UCRL-CR-120671
B239744

Final Report

SEISMIC AND SOURCE CHARACTERISTICS OF LARGE CHEMICAL EXPLOSIONS

V. V. Adushkin
IDG Director
V. N. Kostuchenko
L. M. Pernik
D. D. Sultanov
V. I. Zcikanovsky

January 1995

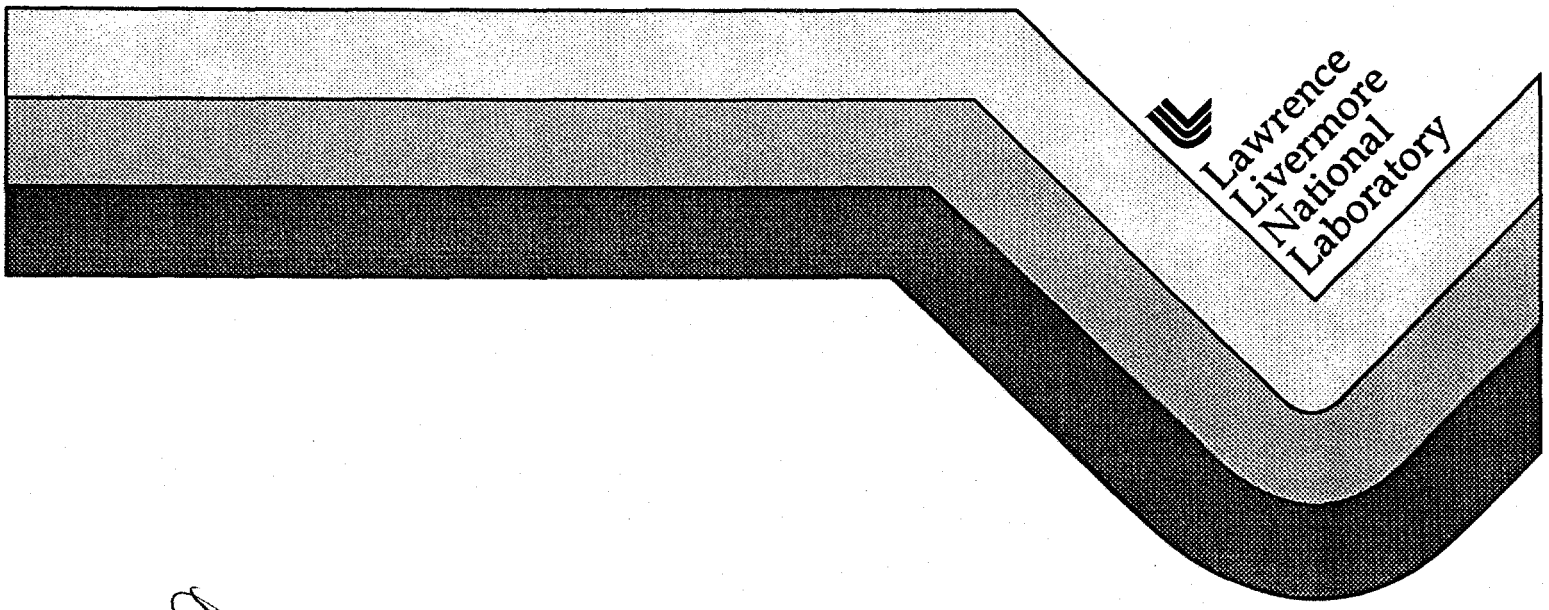

DISTRIBUTION OF THIS DOCUMENT IS UNLIMITED

MASTER

DISCLAIMER

This document was prepared as an account of work sponsored by an agency of the United States Government. Neither the United States Government nor the University of California nor any of their employees, makes any warranty, express or implied, or assumes any legal liability or responsibility for the accuracy, completeness, or usefulness of any information, apparatus, product, or process disclosed, or represents that its use would not infringe privately owned rights. Reference herein to any specific commercial product, process, or service by trade name, trademark, manufacturer, or otherwise, does not necessarily constitute or imply its endorsement, recommendation, or favoring by the United States Government or the University of California. The views and opinions of authors expressed herein do not necessarily state or reflect those of the United States Government or the University of California, and shall not be used for advertising or product endorsement purposes.

DISCLAIMER

Portions of this document may be illegible in electronic image products. Images are produced from the best available original document.

INSTITUTE for DYNAMICS of the GEOSPHERES

FINAL REPORT

SEISMIC AND SOURCE CHARACTERISTICS OF LARGE CHEMICAL EXPLOSIONS

B239744

MOSCOW, 1995

DISTRIBUTION OF THIS DOCUMENT IS UNLIMITED

CONTENT

LIST OF AUTHORS

Adushkin V.V. IDG Director, Professor	–	Scientific Adviser
Kostuchenko V.N.	–	Principal Investigator
Pernik L.M.	–	Researcher
Sultanov D.D.	–	Researcher
Zcikanovsky V.I.	–	Technician

INTRODUCTION

From the very beginning of its arrangement in 1947, the Institute for Dynamics of the Geospheres RAS (former Special Sector of the Institute for physics of the Earth, RAS) was providing scientific observations of effects of nuclear explosions, as well as large-scale detonations of HE, on environment. This report presents principal results of instrumental observations obtained from various large-scale chemical explosions conducted in the Former Soviet Union in the period of time from 1957 to 1989. Considering principal aim of the work, tamped and equivalent chemical exploisons have been selected with total weights from several hundreds to several thousands ton. In particular, the selected explosions were aimed to study scaling law from excavation explosions, seismic effect of tamped explosions, and for dam construction for hydropower stations and soil meleoration. Instrumental data on surface explosions of total weight in the same range aimed to test military technics and special objects are not included.

All the selected explosions were extensively measured by specialists from the IDG who took participation in their conduction. Rock ejection velocity, as well as ejecta flight's height and range were filmed. Gas and dust clouds from the explosions were also observed. Detonation velocity of HE and its conversion into gaseous products of detonation, as well as initial pressure in cavities were measured. Compressional wave in free-field and air shock wave were studied in detail during

the explosions. Seismic and mechanical effects of large-scale explosions determined stability of secured underground constructions, seismic safety of buildings, constructions in nearby populated areas.

In order to carry out the instrumental observations in local zone, special automatic system was designed to turn on the equipment before the explosions.

After the explosions, sizes of dams or craters were measured, as well as topographic measurements of newly developed relief and residual strains inside and on the surface of massifs were conducted. The instrumental observations of the indicated effects and parameters from the explosions allowed to compile large data bank characterizing all the principal explosion's effects. The data bank is intensively used during elaboration of various physical and mathematical models of explosion's effects, for giving recommendations on the effectiveness increase of industrial explosions, and for seismic hazard estimates as well as calculation of explosion effects (air shock wave, contamination by products of detonation, etc.).

The work done under this project used the data bank's portion dealing with seismic effects of large-scale explosions. Seismic sensors used in the measurements of seismic waves in local zone are described. Copies of seismograms at different ranges are presented. The results of the measurements are analyzed and summarized. Geological and tectonic structures of the sites of the explosions are described briefly, as well as the charges and mines design. Parameters of air shock wave are

also briefly described in order to understand total energy sharing between useful work and extra effects.

Results of seismic observations in local zone from two large-scale explosions conducted in hard limestone (marble) massif of Tuwya-Muyun Mountains are analyzed in detail. Seismic source characteristics of the explosions were estimated. High influence of nearby faults crossing the massif on sesimic source parameters was revealed. It will be useful in future to compare the results of the local measurements with regional and teleseismic data. It is important also to conduct such a complex analysis of extensive experimental materials obtained by the Institute from nuclear explosions of different yields.

In principal, the results under consideration demonstrate broad program of possible usage of chemical explosions for industrial purposes. The explosions allowed to decrease expencies and duration of construction, as well as to use local materials in low populated areas with a lack of men resources. The principal task of the IDG in this program was scientific basis of the program from the design and expertise of the large-scale explosions to conduction of instrumental observations and data processing and analysis.

I. Large-scale chemical explosions' catalog

This work is based on the data obtained from several large scale chemical explosions conducted in the Former Soviet Union in the period from 1957 to 1989. Most of the explosions investigated below have been conducted to construct various hydrotechnical constructions and dams aimed for improvement of soil . Some of the explosions have been aimed to investigate characteristics of craters and seismic effect. The explosions yields ranged from several hundred ton to thousands ton.

Table I.1 presents list of the majority of large scale chemical explosions conducted during indicated time period. The list includes dates, times (Moscow time) of detonation, locations, total explosive weights and number of charges. Correct time in several cases was not determined accurately and then no seconds indicated.

The explosions "Cabulsai" and "Uch-Terek" were conducted for scientific purposes. The "Ach-Su" explosion was aimed to uncover deposite. A.all the other explosions were conducted to create dams: hydrotechnical, for improvement of soil and antiavalanches.

Any large scale explosion is a source of scientific information. That is why most of the explosions were well equiped to conduct observations: filming, seismic and acoustic measurements, and other geophysical measurements. Table I.2 presents a list of explosions including parameters measured in experiment.

Chapter III presents detailed information on each of the explosions except "Medeo-II", "Ach-Su", "Quisa" the data from

Table I.1

NN	Explosion title	Date dd mm y	Time (Moscow) hh mm ss	Coordinates long. N deg,min	Coordinates latit.E deg,min	Total weight t	Number of charges
1.	Cabulsai	19.12.57	12-00-00	42 12.3	69 03	1000	1
2.	Tuya-Muyun -I	31.12.59	12-00-0.025	40 21.2	72 35.3	190	1
3.	Tuya-Muyun -II	03.03.60	12-00-0.4	40 21.3	72 35.3	660	1
4.	Medeo-I	21.10.66	06-59-59.1	43 09.4	77 03.4	5293	5
5.	Medeo-II	14.04.67	09-00	-"-	-"-	3941	10
6.	Baipaza	29.03.68	09-50	38 15.8	69 07.2	1854	12
7.	Ach-Su	26.12.72	14-28	42 57.4	46 52.4	552	9
8.	Burlykya	08.02.75	09-59-59.3	41 52.7	73 15.6	702	5
9.	Tyrnyauz	31.12.77	15-00	43 23.2	42 53	833	6
10.	Alindja-gai	04.09.84	13-00-01	39 14.6	45 42.7	689	2
11.	Quisa	16.12.84	14-00-36	42 31.2	43 38.5	437	2
12.	Uch-Terek	11.06.89	10-59-48	41 43.5	73 15	1623	2

Table I.2

Explosion title	Filming	Compress. wave in massif	Seismic measurements		Air shock wave
			nearby	far field	
Cabulsai	*	*	*	*	
Tuya-Muyun -I	*	*	*		
Tuya-Muyun -II	*	*	*		
Medeo-I	*		*	*	
Medeo-II	*		*	*	
Baipaza	*	*	*	*	
Ach-Su	*				
Burlykya	*	*	*	*	*
Tyrnyauz			*		*
Alindja-gai	*		*		*
Quisa	*				*
Uch-Terek			*	*	*

which were not saved and/or were not obtained in the amount proper for following analysis.

II. Equipment used in observations

Specially designed equipment was used to measure different parameters from large-scale explosions at close and remote sites. This chapter is devoted to brief description of sensors and other equipment mainly designed to measure compressional waves propagation velocities and those of displacement and particle velocity history.

1. Sensor IMSG is designed to measure particle velocity in the soil in the range from 0.10 to 100 m/sec with peak possible displacement of 30 mm.

The sensor sensitivity is of 50 mVsec/cm. Measuring coil resistance is of 30 Ohm. Figure II.1 shows principal scheme of the sensor. Operational principle of the sensor is as follows. When the sensor's shell (2) is moved by adjacent soil to which the sensor is attached, relative motion of the shell and seismic mass (1) occured. The seismic mass is represented by a constant magnet of cylindrical shape. A coil (3) with two circuits (electromeasuring (4) and electromagnetic (5)) is hardly attached to the shell.

Electric force is arised in the electromeasuring circuit when the sensor is moved. The electric force is proportional to the relative velocity between the shell and the constant magnet. Resulting signal's recording is conducted on a trace oscilloscope MPO-2. To reduce signal when particle velocity is very high, additional resistor was placed in the circuit of

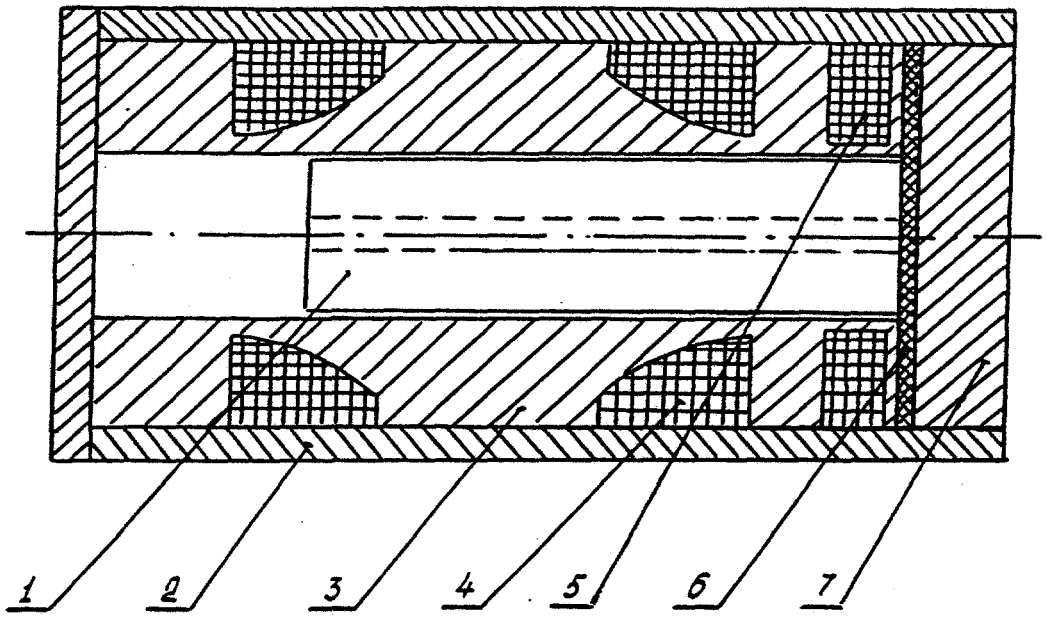

Figure II.1 Principal scheme of IMSG sensor

trace oscilloscope.

Electromagnetic coil circuit was installed to establish constant magnet into the edge position by giving to the coil constant voltage of 24 V. After moved to the edge position, the constant magnet was attached by steel cork (7) in this position. Attraction force of the cork and the magnet is controled by a thickness of nonmagnetic flank (6). After being installed the electromagnetic coil was swithced off.

Records are deconvolved by following formula:

$$U = \frac{(Re+Rs+Rad+Rtr)1}{Str\ Ss}$$

where U is the particle velocity, cm/sec; Re is the resistance of the line, Ohm; Rs is the sensor resistance, Ohm; Rad is the additional resistance, Ohm; Rtr is the trace resistance, Ohm; 1 is the record amplitude, mm; Str is the trace sensitivity mm/μa; Ss is the sensor sensitivity; $\frac{\mu V\ sec}{cm}$.

By integrating velocity records it is possible to get ground displacement as a function of time. Compressional wave velocity can be estimated from arrival times at different IMSG sensors placed at fixed distances from each other.

The sensors calibration was carried out by throwing of a magnet from different heights. Sensor sensitivity was determined from velocity of a magnet in the impact moment or from total path to a given time.

In order to measure particle velocity inside a rocky massif special drillholes have been drilled to epicenter of explosions with a length of 0.5 to 3.0 m and a diameter of 70 mm. A small

amount (10-15 cm^3) of cement was intruded in a borehole by specially designed equipment. Sensors were pressed in the cement to touching hard rock at the boreholes bottoms. The boreholes were wholly cemented after the sensors establishment.

2.GIS sensor is designed for measuring of particle velocity of ground motion under detonation waves loading. Operation principle of the sensor is based on measuring of sensitive element displacement relative to two-sectional induction coil attached to the sensor shell. The inner space of the coil is filled by viscous polimethiloxidance liquid (PMO). Inertial element's equation of motion has following common form:

(1) $$m\ddot{x} + c\dot{x} + kx = m\ddot{y},$$

where m is the mass of the inertial element; x is the displacement of the inertial element relative to the sensor's shell; c is the coefficient of relaxation; k is the regidity of the string to the inertial element; y is the sensor's shell displacement.

For high coefiicient of relaxation it is possible to write

$$c\dot{x} = m\ddot{y} \text{ или } \dot{x} = \frac{m}{c}\ddot{y},$$

and after integrating without a constant one can get

(2) $$x = \frac{m}{c}\dot{y}.$$

Thus, the sensitive element's of the sensor inclination is proportional to the velocity of the shell or particle velocity in massif where the sersor is placed.

GIS sensor was designed in two versions in order to measure

vertical (GIS-V) and horizontal (GIS-H) components of motion. Sensitive element of GIS-V sensor (Fig. II.2) (cylinder heart) is attached by low-rigidity spring in the inner space of the coil made from organic glass. Sensitive element diameter and liquid viscosity is chosen by the desired velocity amplitude to be measured.

To reduce frictional effects on the heart from the coil walls when horizontal motion is strong, two rows of rollers (three in a row) are used.

The coil has two wires which are separated into two sections in order to increase linearty range of inductivity variations. Sensetive element is attached by a spring which holds the element in the middle position relative to the upper and lower wires. The spring rigidity is chosen to get natural frequency of oscillations in the air in the range from 2.5 to 3 Hz.

The shell protects the sensor from mechanical damages. The shell is filled by PMO liquid providing reliable hermeticity of the sensor under high pressures and allowing inhermeticity of the inner space. When temperature changes, PMO liquid flows through the capillaries near the cork and screw into the coil and back into the shell. Such a connection prevents air bubble creation in the coil when temperature drops down.

GIS-H has the same principal operational procedure, but has two springs adjusting the sensitive element to the central position. The differential scheme was chosen for electrical

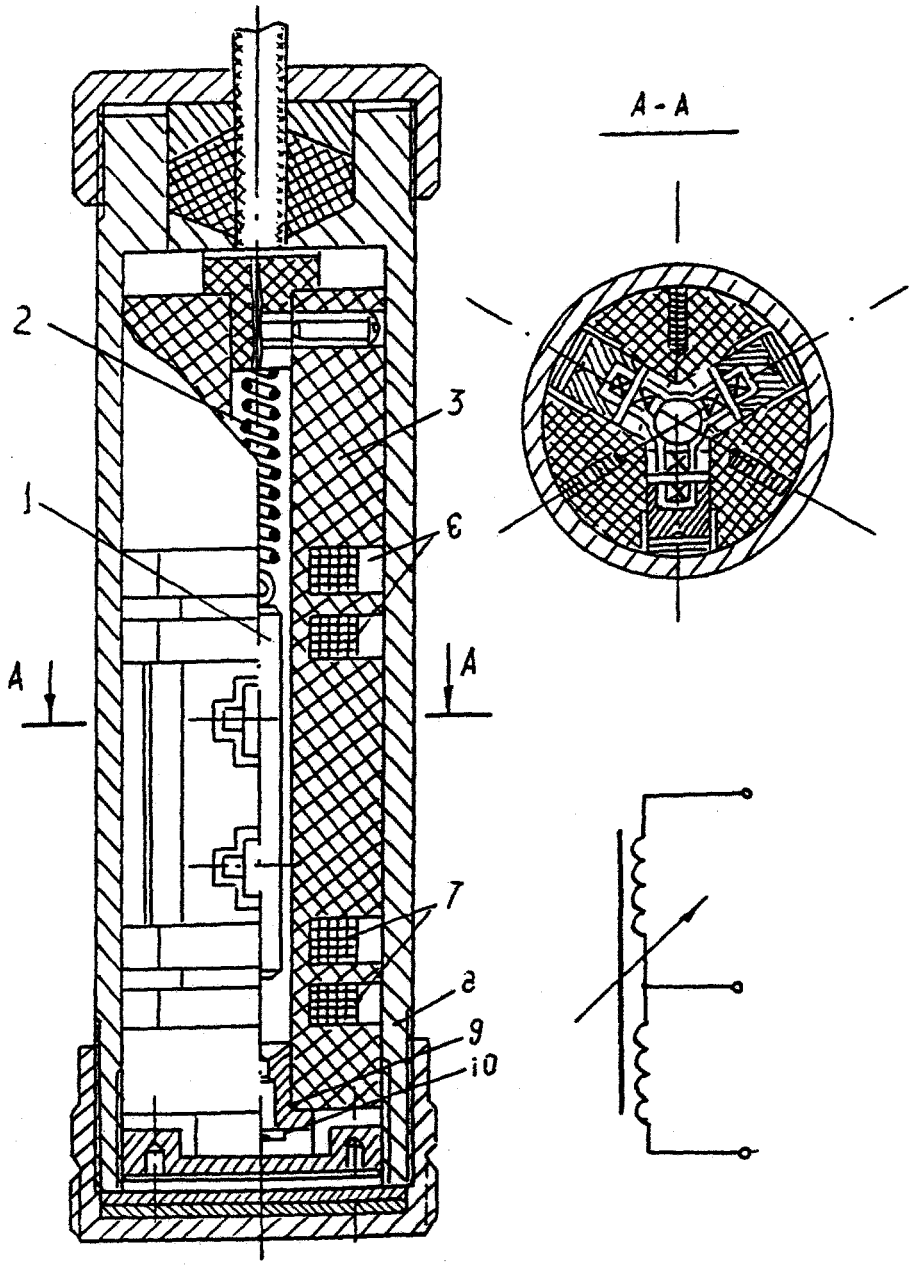

Figure II.2 GIS-V sensor. 1-sensitive element, 2- spring, 3-coil, 4-roller, 5-roller´s axis, 6,7- working wires, 8-sensor´sshell, 9-cork, 10-screw.

circuit of the sensor. The scheme provides displacement less than ±3 mm.

Principal technical characteristics of the GIS sensor are following.

Measured velocity range, m/s:	
GIS-I	0.1- 3.0
GIS-II	0.5-15.0
GIS-III	1.0-30.0
Frequency response linearty range, Hz	
GIS-I	0.9- 80
GIS-II	0.4-250
GIS-III	0.1-350
Acceleration range, g	0.01-300
Maximum connecting wire length, m	1000
Environment temperature range, C^{o}	-20 - +50
Lenght, mm	less than 160
Diameter, mm	38
Mass, kg	less than 0.6

3.VIB-A seismometer is designed to measure partical velocity of vertical and horizontal ground motion in the frequency range from 5 Hz and higher and peak displacement less than ±10 mm. Measuring velocity range is from 0.1 cm/sec to 10 m/sec.

VIB-A seismometer is of pendulum type with magnetic-electrical transducer. There is no special damping of natural oscillation.

Principal characteristics of the sensor are following. Natural period of oscillations for vertical component measuring T_1=0.6 sec.

Natural period of oscillations for horizontal component measuring T_1=0.4 sec.

Scaled lenght l=10 cm.

Induction coil resistance of transducer Rs=5 Ohm.

Coefficient of electromechanical coupling 0.01 10^8 CGSM.

4.VIB-V seismometer is designed to measure higher particle velocity than VIB-A. The range of possible displacement is ±50 mm. VIB-V is also of pendulum type sensor with magnetic-electrical transducer and also has no damping of natural oscillation.

Osh-9 oscilloscopes were used to record signals from VIB-A and VIB-V seismometers. The Osh-9 oscilloscope has usual traces. When measurements were carried out in field conditions oscilloscopes amortization by special pad on springs was used to reduce strong motion.

5.VEGIK seismometer was designed to measure separately vertical and horizontal components of ground motion with amplitudes from 0.001 to 2 mm in the frequency range from 0.01 to 1 sec. This sensor is of pendulum type with magnetic-electrical transducer and adjustable magnetic damping.

The sensor (Fig. II.3) contains mechanical system including

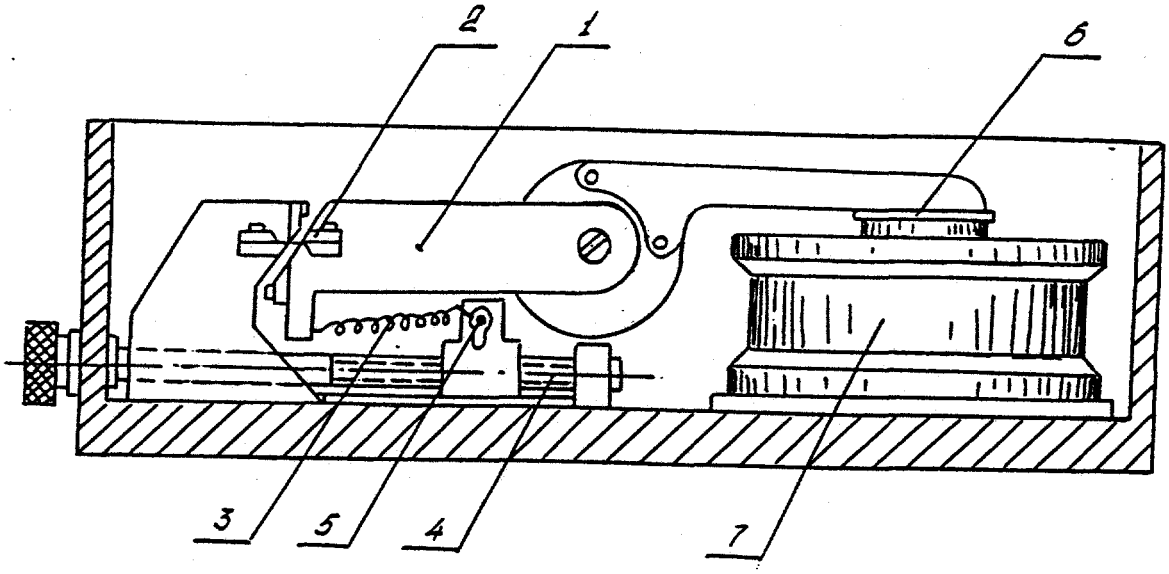

Figure II.3 Vibrosensor VEGIK (schematic cross section).

the pendulum with seismic mass (1) rolling at a crest-like chassis (2) and the spring (3) which strain and position is adjusted by the screws (4) and (5). Due to these screws it is possible to change natural period of oscillations from 0.5 to 2.5 Hz for vertical component measurements.

To measure horizontal component of motion. The spring is detached and the sensor's shell is moved at 90^{o} around horizontal axis and then is attached by three screws which serve to adjust inclination angle and seismic mass stable position. To provide the pendulum stablity the sensor's shell is established with little inclination. Inductive element of the sensor consists of the coil (6) attached to the pendulum with two wires and the magnetic system (7) installed at the shell. From the two wires of the coil, one is usually shorted or connected through small resistor and operates as a damping circuit. The second one is connected to the recording system.

Principal parameters of the sensor are following:

pendulum natural period T_1=1.2 sec;

damping D_1=0.5-0.9 (from critical);

scaled length l=10 cm;

damping inductive coil resistance R_{m2}=30 Ohm;

transducer inductive coil resistance R_{m1}=55 Ohm;

electro-mechanical coupling coefficient 10-30 $\frac{V\ sec}{m}$;

size 30x13 cm, height 11 cm;

weight 9 kg.

6. Pendulum seismometer S5S with magnetic-electrical transducer and adjustable magnetic damping is designed to record by galvanometer ground and constructions motion induced by explosions and earthquahes. Displacement range is from 0.01 micrometer to 15 mm with frequency range from 0.01 to 5 sec.

S5S seismometer has double seismic mass system with pendulum chassis (Figure II.4). The pendulum consists of two massive constant magnets with magnetic conductors (2) (Figure II.5) connected by rigid bar (1) balanced on the cross-like chassis (3) to pad (9). The spring (4) is attached by one edge to the roller (5) moving along adjusting screw and by other edge to the bimetallic thermocompensator (6) attached to the pendulum. Measuring and damping coils (7) are hardly attached to the pad. The pad can be attached by the screws (8) to the shell basement (10) in one of two positions: measuring vertical or horizontal motion with the special steps at the basement allowing to change the angle between the pad and the shell by adjusting the screws (8). The angle changing allows to change pendulum's natural period. Natural period can be adjusted gradually when the pendulum is unbalanced by the roller (5) shift. When measuring horizontal motion the string (4) is adjusted to be in the same plane as the pendulum chassis is or close to it.

Principal characteristics are following:

pendulum's natural period	5 sec;
scaled lenth	42.5 cm;

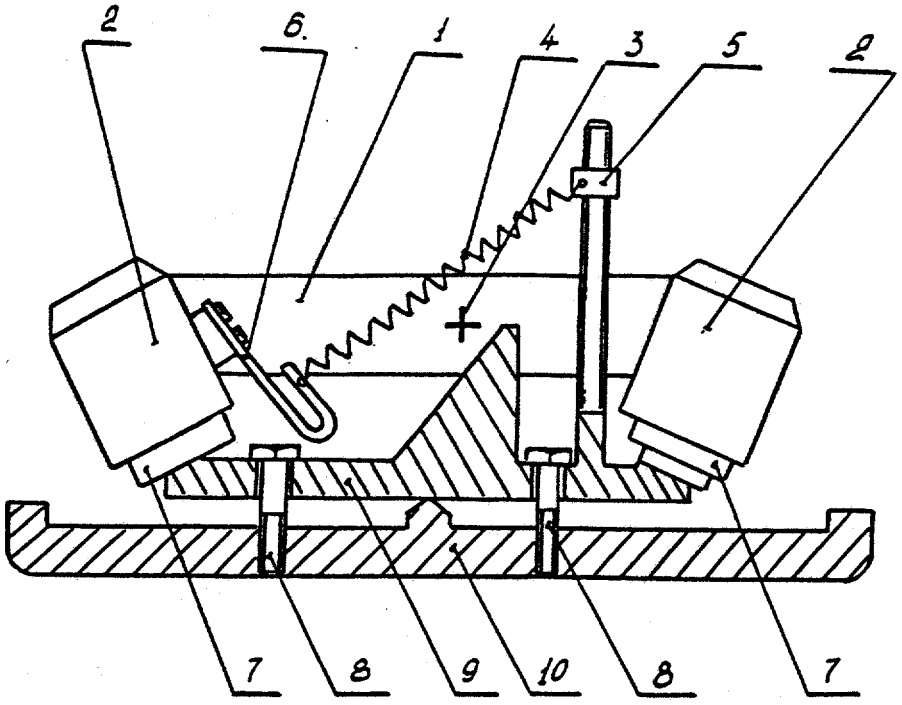

Figure II.4 S5S seismometer (cross section of the sensor for vertica component measuring).

working inductive coil resistance 88 Ohm;

damping inductive coil resistance 88 Ohm;

electric-mechanic coupling coefficient 12.8 $\frac{V\ sec}{m}$;

size 36x16 cm, height 15 cm;

weight 11 kg.

7. Strong motion vibrograph VBP-3 is designed for recording of displacement in vertical and horizontal directions with amplitudes from 0.5 to 200 mm and frequency range from 100.0 to 1.0 Hz. As well as S5S, the vibrograph has masses, mechanical system with pendulum chassis.

Principal parameters are following:

natural period 1.6 sec;

damping coefficient 0.7-1.0 (from critical);

scaled lenght 65 cm;

transducer's coil resistance 55 Ohm;

electric-mechanical coupling coefficient 0.1 $\frac{V\ sec}{m}$;

size 23x23 cm, height 15 cm;

weight 9.6 kg.

Frequency responces of VBP-3 and VEGIK sensors with galvanometers GB-III are shown in Figure II.5. As clear from the Figure the frequency responces are close to constant in the working range.

8. ISF sensor is designed to measure propagation velocity in the closein zone.

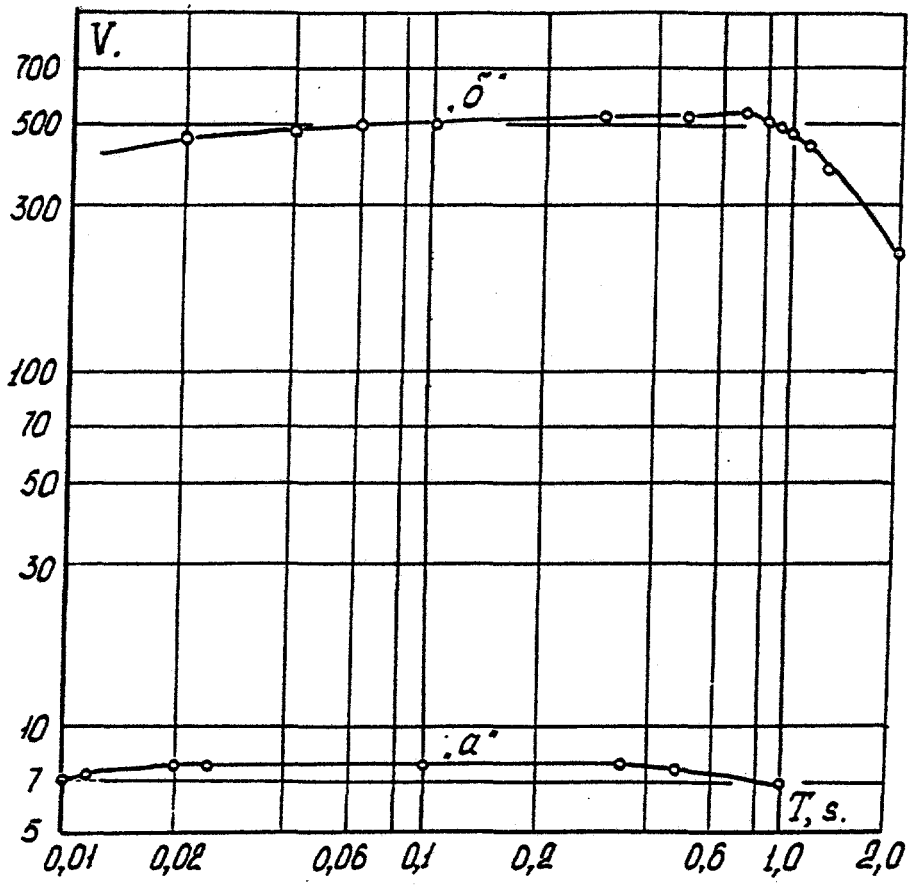

Figure II.5 Responces and gains (β-reduction coefficient)

a- VBP-3 (β=1)

b- VEGIK (β=2)

There are two ends of disconnected electic circuit in the shell of the sensor. These ends are represented by hard contactors. There is a gap of adjustable thickness between the contactors and the bottom of the shell.

The gap thickness is of 0.10 mm during experiments. Under strong loading the shell bottom concaves and connects the contactors shorting the circuit.

Thus, arrival times compressional wave are determined by the sensor. Several sensors established at known distances from the shot point with known baselines allow to estimate velocity of propagation.

The sensor time accuracy is determined by particle velocity in compressional wave in a given point. When particle velocity is of 10 m/sec time accuracy is of $\frac{0.1 \text{ mm}}{10 \text{ m/sec}}$ = 10 microsec. If to assume usual baseline length of 5 m and compressional wave velocity of 5 km/sec the error induced by operation time of the sensor is of 1.0 %.

9. Seismometer SM-2 is designed for oscillations' measuring in the range from 0.7 to 200 Hz and displacement amplitudes from 10^{-4} to 3 mm. The sensor allows measuring any component of motion.

The seismometer is assembled at the hard basement. The shell of the sensor is attached to the basement by screws. All the principal parts of the seismometer are assembled at the shell. They are the pendulum, magnetic system, coordinate

mechanism with two adjusting screws, and central and axial arresting devices.

The sensor's pendulum is hung on elastic cross-like substitutable chassis and is held in the stable position by cylindrical spring.

Bimetallic thermal compensator is attached to the pendulum allowing stable position don't to be changed with temperature variation of 20°C. There is a coil with working and damping loops attached to the pendulum. The shell design allows to use the seismometer for measuring of vertical as well as horizontal components of motion.

Principal sensor characteristics are

pendulum natural period 1.2 sec;

scaled length 8.7 cm;

transducers inductive coil resistance 130 Ohm;

dampind inductive coil resistance 45 Ohm;

electric-mechanical coupling coefficient 37 $\frac{V\ sec}{m}$;

size 23x16.7 cm, height 14.5 cm;

weight 5.5 kg.

SM-2 seismometer was designed to substitute for VEGIK seismometer. Having almost the same technical characteristics it has higher hermeticity, thermal compensation, and it is simplier to install for recording different components of motion, more reliable arresting device and substitutable chassis creating rotation axis of pendulum.

10. SM-3 seismometer represents an updated version of SM-2 differing only by wider ranges of working parameters. Natural period is Ts=2 sec and maximum coil displacement is of 5 mm.

Principal characteristics are following:

scaled length 8.5 cm;

transducer's inductive coil resistance 65 Ohm;

damping inductive coil resistance 65 Ohm;

electric-mechanical coupling coefficient 20 $\frac{V\ sec}{m}$;

size 23x16,7 cm, height 14.5 cm;

weight 5,5 kg.

11. SMP-2 seismograph is the horizontal seismograph with mechanical recording system, electromagnetic damping and continuous recording. It is designed to measure earthquakes with intensity of 3 to 7 balls. In the range from 0.2 to 4 sec the sensor measures ground displacement.

A set of two sensors are usually used to measure two horizontal components. The pendulum represents a massive cylinder of 6 kg total weight hung at four steel plates 0.15 to 0.2 mm thick which are attached to the sensor basement. Each of the plates is pressed to the pendulum from one side and to corresponding bar from another one side. The plates are installed in such a way to avoid shear loading. To prevent disturbing vibrations of the mass on the chassis each couple of the plates has a shape of a cross. The pendulum rotation axis is close to the line where two planes of two couples of the plates

intersect and almost perpendicular to the basement. Copper plate is attached to the bottom of the cylinder. The plate serves as a damping device. Damping is conducted by two constant magnets which can be moved along a roller to adjust damping coefficient. Magnifying handle presented by light aluminum tube is attached to the side surface of the cylinder. The tube edge holds a pencil. To reduce friction the pencil has a conterweight.

A spring mechanism of recording equipment forces and holds a drum and rolls. There is a bar with a screw-thread inside the drum allowing screw recording. Rate adjusting mechanism give an aweraged linear drum surface velocity of 30 mm/min. The rate adjusting mechanism consists of two blades attached at the output axis of the mechanism. A day long operation is available with a rate of 30 mm/min.

Time marks are presented by gaps in records' lines which are inducted by electric current going through electromagnet which moves the pencil up through a swivel system. There is also independent timing mechanism represented by electromagnet with a handle at the anchor. One time a minute (from stationary time service) an electric impulse was passed through the electromagnet wire. The handle drops to the drum at this moment and makes a mark on the record's line. Time marker is included in the circuit of the pencil which is available at the station for time marking. The drum is covered by smooth paper band (fine paper or copier). This band is smoked and recording is done by sharp blade over the smoked surface.

Principal characteristics are following:

pendulum's natural period 5 sec;

damping coefficient 0.46;

scaled length 10 cm.

12. SKM-3 seismometer is used to measure seismic waves in the period range from 0.1 to 3 sec and amplitudes of 10^{-5} to 1 mm. The sensor was designed in two versions: horizontal seismometer SHKM-3 and vertical SVKM-3. The sensor is of electromechanical type with oscilloscope recording.

Characteristics are following:

natural period 1.6 sec;

scaled length 16.5 cm;

transducer inductive coil resistance 40 Ohm;

damping inductive coil resistance 40 Ohm;

electric-magnetic coupling coefficient 65 $\frac{V}{m}\,\frac{sec}{}$.

13. Seismometer SK is used to measure seismic waves in the period range from 0.2 to 10-15 sec and amplitudes of 10^{-3} to 5 mm. The seismometer is designed in two versions: horizontal seismometer SHK and vertical SVK. The seismometer is of electromechanical type with oscilloscope recording.

Characteristics are following: for SHK/SVK

natural period 6 to 35 / 7 to 25 sec;

scaled length 27/10 cm;

inductive coil resistance 26.5/26.5 Ohm;

electromechanical coupling coefficient 5.5/21 $\frac{V\ sec}{m}$.

14. Inductive velocity sensor IDS-3 was used to measure seismic waves propagating in hard rocks from explosive sources and having amplitudes from 0.01 to 10 m/sec and periods from 0.5 to 20 microseconds.

Principal scheme of the sensor is shown in Figure II.6-a. Soft seismomass's chassis allowed to avoid high-frequency parasitic oscillations. Prestrained springs provide the sensor operation in any position, i.e. it is possible to use the sensor in measuring vertical as well as horizontal components of ground motion. Thick gap between a magnet and two-section coil (2) allows is not directed along the sensor axis. The sensor directivity is shown on Figure II.6-b.

The sensor characteristics are following:

natural period 12 Hz;

doubled amplitude of seismomass displacement 17 mm;

sensitivity 25 $\frac{mV\ sec}{mm}$;

coilsresistance 3000 Ohm;

diameter 54 mm. length 74 mm;

weight 0.36 kg.

The sensor were established in drillholes in rocky massif and were fixed by special clue.

15. Pressure recorder SD-725 was used to measure shock waves in the air. The recorded natural period has been no less than 20

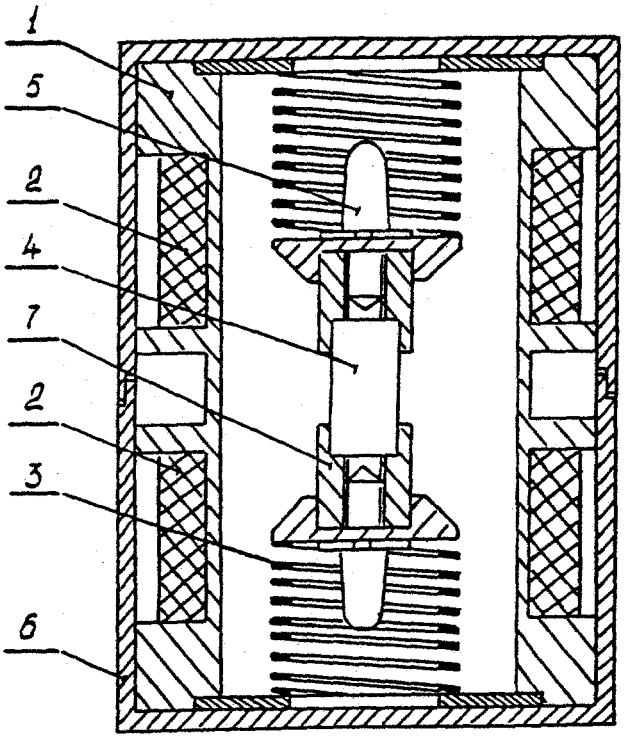

Figure II.6-a Inductive sensor of velocity IDS-3. 1-coil. 2-twosectional wire, 3-intruding springs, 4-constant magnet, 5-limits. 6-shell, 7-pole peaks.

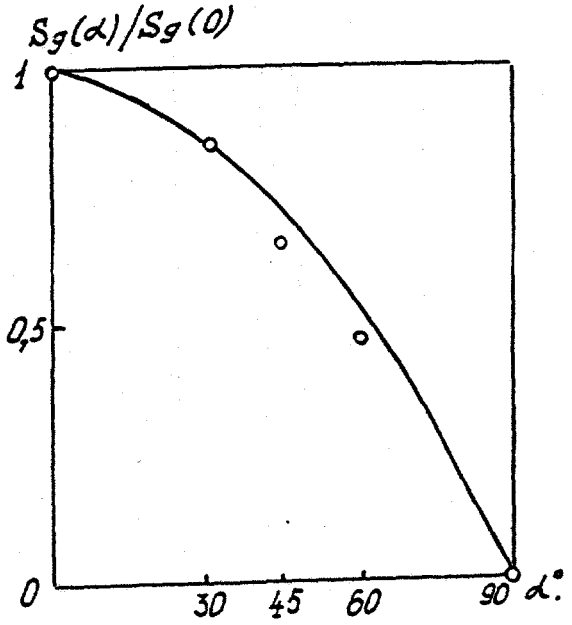

Figure II.6-b IDS directivity pattern. 1-cosα, 2-experimental points.

Hz. Recording was conducted on smoked paper covering a rotating drum. The sensor with total recording time of 8 and 30 sec were used. During this time the drum makes 6 total loops with forward displacement of 2 mm per one loop. Linear band velocity was of 190 and 50 mm/sec respectively. The sensor sensitivity was of 0.007 kg/cm^2 and 0.02 kg/cm^2.

III. Measurements result.

III 1. Cabul-Sai explosions

A series of underground chemical explosions with yields from 10 kg to 1000 tons was conducted in fall of 1957 within theSouthern Kazakhstan. The explosions were fired in consolidated non-rock soil. Crater creation and study of ejection mechanism were two principal goals of the series. To investigate these phenomena, the filming of motion of the surface and debris flight were conducted. Also the distribution of the ejecta around the craters by radioactive isotopes as well as the profiles and sizes of the craters and walls were measured. Explosion generated seismic waves parameters in the upper layers were also measured in the local zone. Moreover, seismic waves from 1 kt explosion were detected by the network of the Soviet Asia seismic stations.

To conduct the series a spacious valley with the summer drying river Taganas-Sai to the south of the railway station Cabul-Sai was chosed. The valley is surrounded by smooth hills. Four test sites were used. The first layer of sediments with a thickness of 5 to 25 m was formed by loamy soil. The principal layer of blue clay underlied. Ammonium nitrate was used as an explosive. The charges with an yield of 10 kg were detonated in the drill-holes. 80-120 kg charges were placed in the cavities created by the smaller explosions. To place 1000 and 10000 kg charges the special cavities in the sides of dug-holes were

excavated. The chamber of a size $8_x 20$ m^2 in plane and 8 m height was created for the charge of 1000 tons. The charge was centered at the depth of 40 m from the free surface in blue clay. The loamy soil layer thickness above the chamber was of 10 m.

Several boreholes of different depth were drilled at the test sites. Cores of soil were extracted from the boreholes. These cores were analyzed in laboratory to measure granulometric content, specific and volume weights, water content and some other parameters. Table III.1 presents the data obtained from the borehole N12.

Table III.1 Physical and mechanical properties of soil.

	Soil content	Grain sizes (%), mm				Volume weight, g/cm^3		
		2.0-0.05	0.05-0.005	0.005		natural structure	skeleton	
6	fine clay	1.64	28	70	2.38	2.01	1.65	22.2
40	fine clay	4.0	20	75	2.26	2.00	1.60	25.0
80	sand and clay	44.0	18	38	2.50	1.72	1.20	43.7
100	clay rough	26	39	35	2.56	1.92	1.53	25

The cores were also studied in the conditions of volumetric compression of 25 kg/cm^2 . Averaged values of bulk modulus was

of K=176 kg/cm^2 at the depth of 6 m and K=380 kg/cm^2 at the depth of 40 m.

Oscillations measurements were carried out on the free surface and in vertical plane passing through the sensor and the shot point.

Due to high amplitudes of displacement near the craters thesensors sensitivity were reduced to low level.

A. System of measurements

The depths of the charges emplacement was chosen from the geometrical scaling relationship:

$$\frac{h_1}{h_2} = \frac{\sqrt[3]{q_1}}{\sqrt[3]{q_2}}$$

where h_1 and h_2 are in m, and q_1 and q_2 in kg. For all the explosions the ratio $h/\sqrt[3]{q}$ was in the range from 0.4 to 0.7 except the two charges of 1000 kg which were conducted at the depth of 15 m.

Soil oscillations were usually measured at the surface along the profiles. The source/receiver distances and the profile length were dependent on the charge weight and also were governed by geometrical scaling law. In several cases, however, the sensors spacing was smaller in order to study some details of wave propagation and seismic phases identification. Besides the main goals, the engineering problem of wave-fundament interaction was also investigated and three couples of VEGIK sensors were installed with 15 m spacing.

Vertical (Z) and radial (X) components were measured by the sensors installed in the vaults at the depth of 0.5 m. The vaults were filled by soil, especially at closer distances. Special procedures were fulfilled to harden the soil/sensor contact. To control the records, VIB-A sensors measuring transversal component of motion (Y) were installed in some cases. Transversal component occured to be very low and is not considered below.

VIB-A sensors were installed deeper than 0.5 m in some cases. These sensors were placed at the depth of 15 m for the explosions of 1000 kg. The dug-holes created for the following explosions were used to place VIB-A sensors. During the explosion of 1000 tons sensors were attempted to be installed deeper, at the depth of 40 m in the specially drilled borehole of 350 mm diameter. Two sensors (Z and X component) were mounted in the special container of 70 cm height. After installation the containers were isolated by melted tar. The containers were placed in the boreholes by the special system of metal tubes.

The records from these sensors have shown that the system of container installation and insulation should be improved.

At closer distances seismic sensors VBP-3 and VIB-V were used, and at larger distances - VIB-A and VEGIK. The distance to the closest sensor was dependend on a crater diameter and ejecta wall height. The diameter changed from 3.5 m for 10 kg explosion to 100 m for 1000 tons explosion. Such a distance garantees that a sensor can be digged out and used next time. Such a system of

sensors allowed to correlate different seismic phases along the profile as well as to establish the parts of the profile where the correlation is disturbed by new phases arrivals and interferention.

To compare the records from the explosions of different yield, q, at different distances, r, parameter

$$p = \frac{r}{\sqrt[3]{q}}$$

is used below. The parameter is the scaled distance, where the charge weight is given in kg and the source/receiver distance in meters.

The shot time was obtained from the circut wrapped around the detonator and the signal was recorded by oscilloscope. All the oscilloscopes also had common null-mark from automatic equipment.

B. 1000 tons explosion

The explosion of 1000 tons was detonated on 19 December, 1957 in 12:00:00 (Moscow time).

The explosion was conducted at the test site N4 inside the valley with nondeveloped relief. The ammonium nitrate charge was placed in the chamber with 8x20 m plane size and height of 8 m excavatedin blue clay. The charge was centered at the depth of 40 m. The loamy soil layer of 10 m covered blue clay above the shot point.

Within the valley at the range of 1800 m from the shot point the borehole of 120 m was drilled. By using this borehole

several seismic profiles were investigated. The principal profile range was of 900 m lenght. A set of travel time curves was obtained for this profile from six explosions points. Geological section and velocity distribution were retrieved from these curves. From these data, the upper loamy soil layer thickness varies from 5 to 12 m. Longitudinal wave velocity in this layer was from 430 to 500 m/sec. Brown-green clay layer 2.5-3 m thick was noted below the loamy soil layer. Wedges of the clay layers were traced along the profile with compressional wave velocity of 1750 m/sec. In the underlying blue clay laeyr V_p is of about 1900 m/sec. The lower boundary of blue clay was not detected by seismic sounding.

Two profiles of seismic sensors were established due to the valley relief. The first profile 800 m long was oriented perpendicular to the center of the longer side of the chamber due to symmerty reasons. VIB and VBP-3 sensors were used with 100 m spacing beginning from 100 m (predicted crater radius).

The second profile oriented along the valley began from 600 m with the most distant point at 4000 m. The angle between the two profiles was of 45^{o}. From 600 to 1600 m the sensors spacing was of 200 m. At the distances of 1600, 2000, 3200 and 4000 m trippled couples of VEGIK sensors with the spacing of 15 m were established.

Displacement amplitudes as measured by VBP-3 and VEGIK sensors at different distances are presented in Figure III.1. Travel time curves are shown in Figure III.2. The explosion was

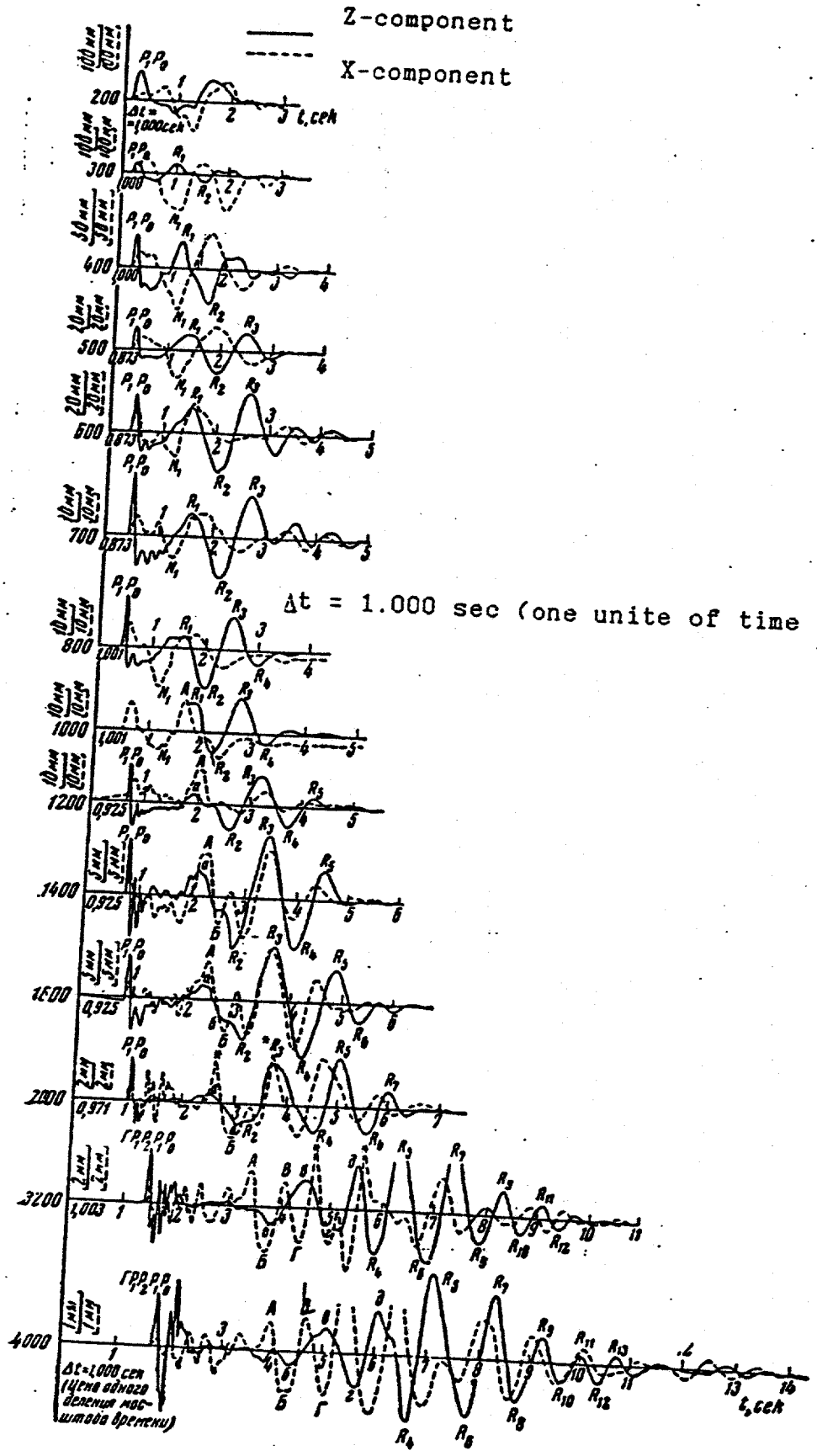

Figure III.1 Disolacement at different distances.

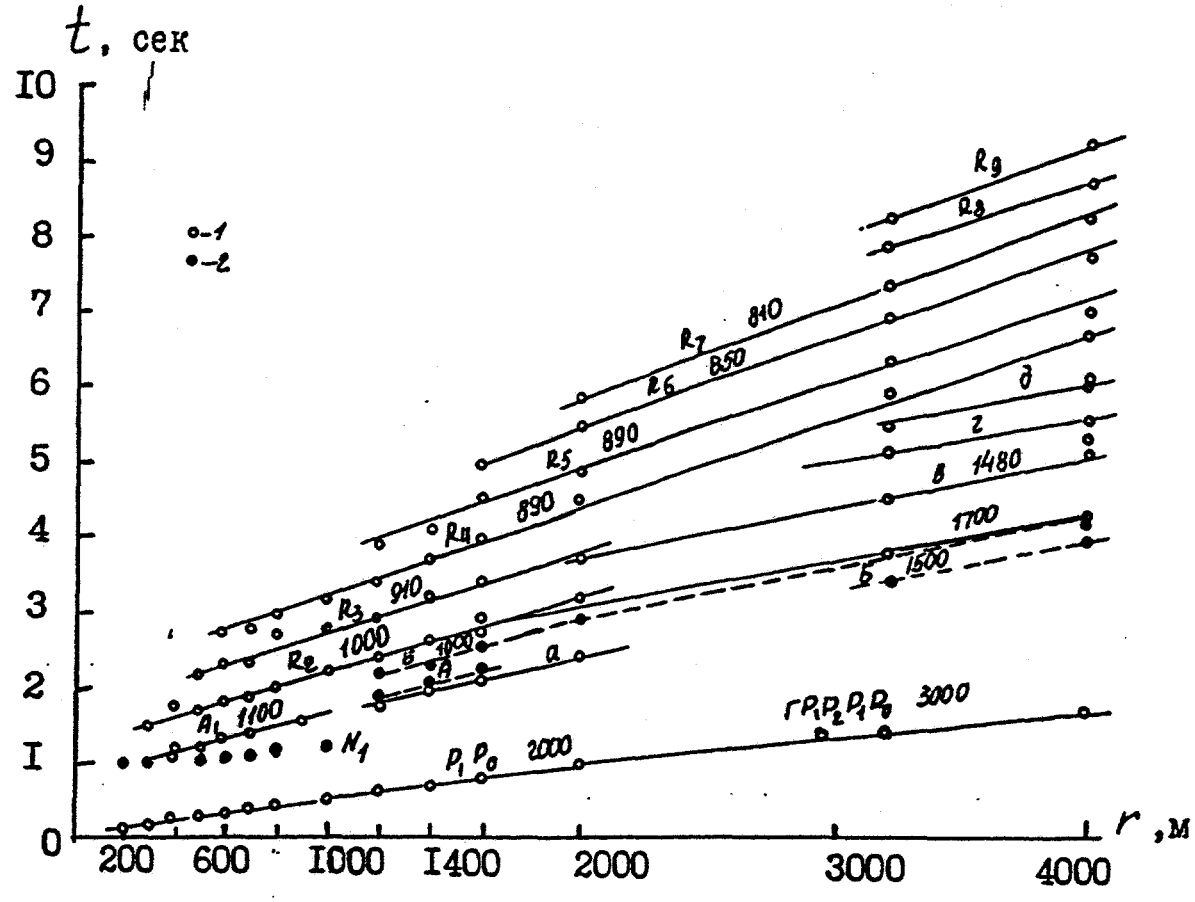

Figure III.2 Summarizing time/distance curve. (1-Z-component; 2-X-component.

detonated in blue clay at the depth of 4 times lager than the loamy soil layer thickness. Hence, the first sharp arrivals at the records are associated with P_1P_o wave and lay at straight line to the distance of 2000 m. This wave velocity Vp_1p_o = 1900 + 2000 m/sec is consistent with blue clay. At the distance of 2000 m the travel time curve has a break. Straight line drawn through the three points cut a time to = 0.3 sec on the time axis. One can suppose that this branch of travel time curve corresponds to a guide wave propagating along deeper interface.

If to assume horizontally layered structure then this guide wave velocity is of 3000 m/sec. From relationship:

$$t_o = \frac{2H \cos i}{V}$$

where i - is the critical angle, one can obtain the interface depth of H=400 m which obviously corresponds to the blue clay lower boundary.

The longitudinal wave under consideration has sharp arrivals along the profile with upward and outward first motion and substantially larger Z-component than X-component. This feature is consistent with close to vertical wave front incidence. One characteristic feature of the compressional wave is a decrease of positive phase duration with increasing distance. This feature is not explained yet.

Rise time in P_1P_o-wave is larger at X-component. The difference decreases with distance. Due to these phenomena, the travel time curves obtained from maximum amplitudes of X- and Z-component approach the travel time curves from the first

arrivals when distance increases. First maximum amplitudes of Z- and X-components effectively decrease with distance but not so fast as amplitudes of guide wave at the test sites N2 and N3. Relatively high-frequency coda of the longitudinal wave with periods from 0.12 to 0.2 sec arrives beginning from 400 m. The coda duration increases with distance. It is hard to interprete phase in this coda due to complexity of records. One can assume this wave train as reflected waves in the loamy soil layer.

Next distinct seismic phase is the first minimum at X-component which marked by character N_1 at the records and travel time curve. This phase is well traced in the distance range from 300 to 1000 m. This phase is characterized by intensive displacement of soil to the shot point and low vertical displacement amplitude. At the epicentral distance of 300 m, for example, horizontal displacement amplitude reaches 150 mm and Z-component as low as 50 mm. Clockwize elliptical partical motion is observed. This phase may be interpreted as a converted P_1S_1-wave reflected by the lower blue clay boundary. But this kinematic constraint is not enough for unambigious interpretation. It is possible that the particle motion is related to the special features of caving explosion discussed above. This assumption is partially confirmed by long duration of the phase (period of about 1 sec) and fast attenuation with distance.

Besides distinct refracted and guide longitudinal waves several clear wavetrains are observed. These wave groups became

more distinct at larger distances and by some features (partical motion trajectory shown in Figure III.3, component ratio, dispersion) can be interpreted as Rayleigh surface waves. These wavetrains consist from successive phases marked at the records by character R and indexes 4, 5, 6 etc. Phase velocity decreases with increasing index from 880 m/sec to 800 m/sec. Oscillations period decreases from 1.0 to 0.7 sec. Group velocity is from 300 to 500 m/sec.

Phases R_1, R_2 and R_3 at closer distances are not so clear at vertical component, possibly due to different phase interference. These phases are also characterized by energy transmission to following phases and disappearance of earlier phases.

Mean parts of the records at all the epicentral distances are very complex and hard to interprete. Travel time curves constructed for the phases from these parts of the records are not reliable due to strong distortion by different phases. It is also worth noting that natural periods of sensors were not long enough to measure waves with periods longer than 1 sec. Thus, high shape distortion may be common for first two phases of these waves.

Inspite the discussion above, it is possible to note that beginning from 800-1000 m long-period oscillations are formed after body waves arrivals with horizontal component amplitude compatible with vertical at close distance and larger with distance increase. This feature is very distinct at the

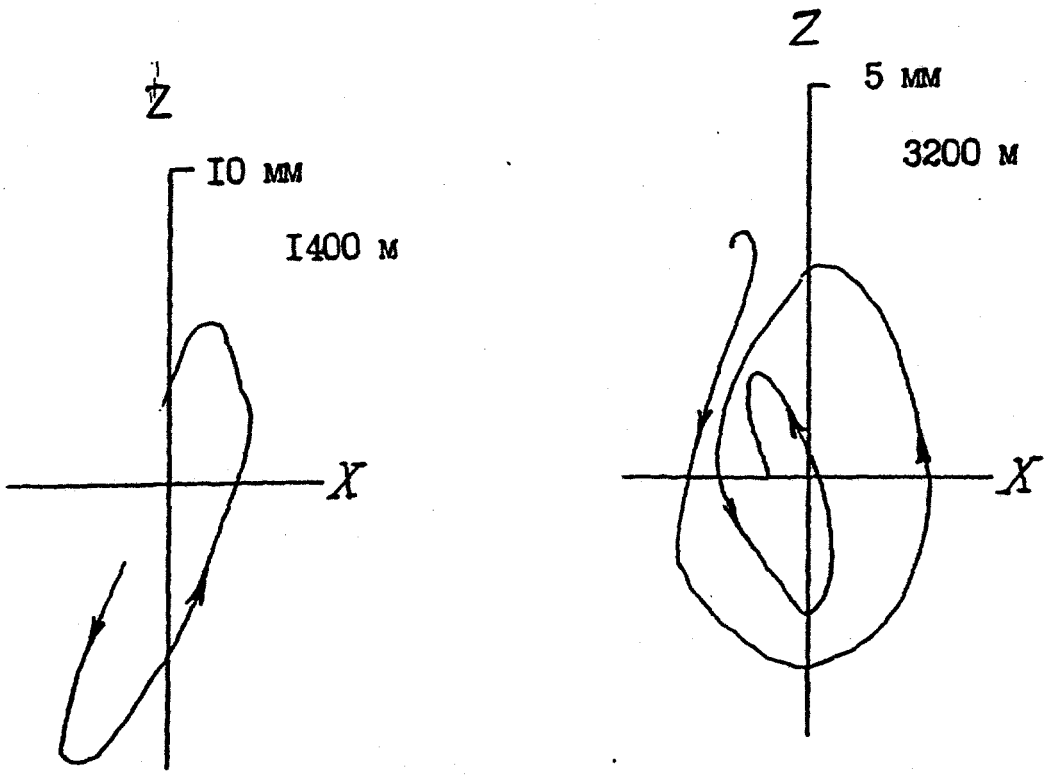

Figure III.3 Particle trajectory in Raileigh wave.

distances 2000 and 3200 m where VEGIK sensor were installed. At these distances records show corners (see Fig. III.1) related to impact of pendulum due to high amplitude of displacement. Vertical component's records do not show such a feature. Predominant horizontal motion in phases marked by A, B, C and D was mentioned by personnel settled at the distance of 2000 m. Similar to the phases mentioned for different test site these phases can be related to N successive phases. The number of phases in the group of horizontal oscillations and their durations increase with distance.

Let us consider now quantitative characteristics of seismic waves measured from 1000 tons explosion. The most interesting distance range is, of course, where displacement amplitude is larger than 10 mm. The data here are unique. Consider P_1P_o wave. As mentioned above, τ_2^A decreases with increasing epicentral distance. Figure III.4 displays this decrease for both components in the distance range from 200 to 2000 m. Analytic interpolation gives following relation:

$$\tau_2^A = \frac{1.3}{r^{0.34}}.$$

τ_2 for the first arrivals at the distances larger than 2000 m lay out of the relation. It confirms the assumption of guide wave coming ahead of P_1P_o at this distance.

Figure III.5 displays the relationship between displacement amplitude in P_1P_o-wave and epicentral distance for horizontal and vertical components separately. Log-log scale graphs shows

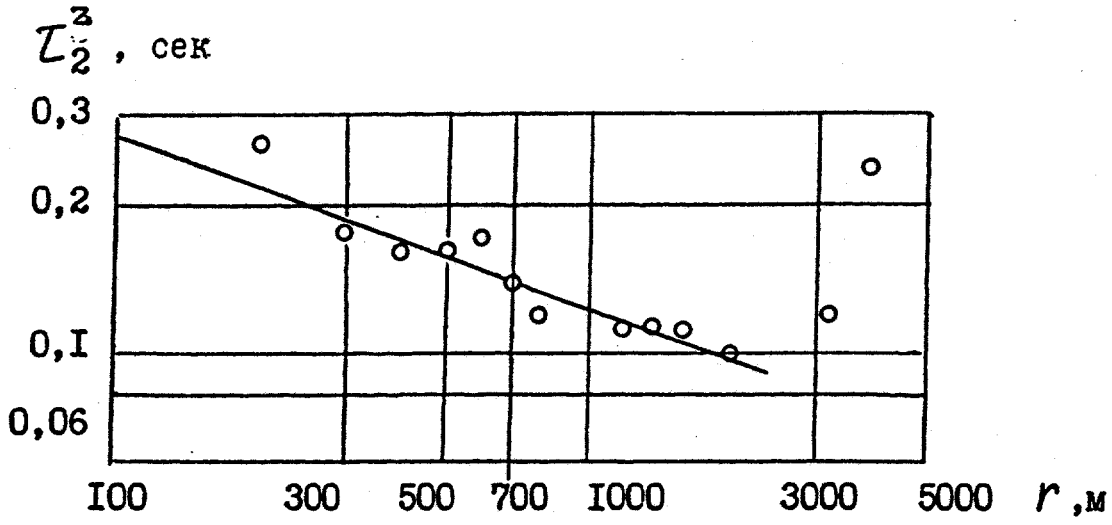

Figure III.4 Rise time in P_1P_o wave as a function of distance.

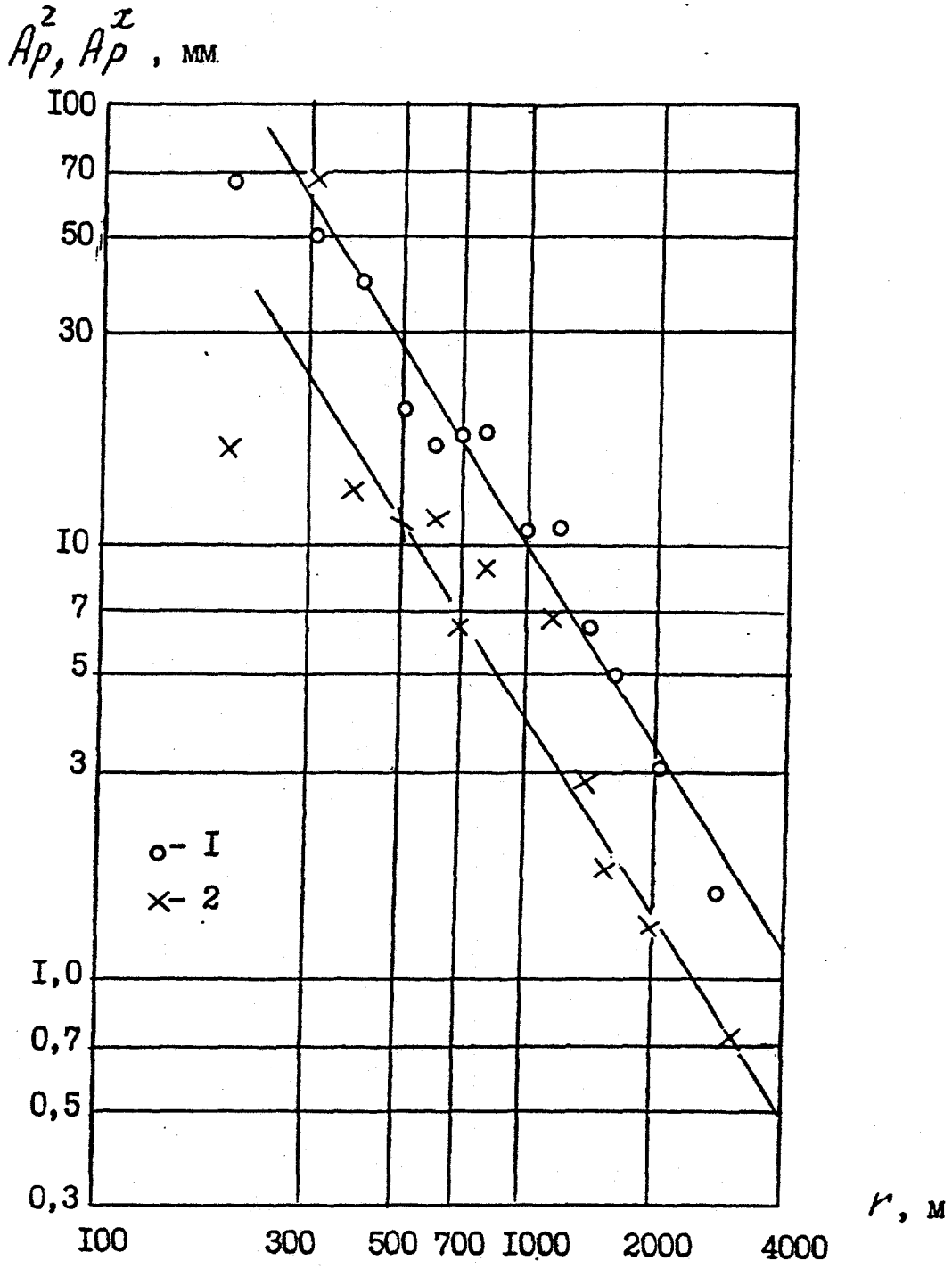

Figure III.5 Peak displacement, P_1P_0, in P_1P_0-wave as a function of distance . 1-A_P^z phase; 2-A_P^x phase.

that:

a) both components attenuate with distance similar in the limits of accuracy;

b) vertical component is 2-2.5 times larger than horizontal;

c) at the distances from 200 to 300 m vertical displacement is of 50 to 70 mm;

d) vertical displacement amplitude attenuation with distance can described by experimental relationship:

$$A^{Z}_{P_1P_0} = 3\ 10^{5}\ r^{-1.5}\ \text{mm}.$$

Figure III.6 presents peak particle velocity as a function of distance as measured by VIB sensors at the two profiles: short and long. As clear from the Figure, it is impossible to interpolate measured velocity values by one empirical relation. The short profile's measurements, where data scattering is lower, can be described by approximate relation:

$$U^{Z}_{P_1P_0} = 4.5\ 10^{8}\ r^{-1.5}\ \text{cm/sec}.$$

Exponent -1.5 is consistent with that of displacement measured by different sensors. It is worth noting, that at the distance of 100 m particle velocity is of about 600 cm/sec. N-wave produces similar displacement at closer distances. The nature of N-wave is not clear yet. Horizontal displacement in N_1 and N_2 phases of this wave as a function of distance is shown in Figure III.7. Measurements of N_1 phase in the range from 200 to 1000 m are interpoleted by relationship

$$A^{X}_{N_1} = 10^{8}\ r^{-1.7}\ \text{mm}.$$

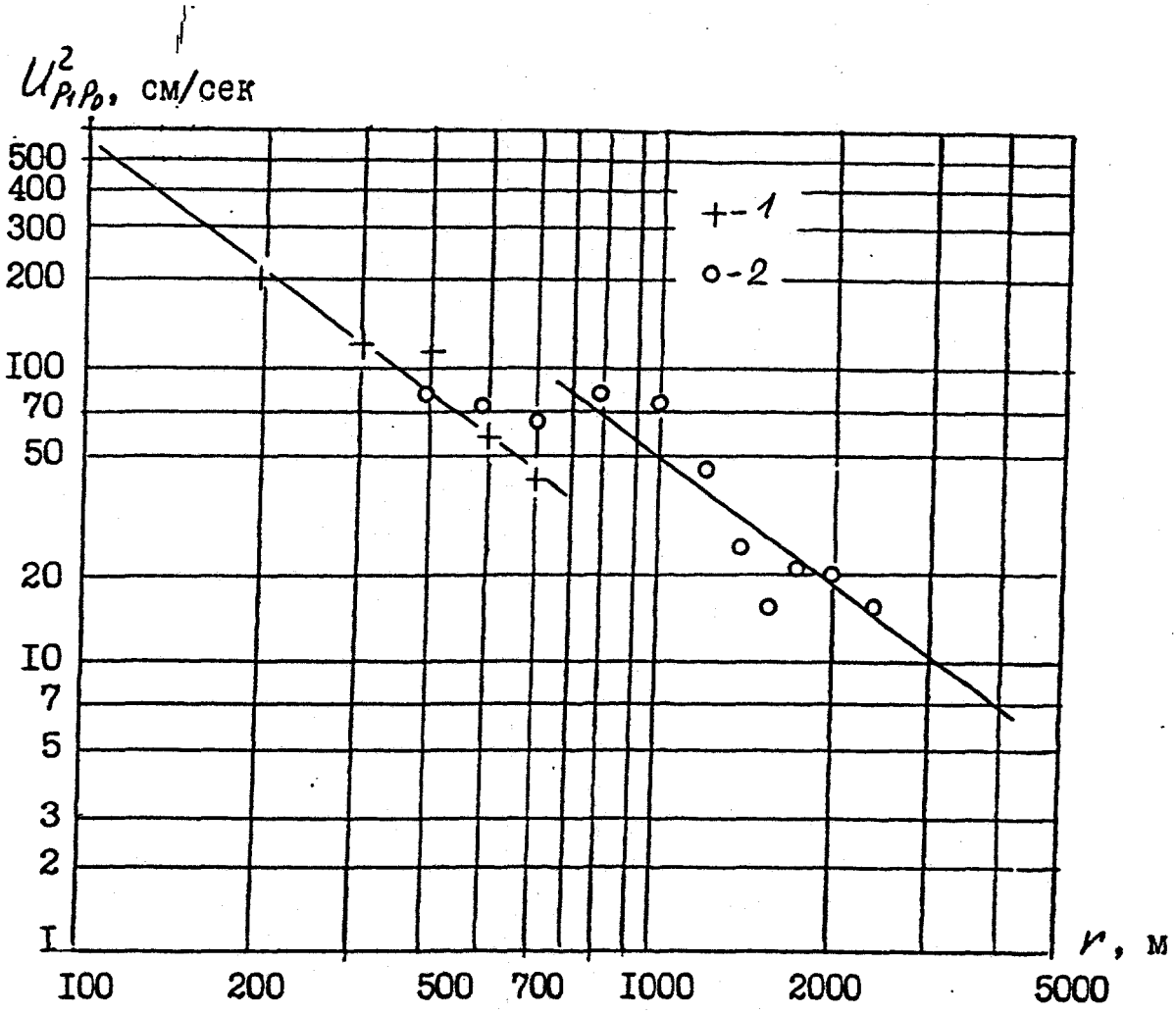

Figure III.6 Peak vertical particle velocity $U^2_{P_1P_0}$, VS. distance.

1-short profile, 2-main profile.

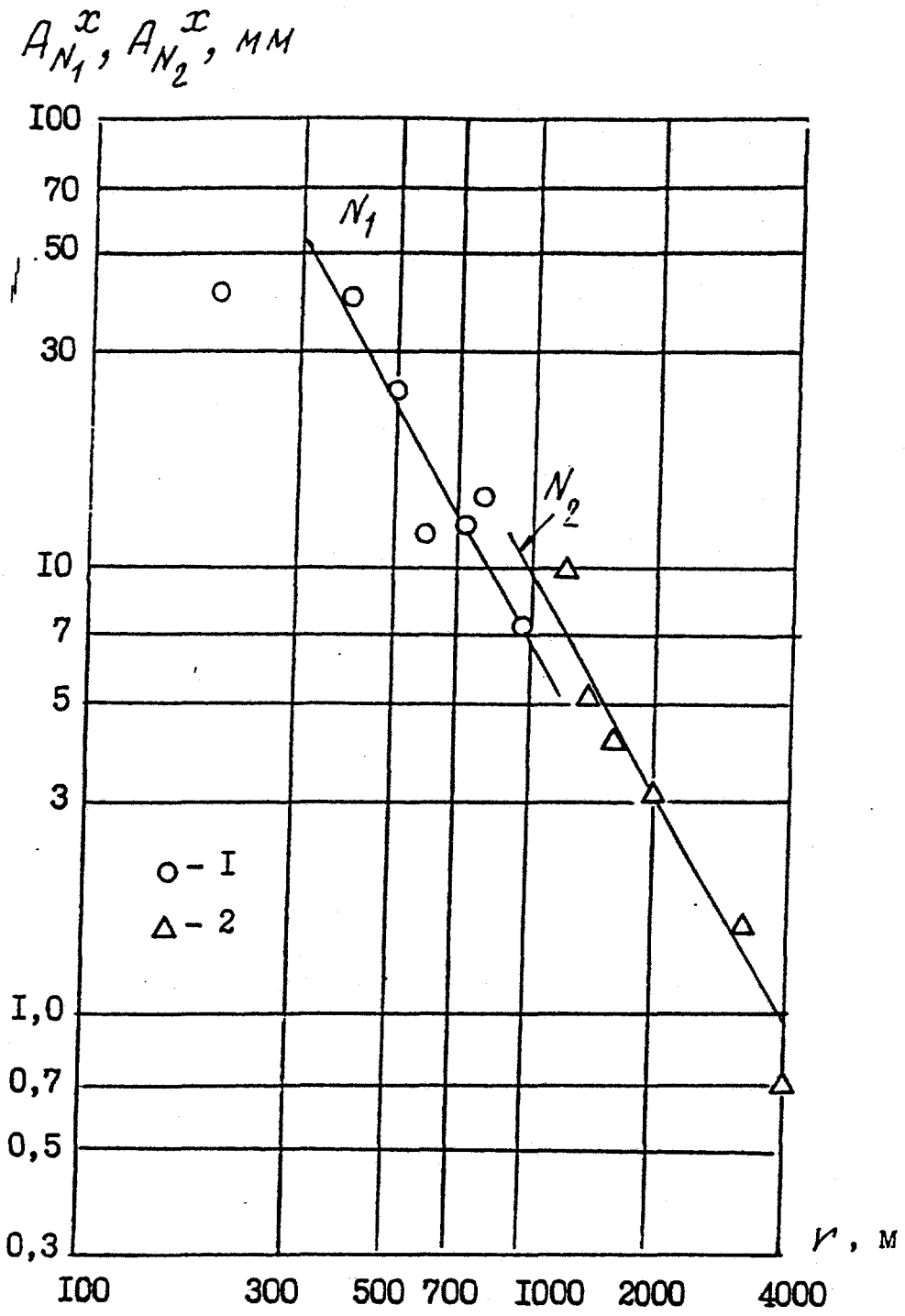

Figure III.7 Peak horizontal displacement, A^z_R, in N, and N2, $A^x_{N_1}$, and A_{N_2}, VS. distance.

High-frequency N_2 phase measurements in the range from 1200 to 4000 m are interpolated by relationship

$$A^X_{N_2} = 1.6\ 10^8\ r^{-1.7}\ mm.$$

Figure III.8 displays displacement amplitude/distance relationships for several phases mentioned above as a group of surface waves of Rayleigh's type. Amplitudes of different phases and curves are marked by different symbols. R_1 and R_2 phases are traced to distance of 800 to 1000 m. Amplitude curves interpolate the data by relations:

$$A^Z_{R_1} = 40\ 10^8\ r^{-2}\ mm$$

and

$$A^Z_{R_2} = 10^5\ r^{-1.4}\ mm.$$

The amplitude of R_2 phase at the distance of 300 m reaches 50 mm. Beginning from phase R_3 the pattern abruptly changes. Energy transmission to later phases is observed. Phases appeare at different epicentral distances (R_3 at 400 m, R_4 at 700 m, R_5 at 1200 m, etc.). Amplitude/distance curves have peaks, i.e. increase from the beginning, reach maximum value and then decrease with index number (17 mm for R_3, 6.5 mm for R_4, 3.8 mm for R_5, etc.). Ordinates of straight line BB decrease with distance as

$$A_R = 2.4\ 10^4\ r^{-1.1}\ mm.$$

It is known from literature, that surface wave dispersion is related to velocity structure. Vice versa, from geological section and velocity distribution it is possible to estimate

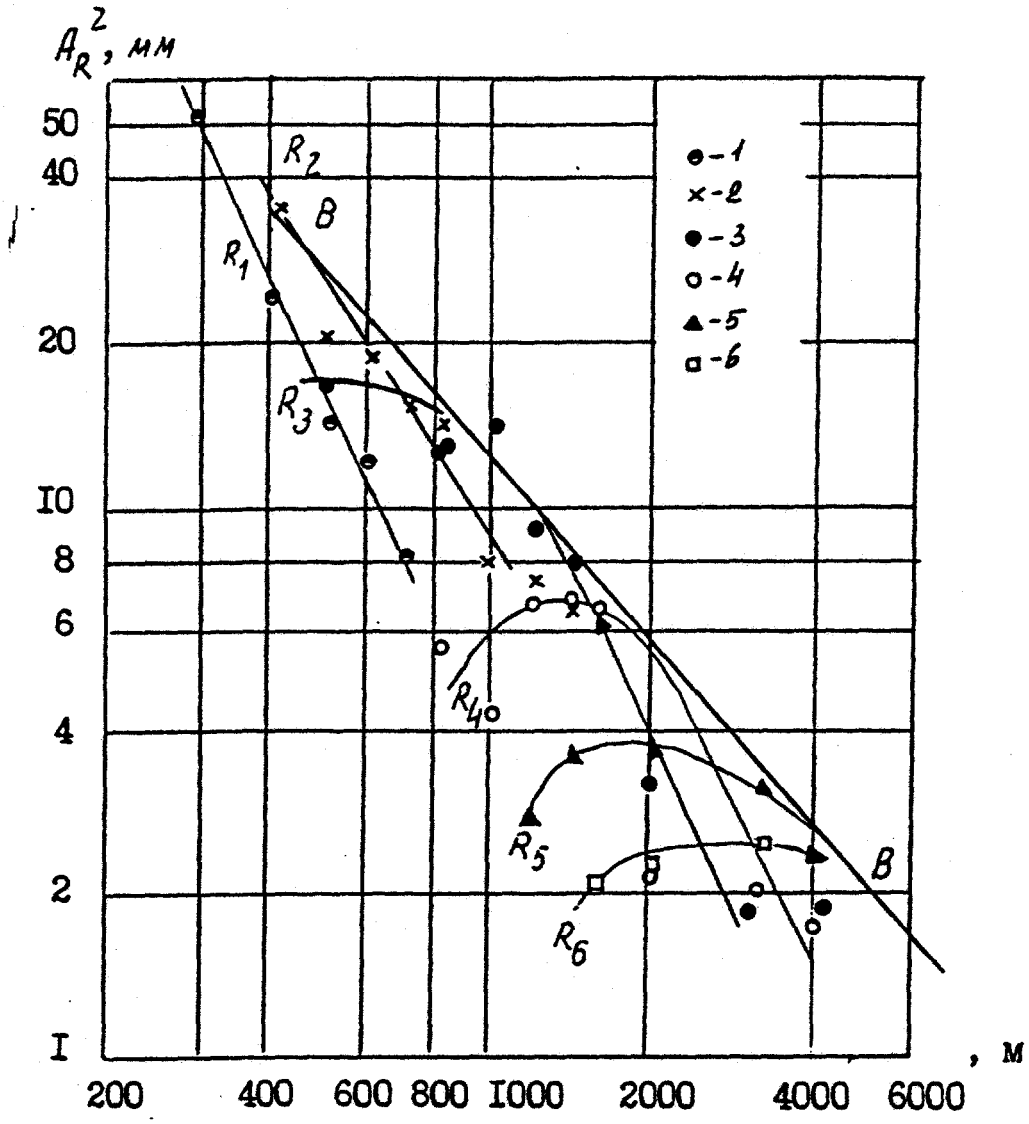

Figure III.8 Vertical displacement in different phases of R-wave VS. distance.

1-phase R_1; 2-phase R_2; 3-phase R_3; 4-phase R_4; 5-phase R_5; 6-phase R_6.

maximum and minimum phase and group velocities. For example, for a layer above halfspace, phase velocity of short surface waves approches Rayleigh wave velocity in the upper layer and phase velocity of long-period surface waves - to the Reyleigh wave velocity in halfspace. In the latter case, the upper layer does not play any role in signal propogation. Short- and long-wave length concept is related to wavelenght λ and layer thickness ratio. If $\lambda/H<1$, the wave can be considered as short: if $\lambda/H>10$ thewave is long.

Consider the results of the measurements at the sites N2, 3 and 4. Table III.2 presents geological section and velocity distribution of the sites.

Table III.2 Geological section and velocity structure of test sites N2, 3 and 4.

N layer	Soil type	Layer thickness H,m	Compressional wave velocity, m/sec
1	Loamy soil	6-10	500
2	Blue clay	400	1800-2000
3	Sandstone (assumption)	unknown	3000

Consider two schems of surface wave generation:

1) loamy soil - layer; blue clay - halfspace;

2) blue clay - layer; "sandstone" - halfspace.

Table III.3 contains periods, phase velocities and wavelengths as well as λ/H ratio for both schems.

Table III.3 Wavelength / thickness ratios.

Charge weight C, kg	Period T, sec	Phase velocity m/sec	Wavelength m	λ/H_1	λ/H_2
100	0.17	330	55	9	0.14
1000	0.27	370	100	17	0.25
10000	0.35-0.5	400-800	150-400	25-67	0.4-1.0
1000000	1.0	800-1100	700-1200	117-200	1.7-3.0

As clear from Table III.2 surface waves from all the charges are "long" for loamy soil layer. Thus, this layer does not influence the surface wave. One can assume that surface wave is formed in the blue clay layer with a thickness of 400 m laying on the sandstone layer. Compressional wave velocity in the latter, from the data of the main explosion is estimated as 3000 m/sec.

If to assume that $V_R = 0.92V_S$ (V_S-shear wave velocity) and $V_S = 0.5V_P$ then in sandstone $V_R = 1400$ m/sec which is maximum possible phase velocity of dispersing surface wave. Maximum phase velocity obtained during the 1000 tons explosion was of 1100 m/sec that is lower than predicted. Thus, second scheme of the surface wave generation seems more suitable. But following phenomena is unclear. If to apply an assumption of compressional, shear and surface waves velocities ratios to blue clay then minimum observed phase velocity $V_R = 330$ m/sec

predicts Vs of 360 m/sec. In this case V_s/V_P is in the range from 0.18 to 0.2 but not of 0.5 to 0.6 as usually. This velocity ratio seems unlikely for soil under consideration, since only plastic soil with nigh water content show such a ratio.

It is possible to suppose that some pecularities can be explained by low epicentral distances where surface waves are not wholly formed and equipment had low sensitivity which did not allow to detect surface wave with lower phase velocity.

III.2 Tuwya-Muyun explosions

Underground chemical explosions' testing were conducted in the drainage mine of the former ore deposite Tuwya-Muyun (Osh Region, Kyrhgyzstan). The mine is an underground horizontal, almost straight tunnel with total length of 2.5 km.

TNT charge of 190 tons was placed in the special mined chamber at the distance of 2280 m from the mine mouth. The charge was centered at the depth of 177 m, 7 meters from the axis of the mine. Absolute elevation was of 1084 m (see Figure III.9).

The second charge with the total weight of 660 tons was placed in the mine chamber situated at the distance of 2190 m from the mine mouth. The charge was centered at the depth of 203 m, 70 meters from the axis of the drianage mine. Absolute elevation of the charge was of 1035 m.

The region of the experiment represents mountainous country with maximum elavation difference of 400 m. The mine mouth absolute elevation was of 1070 m.

From hydrogeological survey, the mine Tuwya-Muyun crosses massive hard limestone of light-grey color.

There is strong karstification in the massif. The largest karst water-filled cavity with total volume of several thousands cubic meters is situated at the distance of 1350 m from the mine mouth. It is supposed that this cavity is connected by cracks to different karst cavities situated above the mine.

The limestone massif is crossed by a set of parallel cracks

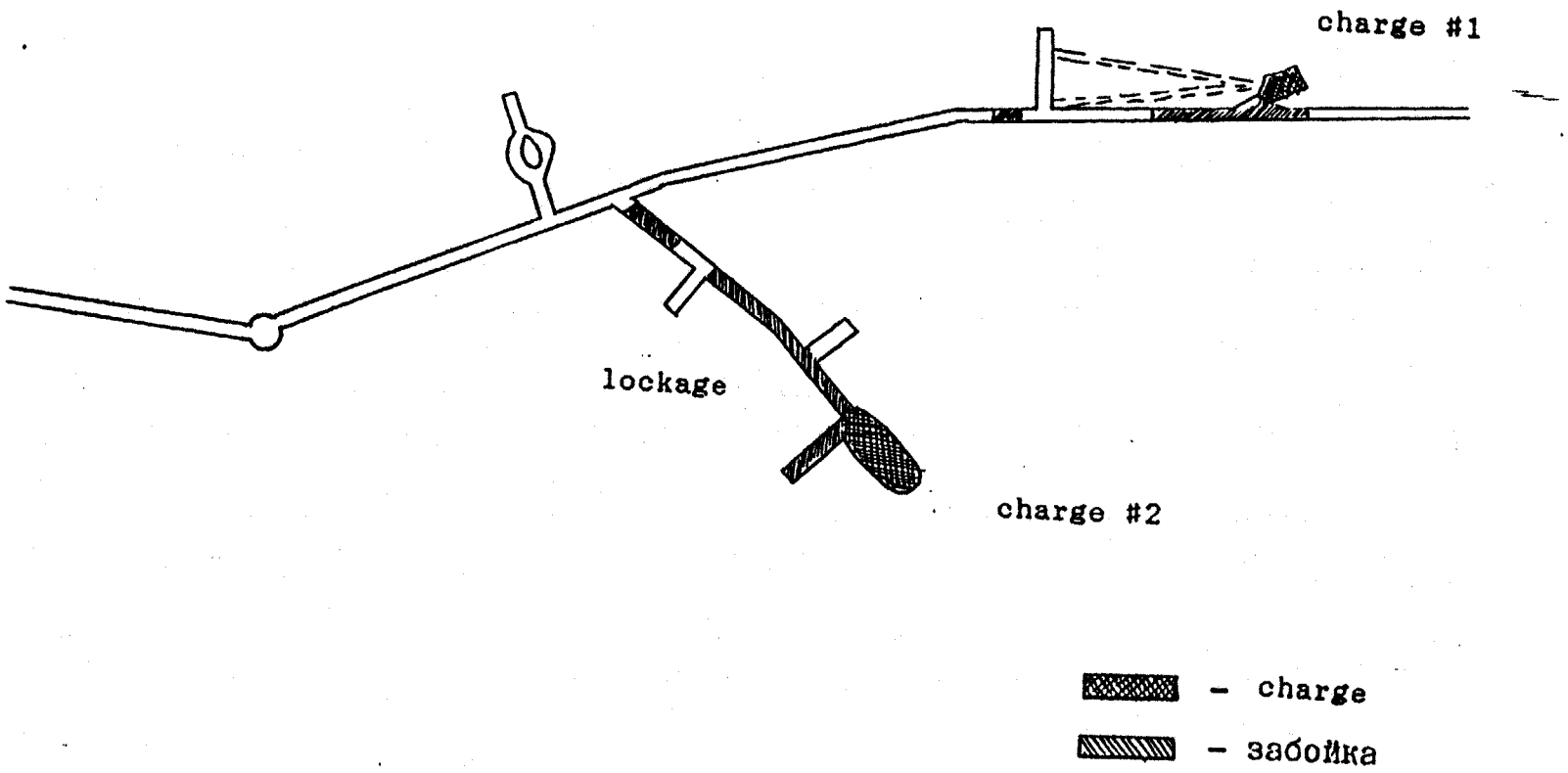

Figure III.9 Charges positions in the mine.

of 60^{o}-70^{o} dip. There are discontinuities along the cracks. The largest discontinuities were observed at the distances of 120 m, 150 m, 750 m, 1925 m and 2000 m from the mine mouth.

The first explosion was detonated through 4 detonating wire DSH-V which were placed in the wooden cover and metallic tube of 100 mm diameter. The tube was used from the charge to 70 m in the mine. Outer ends of the detonating wires was initiated by 4 instant electrodetonators ED-8-56 with nichrom bridge. The detonators were fired from doubled line layed in the mine from the control automatics.

The electrodetonators were connected to the sapping line only when preliminary work and safety precautions were finished 2 1/2 hours before the explosion.

The charge was blocked up in two stages. At first stage the end of the mine was blocked up during the mine chamber excavation. Then after the charge packing, detonators establishment and DSH laying, the second stage was fulfilled.

The blockage was formed from two parts of 20 m and 5 m respectively with the distance of 35 m between them. Blocking was fulfilled from crashed rock excavated from the chambers N1, N2 and the first drift. The blockage near the charge and tubes partially contained sacks of soft soil. Near the mine a log wall was constructed which covered the main part of the mine cross-section and protected the wires and equipment.

The chamber for the second charge of 660 tons was prepared at the end of the second right drift of 70 m length located 2165

in from the mine mouth (see Figure III.9). The chamber sizes are following: length - 22 m, mean width - 7.3 m and mean height - 6 m. The total chamber volume was of 930 m^3.

660 tons of explosive were placed in the chamber including 75 tons of trotyl in bars packed in standard wooden boxes and 585 tons of trotyl in sacks. Mean density of the charge was of 0.71 t/m^3.

The charge detonation was initiated by two primers. The primers were installed in the charge at the height of 2.5 m from the chamber bottom., 8 and 11.5 m from the closest to wallof the mine chamber respectively. Each primer was formed from 15 kg of detonite and 2 kg of grained trotyl. Two detonating wires DSH-V were layed from the mine to each primer in wooden cover and metallic tube. Four electrodetonators ED-8-56 with nichrom bridge fired the detonating wires.

The blockage had two parts: 40 m from the charge and 10 m from the end of the first part was the second block of 10 m length. Crashed rocks and sacks filled by rocks were used to block up the drift.

A. Observation procedure in local zone

Observation procedure in the local zone of powerful underground explosions is based of the results and experience of similar experiments with low-yield chemical explosions. Scaling law was used to predict seismic wave parameters and to choose proper procedure of record and equipment characteristic.

From scaling law, two explosions of total yield q_1 and q_2 respectively conducted in similar conditions (geometrical similarity of shapes and positions of the charges relative to main interfaces and inhomogenities) produce equal particle velocities in stress wave at the distances R_1 and R_2 if they are governed by following relationship:

$$\frac{R_1}{\sqrt[3]{q_1}} = \frac{R_2}{\sqrt[3]{q_2}}.$$

Temporal characteristics of the signals at the distances R_1 and R_2 ("reduced distances") are also governed by the same law:

$$\frac{T_1}{\sqrt[3]{q_1}} = \frac{T_2}{\sqrt[3]{q_2}}$$

which controls relationships between all other parameters. For example, maximum or reached at a given time displacement meets following relationship:

$$\frac{W_1}{\sqrt[3]{q_1}} = \frac{W_2}{\sqrt[3]{q_2}}$$

and maximum accelerations

$$\frac{\ddot{W}_1}{\sqrt[3]{q_1}} = \frac{\ddot{W}_2}{\sqrt[3]{q_2}}.$$

It is convenient to use charge radius R_{oc} instead of charge weight q or energy E. For trotyl charge of normal density and specific energy of E = 1000 kcal/kg, charge radius is $R_{oc} = 0.053\sqrt[3]{q}$ where q-is the weight in kg, R_{oc} is the radius in meters.

For explosives with different specific energy, ε, following

relationship is used:

$$R_{oc} = 0.053 \sqrt[3]{\frac{\varepsilon}{1000}}\, q \ .$$

When using R_{oc}, relative distances and temporal characteristics are proportional to the charge radius.

Temporal characteristics of seismic signals increase with increasing charge yield. This feature provides an opportunity to use equipment with standard channels responses (not high frequency) that simplifies the recording procedure and by using in many cases standard oscilloscopes.

The actual experiment layout allowed to observe seismic wave generation and development processes beginning from the charge chamber wall to a distance of 400 to 500 times R_{oc}. Observational points were placed in the mine as well as at the surface of the mountain.

Moreover, the explosive chambers were so accessible that an experiment on temperature measurements in the nearby zone of the chambers were conducted. Also, some special observations of the underground mine were carried out during the explosions.

Some optical observations were fullfiled by AKS-2 cameras. Motion of the epicentral zone of the mountanious massif during initial period of the second explosion was filmed by the special long focus cameras and photo-registers.

B. Observation's results

The first explosion of 190 tons was detonated at

12:00:0.025 (Moscow time) on 31 December, 1959.

The researchers who have been at the control point and evacuation region (300 and 600 m respectively from the mine mouth and 2.5 km from shot point) have feeled substantional initial shock and following ground motion of several seconds duration. Tracks and cars in the evacuation region have also been moved.

Weak shock wave with following increasing whistle due to air ejected from the mine were observed in 6-8 seconds after the shot. The air ejection from the mine was also obserwed by dust cloud propagated near ground surface with a shape of horizontal torch to a distance of 100 m from the mine mouth. The air ejection was observed during about 10 seconds. After that, back motion possibly began from the mine mouth to shot point.

The small dust cloud of several meters height was observed above the mine mouth during this period of time. The cloud was drifted and dissipated by wind.

Sharp distinct sound similar to generated by distant surface explosion was observed in 26 minutes. Black (several hundreds meters height) cloud arised above the mine.

The second explosion did not generate air ejection or sound from the mine. The mine mouth survey in 30-35 minutes after the first explosion showed that air flow in the mine was normal with a little increase of air velocity: water output from the mine did not change.

Followed surface survey around the epicentral zone have

shown that gaseous products' of detonation ejection occured near the mine and several drifts connected to the mine, upper horizons and tunnel. Gaseous products' of detonation trace moved by wind was observed to a distance of 2 to 3 km.

Gaseous products of detonation coming from the mine were observed during several days.

Concret constructions around the mine mouth were destroyed and thrown to a distance of 20 to 30 m as well as automatic cables, tubes and bars from the mine.

Rocky embankments (from 50 to 100 m from the epicenter), fundament's fragments (150 to 300 m from the epicenter) and walls constructed from saman bricks (350 to 400 m from the epicenter) were not damaged at all. Constructions situated in the populated areas Kopurbashi (2.5 km) and collective farm Chapaeva (2.0 km) have not been damaged too. Avalanches in the epicentral zone and r. Aravan canyon were not observed.

The results of the mine detailed survey conducted in 6 days after th shot were as followes:

The first part of the locking of 20 m lenght has conserved to a distance of 14 to 15 m from the chamber. Gaseous products of detonation were not ejected through this lock. The first 5 to 6 m, however, were totally destroyed. A hole, apparently preexisting karst cavity, with a size of $1.5_{\times}1.5$ m in section was found near the conserved part of the first lock under the mine. Gaseous products of detonations should be ejected through this hole. This ejection was so powerful that iron rails were

lifted by 1 m and the second lock was totally destroyed.

All the attachements established in the mine. tubes and drifts and behind the equipment room were destroyed and thrown around.

Rock used in constructing the second lock and soil were ejected from karst cavities closed by bar's walls were thrown around as an even layer to a distance of 300 m from the chamber.

The railway installed in the mine has been destroyed to a distance of 100 m from the second lock and lifted by 0.5 to 0.8 m above the mine bottom. Ejected rocks occured above the railway.

The highest embankment of bars, soil, ventilator parts, water and air tubes was situated near the bar's wall adjacent to the mine. It was of 1.5 m height.

The mine portion at the distance of 1500 m from the chamber, the mine and tube as well as initial parts of side drifts were covered by a layer of soil dust mixed with huge amouth of ashes (pure carbon created during trotyl explosion since trotyl has a negative oxigen balance). This layer thickness on the walls of the mine was of 1 cm from the point of gas ejection to the equipment room with decreasing thickness beyond.

Laboratory dust investigations conducted in a laboratory of a local coal mine have shown that the ashes are not explosive.

Reinforcements and karst cavities were not destroyed beyond the equipment room. The equipment room itself was not damaged but covered by ashes.

Side drifts bisides left one situated at a distance of 44 m from the shot center also were not damaged.

In the left drift, the wall closer to the shot was destroyed to a distance of 0.5 to 0.7 m. There was no observed volume increase in karst cavities strengthened by bars which were damaged by explosion.

The results of the detailed survey of the mine in the epicentral zone allow to make some conclusions on the explosion development and in particular to find out the cause of the second explosion in 26 minutes after the first one. During the explosion in the mine chamber as a result of cavity creation gaseous products of detonation ejection occured. At first, gaseous products of detonation have been ejected through the karst cavity beneath the first lock. Then the end part of the first lock had been destroyed and gas filled the room between the first and socond locks. Gage installed in the wooden box opened in the space between the locks showed that pressure began to increase gradually straight after the explosion. Pressure of 0.8 kg/cm^2 was measured in 1 second after the explosion. Gage installed near the equipment room measured relatively slow and long (~25 sec) pressure increase to a value of 0.3 kg/cm^2. These data allow to assume that the second lock 5 m long was destroyed more or less gradually and air in the mine behind the second lock was moved relatively slow by gaseous products of detonation.

At the same time, air and gaseous products of detonation

were slowly moved through the mine and this process was filmed by the camera installed near the epicenter.

Gas ejection from the mine was observed in 8 seconds after the explosion and from the drift situated near the mine approximately in 15 seconds after the explosion.

During ten seconds after the explosion (when filming was conducted) the velocity of gas ejection from the mine was low and the smoke cloud height was of 40 to 50 m. This cloud was moved by wind.

From a film recorder by another camera it is possible to conclude that in 20 seconds after the explosion gas ejection from one of the horizontal drifts of the upper horizons.

Presumably, this period of gas motion inside the mine was not related to severe damages.

Normal venting of air inside the mine, drifts and other parts of the system was established when pressure decreased to the atmospheric level. This caused the mixing of pure air moving through the mine and gaseous products of detonation from the chamber.

Gaseous mixture created by this process should contain oxigen, CO and some amount of water (from karst cavities) as well as hard particls of carbon. The mixture exploded in 26 minutes after first explosion. The second explosion destroyed concrete constructions around the mine mouth and reinforcing bars in the mine.

The explosion of 660 tons was conducted on 3/03/1960 in

12:00:0.4 (Moscow time).

All the participants of the experiment feeled strong shock and following ground vibrations to a distance of about 2.5 km at the elevated plane as well as in the valley of the r.Aravan.

Two seconds after the explosion a narrow vertical jet of black gas was ejected from the mouth of the main mine. In 1 second after that, intensive ejection of gaseous products of detonation began from the mouth of two another vertical drifts situated near the main mine and from the central tunnel. Gas jet averaged velocity during first seond was of 50 m/sec. In several seconds a flame was observed near the base of the gas jets. Flame was observed diring 5 minutes with a continious gas ejection. Intensive uplift of gas jets during 40-60 second caused those of upper edge uplift at a height of 1.5 to 2.0 km.

Gas jets throwed from the mine stones of several kilogramms weight and parts of wooden bars flyed to a distance of 500 m. In several seconds after gas ejection air motion from the main has begun followed by black jet of gaseous products of detonation ejection from the mouth of the drainage mine. The latter jet was burned in 30 seconds and huge jet of fire of 100 m length was created. The gas jet as well as flying rocks, soil, rails, tubes and bars destroyed the roof of diesel and compression station situated behind the mine mouth at a distance of 40 m and wooden kitchen at a distance of 100 m was damaged. The ejecta from stones, tubes, rails and bars formed a narrow band of 400 m length along the mine axis.

Total gas ejection from vertical drifts near the main mine and drainage mine occured during 6 to 8 minutes. Burning of gas where it ejected into the atmosphere was not followed by explosions.

Five minutes after the explosion, sharp ejection of gas and flame initition were observed from a drift situated near the explosion epicenter but did not connect to the chamber.

The second explosion was observed in 19 minutes near the mine. Small cloud generated by this explosion lifted to a height of several hundreds meters. Detailed survey of the epicentral zone gave following results:

The rocky massif in the epicentral zone was not damaged; several small cracks opened to a width of 2 to 3 mm in the zone of 12 m radius in the upper rocky layer; some stones separated from the massif by preexisting cracks were moved with edge damage to a radius of 300 m.

Larger cracks were created in unconsolidated soil and at the surface of tunnels. Partial damage of the tunnels and the upper surface subsidence of 5 to 10 cm were observed to a distance of 150 to 200 m. Vertical slopes in loamy soil were damaged to 350 m. Drifts in loamy soil of circle and square shape with a depth of 15 and 5 m and situated at a distance of 250 and 350 m respectively were not datаged.

The upper part of the main mine and near by vertical drifts' mouths were totally damaged.

Whole vertical cracks in 25 cm thick longitudinal concrete

walls of a pool (5x20x2 m) situated at a distance of 250 m from the epicenter in loamy soil were created as a result of the explosion. A pool of 4x10x2 m size with concrete walls of 20 cm thickness at a distance of 200 m was damaged more severely: two walls falled down. Continuous concrete and iron-concrete fundaments and basement's parts of walls consructed from stones at a distance of 180 to 200 in were not damaged.

Residuals of the walls of one story houses constructed from bricks with clay grout situated at a distance of 250 m were additionally damaged.

The drainage mine after the explosion is characterized by following data.

In the range from 100 m from the mine mouth to the embankment at 980 m wooden bars, railways, cables and tubes for compressed air were totally destroyed and mainly thrownfrom the mine; lower part of the mine is filled by liquid mud (fine soil mixed with ground water) of 40 to 60 cm thickness near the embankment.

Wooden reinforcement near the embankment at a distance of 980 m is totaly destroyed with materials, bars and part of soil (clay) ejected by gas jet to a large distance from the embankment. But the volume increase of an arch in hard rock was not observed, however. Part of soft soil stayed at the bottom near the embankment formed a hill of 1.2 m height. This hill caused water level increase behind the embankment to a distance of about 500 m.

Beginning from 1500 m the mine is dry. Railways and tubes were damaged but without substantional shift. The equipment room was severely damaged due to destroying of the front wooden wall by gas jet. The wall parts moved by gas jet to back wall destroyed oscilloscopes and automatic equipment. High temperature gas jet caused destroying of films in cassettes. There are no traces of burning inside the mine and equipment room.

Wooden bars reinforcingthe wall near the embankment at a distance of 980 m and near the place of the mine junction of left and right drifts and the tube are totally destroyed, but no wall collapse was observed.

The inital stage of rock destruction such as longitudinal cracks was observed between the mine and the tube.

From the data of preliminary observations conducted by special group, the charge lock in right drift was totally ejected. Right drift to a distance of 30 to 40 m from the mine was not damaged. Near the end of the drift's large wall and roof collapse were observed. Natural mine ventig was not disturbed.

C. Stress wave parameters in local zone of underground explosions

Stress wave parameters during the two experiments were measured by equipment installed in the mines at a depth of 200 to 250 m beneath the surface. It allowed to assume that measured

values did not differ strongly from those of should be measured in homogeneous space.

It is convenient to begin with the simpliest characteristic of stress wave. Velocity of propagation is the first claimant.

1. Compressional wave velocity estimation

Compressional wave velocity estimation was carried out with higer accuracy during the first experiment. Some sensors installed near the oharge chamber were not operational during the second experiment.

Velocity measurements were conducted by the IMSG, ISF, INS, VIB-A and VBP sensors. All these sensors have made it possible to measure compressional wave arrival times but with different accuracy.

The ISF and IMSG sensors were used to estimate propagation velocity at the closest distances during the first experiment.

The ISF sensors established at the distances of 3.0, 10.0, 20.0, 30.0 and 44 m were connected to the MPO-2 oscilloscope with filming rate of 5 m/sec. (The sensor marking the zero time of the shot was established at the charge/soil interface, i.e. at a radius of the charge). The signals from the IMSG sensors at the distances of 10, 20, 30 and 40 m were recorded by the MPO-2 oscilloscope. Absolute accuracy of the first arrival measurements for 5 m/sec rate is of 0.2 mm on the film, i.e. 0.04 msec.

The next sources of estimation errors are unaccurate

measurements of the distance between the sensors and oscilloscope filming rate. The sensor to sensor distances were measured with an accuracy of 0.3 to 0.5 m, i.e. relative accuracy is of 3 to 5 percents.

The filming rate was determined from time marks of 500 Hz standard oscillator. The accuracy of this time mark is garanteed to be as low as 2%. Thus, total maximum error of arrival time determination is of 10%.

Arrival time estimation error decreases with distance since absolute time and base line lenth also increase. Actual accuracy of propagation velocity estimation is higher than accuracy of arrival time estimation since velocity is determined by several sensor measurements. Table III.4 presents the data on the first arrivals as measured durind experiment N1.

Table III.4

Range, m	Sensor type	Arrival time, msec	Notes
10	ISF	1.15	Time is given from true
20.0	ISF	2.75	zero of the shot
19.5	IMSG	2.8	
29	IMSG	4.3	
39	IMSG	4.4	
43.5	IMSG	6.35	
43.5	IMSG	7.25	
43.5	ISF	6.75	
43.5	INS	6.75	
100	VIB	13.0	
240	VIB	35.0	
460	VIB	75.0	
800	VIB	128.0	
1550	VIB	247.0	

Free field measurements show that longitudinal wave velocity is of 6200 m/sec. Averaged in the range from 0 to 1350 m the velocity also is of 6200 m/sec.

Thus, longitudinal wave velocity is constant in the range of measurements and is equal to 6200 m/sec.

2. Characteristic features of velocity/time function on stress wave

The VIB-A and IMSG sensors' records were used to analyse the character of particle velocity/time function since those are velocity transducers. The VBP-3 sensors were also used. The latter were installed at the three distances to compare to the records of the VBP-3 at the free surface.

Figure III.10 displays some copies of typical VIB-A and IMSG sensor's records of particle velocity as measured in stress wave. Characteristic feature of the records is a finite rise time, i.e. finite time for particle velocity to reache its maximum. The values t_r for different ranges as recorded during the experiments N1 and N2 are presented in Table III.5.

Table III.5 Rise times as measured in the experiment N1

R, m	19.5	29	42.5	43	44	44	100	100	100	240	460	800	1550
t_c,msec	1.5	1.6	1.9	1.9	1.6	1.4	3.4	1.7	5.1	6.9	7.3	8.0	10
Sensor type	IMSG	-"-	-"-	-"-	-"-	VIB	-"-	-"-	-"-	-"-	-"-	-"-	-"-

As clear from the Table, peak particle velocity is reached by different times. Rise time value increases relatively fast to a distance of 70 R_c. At larger distances, rise time grows not so fast. It is worth noting, however, that t_r in the nearby zone needs to be analysed more carefully since the records in this zone are not usuall. For example, the IMSG sensors installed at distances of 10 and 20 m in the experiment N1 gave the records with bends when particle velocity rises to peak value.

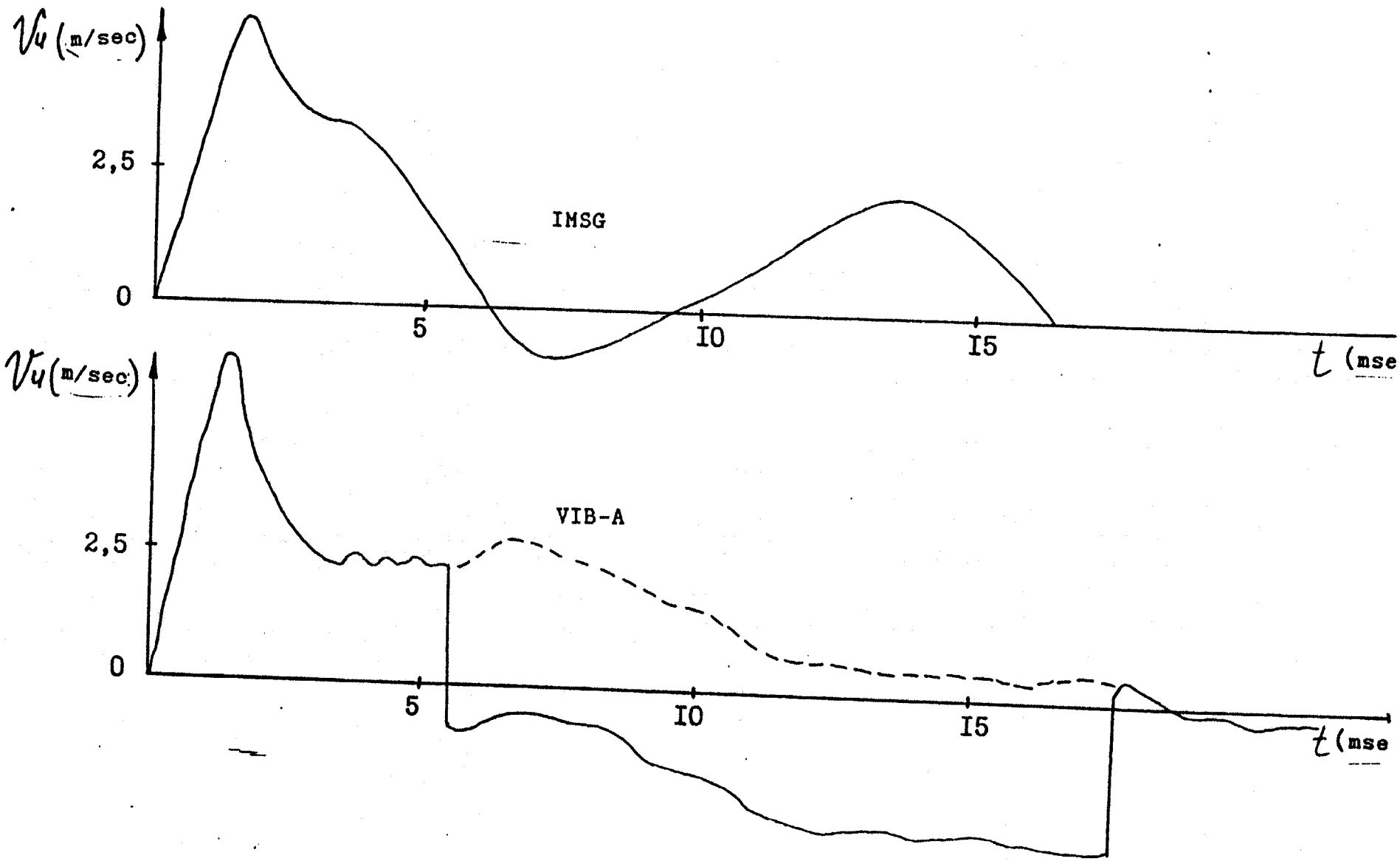

Figure III.10 Particle velocity records at a distance of 44m in the mine.

A reason for signal disturbance may be misorientation of the sensors to the center of the explosion (designed accuracy of orientation is of several degrees). Also it is possible that wavefield around the nonspherical charge is not spherical in the nearby zone.

Since wave front is not vertical as in shock wave and rise time increases with distance propagation velocity of peak particle velocity is lower than that of the first arrival. Averaged value of peak particle velocity propagation velocity is close to measured from first arrivals and is of 6000 m/sec.

If measuring propagation velocity of peak particle velocity in the closest zone from 0 to 15 R_c (experiment N1), the velocity is of 5800 to 5900 m/sec. It was mentioned above that stress wave velocity in hard rocks is constant in the range of measurements with adopted accuracy. At larger distances, where stress wave can be considered as elastic wave this velocity is the same. Thus, one can conclude that near the charge (from 3 R_c) stress wave velocity is practically as large as sound speed. Propagation velocity of peak particle velocity is a little lower (less than 8%).

The positive phase durations, t_{pos}, as a function of distance are presented in Table III.6 for the experiments N1 and N2. The VIB-A sensors data were used to calculate t_{pos} values.

The IMSG sensors records were not used to estimate t_{pos} since container deformations cause the tail part of the records disturbance.

Table III.6 The results of compressional wave parameters measurements in the mine, experiment N1

NN	Distance from the charge center, m	Sensor type	Sensor orientation	Peak particle velocity, cm/sec	Peak displacement, mm	Rise time t_r, msec	Positive phase duration, msec
1	10	IMSG	R	2200	-	1.3	-
2	19.5	IMSG	R	2700	-	1.5	-
3	29	IMSG	R	800	-	1.6	-
4	42.5	IMSG	R	540	-	1.9	-
5	43	IMSG	R	480	26	1.9	-
6	44	IMSG	R	500	26	1.6	-
7	44	VIB-A	R	600	30	1.4	17
8	100	IMSG	R	130	-	-	-
9	110	IMSG	R	90	-	-	-
10	100	VIB-A	R	210	20	3.4	18
11	-"-	-"-	R	200	21	1.7	18
12	-"-	-"-	R	120	13	5.1	27
13	100	VBP-3	R	-	1.7	-	23
14	240	VIB-A	R	55	5.0	6.9	26
15	240	VIB-A	Z	17	1.2	5.7	14
16	240	VBP-3	R	-	3.4	-	23
17	460	VIB-A	Z	6.2	0.6	4.4	19
18	460	VIB-A	R	12	2.1	7.3	29
19	460	VIB-A	Z	9.6	0.7	4.4	16
20	460	VIB-A	R	13	2.0	7.3	31
21	460	VIB-A	H	1.9	-	-	-
22	460	VBP-3	R	-	1.1	-	23
23	800	VIB-A	H	0.54	-	-	-
24	800	VIB-A	R	4.6	0.8	8	34
25	1550	VIB-A	Z	0.4	-	-	-
26	1550	VIB-A	R	1.0	-	10	29

As clear from the measurements, positive phase duration in compressional wave increases with increasing distance. But scattering of the data does not allow to construct reliable quantitative relationship in the full range of measurements.

It is worth noting that vertical components of motion appear at some records of sensors installed in the mine. Vertical component is not larger than horizontal, but it should be considered in velocity or displacement principal vector amplitude's calculations.

3. Peak particle velocity measurements results.

The data measured by the IMSG, VIB-A and INS sensors were used to estimate particle velocity in compressional wave. The IMSG and VIB-A sensors are velocity transducers themselves. The INS sensor gives averaged velocity in some displacement range. The measurements of all the sensor are in good consistance.

Tables III.6 and III.7 present the results of the records processing.

Figure III.11 displays the peak particle velocity , V_{max}, as a function of distance. As clear from the Figure, this function can be represented by one term power low in the range of measurements from 3 R_c to 500 R_c

$$V_{max} = 3.6 \left[\frac{q^{1/3}}{R}\right]^{1.75}$$

where V_{max} is the peak particle velocity in m/sec, R is the source/receiver distance in m, q is the charge weight in kg.

Table III.7 The results of compressional wave parameters measurements in the mine, experiment N2

NN	Distance from the charge center, m	Sensor type	Sensor place and position	Sensor orientation	Peak particle velocity, cm/sec	Peak displacement, mm	Rise time t_r, msec	Positive phase duration, msec
1	43	IMSG	dug-hole =1 m	R	1080	-	2	-
2	64	IMSG	-"- =2 m	R	790	-	3	-
3	64	IMSG	-"- =2 m	R	940	-	3.8	-
4	64	IMSG	-"- =1 m	R	765	-	3.4	-
5	64	IMSG	-"- =1 m	R	700	-	4.1	-
6	64	IMSG	-"- =1 m	R	620	-	3.4	-
7	72	IMSG	-"- =2 m	R	453	-	8	-
8	92	IMSG	-"- =1 m	R	317	-	10	-
9	145	VIB-A	mine,niche	R	148	21	10.3	28.5
10	369	VIB-A	-"-	Z	7.90	1.1	6.75	24
11	369	VIB-A	-"-	R	22.5	4.0	9.0	33
12	369	VIB-A	-"-	R	26.5	4.6	8.24	33
13	369	VIB-A	-"-	Z	13.2	1.7	4.5	25.5
14	369	VIB-A	-"-	H	5.6	0.8	9.0	27
15	710	VIB-A	-"-	R	8.6	1.8	12.0	37.5
16	710	VIB-A	-"-	Z	2.6	0.7	-	-
17	1460	VIB-A	-"-	R	2.3	0.6	20.2	42
18	1460	VIB-A	-"-	Z	1.0	0.2	19.5	33

x/ the charge in the experiment N2 had clongated, non-spherical shape. The distance from a sensor to the center of the charge was estimated as the distance from the closest charge surface plus 4 m=R_c.

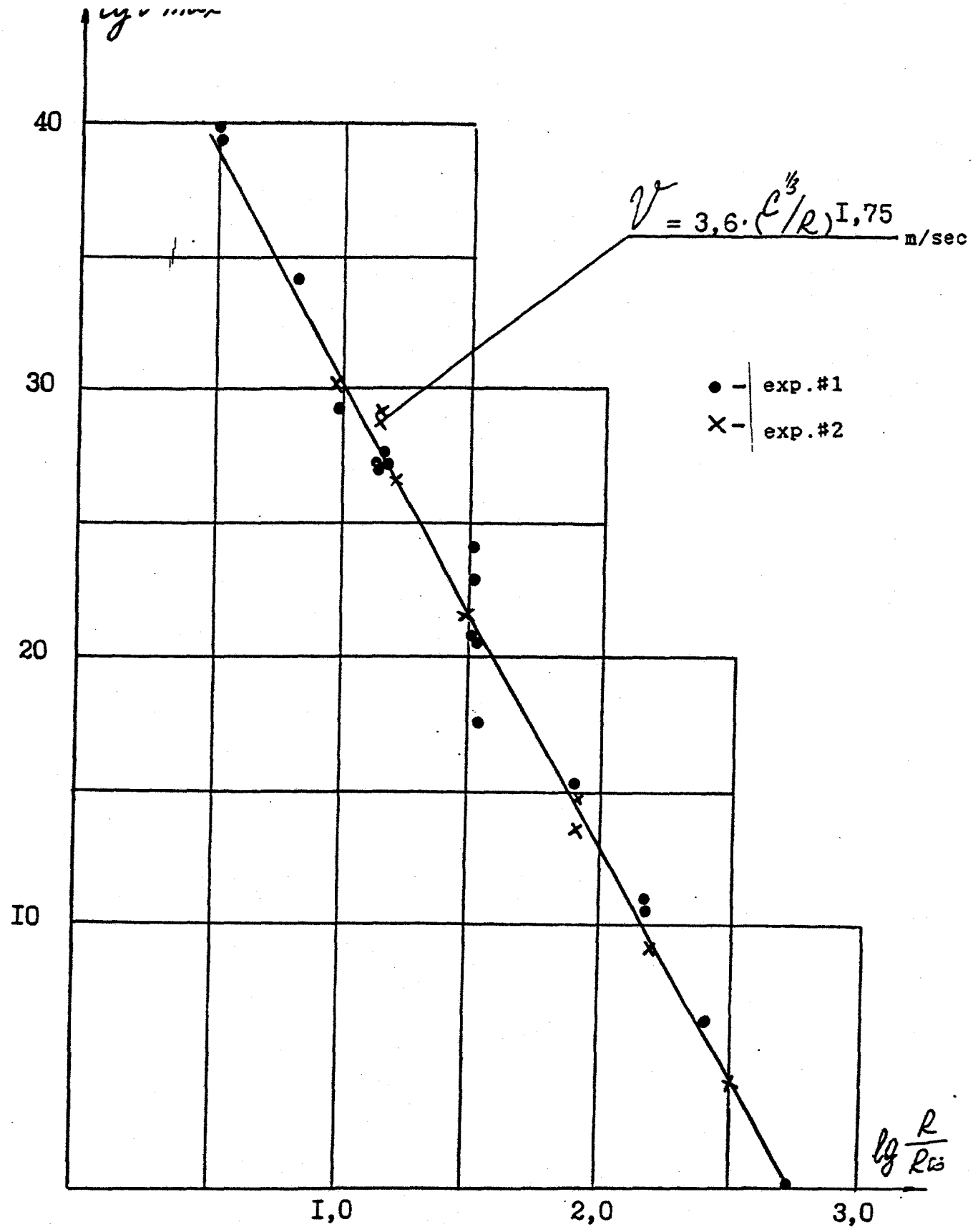

Figure III.11 Peak particle velocity in the mine VS. distance (log-log scale).

D. Free surface measurements

Wave-field at the free surface of the massif, as followed from the records survey, is much more complicated than in the mine. Even the records at the closest distances showed more sophisticated pattern of displacement than at similar distances in the mine. The records complexity increases with distance.

Wave-field complexity as observed at the free surface during underground explosion is caused by wave reflection from the free surface which generates two extra wave: reflected longitudinal and shear waves. Moreover, new type of wave arises near the surface - the surface wave. So, from a simple signal in compressional wave as it observed in the mine, wave train of seismic oscillations arises and propagates at large distances. The influence of geological structure and relief on the generation of complex wave-field is a sophisticated problem which has not been solved yet.

Qualitatively, the wave pattern observed at the surface during the underground explosion is similar to different experiments in different geological conditions. Two principal waves were distinguished from the records and discussed below. They are compressional wave, P, K, (longitudinal wave) which causes the dome-like uplift of the surface in the epicentral zone, and surface wave, R.

Compressional wave's averaged velocity as estimated from

time/distance curve is of 5260 m/sec. This value is lower than measured in the mine. It is to be noted, however, that compressional wave velocity varies and differs at various sections. The complex relief and the upper layers inhomogeniety are the reasons for that.

Peak displacement and particle velicity amplitudes are related to the initial part of the records, i.e. compressional wave, to the distance of 100 R_c to 150 R_c. Surface wave amplitude is higher at larger distances.

The principal measured parameters in compressional wave are following:

a) particle velocity measured straight from the VIB's records as well as from the slopes of the VBP's records;

b) rise times to peak velocity, t_r, (from VIB's records);

c) peak displacement, W_{max}, straight from the VBP's records or by integrating of particle velocite (VIB-A records);

d) displacement rise time, τ, (from VBP's records) or positive phase duration, t_{pos}, (VIB records). The values actually are the same.

Tables III.8 and III.9 present the parameters. Finite rise time to peak velocity is a characteristic feature of the records at free surface as well as in the mine. Tables III.8 and III.9 show that rise time increases fast with increasing distance to ~299 R_c, and then increases a little.

As mentioned above, three components of motion were usually measured. So, the principal vector of particle velocity in

Table III.8 Compressional wave parameters at free surface.

Experiment N1

Epicentral distance $R_э$, m	Distance from the charge center $R_г$, m	Sensor orientation	Rise time $t_г$, msec	Positive phase duration $t_{пол}$, msec	Peak particle velocity V_{max}, cm/sec	Peak displacement V_{max}, mm	Peak acceleration W, g	Notes
0	177	vert.	10	100	108	38	10.8	VIB-A
0	177	rad.	2.5	-	9.8	-	3.9	-"-
0	177	azimuth.	-	-	25	-	-	-"-
0	177	vert.	-	80	-	25	-	VBP-3
200	270	vert.	10.0	46	63.2	14.2	12.4	VIB-A
200	270	rad.	5.2	63	70.0	21.0	20.6	-"-
200	270	azimuth.	3.4	44	28.0	3.0	8.2	-"-
205	300	vert.	16.6	62	39.0	14.5	2.4	-"-
205	300	rad.	13.5	52	64.2	11.5	4.8	-"-
205	300	azimuth.	-	28	11.0	1.3	-	-"-
205	300	rad.	-	40	0	2.3	-	VBP-3
205	300	azimuth.	-	30	0	2.0	-	-"-
370	412	vert.	26.0	53	26.4	7.9	1.0	VIB-A
370	412	rad.	-"-	-"-	>52	-	-	-"-
370	412	azimuth.	31.0	57.7	7.5	2.0	0.24	-"-
370	412	vert.	26.6	51.0	19.5	4.9	0.73	-"-
370	412	rad.	-	-	>30	-	-	-"-
370	412	azimuth.	47.7	75.0	16.8	5.4	0.37	-"-
430	467	vert.	15.0	34.0	12.3	2.16	0.8	-"-
430	467	rad.	16.5	44.0	11.6	2.8	0.7	-"-
430	467	azimuth.	10.5	15.8	7.5	0.6	0.7	-"-
430	467	vert.	-	30.0	-	1.6	-	VBP-3
750	765	vert.	18.7	40.0	5.45	1.33	0.30	VIB-A
750	765	rad.	19.0	75.0	4.55	1.74	0.24	-"-
750	765	azimuth.	19.0	38.0	3.58	0.63	0.20	-"-
750	765	vert.	-	35.0	-	0.63	-	VEGIK
750	765	rad.	-	45.0	-	0.52	-	-"-
750	765	azimuth.	-	50.0	-	0.63	-	-"-
1450	1450	vert.	32.0	50.0	1.18	0.25	0.05	VIB-A
1450	1450	rad.	44.0	70.0	1.71	0.62	0.04	-"-
1450	1450	azimuth.	30.0	46.0	0.97	0.19	0.08	-"-
1450	1450	vert.	-	40.0	-	0.23	-	VEGIK
1450	1450	rad.	-	40.0	-	0.25	-	-"-
1450	1450	azimuth.	-	55.0	-	0.10	-	-"-

Table III.9 Compressional wave parameters at free surface Experiment N2

Epicentral distance $R_э$, m	Distance from the charge center $R_г$, m	Sensor orientation	Rise time $t_г$, msec	Positive phase duration t_{pos}, msec	Peak particle velocity V_{max}, cm/sec	Peak displacement V_{max}, mm	Sensor	Notes
1	2	3	4	5	6	7	8	9
0	204	vert.	24	115	98.4	74	VIB-A	
0	-"-	-"-	15	120	256.0	173	-"-	
0	-"-	-"-	-	92	100	56	VBP-3	
105	205	rad.	18	90	177.0	67	VIB-A	
105	-"-	azimuth.	10	105	52.5	19.2	-"-	
105	-"-	vert.	-	100	100	51.0	VBP-3	
105	-"-	rad.	-	120	-	71.0	-"-	
165	248	vert.	30	115	152.0	48.6	VIB-A	
165	-"-	rad.	12	120	71.5	33.1	-"-	
165	-"-	azimuth.	30	115	53.0	17.1	-"-	
165	-"-	vert.	-	60	120	38.0	VBP-3	
165	-"-	rad.	-	75	-	23.4	-"-	
125	246	vert.	17	112	167	65.0	VIB-A	
125	-"-	rad.	17	85	117	43.5	-"-	
125	-"-	azimuth.	19	60	24.5	10.0	-"-	
125	-"-	vert.	-	85	120	60.0	VBP-3	
125	-"-	rad.	-	100	-	52.0	-"-	
365	410	vert.	9	31	27.0	4.2	VIB-A	
365	-"-	rad.	15	42	19.4	5.8	-"-	
365	-"-	azimuth.	7	12	9.4	0.3	-"-	
365	-"-	vert.	-	32	21	4.2	VBP-3	
365	-"-	rad.	-	45	-	4.1	-"-	
345	392	vert.	26	55	29	7.8	-"-	Loamy soil, depth of 7 m
345	-"-	rad.	29	195	65	63.0	-"-	
345	-"-	azimuth.	27	59	21	6.0	-"-	Loamy soil, depth of 7 m
345	-"-	vert.	34	65	44	15.6	-"-	
345	-"-	rad.	52	143	37	29.0	-"-	---
345	-"-	azimuth.	45	72	36	12.5	-"-	
580	630	vert.	-	31	16.5	3.0	VBP-3	
580	-"-	rad.	-	100	-	5.0	-"-	
715	732	vert.	24	44	11.5	2.9	VIB-A	
715	-"-	rad.	19	63	7.0	2.2	-"-	
715	-"-	azimuth.	19	45	4.3	0.9	-"-	

1	2	3	4	5	6	7	8	9
715	-"-	vert.	-	33	5.5	1.5	VIB-3	
715	-"-	rad.	-	65	-	1.8	-"-	
715	-"-	azimuth.	-	35	-	0.6	VBP-3	
1070	1070	vert.	-	32	5.2	1.05	VEGIK	
1070	-"-	azimuth.	-	30	-	0.4	-"-	
1070	-"-	rad.	-	-	-	-	-	Clipped
1450	1450	vert.	20	53	4.6	1.0	VIB-A	
1450	-"-	rad.	20	71	3.5	1.4	-"-	
1450	-"-	azimuth.	18	48	1.6	0.3	-"-	
1450	-"-	vert.	20	27	1.6	0.32	VEGIK	
1700	-"-	vert.	-	22	1.0	0.13	-"-	
3000	1700	vert.	-	22	0.2	0.003	-"-	
2600	3000	vert.	12	27	0.64	0.11	VIB-U	
2600	2600	rad.	35	60	1.06	0.37	-"-	
2600	-"-	azimuth.	18	50	0.78	0.25	-"-	

compessional wave was analysed during the processing of the data obtained by the VIB-A sensors at the free surface.

Power law was adopted to describe peak amplitude of the principal vector of particle velocity as a fuction of the yield and distance:

$$V_{max} = 13.5 \left[\frac{q^{1/3}}{R}\right]^2, \text{ m/sec}$$

where q is the weight of the charge in kg, R is the distance in meters.

It is interesting to consider each component of particle velocity separately. Azimuthal or transversal component is usually two to three times lower than vertical and radial components. So it is eliminated from the following analysis.

Peak vertical velocity, V_{zmax}, dependence on distance occured to be the same as for the principal particle velocity, V_{max}, but with different coefficient:

$$V_{zmax} = 8.9 \left[\frac{q^{1/3}}{R}\right]^2, \text{ m/sec}$$

The VBP-3's records processing confirms the relationship obtained from the VIB-A's data on the attenuation, but coefficient is defferent:

$$V_{zmax} = 7 \left[\frac{q^{1/3}}{R}\right]^2, \text{ m/sec.}$$

Doubled peak particle velocity measured in the mine differs from the value of the principal vector amplitude measured at the free surface to a distance of 400 R_c. Then this difference almost disappears.

2. Surface wave

Surface wave, R, becomes noticable from a distance of 350 to 400 m in the two experiments. From 500 to 600 m the amplitude of surface wave prevails in the velocity and displacement records. Partical trajectory in surface wave is usually in vertical plane along the radius with counterclockwise motion (Figure III.12).

Surface wave nature of the oscalllations is confirmed by comparison of the records at the free surface and in the mine. Phase velocity measured from time/distance curve of the first maximum phase of vertical component is of V_R = 1840 m/sec. It is to be noted that arrival velocity of this wave may differ from phase velocity.

The measured kinematic parameters of surface wave are following : period, T, and amplitude, A. Vertical and horizontal amplitudes are approximately equal.

Table III.10 summirizes the measurements for the two experiments.

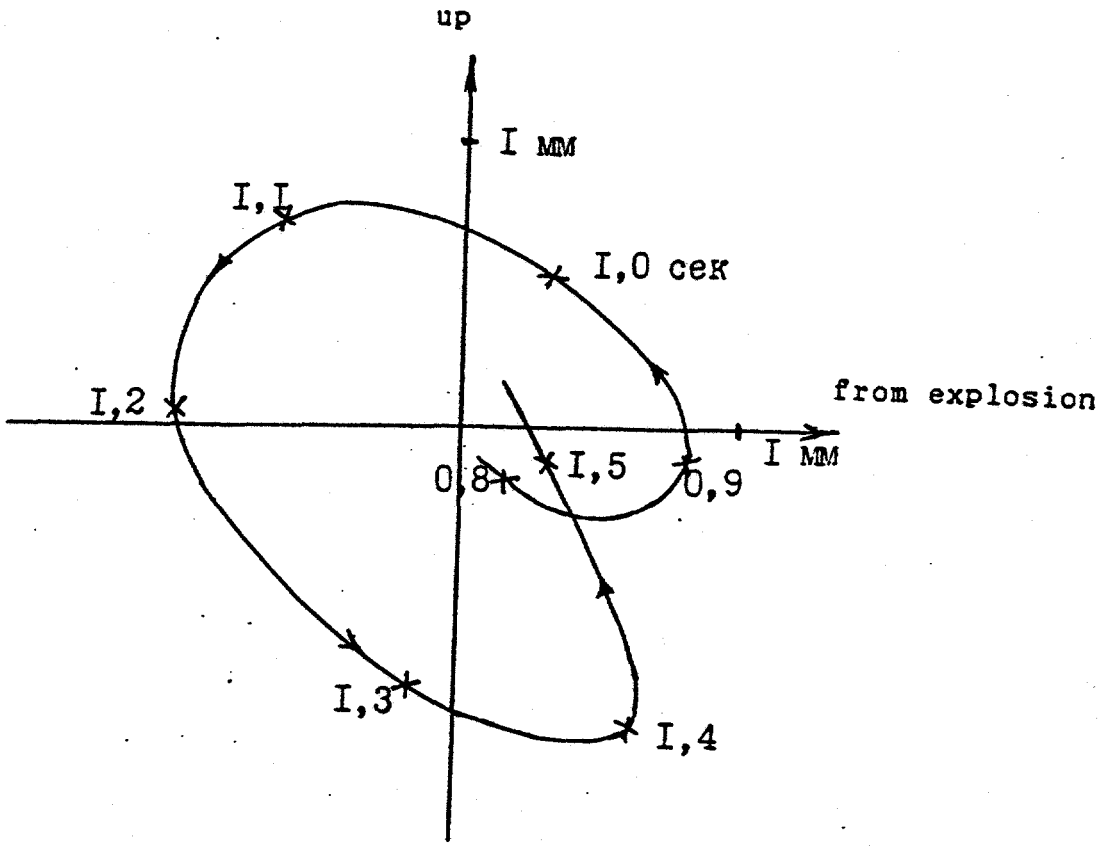

Figure III.12 Particle trajectory in surface wave at 1700m.

Table III.10

NN	Epicentral distance R_e, m	Peak vertical displacement W_z, mm	Period T, sec	Notes
Exp. N1	430	1.5	0.33	
	740	0.8	0.36	
	1450	0.42	0.37	
Exp. N2	365	4.7	0.55	
	580	2.8	0.57	
	715	2.7	0.55	
	1070	1.8	0.55	
	1450	1.0	0.57	
	1700	1.0	0.53	
	3000	0.3	-	

The parameters of this wave are considered depending on the epicentral distance.

From the data obtained in the experiments N1 and N2, the amplitude and period of surface wave may be represented by following relationships

$$\frac{w_z}{q^{1/3}} = 0.32 \left\{\frac{q^{1/3}}{R}\right\}^{1.15} ; \quad T = 0.06\, q^{1/3}$$

where w_z is the peak displacement in mm, q is the charge weight in kg, R is the epicentral distance in m, T is the period of oscillations in seconds, i.e. the parameters of surface wave are governed by geometrical scaling.

To analyse surface wave more carefully a longer profile of seismic observations is needed.

E. The results rock temperature measurements

Temperature measurements were conducted only during 190 tons explosion. To install temperature sensors a borehole N1 of 46 mm diameter and 29 m depth was drilled to the center of the chamber. The borehole mouth was at a distance of 44 mm from the center of the chamber. Thus, the borehole bottom was at a distance of 15 m from the center of the charge (5 R_c).

The borehole N1 was used to measure the initial temperature and to install three temperature sensors. It was supposed that the borehole would not be collapsed during the explosion and could be used to measure temperature in some points straight after the explosion. The borehole survey in 7 days after the experiment actually confirmed these assumptions: the borehole N1 was not damaged to a depth of 18.5 m. The space below this level was filled by crashed rock.

The sensor installed at the bottom of the borehole was not operational due to cables damage. There was not measured any temperature increase at the distances larger than 25.5 m from the charge center. That is why the borehole N2 was drilled and temperature measurements were conducted in this borehole The borehole N2 has also been drilled horizontally to the center of the chamber to a depth of 39 m. But after the extracting of drilling tubes, the borehole has collapsed from 33.6 to 39 m.

The borehole mouth/chamber center distance was of 44 m.

Two temperature sensor: N08 and N22 were used in turn tc measure temperature in the borehole N2 to a distance of 33.6 m. The sensor N08 has been intially installed at the bottom of the borehole (33.6 m). Stable temperature measurements were reached in 2 hours after the installation. Low thermal conductivity is a reason for that. The sensor was moved closer to the mouth after each measurement session. The distance of the shift was fixed and the sensor stayed in the position from 3 to 6 hours. Thus, temperature along the borehole was progressively measured by the one sensor N08.

The sensor was extracted from the borehole and calibrated after one measurement cicle. New cicle of measurements was also begun from the bottom. But this cicle was not finished since the sensor was catched at a depth of 31 m presumably due to wall collapse. Crashed rocks did not allow the sensor to be moved back. The sensor N22 was used in following measurements. It has been calibrated before usage. The measurements by the the sensor N22 was carried out in reverse sequence: from the mouth to the bottom and back. After the first cicle of measurements the sensor has been calibrated again. Two calibrations comparison has shown that the sensor worked stable.

The sensors were established in the borehole by specially designed tube system constructed from tube pieces of 15 m lenght and 15 mm diameter. The system has been dismounted then the sensor installed. Backward motion of the sensor was conducted by

wires connecting the sensor and recording equipment. In the cases when the sensor was moved from the mouth to the bottom the tube system was not dismounted but moved 3 or 4 meters off the sensor. This procedure was fullfiled to prevent temperature field disturbance by metallic tube.

The borehole N2 was of 39 m lenght. Sensor installation into the borehole N2 was fullfilled straight after evacuation of drill equipment from it. But the sensor could not be established at the bottom, however. Lower part of the borehole evidently was drilled in crashed rock.

The sensor N08 was established at maximum distance of 33.6 m from the borehole mouth, i.e. 10.4 m from the charge center. Then moved to maximum depth the sensor was stoped several times by wall bends, i.e. lower part of the borehole was uneven. For example, at first time when the sensor has been moved back the sensor was stoped at a depth of 33 m. When moved back the sensor was stoped at a depth of 32 m by such a bend. Fortunately, the sensor was uncatched by not strong impulse by wires.

Following motion was relatively even confirming flat walls of the borehole. The first stage of measurements was finished by the sensor extraction and calibration. Temperature was measured in ten points from 33 to 15 m. The sensor was installed at the depth of 33.6 m on the second stage of measurements, i.e. 0.6 m deeper than during the first stage. But the sensor was stoped at the depth of 31.2 m from the borehole mouth then moved back, however. Presumably a reason for that was the wall collapse

since it could not be moved again.

Almost all the measurements of temperature after 190 tons explosion were conducted in the borehole N2. Only the limited number of measurements from the borehole N1 are availbale which expands the results from the borehole N2. Temperature increase was observed to 8 to 9 radia of the charge. The closest to the charge point in the borehole N1 was at the distance of $9.2R_c$. Hence, is it natural that no temperature increase was not detected in that borehole.

Thus, temperature measurements were conducted only in one direction from the charge. So, the estimate of total thermal energy of the rock heated above 19°C in only approximate. It was assumed that the distribution of temperature around the charge is symmetric and thermal isolines are spherical. Total energy was estimated from the relationship:

$$Q = \int_{R_1}^{R_2} 4\pi r^2 \rho C \, \Delta T(r) dr$$

where Q is the thermal energy, ρ is the density, ΔT is temperature increase, C is the specific energy. It was adopted in the calculations that ρ = 2700 kg/m^2 and C = 0.2 cal/g °C. (Specific energy was not specially estimated of the rock used. The value of C was borrowed from a handbook for marble: granite has specific energy of 0.21 cal/g °C).

Total thermal energy estimation was conducted for separated parts where $T^o = f(R)$ function was approximated by straigh line. Table III.11 presents the values of thermal energy of each part

separately. Total energy in the range from 10 to 16 m from the charge center is of 4.28 10^{10} cal, as follows from the Table. The calculations above did not take into account thermal energy in the central region. The soil closer than 10 m to the center, however, was heated too, with temperature increasing contineously to the surface of the cavity at a depth of 39 m. Thus, one can assume that temperature increased evenly from 3.6 to 39 m (33.6 is the furthest observational point). It is hard, however, to determine the distribution of temperature in this region since a function $T^{o}(R)$ is not known and extrapolation is too complex. It is only possible to estimate minimum energy concetrated in a spectral layer between R = 5 m and R = 10 m if to consider constant temperature throughout the layer to be equal to the temperature at R = 10 m ($28^{o}C$). This temperature value gives thermal energy of 1.8 10^{10} cal. Total thermal energy in the rocks around the explosion in the zone of mine charge radius should be as large as 6.08 10^{10} cal. Total energy release of the trotyl charge of 190 tons with a density of 0.71 g/cm^{3} is of 190 10^{7} 800 10^{3} = 1.52 10^{11} cal.

Thus, approximately 40% of total energy release during the explosion transforms into thermal energy, i.e. heating of the rocks in nearby zone. It should be noted that this estimate is only approximate and actual energy transform could be higher or lower. Futher investigations are desirable in the nearby zone of the explosion during drilling of control dug-holes.

Table III.11

Inner sphere radius R_1, m	Outer sphere radius R_2, m	Thermal energy Q, cal
10	12	$11\ 10^9$
12	14	$8.9\ 10^9$
14	16	$8.1\ 10^9$
16	20	$10.2\ 10^9$
20	26	$4.6\ 10^9$
	Total:	$4.28\ 10^9$

The results of crashed rock zone study

The zone of crashed rocks was not investigated specially. The study was conducted when the borehole for temperature measurements was drilled. What is why the data on crashed zone are not systematic. The data considered below were obtained during the drilling of the two horizontal boreholes of 46 mm diameter.

1. Experiment N1

The boreholes N1 and N2 were used to obtain the data on the crashing of the rocks around the explosion.

The borehole N1 has been drilled from a dug-hole perpendicular to the mine. The borehole mouth was situated in 10 m from the mine and 44 m from the center of the charge cavity. A little slope was designed of the borehole: the mouth was of 1 m

above the mine floor and the bottom of 2 m above the floor. The distance from the center of the chamber to the bottom of the borehole was of 15 m. The borehole was drilled in light-grey fine-grained hard limestone crossed by sparce layers of calcite.

The borehole N1 was partially destroyed by the explosion: the borehole testing by special tool mounted of tube pieces has shown that the borehole collapsed at a distance of 27.5 m from the center of the charge. From the fact that a cable of 10 mm diameter covered by hard alloy was cut, the borehole was damaged by strong differential motion in the rocky massif. The portion of the borehole N2 from the mouth to collapsed zone was not disturbed as follows from the bbsence of any bends or cracks during testing.

The borehole N2 was drilled from the same dug-hole. The borehole mouth was at a distance of 1 m from the mine. The total borehole length was of 39 m.

Table III.12

Interval, m	Core output, %
00 - 3.00	75
3.00 - 4.60	85
4.60 - 7.30	87
7.30 - 13.60	19
13.8 - 19.40	20
19.4 - 26.40	2.9
26.4 - 31.40	16.0
31.40 - 39.0	2.8

Low core percentage can be partially explained by improper drilling regime: the borehole was drilled by tubes of different length from 1.6 to 3.0 m in the begining to 7 to 8 m in the end. Small size of the crown in the end caused extra crashing of the rock cores which were wipped out by water.

Sharp drop of the core percentage, as clear from the Table, started from 19 m and persisted to the end of the borehole. Some output increase between 26.4 and 31.4 m has not been explained and presumably is not of any significance. Explosion-induced rocks crashing is considered as a main reason of output drop.

Drilling liquid came back totally to the depth of 19m. A part of the liquid was lost after 19 m, and finally, water disappared at all in the end of the borehole. From 33 m to the end of the borehole drilling water became black. It is

consistent with the rocks crashig and gaseous products of detonation venting into cracks.

Then the borehole N2 has been finished, temperature sensor was installed into it. But due to the borehole collapse the sensor could not be moved below 33.6 m level. The borehole survey has shown that begining from 31 m the walls were damaged: some bends and falling out of small stones were feeled which closed the borehole section.

From the data considered above it is possible to estimate the cracked zone radius and the cavity size.

1. Actual radius of the zone of intensive cracking can be estimated from the results obtained in the boreholes N1 and N2. In the borehole N1 the radius of the zone is, evidently, the distance to the borehole collapse of 27.5 m or mine charge radius.

Core output percentage was used to estimate the radius of the zone of intensive damage of the rocky massif. Table III.12 contains necessary data. Sharp percentage drop occured at a distance of 19 m, i.e. the zone of intensive cracking is as large as 25 m (8.3 R_c). This value is consistent with that of obtained from the borehole N1.

Thus, the upper limit of the zone of intensive cracking of the rocky massif by underground chemical explosion of 190 tons is of 25 to 27 m or 8 to 9 charge radia. Temperature increase in the same zone confirms indirectly the size of the zone of intensive cracking.

2. Some constrains on the radius of explosion produced cavity can be obtained only from the data from the borehole N2. The lenght of the borehole was of 39 m with a distance from the mouth to the charge center of 44 m. The cavity surface has not been crossed by the borehole. Thus the cavity radius was not larger than 5 m or 1.7 R_c.

But considering nonspherical shape of the chamber, the size of the cavity is only approximate.

2. Experiment N2

Study of the crashed zone after the second explosion of 660 tons was not conducted. The mine has collapsed in several places and the chamber was not accessable. Only the data from the borehole N2 drilled before the explosion were available. The borehole N3 has been drilled to the center of the charge.

The borehole N3 has been drilled from the mine beginning from PK N210. The borehole mouth was at a height of 1.5 m from the mine floor and at a distance of 92 m from the charge center. The borehole lenght was of 70 m with core output of 23.65 m or 38%. Low core output can be explained by usage oflong tubes and calcite inclusions. From 0 to 18 m the borehole was drilled in dense fine-grained hard limestone with rare gneiss and calcite intrusions. Core output was from 47 to 97% in this range. From 18 to 26 m the borehole opened middle-grained white sugar-like hard limestone with sparce layers of calcite. From 26 to 56 m dark-grey dence limestone is crossed by sparce calcite layers.

Middle-grained white hard limestone was between 56 and 70 m. There were no sharp transformations from white to grey limestone. Grey limestone is the most competent rock followed by middle-grained white, and large-grained white limestone with large calcite inclusions is the weakest rock. In principle, the rocks around the explosion N2 differ from those of the first explosion. They are weaker due to high content of calcite inclusions and sugar-like limestone.

III.3 Medeo explosion

Medeo antiavalances dam has been created by two directed explosions.

The first explosion was conducted on 21 of October, 1966, 4:59:59.1 GTM. The charges of total weight of 5293 tons were detonated at the right side of r. Malaya Almaatinka. Figures III.13 and III.14 display the schemes of the charges positions. The charges were detonated with some time delay. The first row charges of 1689 tons total mass were fired in the beginning. As a result of these explosions an outcrop plane has been created. The second, main explosion of 3604 tons total mass was directed to this plane. The second explosion was fired in 3.56 sec after the first.

A dam of 61 m height has been created by this explosion (see Figure III.14). The base of the dam was of 500 m long with total dam volume of 1.5 10^6 m^3.

A. Seismic observations

1. Seismic observations were conducted in order to study seismic effect of the explosion and to estimate the size of seismic hazard zone as well as seismic intensity vs. distance relation. Macroseismic data were collected in the closest populated areas and Alma-Ata city after the explosion. Measured and observed data being considered together allow to reevaluate and correct existing theoretical predictions and to test their applicability to seismic effect of large-scale explosion

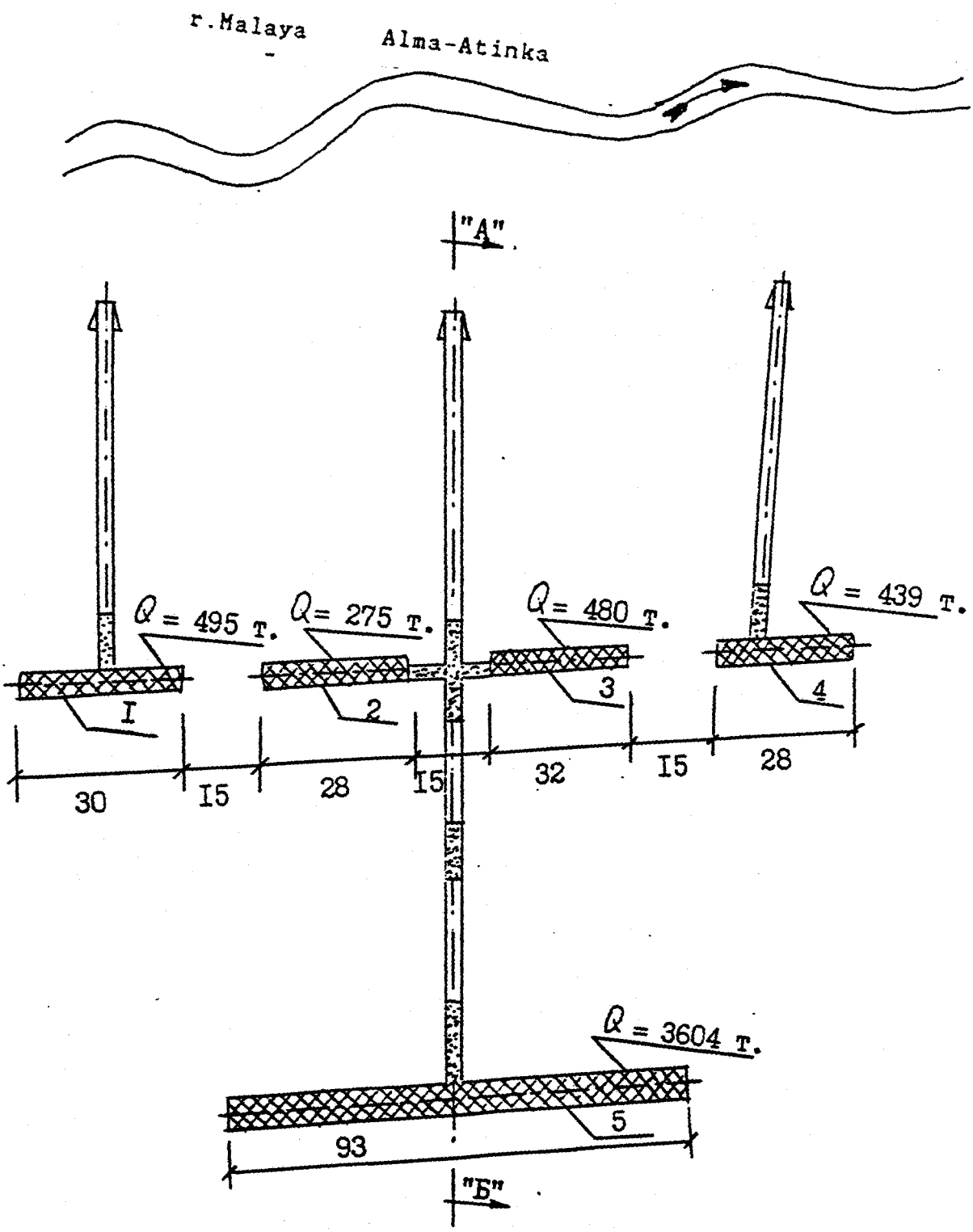

Figure III.13 Charges positions in the first explosion series 2: October.

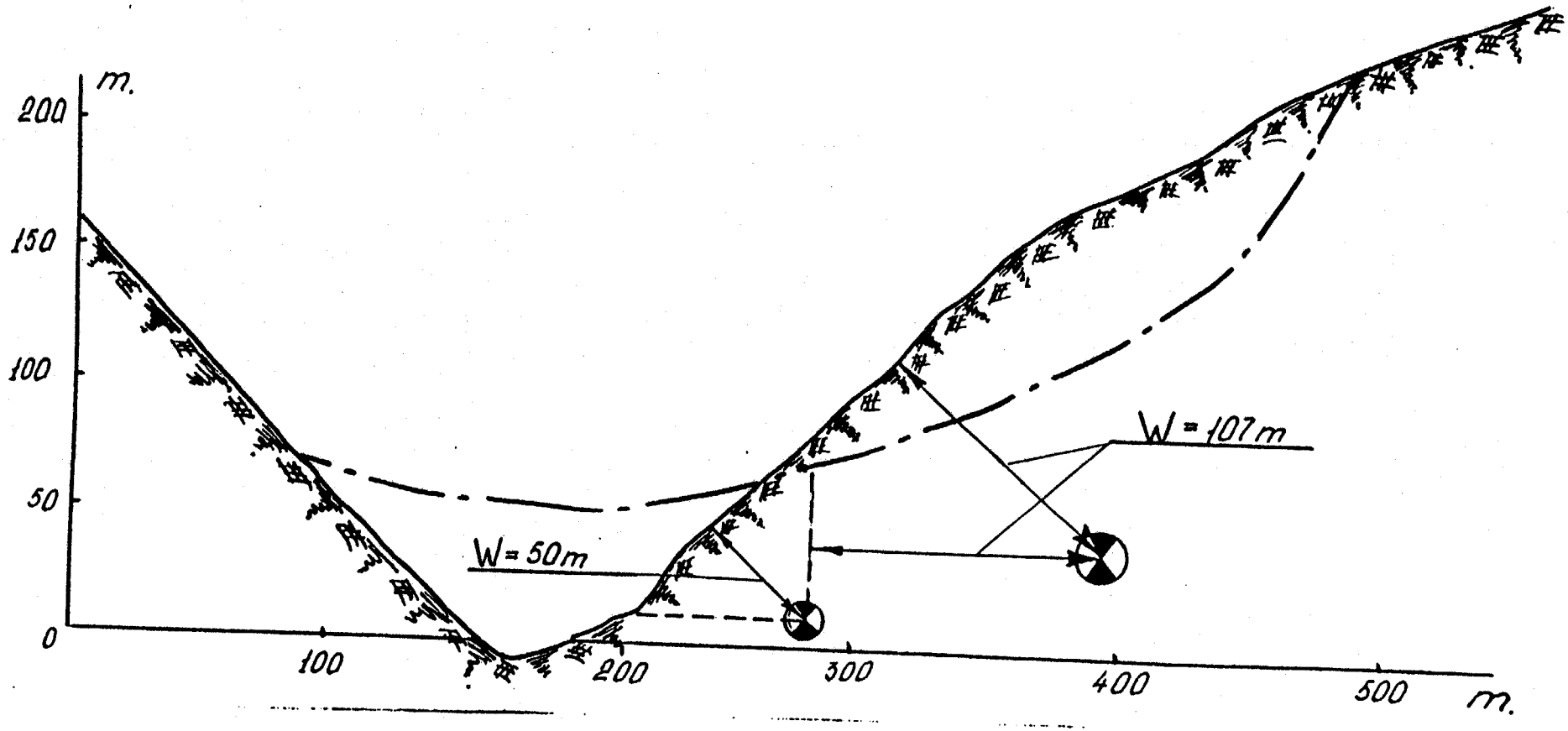

Figure III.14 Cross section of the Medeo dam

conducted in a region with complex relief.

Another problem under consideration was to compare wave fields generated by directed explosion near oblique free surface and contained concentrated explosion near the horizontal free surface. Seismic waves directivity was also studied.

Intensity and polarization of seismic oscillation were studied in the conditions of complex relief. The main problem was to study vibrations of canyons walls surfaces which look like high dams such as Nurek, Toktogul ant other dams.

In the zone of six to eight ball intensity the observations were prepared to estimate the influence of upper low-velocity layer covering hard rocks on seismic intensity.

The entire observational program also included huge complex of seismic engineering tasks conducted by different institutions. Soil and constructions vibrations were one of the tasks. Principal problems to be investigated were as follows:

a) typical construction behaviour under strong motion;

b) soil/typical construction interaction;

c) micro seismic regionalization by the data of large scale explosion.

The records in the range from 20 to 300 km also can be used to solve a number of seismological problems (crust structure, explosion magnitude, etc.).

A system of 24 evenly spaced observational points in the range from 1.1 to 20 km has been established. This system gave an opportunity to study seismic effect of the explosion and to

collect ground truth data on the dynamic parameters of seismic waves vs. distance. 13 recording stations supplied by POB-12 or N-700 oscilloscopes were installed. Filming rate was of 120 mm/sec (in the range to 5 km) and 40 to 50 mm/sec in the range from 5 to 20 km.

Three components of motion were measured at each observational point (vertical, Z, radial, X, and transversal, Y). In the nearby zone VBP and test SM-2 sensors were used. S-5S, SVKM, SK and VEGIK seismometers were established further. Predicted values of ground motion were used to adjust the gains of the seismometers.

Figure III.15 presents the observational points positions relative to the explosion. General information (range, azimuth to the epicenter, seismometer type, type of motion measured) is summarized in Table III.12. the observational points numbering in the Table and Figure is the same.

Automatic control of the equipment was used in the zone closer than 2 km due to safaty reasons.

The observational points were established in different azimuths to provide an opprtunity to study seismic wave generation directivity (see Table III.12).

In order to study parameters of canyons walls oscillations in two gates having similar configuration three component of ground motion were measured by seismographs established at the bottom of canyons as well as at the both slopes. Altitude difference was of 130m. The first gate (observational points

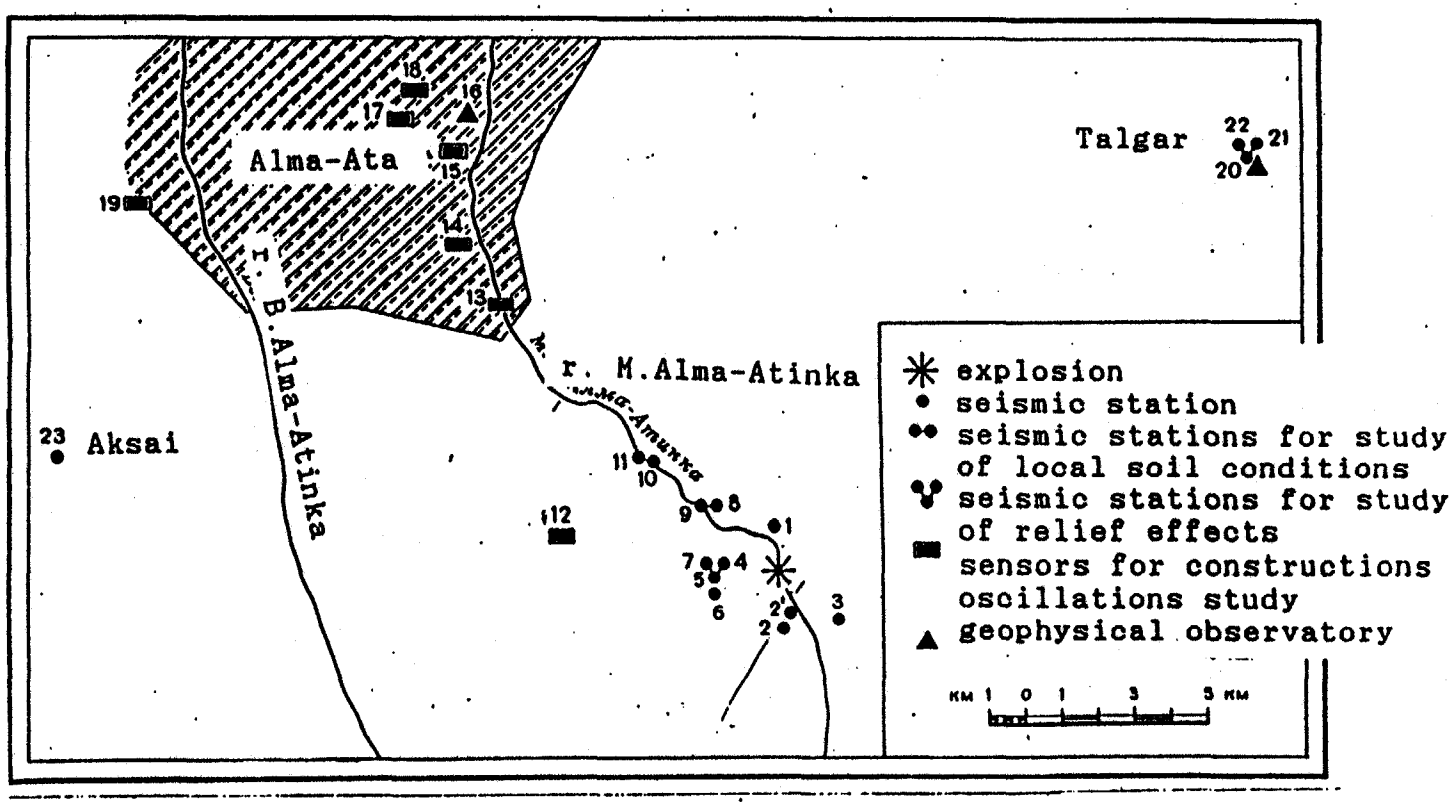

Figure III.15 Locations of seismic observation point closer than 20 km to the epicenter.

Table III.12 General information about seismic observations during the explosion

NN	Title	Distance, km	Azimuth, o	Sensor type	Compo-nents	Place of installation
1	2	3	4	5	6	7
1	"X year of Kazakhstan" resort	1.1	354	VBP	X,Y,Z	Unconsolidated layer
2	Gorel'nik spring	1.7	185	VBP	X,Y,Z	Hard rocks, valley bottom
2*	Tourist base "Gorel'nik" *)	1.2	175	VBP	X;Y	One stage house roof
	-"-				X,Z	Soft layer near the house
	-"-				X,Z	Hard rocks
3	Sarysai spring	2.1	126	VBP	X,Y	Valley slope (south) hard rock
4	Valley south to "Prosveshenetz" resort	1.8	267	VBP	X,Y,Z	Canyon slope (west) hard rocks
5	-"-	1.9	267	VBP	X,Y	Canyon bottom hard rocks
6	-"-	1.9	267	SM-2	X,Y	-"-
7	-"-	1.2	268	VBP	X,Y	Canyon bottom (east)
8	Mine station	2.2	312	VBP	X,Y	Malaya Almaatinka valley slope, hard rocks
9	-"-	2.3	312	VBP	X,Y,Z	Bed of Almaatinka river, soft soil
10	"Sov.Ministrov" resort	4.5	316	S5S	X,Y,Z	Malaya Almaatinka valley slope, hard rocks
11	-"-	4.6	316	-"-	X,Y,Z	-"- -"-, soft soil
12	Astronomy observatory	7.6	280	S5S	X,Y	Big telescope basement
	-"-	7.6	280	-"-	X,Y	Soil close to basement
13	Panel building (Lenina, 103)	10.5	313	-"-	X,Z	Four stage house, under floor
					X	2,3,4 stages
					X	under roof

1	2	3	4	5	6	7
14	Panel building (Lenina, 89)	12.5	315	-"-	X,Z X,Y X,Y X,Y X	Ground, 20 m from house Under floor Ground stage First stage Second stage
15	Three stage house brick	14.5	323	VEGIK	X,Y,Z X X,Y	Ground near house Under floor Roof
16	Seismic station Alma-Ata	15.3	326	VEGIK SK SK SMP	NS,EW Z NS,EW Z NS,EW NS,EW	Station under floor -"- -"- optical recording from a pendular -"- mechanical seismographs
17	Seven stage building (Kommunisti-cheskay and Gogol corner)	16.1	320	VEGIK	X,Y,Z X X,Y,Z X	Ground near house Under floor Under roof Third floor of unfinished part of the house
18	Panel, four stage house (Panfilova 37-41)	16.5	324	VEGIK	X,Y,Z X X,Y	Ground near house Under floor Roof
19	Panel two stage house (sixth microregion)	20.2	300	VEGIK	X,Y,Z X X,Y	Ground near house Basement Roof
20	Geophysical observatory CSE "Talgar"	17.3	49	SKM	NS,EW	Mine in granite
	-"-			SK	NS,EW Z	-"-
	-"-			CHISS		-"- (frequency separating seismic station)
	-"-			VEGIK	NS,EW Z	Mine, (DSS equipment)
21	-"-	17.7	49	VEGIK	NS,EW Z	Canyon slope (north)
22	-"-	18.1	49	VEGIK	NS,EW Z	Canyon slope (south)
23	Aksai	23.2	280	VEGIK	NS,EW Z	Four stage building basement

*) Stations are installed by "Souzvzryvprom" and IPE RAS.

from 4 to 7) was oriented perpendicular to the supposed path of seismic ray. The second gate (Right Talgar river canyon, points from 20 to 22) axis has a small angle to seismic ray.

To compare seismic wave parameters on hard rocks outcrops and unconsolidated layers of small thickness three component stations in the points 2, 8-9 and 10-11 were established at hard rocks as well as on nearby soft layers (alluvium and delluvium). The distance between compared points was not larger than 100 m.

To solve the tasks of seismic engineering six observational points have been installed (NN 13-18). Figure III.15 and Table III.13 describe seismometer positions and briefly characterize the constructions.

In order to measure seismic signals from the Medeo explosion in proper way, rates and gains were specially adjusted at the geophysical observatory CSE "Talgar" and the seismic station "Alma-Ata". So, seismographs SKM (frequency band from 0.1 s to 1.4 s), SK (from 0.3 to 10 sec), and CHISS (frequency separating seismic station with seven semioctave filters in the range from 4.2 to 0.03 sec) were specially prepared at the station "Talgar". Moreover, standard equipment was also operational. VEGIK equipment (frequency band from 0.1 sec to 1.2 sec) has been established at the seismic station "Alma-Ata". Optical recording straight from OK pendulum was also arranged.

Six seismic stations of the USSO have also been rearranged in similar way. The farthers station was at a distance of about 200 km. Other stations of the CSE and USSO situated at larger

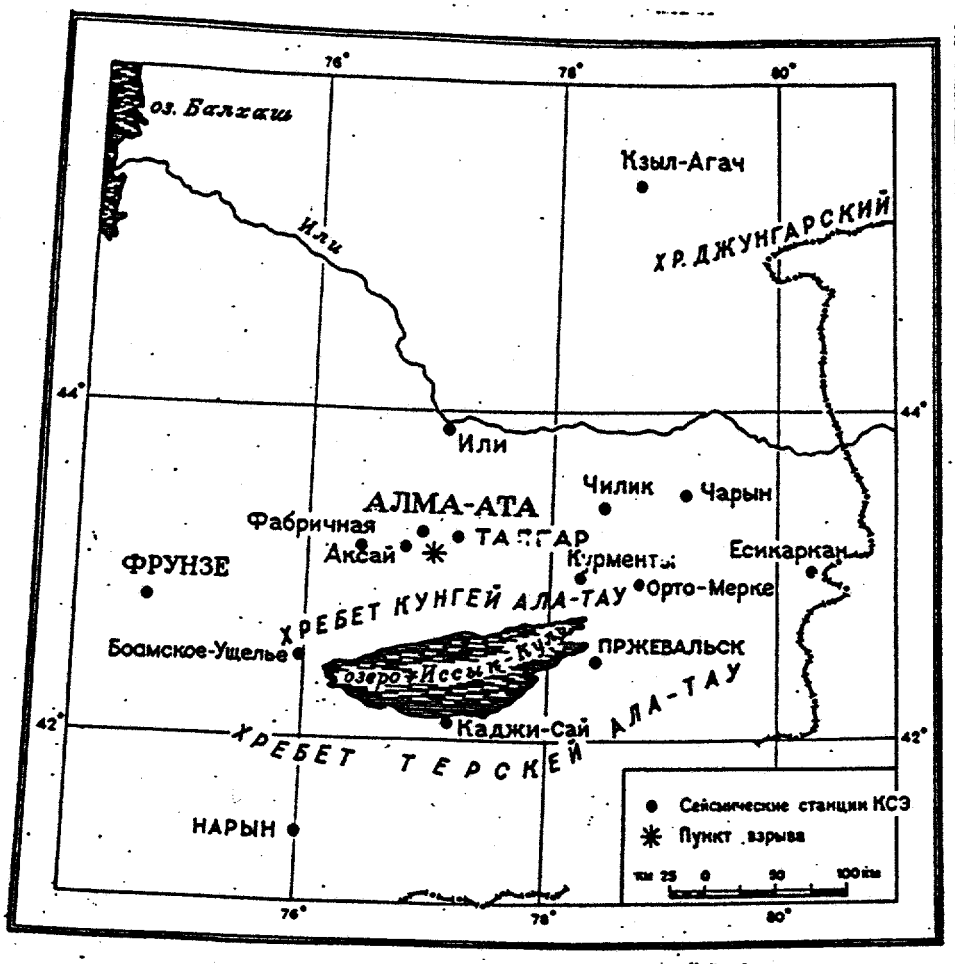

Figure III.16 Seismic stations closer than 300 km.

List of names and titles of Figure III.16

озеро Балхаш	-	L. Balkhash
р. Или	-	r. Ili
Хр. Джунгарский	-	Ridge Jungar
Или	-	Ili
Алма-Ата	-	Alma-Ata
Фрунзе	-	Frunze
Хребет Кунгей Ала-Тау	-	Ridge Kungei Ala-Tau
Хребет Терский Ала-Тау	-	Ridge Terskii Ala-Tau
Пржевальск	-	Prijevalsk
Талгар	-	Talgar
Нарын	-	Naryn
Чилик	-	Chilik
Чарын	-	Charyn
Озеро Иссык-Куль	-	Lake Issyk-Kul
Пункт взрыва	-	explosion
Сейсмические станции КСЭ	-	CSE seismic station
Аксай	-	Aksai
Фабричная	-	Fabrichnaya
Есикаркан	-	Esikarkan
Орто-Мерке	-	Orto-Merke
Боамское ущелье	-	Boam Canyon
Кзыл-Агач	-	Kzyl-Agach

///

distances worked in routine regime.

3. Readable records were obtained at all the installed stations. From all the data measured, the time delay between the first and second explosions was of 3.56 sec.

Averaged value of longitudinal wave amplitudes ratio of the first and the second explosions was of 1.46 in nearby zone and of 1.6 at larger distances. Rayleigh wave amplitude ratio was of 1.6. Body wave arrivals from first and the second explosions are distinct at all the records. Surface waves related to the first and the second explosions could be separated only to a distance of 20 km.

Preliminary data processing has shown that the first explosion has been fired 0.1 sec before the third signal of the special program of announcement of the Alma-Ata radio station. The first explosion absolute time was 04:59:59.1 and the second 05:00:02.7 GMT.

Longitudinal wave velocity in granite (where the explosions were detonated and nearby stations were placed) within first two kilometers was of 5.2 km/sec. Apparent velocity eventually increases with distance: in the range from 10 to 30 km the velocity is of 5.4 km/sec, from 20 to 50 kmis of 5.9 km/sec. Averaged velocity from the "Talgar" station data (the station is at granite outcrop) is equal to 6.0 km/sec. Other stations showed a little lower values: Aksai (23 km) is of 5.4 km/sec, Fabrichnaya (51 km) is of 5.8 km/sec or (85 km) of 6.1 km/sec. P-wave velocity from more distant stations is of 6.2 km/sec.

4. Seismic waves and their dynamic characteristics. Four principal wave types were distinguished from the explosion in the Medeo valley:

a) High-friquency longitudinal wave P_{hf}. Expected period of oscillations in this wave is of 0.15 sec. Particle velocity, U, in this wave was calculated by relationship

$$U = 700 \frac{Q^{2/3}}{r^2} \text{ cm/sec}$$

where Q is the charge weight in kg, r is the epicentral distance in m.

Solid line in Figure III.17 presents the calculated values of particle velocity of an explosion of 3600 tons. It is worth indicating that the theoretical values were not corrected on soft soil layer and relief effects. This wave was identified to a distance of 150 km with the most distinct nature up to 20 km. The theoretical and observed values coinside relatively well: period practically is not distance dependent and in average is of 0.10 to 0.15 sec (Figure III.17). The amplitude of displacement is of 6 mm at a distance of 1 km and attenuates as r^{-2}. Velocity amplitude at 1 km was of 17 cm/sec. Inside the city center (15 km) particle velocity wass of 0.08 cm/sec (Figure III.18).

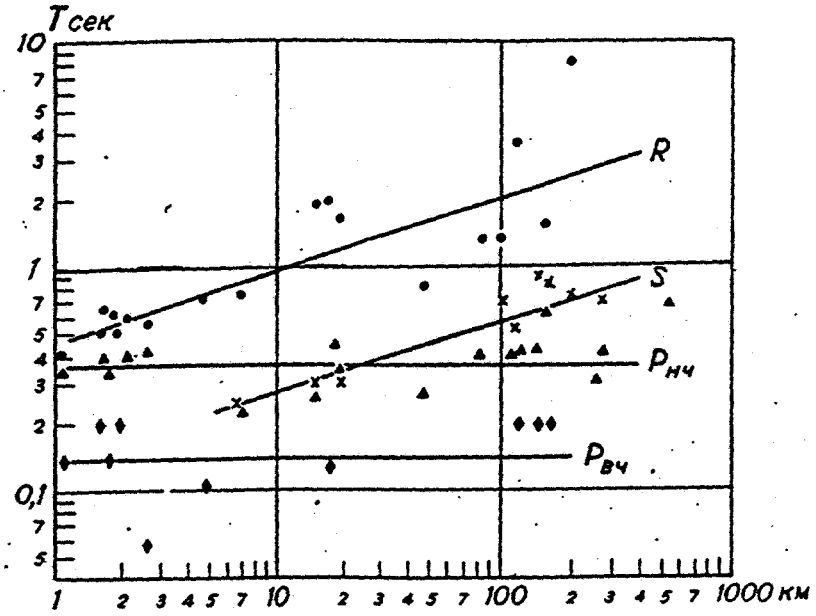

Figure III.17 Period VS. distance in different seismic phases.

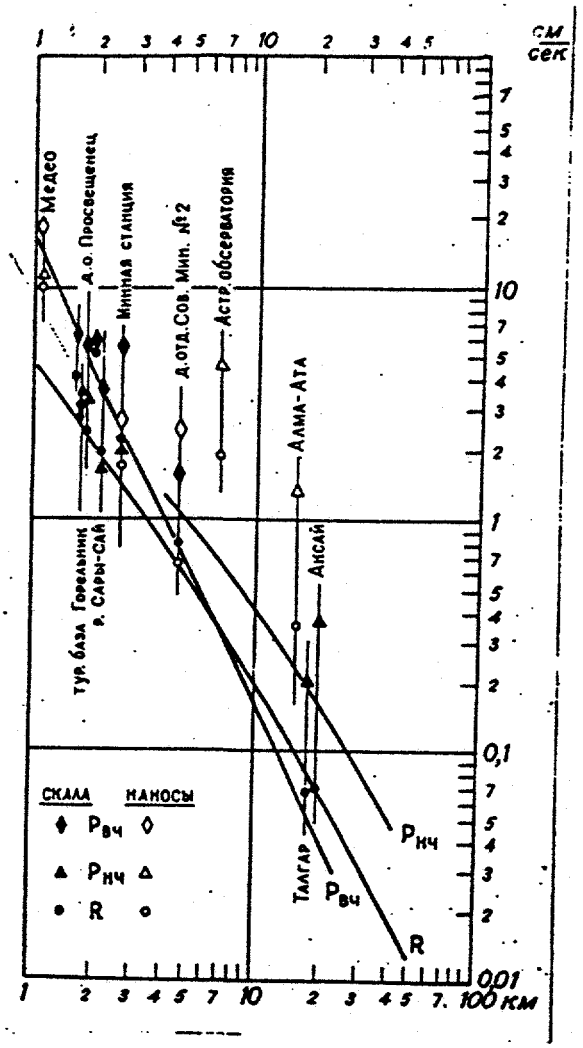

Figure III.18 Peak particle velocity VS. distance in principal seismic phases.

List of names and titles of Figure III.18

Медео	-	Medeo
д.о.Просвещенец	-	Proveshenecz
Минная станция	-	Mining station
д. отд. Совю Мин. N2	-	Sov. Min. N2
Астр. Обсерватория	-	Astranom. observatory
Алма-Ата	-	Alma-Ata
Аксай	-	Aksai
тур. база Горельник	-	Gorelnik
р. Сары-Сай	-	r. Sary-Sai
Талгар	-	Talgar
скала	-	hard rock
наносы	-	sediments

Table III.13 CSE seismic station measured the explosion signal in the range from 40 to 300 km

Title	Distance, km	Azimuth, °	Seismometer type
Fabrichnaya	49	275	SKM *
Ili	84	5	SKM *
Kurmenty	101	99	SKM *
Boam canyon	113	231	SKM long period *
Boam canyon	113	231	SKM
Kadgi-Sai	115	175	SK and SKM
Chilik	120	73	SKM *
Przhevalsk	133	122	SK and SKM
Orto-Merke	143	97	SKM
Charyn	180	76	SKM *
Frunze	201	262	SK
Naryn	219	206	SK and SKM
Esicarkan	264	92	SKM
Kzyl-Agach	284	27	SKM

* - optimal recording parameters were established.

This wave is of hignest intensity in nearby zone.

b) Low-frequency longitudinal wave P_{lf} was identified thoughout the network. This wave amplitude was estimated from the data obtained during test explosions with maximum weight of 17 tons. Figure III.18 shows predicted amplitudes of particle velocity in P_{lf} from an explosion of 3600 tons. Predicted period is of 0.4

sec. The period of P_{1r}-wave was in the range from 0.3 to 0.45 sec and did not change from 1 to 300 km. Displacement amplitude at 1 km was of 10 mm and farther in the range from 15 to 20 km varied from 0.15 to 0.50 mm depending on soil conditions. Displacement amplitude in this wave at 100 km was of 0.01 mm. Particle velocity was of 12 cm/sec, 1.3-0.2 cm/sec, and 0.016 cm/sec respectively and are coinsistent with measured displacement values. The experience on dynamic parameters investigation showed that P_{1r}-wave usually is less intensive in comparison to Rayleigh and P_{hr}-wave. The Medeo region is ananamalous in this respect: maximum amplitude of particle velocity is related to P_{1r}-wave everywhere except the closest points. Thus, P_{1r}-wave is the most dangerous in respect to seismic hazard and building constraction. Preliminary tests have also shown this phenomena.

c) Shear wave was only identified from 7 km. Visible period of oscillations grows with distance in the range from 7 to 300 km. The period at 7 km was of 0.23 sec with that of 300 km equal to 0.7 sec.

d) Rayleigh wave was distinctly identified to a distance of 200 km. Visible period grows with distance from 0.4 sec at 1 km, and 1.1 sec at 15 km to 2 sec at 100 km. Predicted periods in surface wave are very close to measured. Predicted displacement and velocity amplitudes were also well except some points with unusuall geological conditions beneath seismometers.

It follows from preliminary processing, that the measured

dynamic parameters of seismic waves generated by the Medeo explosion were well predicted. Thejretical calculations were conducted on the base of empirical relationships obtained for concentrated explosion fired near the horizontal free surface. It shows no differences between seismic efficiency of a directed explosion detonated near oblique surface and concentrated explosion near horizontal surface. No pronounced seismic wave directivity was also found.

III.4 Baipaza explosion

Baipaza explosion was conducted on 29 March, 1968. It was designed to oreate a dam for power station and to increase water level in Vakhsh river. The place for the shot was chosed in 30 km from Nurek town and 100 km south-east from Dushanbe. Figure III.19 and Table III.14 present original information on the charges positions.

The values of the shortest distance to the surface (SDS) from the charges N11 and N12 correspond to the charges of the first row. The distance from these charges to the oblique surface was of 80 m.

The charges have been placed inside the limestone massif. The massif height above the river was of 300 to 350 m. The slope of the massif wall to the river was as much as 60^{o}.

It was initially announced that the explosion would be fired at eight o´clock, Moscow time. Special radio broadcasting system had been developed and placed in Dushanbe to inform

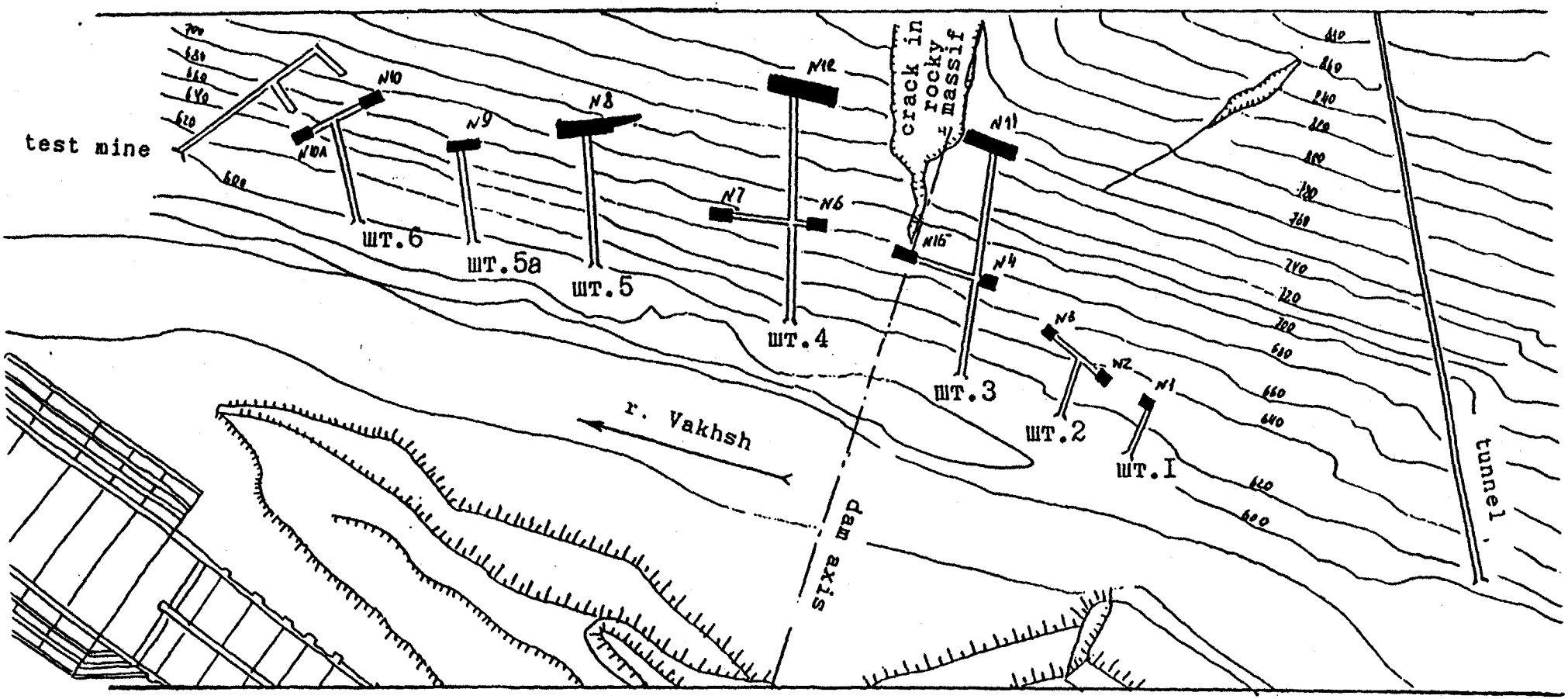

Figure III.19 Charges' positions.

remote seismic stations. Four signals of "correct" time had been merged into the program to refer to the shot time. The signals were similar to the Medeo signals. It was assumed adjusting ofthe first signal to actual correct time or 8:00:00 msk. The explosion time, however, has been shifted by 2 hours due to arrangment reasons. So, the explosion has been detonated 1.73 ± 0.01 sec before the first signal of the "correct" time.

Table III.14

Charge number	Absolute elevation, m	Total weight, t	SDS , m
1	607.9	5.4	19.0
2	607.4	8.6	17.5
3	610.7	25.0	24.0
4	607.5	57.9	34.0
5	603.0	62.7	33.5
6	607.0	61.7	35.0
7	606.2	31.4	30.0
8	597.4	289.0	52.0
9	597.9	62.8	32.5
10	605.3	54.9	32.0
10a	603.4	9.7	23.5
11	608.2	542.0	60.0
12	607.0	642.0	60.0
plane	-	90 (by project)	

The first signal was not specially related to any actually

correct time mark. The explosion has been detonated at 9:50 (Moscow time) with an accuracy of several minutes.

The explosive has been placed in several chambers. Figure III.19 displays the scheme of the charges positions. About 2000 tons of explosive have been used. To avoide damaging seismic effects, the charges were fired with time delay. Table III.15 presents parameters of each charge.

Table III.15

Explosion NN	Charges NN	Total explosion yield, tons	Designed time delay from the first explosion, sec	Actual time delay, sec
1	1,2,3,4 5,6,7	253	0	0
2	11	542	0.5	0.25
3	12	642	0.75	0.38
4	8	289	1.5	1.94
5	9	63	4.0	4.0
6	10, 10a	65	6.0	5.49
7	plane	90	6.0	4.0
		(by project)		

During the initial stage of the explosion development, intensive gaseous products of detonation ejection from the mines going to the charges was observed. The mines N3 and N4 were the first two the ejection occured from.

There was practically no time delay between the explosions N1, N2 and N3. Dome-like uplift of the surface of the mountain

was observed at the same time as gas ejection from the mines N3 and N4. This dome-like uplift was centered above the SDS of the charges N11, N12 as well as NN4, 5, 6 and 7. The unique dome above the charges can be explained by short time delays between the explosions N1, N2, and N3. The dome height above the explosion N1 had been of 6 to 8 m and of about 2 to 3 m above the explosion N2 before the explosion N3 was detonated. This difference in the initial heights with total displacement of 50 m can only be observed as a weak roughness. Gaseous products' of detonation ejection from the main explosions (NN11 and 12) occured from the mines. Thus, the massif has not been damaged to a substantial extent by the explosion N1 in the first row.

Total gas volume estimation have shown that principal ejection was from the mines. Due to this phenomenon, well-developed dome-like uplift was observed without any gas ejection through the surface.

After the dome creating and collapsing, intensive landslide has begun from above the craters. The landslide reached almost the top of the mauntain. The layer thickness was of 10 to 30 m. Sliding process was favoured by the massif structure. The massif structure was formed by layers parallel to the surface with a thickness of 5 to 10 m.

A dam of total volume of 1.5 10^8 m^3 has been created by the exploson. Figure III.20 shows the dam view before and after the explosion. Figure III.21 shows cross-section of the dam. The lowerest point of the dam is near the left bank of the river.

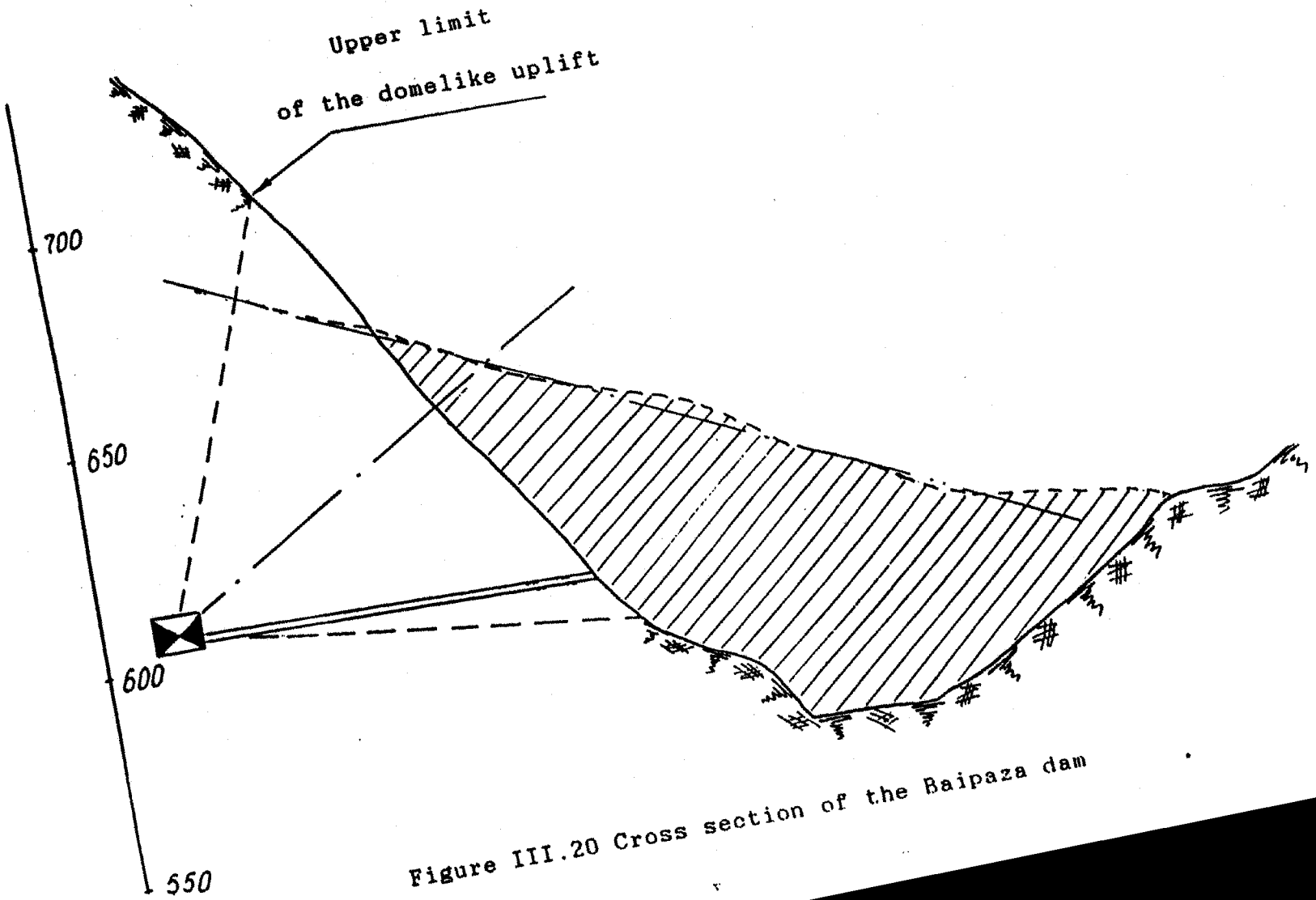

Figure III.20 Cross section of the Baipaza dam

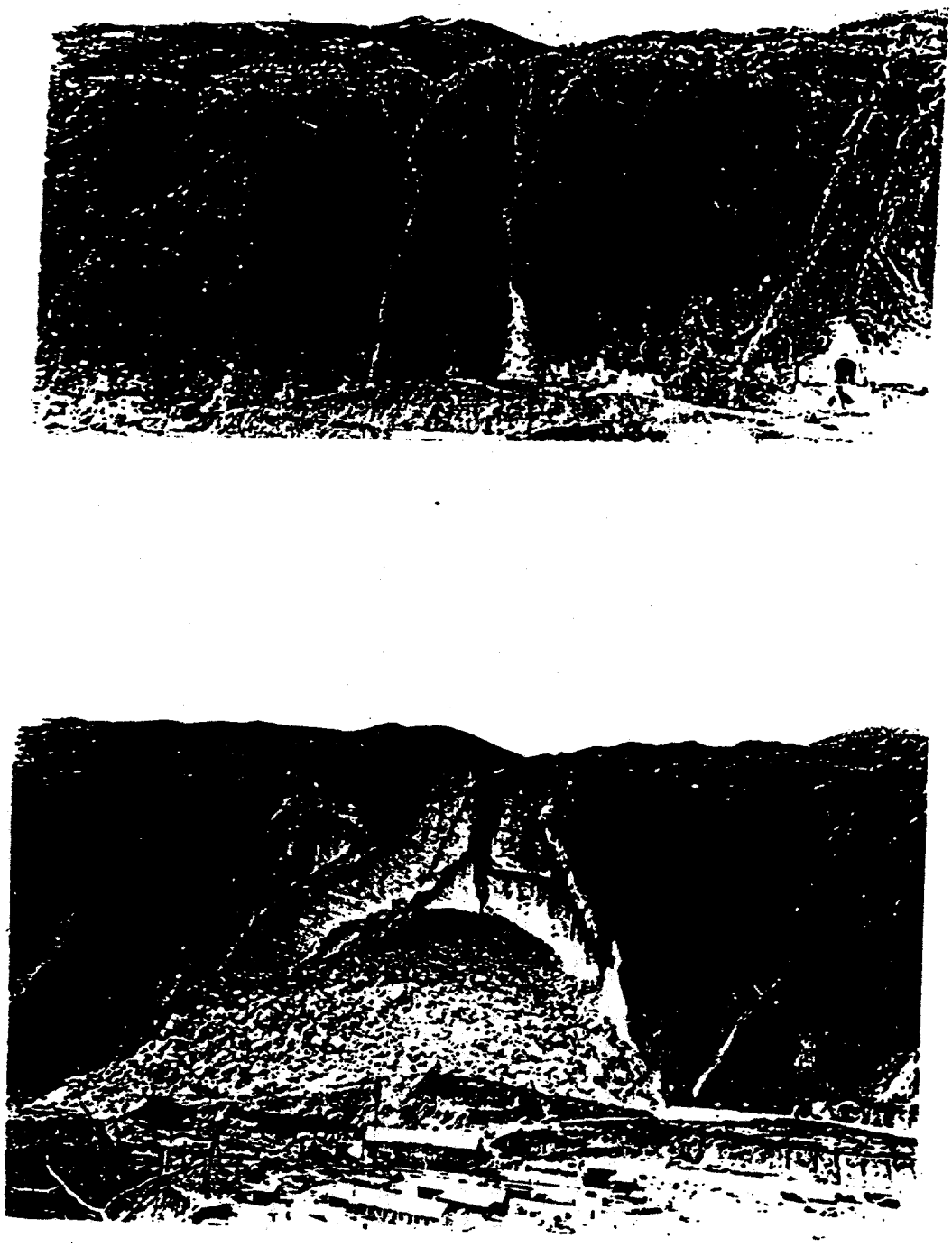

Figure III.21 View of the Baipaza dam before and after the explosion

Absolute height above the water surface was of 50 m at this point. The rocks forming the dam can be separated into two groups. Explosion-formed rocks were finely crashed to a size of several centimeters. Second part of the rocks formed by landslide is characterized by uneven size distribution with large stones predominance.

A. Compressional wave parameters

One of explosion-induced effects on the environment is a compressional wave generation. Medium deformation and kinetic energy of medium are the two principal effects of compressional wave propagation. Also, compressional wave of an explosion fired near free surface provides rock ejection and cavity creation. Considering compressional wave as a principal phenomenon of near-surface explosion, seismic wave measurements have been conducted from the Baipaza explosion. Two observational points were established in the tunnel and the experimental mine (Figure III.19). Source/receiver distance, however, varied due to a series of explosions at different positions. Thus, the seismic wave parameters relationship vs. yield and distance have been obtained. VIB-A seismometers have given the most relaible data. VBP seismometers used to measure particle velocity have given only limited results due to short source/receiver range. S5S seismometers have recorded only first arrivals. Oscillations with the seismometers natural periods disturbed particle velocity records, and the measurements failed.

Peak particle velocity was the principal compressional wave parameter measured. Table III.16 presents the peak velocities measured by each seismometer. Three components of motion were measured in each point. Horizontal components were of much larger amplitude than vertical which was not considered in calculating of total particle velocity vector. Total velocity vector measurements are presented in Table III.17.

Table III.17

$\frac{R}{q^{1/3}}, \frac{m}{kg^{1/3}}$	2.35	2.59	2.84	2.84	3.63	3.92	4.5
V, $\frac{cm}{sec}$	77	49	42	36.5	16.3	23.8	14.7

Figure III.22 displays the same data as a graph. Inspite some scattering observed, the data can be approximized by straight line or by power law

$$V = 630 \left[\frac{q^{1/3}}{R}\right]^{2.3}$$

It is to be mentioned, however, that this relationship is of limited application due to limited distance and yield ranges used.

Only two positive phase duration measurements could be done (Table III.16). They are: 28 msec from 63 tons explosion, and 51 msec from 289 tons explosion, or 0.7 and 0.78 $msec/kg^{1/3}$ respectively. Hard limestone is characterized by value of 0.5 $msec/kg^{1/3}$, from different observations.

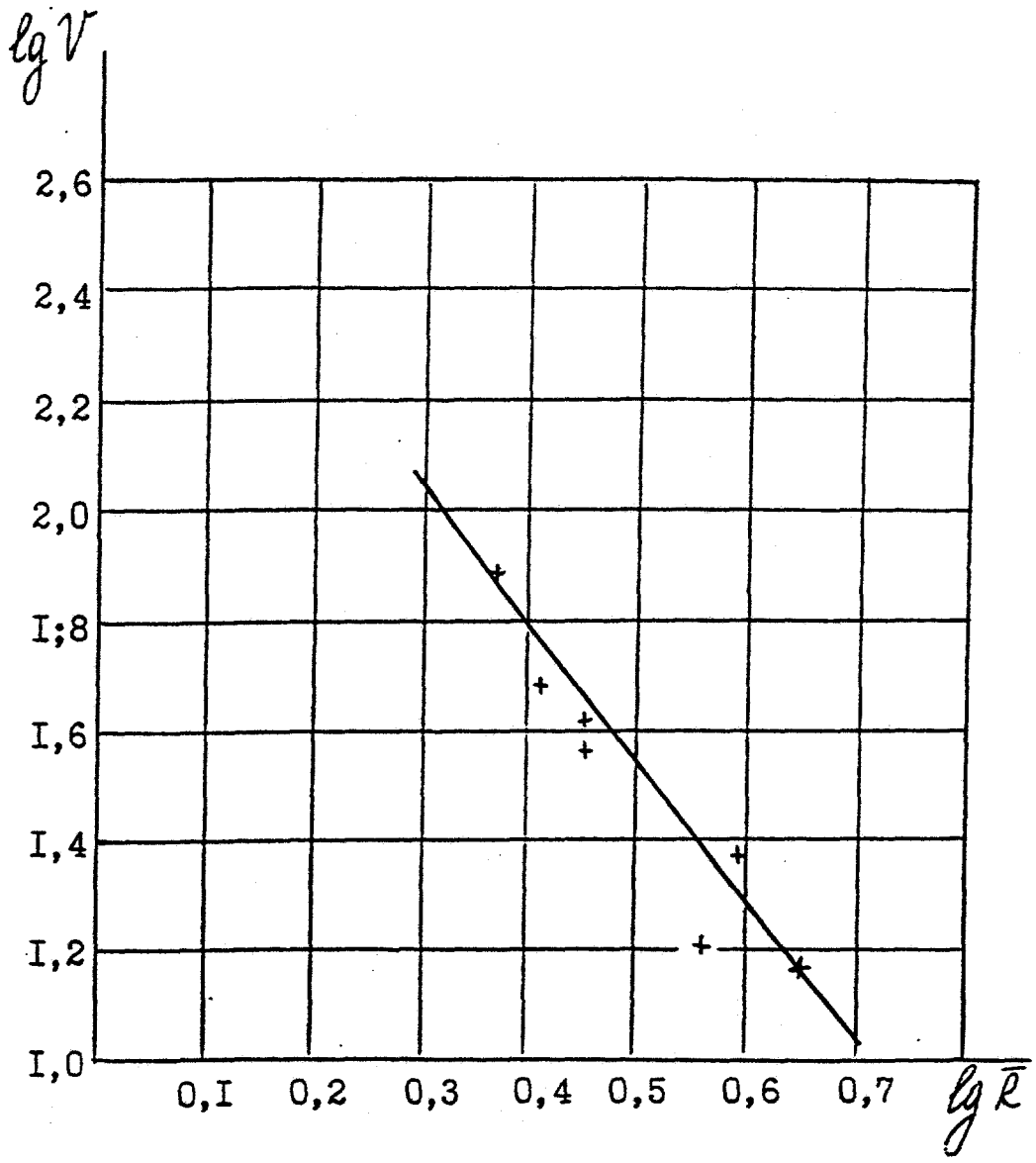

Figure III.22 Curve $V = f\left(\frac{R}{q^{1/3}}\right)$.

Table III.16

Sensor # and orientation	1 expl. R=285m $\bar{R}$=4.5 m/kg$^{1/3}$		2 expl. R=320m $\bar{R}$=3.92 m/kg$^{1/3}$		3 expl. R=245m $\bar{R}$=2.84 m/kg$^{1/3}$		4 expl. R=155m $\bar{R}$=2.35 m/kg$^{1/3}$			5 expl. R=103m $\bar{R}$=2.59 m/kg$^{1/3}$			6 expl. R= m $\bar{R}$= m/kg$^{1/3}$		
	A, mm	V, sm/s	A, mm	V, sm/s	A, mm	V, sm/s	A, mm	V, sm/s	τ_+, msec	A, mm	V, sm/s	τ_+, msec	A, mm	V, sm/s	τ_+, msec
						MINE									
VIB.0647 /$\perp$ mine/	2.5	12.3	2.5	12.3	4.5	22.2	11.5	56.6		7.5	37		14		
VIB.0689 /$\perp$ mine/	2.0	10.0	1.8	9.0	3.5	17.5	10	50		6.0	30	28	12		
VIB.0665 /$\parallel$ mine/	1.8	8.9	3.8	18.8	7.0	34.7	9.5	47		6	29.7	28	6		
VIB.0694 /vertical/	1.3		1		3		6			2			-		
VBP. #6 /$\perp$ mine/	2.3	13.3	2	11.5	4	23	12	69	51	7	40	28	-		
VBP. #66 /$\parallel$ mine/	1.5	8.2	4.5	24.5	7	38	10	54.5		7	38		-		

	R=230m $\bar{R}$=3.63 m/kg$^{1/3}$		R=175m $\bar{R}$=2.14 m/kg$^{1/3}$		R=245m $\bar{R}$=2.84 m/kg$^{1/3}$		R=340m $\bar{R}$=5.15 m/kg$^{1/3}$								
						TUNNEL									
VIB.0661 /$\perp$ mine/	4.0	14.4			11	39.5	2.5	9.0							
VBP.62 /$\perp$ mine/	3.0	14.0			7	33.5	1.5	7.2							
VIB.0670 /$\parallel$ mine/	2.5	7.5													
VIB.AM 134 /$\perp$ mine/	5.0	14.5			13	38									

B. Seismic observations

Seismic measurements have been arranged in the local zone (from 150 to 1500 m) as well as at more distant ranges.

Qualitative data on seismic hazard were of principal importance of these measurements. Oscillation intensity vs. distance was also studied as well as seismic wave generation by unusual explosin as the explosion near almost vertical wall was.

Table III.18

NN	Seismometer position	Range	Seismometer	Channel	Component	Gain
1	Right	600	VBP-3	1		1.26
	bank	-"-	-"-	2	X	1.54
	rock	-"-	-"-	3	Y	1.87
2	Right	700	VBP-3	4		1.56
	bank	-"-	-"-	5	X	1.62
	soil	-"-	-"-	6	Y	1.49
3	Right	2300	S5S	1		8.5*
	bank	-"-	-"-	2	X	-"-
	rock	-"-	-"-	3	Y	-"-
4	Left bank	2300	S5S	4		8.5
	bridge bull	-"-	-"-	5	X	-"-
		-"-	-"-	6	Y	-"-
5	Right	5000	VEGIK	1		22.8
	bank	-"-	-"-	2	X	17.7
	rock	-"-	-"-	3	Y	22.0
			SM-2M	4		26.2
			-"-	5	X	28.6
			-"-	6	Y	30.2
6	Right	7500	VEGIK	1		34.6
	bank	-"-	-"-	2	X	33.4
	rock	-"-	-"-	3	Y	40.0
7	Right	7500	VEGIK	4		47.6
	bank	-"-	-"-	5	X	48.8
	soil	-"-	-"-	6	Y	44.8

*/ Gain from averaged data of S5S seismometers.

Seven observational points have been established to measure seismic wave parameters. Table III.18 summarizes the information on the seismometers. The influence of near vertical wall on the symmetry of seismic wave generation was the principal task of the recordings. Seismic wave was measured only along one

direction, but at the both sides of the river. Figure III.23 and III.24 display the copies of displacement records.

Three-component measurements with vertical (Z), radial (X), and transversal (Y) components have been arranged. The seismometers have been partially attached by cement to hard rocks, and partially digged into the soil.

Three distinct arrivals of longitudinal waves from the three sequential explosions are observed on the records of the closest seismic station (600 m) shown in Figure III.23. Arrival time difference between first and second impulses was of 0.24 sec, and that of between second and third was of 0.18 sec.

Table III.19 presents the measured peak displacement amplitudes (a_n^P), peak particle velocities (V_n^P), and positive phase durations (t_n^P).

Table III.19

Component	Peak displacement, mm			Peak particle velocity, cm/sec			Positive phases duration, sec		
	1	2	3	1	2	3	1	2	3
Z	1.03	3.02	4.6	9.3	24.2	17.5	0.04	0.07	0.06
X	2.21	7.4	5.1	10.5	24.6	17.5	0.065	0.09	0.75
Y	0.37	2.7	4.5	1.4	10.7	15.5	0.035	0.10	0.15

Z- and X-components data show that the largest ground motion is induced by the second row of charges and the smallest - by the first. The ratio of displacements and velocities is of 2.34 to 3.34. The third explosion amplitude is hard to estimate due

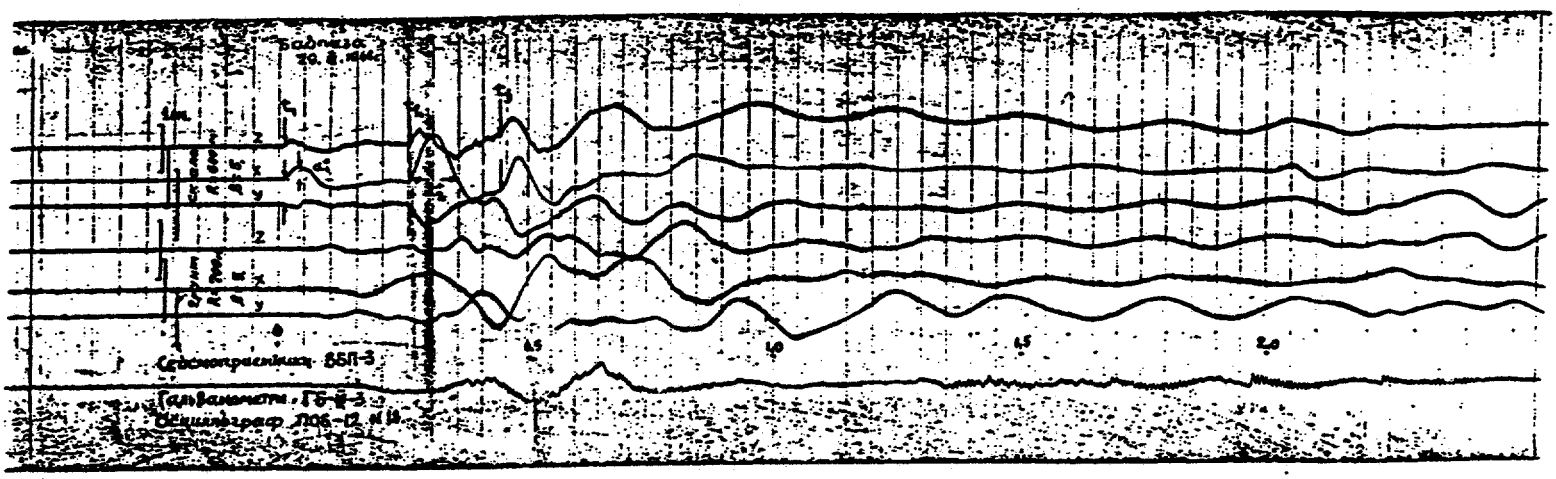

Figure III.23 Displacement oscillograms recorded at the free surface

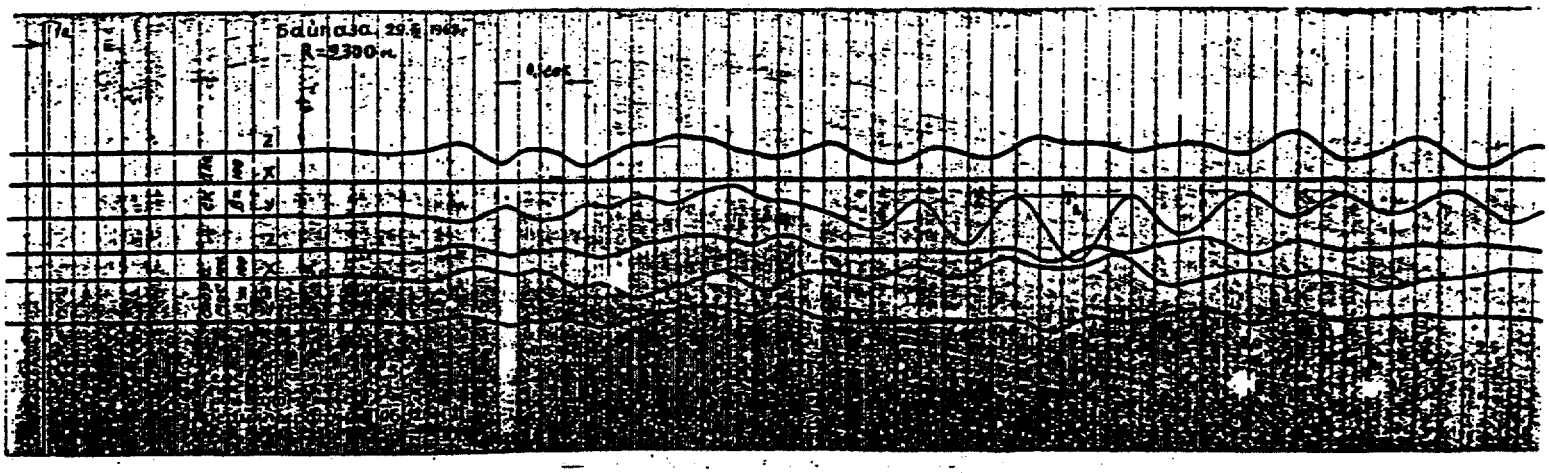

Figure III.24 Displacement oscillograms recorded at the free surface

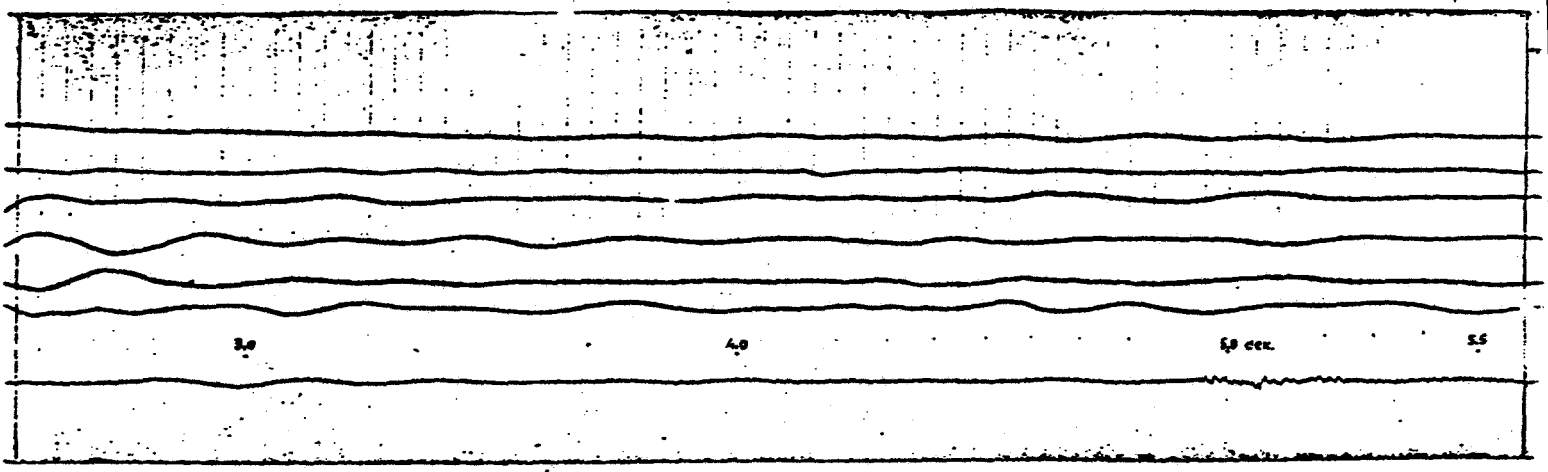

continuation

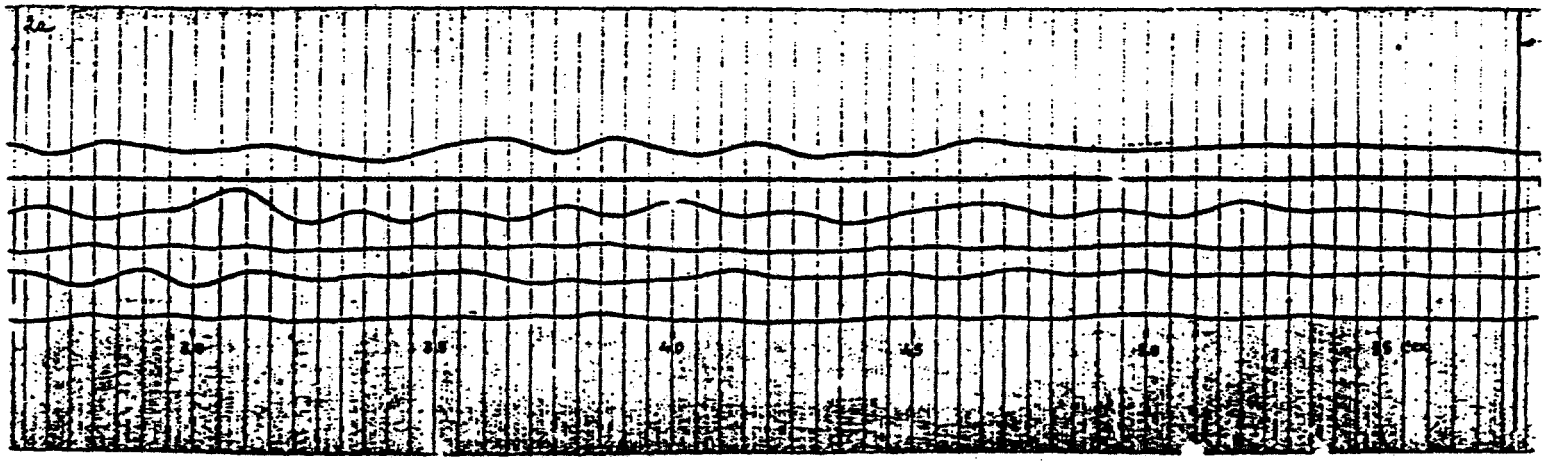

continuation

to strong influence of the second explosion. The highest Y-component has been generated by the third explosion. The three explosions can be separated even at a distance of 700 m. At a distance of 2300 m two explosions are still can be distinguished.

It is hard understanding from one seismogram which charge in which chamber has generated impulses and why Y-component differs from others. This problem is sophysticated by the absence of correct explosion times. Seismic hazard zone along the river can be limited by 700 m as follows from the records. It can not be excluded a possiblity, however, that in the perpendicular direction, along the tunnel, this zone is larger.

The experience on the line charges detonation strictly showes several times higher effect in the direction perpendicular to the line.

There are some (up to 8) weak short period arrivals in addition to the three principal in the first portion of the records. Also, there are distinct arrivals in 2.05, 4.1 and 5.6 sec after the first arrival merged into surface wave of 0.25 to 0.3 sec period and of 4 to 5 mm amplitude.

Displacement amplitude is of 0.5 to 0.6 mm at 2300 m. Two groups of well-developed surface waves with a period of 0.25 and amplitude of about 2 mm, and a period of 0.8 sec and amplitude of 0.3 mm have also been recorded. X-component is the most prominent in the surface waves.

Surface waves with a period of 0.8 to 0.9 sec are distinct

at distances of 5000 and 7500 m. Quazisinusoidal oscillations with a period of 0.19 sec have been recorded in the initial portion of seismograms at a distance of 7500 m.

C. Shock wave in the air

Gages SD-725 were used to measure air shock wave. Overpressure, total momentum and time duration of positive and negative phases have been measured. Two SD-725 gages have been installed inside the equipment site N1a which was oriented perpendicular to the mine at a distance of 645 m from the main charges N11 and N12. Also, two gages have been established inside the equioment site N4 at a distance of 545 m from the mine's N4 mouth (approximately along the mine axis). The distance from the plane charge to the equipment site N1 was of 400 m, and to the equipment site N4 of about 635 m.

The results of the data processing are presented in Table III.20. All the gages have recorded two groups of shock waves with sharp fronts and peak overpressure to 0.03 kg/cm^2, and one wave with gradual pressure increase to 0.008-0.009 kg/m^2. Positive phase duration in this wave was of 0.2 to 0.32 sec. Total (pressure) momentum of all the waves was in average of about 70 $kgsec/m^2$. Equivalent charge weight has been estimated from the total momentum by equation

$$q = \left(\frac{J+R}{35}\right)^{3/2}$$

where q is the weight of the charge in kilogramms, J+ is the total momentum in $kgsec/m^2$, R is the source/receiver distanse.

Table III.20 Acoustic wave parameters as measured by SD-725 sensor

NN	Place	Source/ receiver distance m	Arrival time, sec	Peak over-pressure ΔP_ϕ, kg/cm^2	Positive phase duration τ_+, sec	Pressure impulse I_+, $\frac{\text{kg sek}}{\text{m}^2}$	Over-pressure character
1	Point N1	645	1.90	0.009	0.20	30.0	sharp front
			1.99	0.031			-"-
			4.62	0.009	0.28	14.0	slow increase
			5.62	0.030	0.20	30.0	sharp front
			5.72	0.012			-"-
2	-"-	645	1.90	0.008	0.196	30.0	sharp front
			1.99	0.030			sharp front
			4.58	0.08	0.28	11.0	slow rise
			5.58	0.032	20	28.0	sharp front
			5.68	0.008			
3	Point N4	545	1.60	0.006			slow rise
			1.74	0.032	0.32	35.0	sharp front
			1.88	0.008			-"-
			3.57	0.005	0.24	23.8	slow rise
			3.63	0.022			sharp front
			5.70	0.012	0.50	19.2	slow rise

The equivalent charge weight was equal to 46.5 tons or about 2% from the actual total charge weight.

Thus, fast gaseous products of detonation ejection through the mines during Baipaza explosion has generated shock waves. Relative times of gas ejection from different mines can be estimated from explosion process filming. Table III.21 summarizes these data.

Table III.21

Mine number	Time of gas ejection
1,2, and 3	0.078
4	0.116
5	1.68
5a	4.36
6	6.00
Plane charge	4.00

The first group of shock waves has been generated by the explosions of the charges N1 through N7, N11, and N12. Gas ejection from the explosion N8 has generated second group, and the plane charge has generated the last wave group. It is interesting to note that the first air wave had a shock front recorded at the both observational sites, while other waves changed their character between the two sites. The second wave had a shock wave nature at the observational point N4 and looked smoothat the site N1. The third wave had a reversed character: shock wave at the site N1 and smooth shape at the site N4. Gas

and dust shielding effects from the first group of the charges (N1 through N7, N11, and N12) can explain this phenomenon.

The Medeo explosions were also characterized by gas venting from the mines. But no air wave has been generated despite substantially larger weight of the explosive. Gas ejection intensity is the reason for that. Gas velocity of 200 m/sec was reached during Baypaza explosion with that of the Medeo oneas low as 100 m/sec. Explosion containment, apparently, was weaker of the Baypaza explosion.

III.5 Burlykyay experimental explosion

An explosion at the Burlykyay river was conducted on 8 of February, 1975, at 10 o'clock, Moscow time. The total explosive (zernogranulite 79121) weight was of 702.4 tons. Specific explosive energy was of 1030 kcal/kg.

The experiment site was situated inside Kirgizstan in the Burlykyay river canyon. Canyon walls slope was of 50^{o} to 60^{o} with vertical or even back sloped parts. Intrusive rocks have formed the massif. The content, in principe, can be represented by granite, granite-porfirite and diabase. The rock strength by Protodiakonov scale is of f = 2÷3. Red, red-brown and brown granites prevail. Granites are formed by field spar (60-65 %) and quartz (30-35 %) and have large grained structure and sometimes grain sizes are distributed in wide range. There is some grey diabase and granite-porfirite dikes. The dikes thickness is from 1 to 30 cm, rarely of 5 m, and 25 to 50 m

long.

Two tectonic faults cross the site of the experiment. They are of 60^{o} to 70^{o} dip. One of the faults has a width of 25 to 75 m and other of about 3.5 m. Granites in the fault zone are crashed and cracked . Gouges and traces of offset are visible at the cracks surface. The offset amplitudes in the first fault are of about 10 m, and in the second are of about 1 m.

Several large and small tectonic crack systems also cross the rocky massif. Large cracks have a width from 5 to 20 mm to 200 to 250 mm. The cracks are from 5-10 to 150-300 meters long. Small cracks are from 0.5 to 10-20 mm wide and from 1 cm to 10 m long.

Granite mean bulk weight is of 2.6 g/cm^3. Longitudinal wave velocity is from 1.8 to 3.7 km/sec. Average cracks spacing is of 3.5 to 14 cm with width from 0.2 to 0.7 mm. Blocky structure value is from 3 to 10 cm. Porosity is of 0.2 to 0.8 %.

The Burlykyay explosion contained several charges. The charges positions and the mines to the charges are shown in Figure III.25. Actuall sequence of detonation and the charges masses are presented in Table III.21.

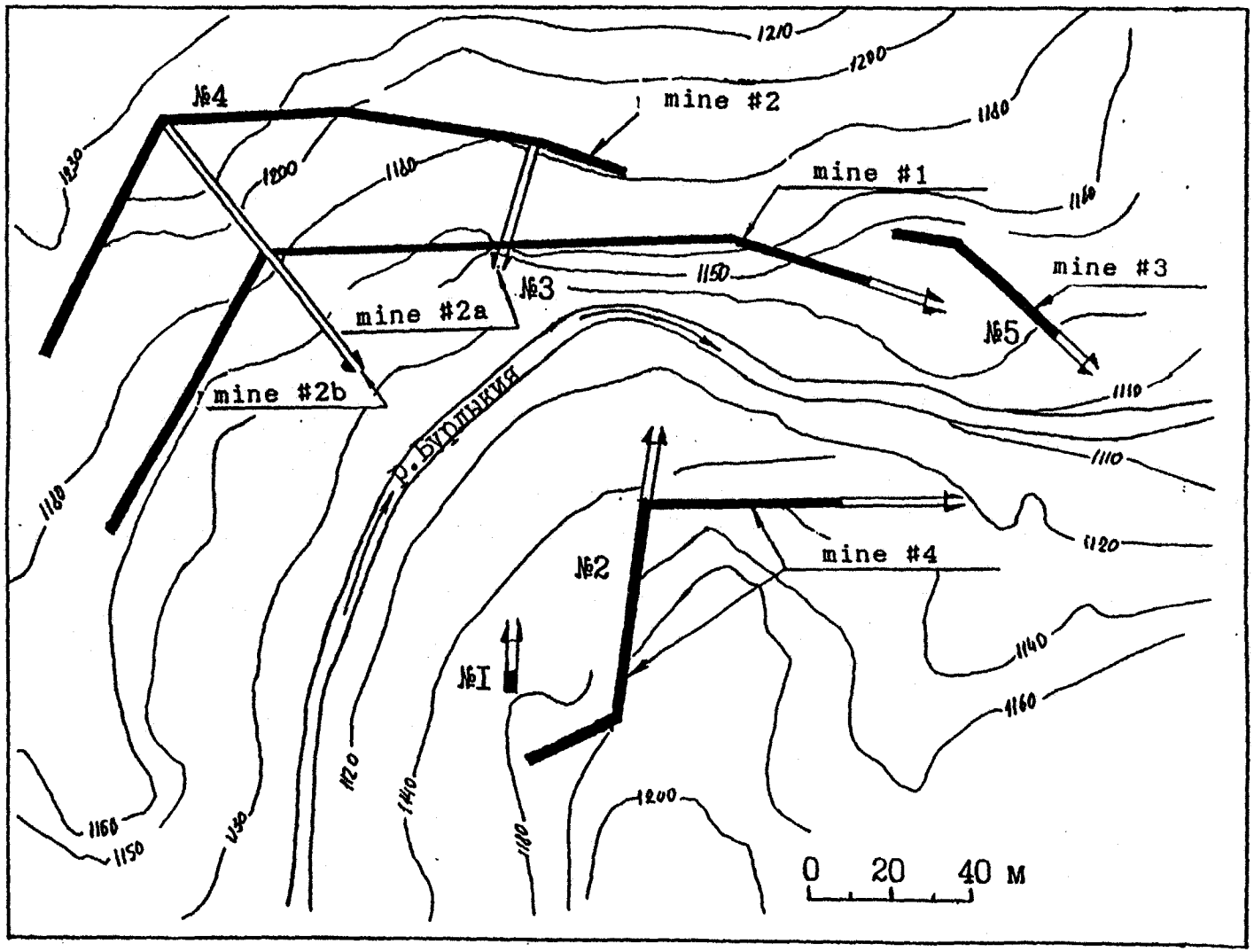

Figure III.25 Mine tunnels scheme: ▬ -charges, ▭ -access tunnels.

Table III.21

NN	1	2	3	4	5
Charge weight in tons	2.3	88	125	470	18
Relative time of detonation, msec	0	35	162	190	280

The first charge has been fired in 9:59:59.282, Moscow time.

A. The explosion observations

1. General pattern of the explosion development.

Filming was used to investigate general pattern of the explosion development. Kinematic parameters of crashed rocks motion were measured. Two optical sites of observations supplied by AKS-4 and AKA-BAF cameras have been established. Figure III.26 displays the sites positions. Filming was carried out in two directions, as clear from the Figure. The right bank peak velocity of a dome-like surface motion was of 15 to 20 m/sec, and at the left side of 25 to 30 m/sec.

2. Air shock wave.

Autorecording gages SD-725 were used to measure air shock wave parameters. Shock wave overpressure was measured. Figure III.26 present the gages positions. Observational sites were at

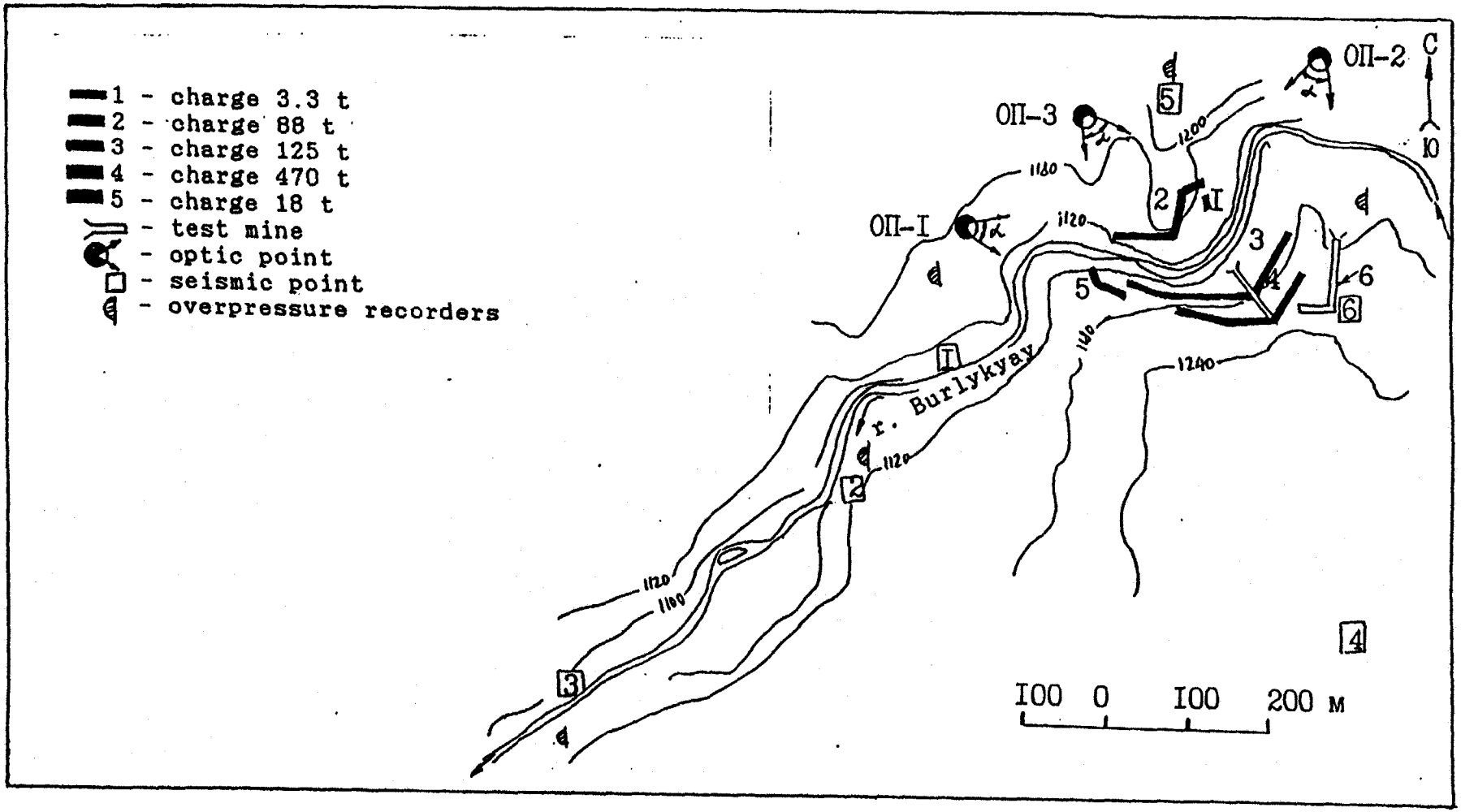

Figure III.26 Observation points location and equipment.

distances of 200, 350, 600, and 1400 m from the explosion. Nearby gages have recorded three groups of shock waves according to gas ejection from the mines. Remote gages (R>500 m) have recorded only one shock wave with almost no rarefaction phase. Dome-like motion in the epicenter also generated long period pressure wave.

3. Compressional wave in the massif.

Parameters of compressional wave inside the rocky massif near the long charge mines of left bank (N1 and N2) were measured. Particle velocity was measured. VIB-A and VIB-V vibrographs as well as induction velocity transducers GIS-3B and liquid velocitymeters GIS were used. The sensors have been established inside the experimental mine perpendicular to the mines N1 and N2.

The mines cross sections are shown in Figure III.27. Also the sensors positions marked by I-IY, are shown. The angle between the line from the sensors positions to the mine axis and horizontal plane is of 10^{o} to 12^{o}. Velocity sensors had been oriented in horizontal plane by different angles to the mines axis and vertically. Vibrographs VIB-A, VIB-V, IDS-3V recording displacement as high as 20 mm were used to measure waves from the additional charge in the mine N1. GIS sensor with maximum measuring velocity of 15 to 30 m/sec were used to measure the main charge wave parameters (the charge was near the testing mine N2). Trace oscilloscopes OSH-9 have recorded the sensors measurements. The oscilloscopes were established near the mouth

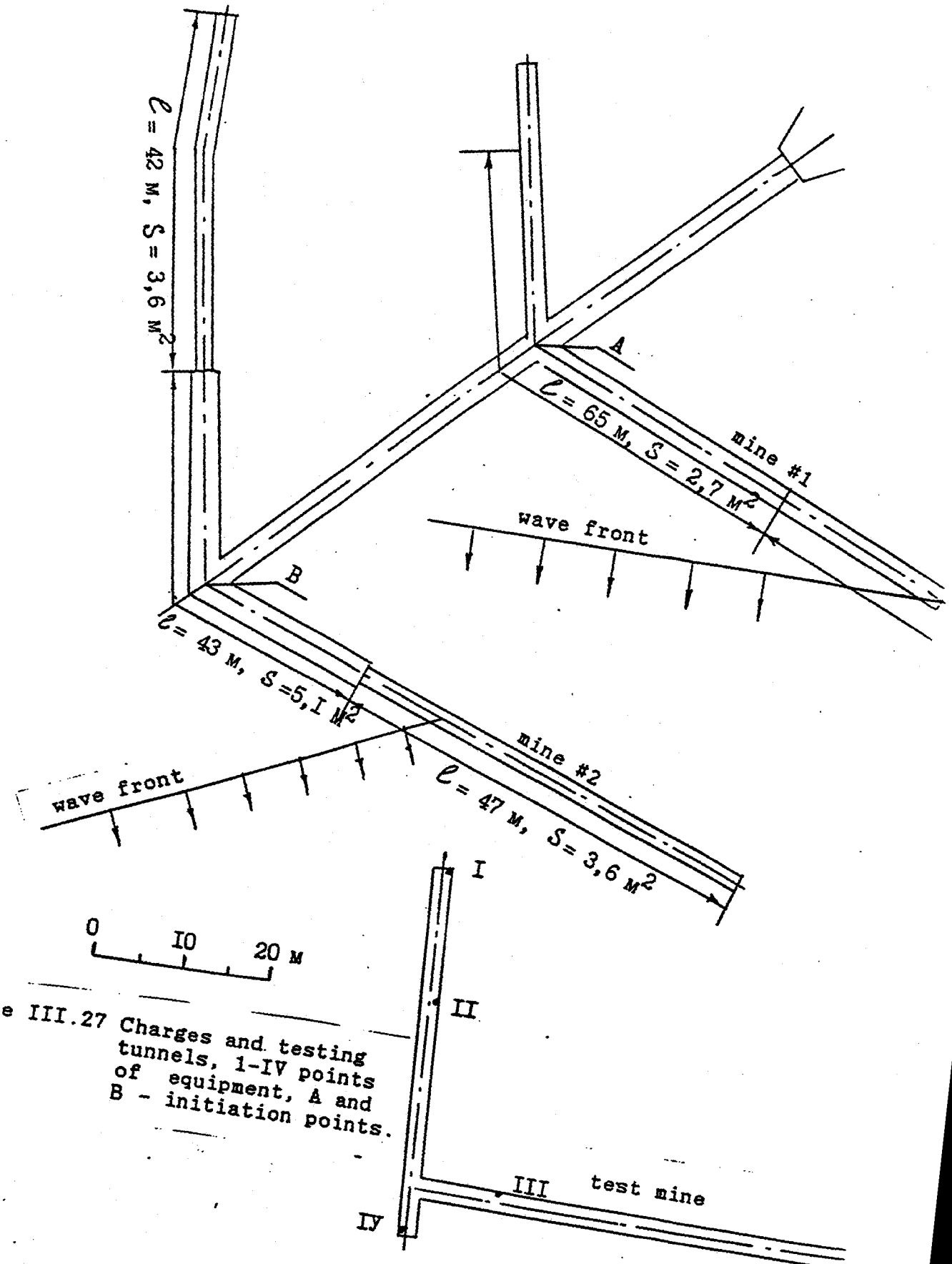

Figure III.27 Charges and testing tunnels, 1-IV points of equipment, A and B - initiation points.

of the testing mine.

Typical oscillograms are shown in Figure III.28. Compressional waves from the right side charge have been recorded the first. The wave from 2.3 tons arrived about 30 msec after the unified time mark, (UTM), and was followed by emerget front of 88 tons explosion. Then the two left side explosions were detected by compressional waves arrivals. The explosion of additional charge in the mine N1 are followed by the main charge explosion in the mine N2.

The sensor data processing results are in Table III.22. Times are given from the "physical zero" which corresponds to the initiation of the additional charge at the left bank. The distances are from the sensors to the mines filled by explosive, and the angles are between the sensors and mines axis.

Positive phase duration in compressional wave generated by the charge placed in the mine N1 can not be measured because of influence of the main explosion compressional wave. Cables rupture did not allow to record whole compressional wave at the closest points N1 and N2. Positive phase duration of 150 and 170 msec have been measured at the third (R = 41.5 m) and fourth (R = 51 m) observational points.

B. Near-field seismic measurements

Seismic waves measurements at the free surface have been carried out in the range from 0.1 to 1 km by S5S seismometers. Figure III.29 reproduces the copies of the records obtained at

Table III.22

R, m to axis of mine 2 (main charge)	R, m to axis mine 1 (extra charge)	V_{max}, m/s (extra charge)	V_{max}, m/s (main charge)	t,ms (extra charge)	t, ms (main charge)	α°, (sensor to mine 2 axis)	α°, (sensor to mine 1 axis)	β°, (axis mine 1 to maximum particle velocity vector)	t,ms (peak velocity from extra charge)	t,ms (peak velocity from main charge)
13	52	1.1	-	20.6	42.5	81±94	84±97	97	29.5	-
27.5	66	0.82	14.6	28.2	46	51±115	54±118	100	38.4	50.7
41.5	79	0.47	4.6	33	52.6	71±128	74±131	110	43.3	-
51	89	0.43	1.8	36	55.5	97±129	100±139	86	50.5	64

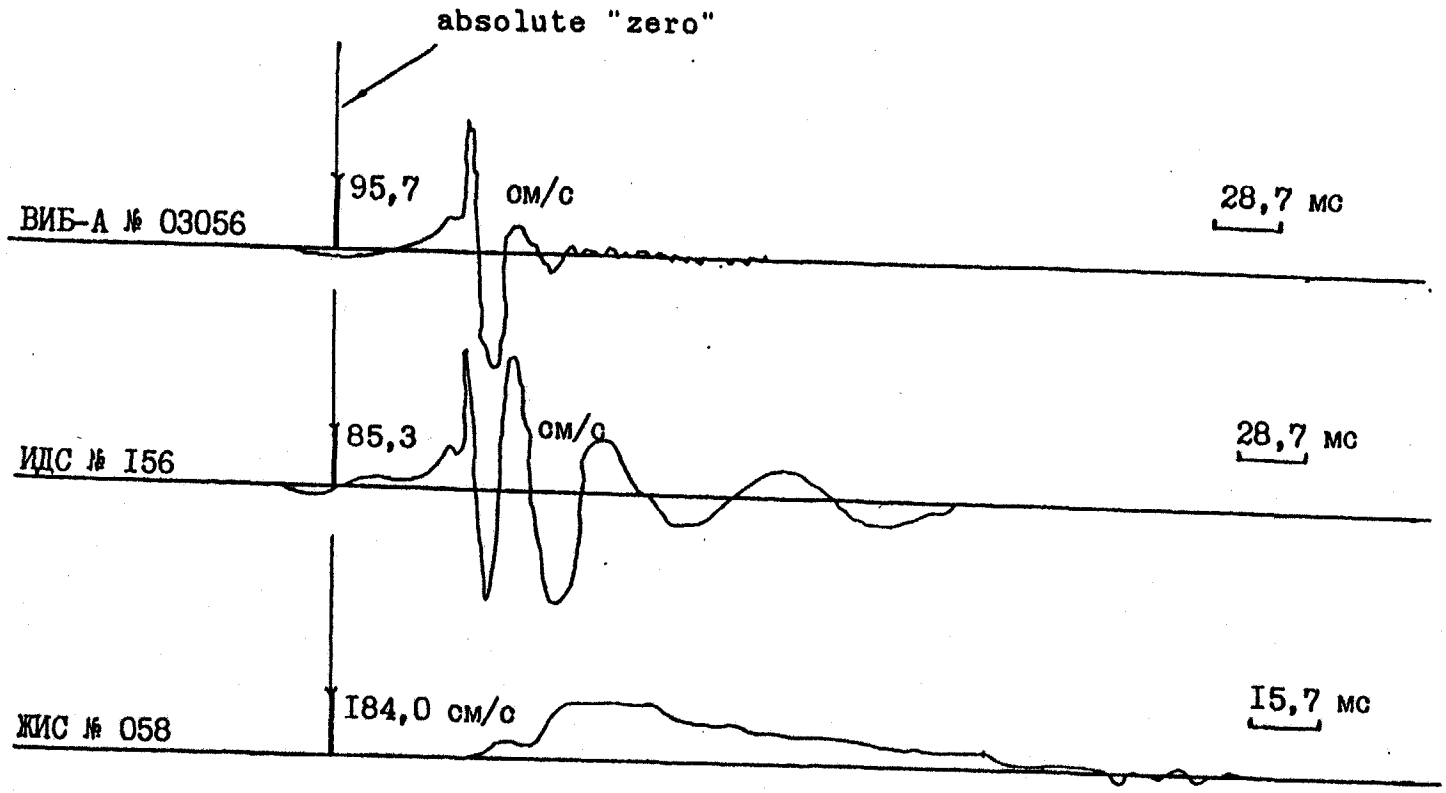

Figure III.28 Particle velocity records measured in the massif (point IV, R=51 m).

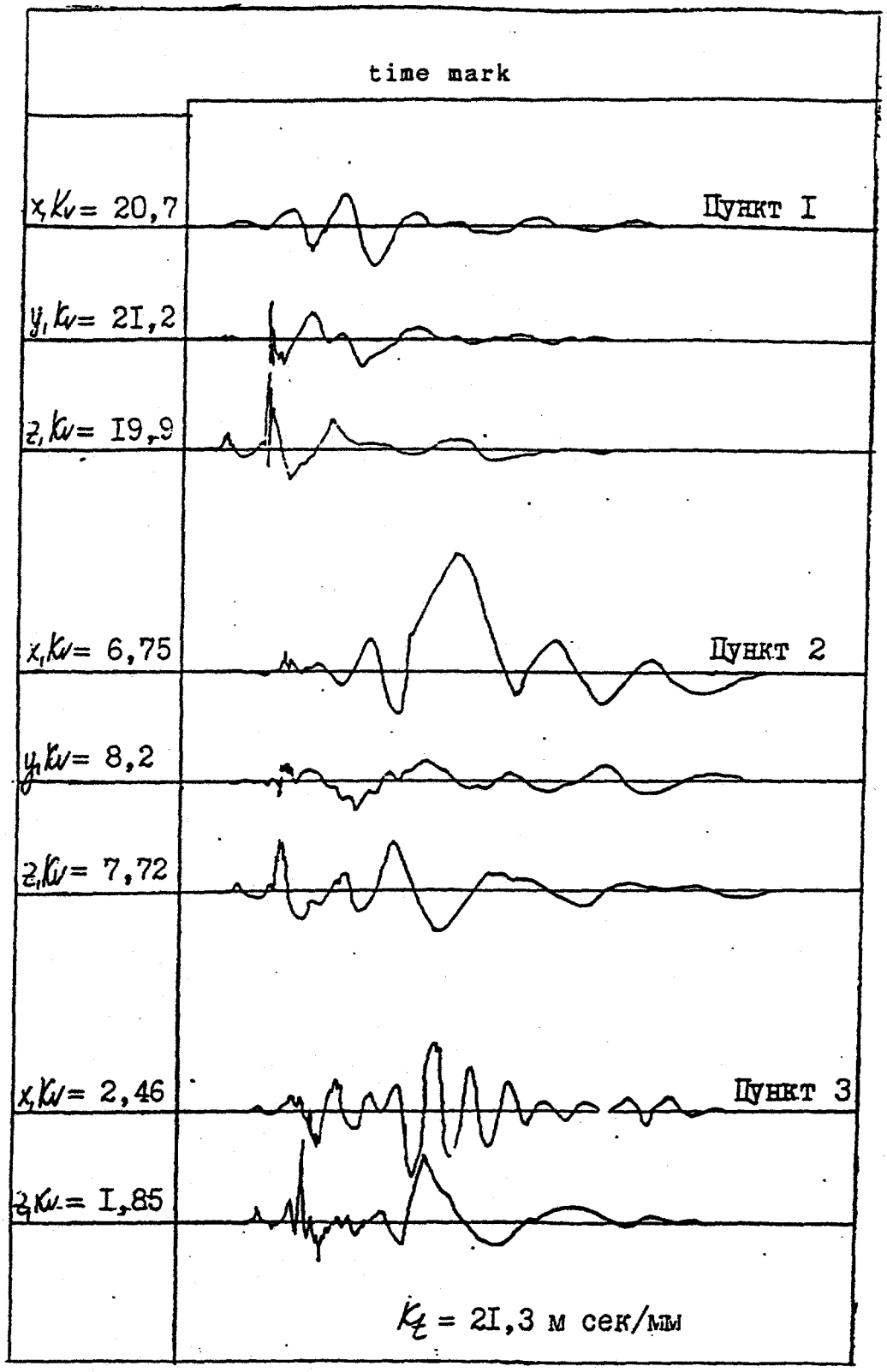

Figure III.29 Records' samples.

the seismic measurement sites 1, 2, and 3. Several wave groups can be distingished. Z-component at the point 3 favours to separate these groups. Three short-period peaks are distinct in the beginning of the record. Time/distance curve has been constructed to analyse these oscillations (Figure III.30). The curve also includes the date from the points 4 and 3 extra to the main profile. Elevation difference has been taken into account and time has been measured from the UTM.

Figure III.30 provides an opportunily to make following conclusions:

1. Time/distance curves of the three peaks are parallel. Thus, they correspont to the same wave type: longitudinal wave.
2. The three explosions "zero" times (88 tons, right side; 125 tons, and 470 tons, left side) can be distinguished.
3. From time/distance curves the sequence of the explosions is as follows: 88-tons explosion has been fired 60 msec after UTM, 125 tons in 190 sec, 470 tons - in 220 msec. Ground motion measured at the fifth point at the right side indicated that 2.3 tons explosion occured 20 msec before 88-tons explosion or 40 msec after UMT.

Unified particle velocity against scaled distance function can be constructed owing to longitudinal waves separation (Figure III.31).

Source/receiver distance was measured from the closest to a sensor charge side with absolute elevation difference taken into account. Relationship obtained by RMS method

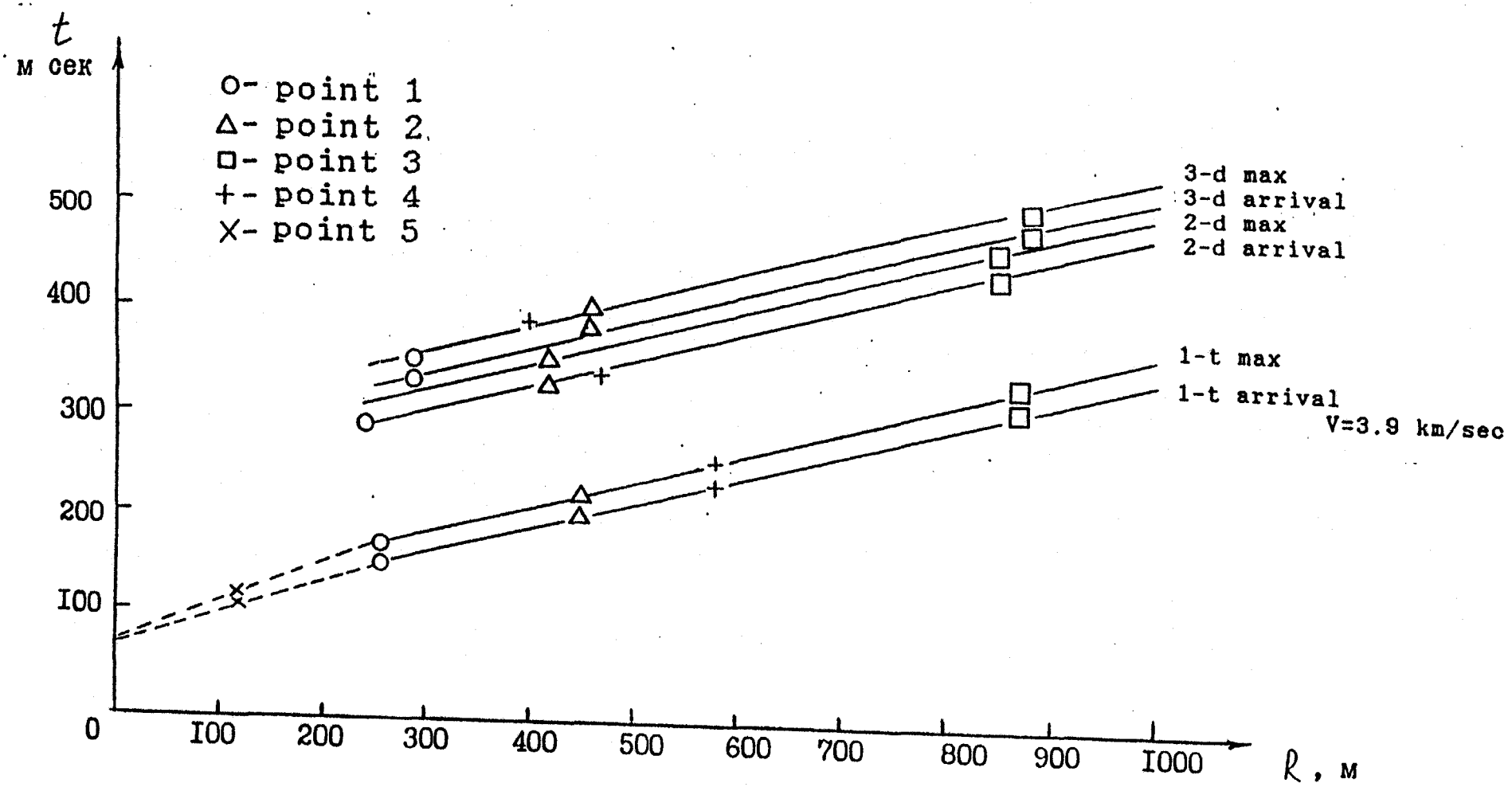

Figure III.30 Time/distance curves.

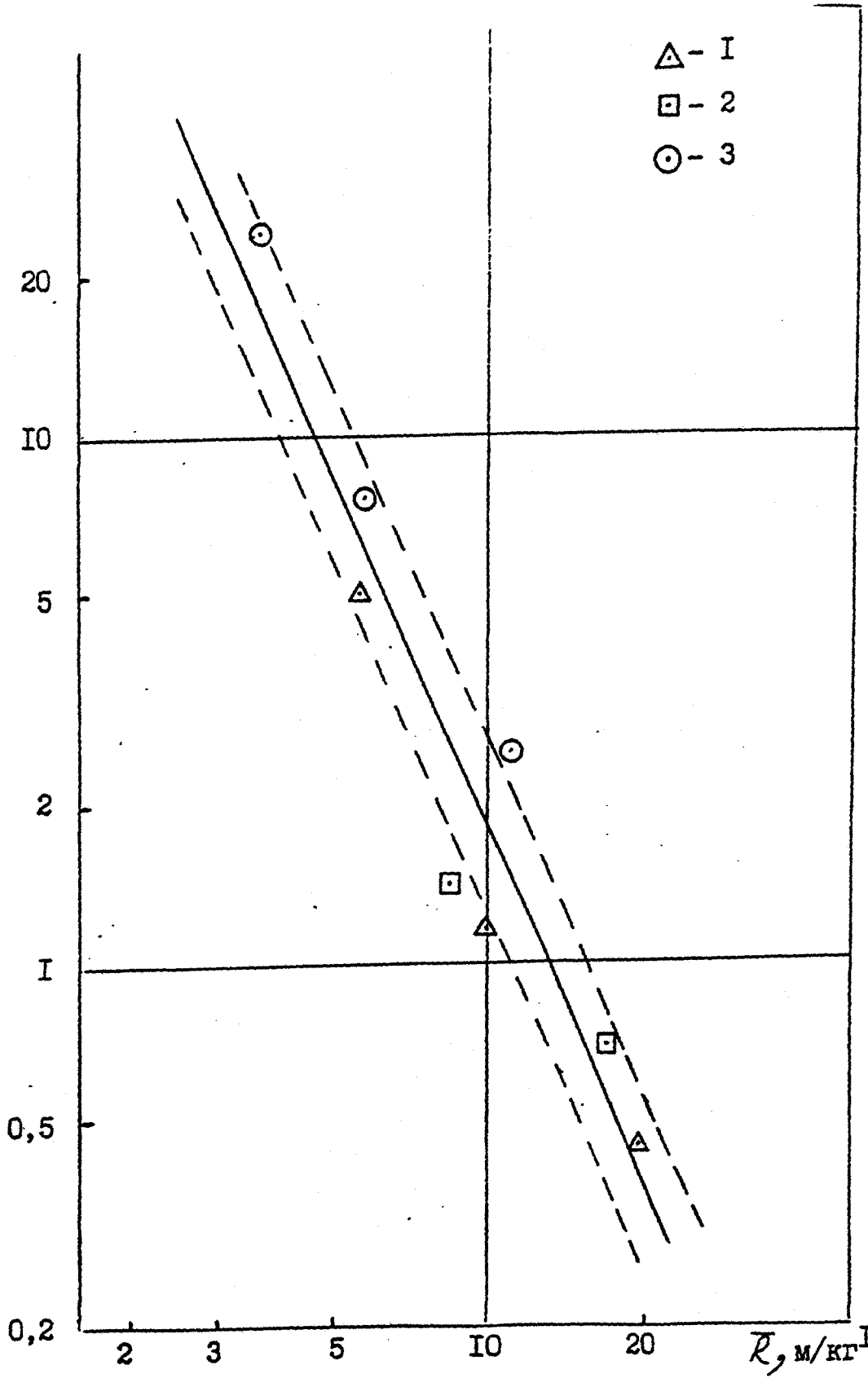

Figure III.31 Peak particle velocity in longitudinal wave vs. scaled distance 1-charge 88 t; 2-charge 125 t.

$$V = 330\left[\frac{q^{1/3}}{R}\right]^{2.25}$$

where V is the particle velocity measured in cm/sec, q is the charge weight in kg, and R is the distance in meters, is show by solid line. Standard deviation, σ=1.48, is shown by dashed line. Standard error of the exponent is of Δ=0.29. Periods of longitudinal waves generated by 88-, 125-, and 470 tons explosions are of 45, 50, and 65 msec respectively.

Table III.23 contains information on peak particle velocities in Rayleigh waves.

Table III.23

Point	1	2	3
V_{RX}, cm/sec	14.5	5.1	3
V_{RY}, cm/sec	10	4.5	-
V_{RZ}, cm/sec	10	7.7	2.2

Periods of Rayleigh waves were of 400 msec with propagation velocity of 2.6 km/sec. Local geological conditions disturbed wave field at the points N4 and N5. Only peak particle velocities could be measured (Table III.24).

Table III.24

Point	4	5
V_x, cm/sec	32	-
V_y, cm/sec	8.3	3
V_z, cm/sec	55	41

Thus, the relationship of the type $V = A(q^{1/3}/R)^n$ has been estimated for particle velocity measured at Z-component along the main profile. The relationship is close to that of concentrated charges (A from 200 to 800, n from 2.0 to 2.3).

Measured values of longitudinal wave periods (T from 45 to 65 msec) are well discribed by relationship $T=4a_m/V_p$, where a_m is the maximum size of the zone of inelastic deformation for concentrated buried explosion, V_p is the longitudinal wave velocity. For chemical explosion in granite $a_m/q^{1/3} \cong$ 0.6 $m/kg^{1/3}$. These values give for a_m=45 m and V_p = 2.6 km/sec a period of 70 msec.

C.Far-field seismic measurements.

Nine portable seismic stations ranging from 5 to 145 km have been deployed to measure three-component (X, Y, and Z) displacement and particale velocity. Six of the nine were in the same azimuth: to the south-west from the epicenter with a deviation of $\pm 15^0$. The three other stations were to the west and south of the epicenter at a distance of 20 to 30 km within the Ketmen-Tube depression where seismic waves amplitude supposed to

be enlarged by thick unconsolidated low-velocity sediments.

Also, special measurements were conducted inside (crest and basement) Toktogul power station aiming to get knowledge about seismic wave effects on such a construction. Horizontal components of the sensor were oriented along and perpendicular to the construction.

Table III.28 summarizes the information about the seismic stations. Figure III.32 presents the relative positions of the stations. Source/receiver distances have been obtained from a 1:100,000 scale map. Due to inhirent map errors the seismic stations locations and azimuths were of about 0.5 to 1 km and from 2^{o} to 3^{o} (Toktogul town, Toktogul station, Kara-Kul, Andizan).

The site of the experiment was situated within Tan-Shan mountains which are separated into few parts. The seismic stations were placed inside two of them: central part which is to the north-east from the Fergana Ridge (stations one through five), and southern which surrounds the Fergana Ridge and the territory to the south and south-west from it. (Kara-Kul, Tohtogul power station, Tashkumyr, and Andyzan stations). The Central Tan-Shan includes a system of mountains and valleys. The Ketmen-Tube depression is one of the valleys. It is surrounded by the Talass and Sasumyr Ridges from the north, and the Takhtalyk and Kakerim-Tau Ridges from the south. The Ketmen-Tube depression is elongated from the north-west to south-east. The lenght in this direction is of 100 km. The depression elevation

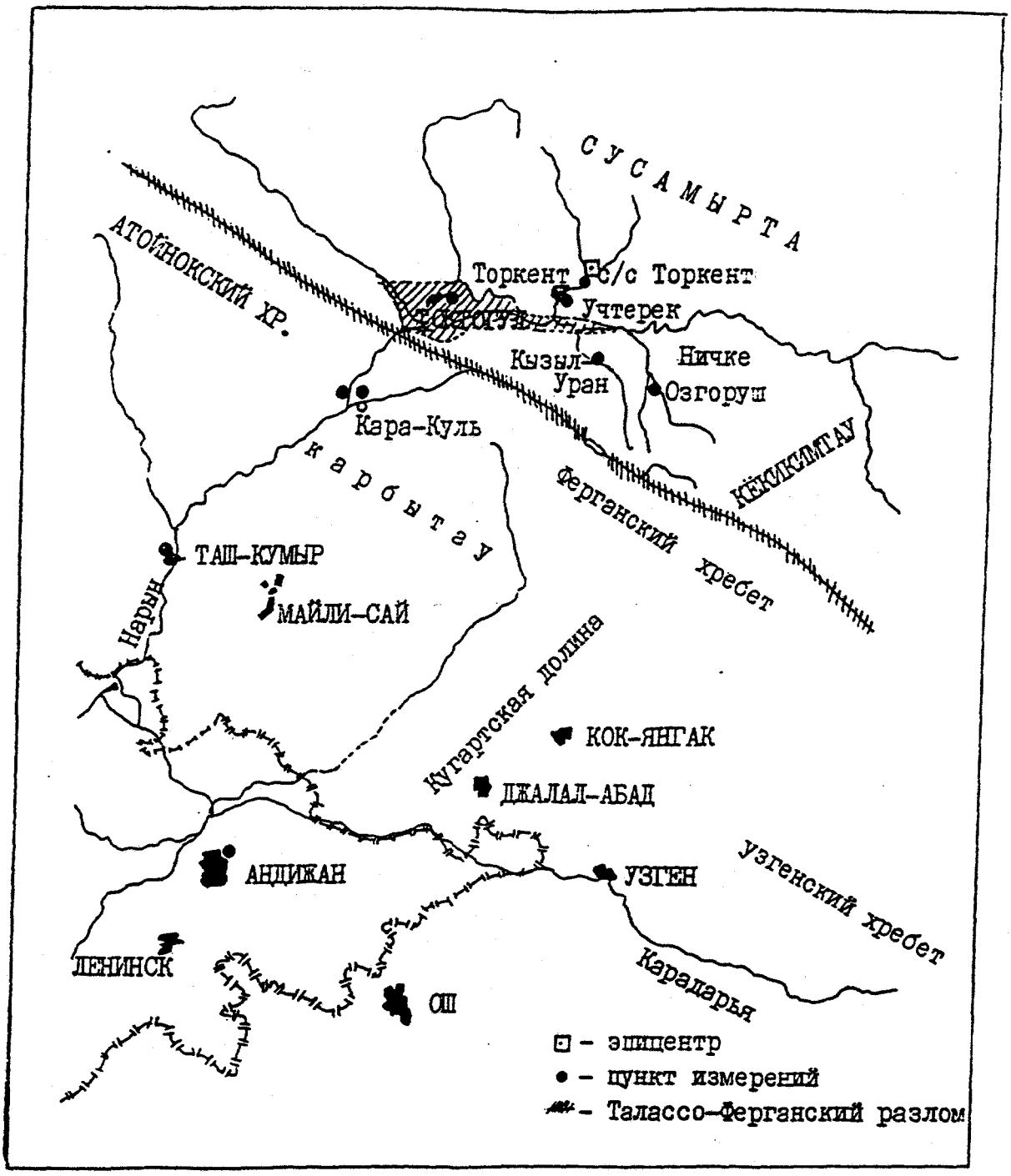

Figure III.32 Sheme of the site.

List of titles and names of Figure III.32

СУСАМЫРТА	-	Susamyrta
Атойнокский Хр.	-	Atoinokskii Ridge
Ферганский хребет	-	Fergana Ridge
Кугартская долина	-	Kugartskaya valley
Узгенский хребет	-	Uzgen Ridge
Торкент	-	Torkent
с/с Торкент	-	s/s Torkent
Уч-Терек	-	Uch-Terek
Токтогул	-	Toktogul
Кызыл-Уран	-	Kyzyl-Uran
Ничке	-	Nichke
Озгорушь	-	Ozgorush
КЕКИКИМТАУ	-	Kekikimtau
Кара-Куль	-	Kara-Kul
Карбытау	-	Karbytau
Таш-Кумыр	-	Tash-Kumyr
Майли-Сай	-	Maili-Sai
Кок-Янгак	-	Kog-Yangak
Джалал-Абад	-	Jalal-Abad
Андижан	-	Andijan
Ленинск	-	Leninsk
Ош	-	Osh
Нарын	-	Нарын.
Узген	-	Uzgen

increases from about 770 m in the south-west part to 1800 m in the south-east part adjacent to the Takhtalyk Ridge. The Ketmen-Tube depression represents a basin of river Naryn. Rivers Torkent, Chichkan and Uzunakhmat coming from the Talass and Sasuman Riges are the principal right Naryn tributaries and Saregata and Kambarata - the left tributaries from the Takhtalyk Ridge. Two closest observational points (Torkent seismic station and Torkent town) were situated near Torkent river. The seismic station Kyzyl-Uran was placed near the river Saragata, on one of the r. Kambarata tributary - village Ozgorush, on r.Chichkan - Taktogul town. Beyond the Ketmen-Tube depression, near the place where right tributary r. Carasu flows into r. Naryn, observation site was situated in Kara-Kul. Kara-Kul is near the Fergana Ridge, observations were also fulfilled at the Toktogul hydropower station and nearby canyon wall. Next observation point was inside town Tashkumur where r. Naryn coming out of Fergana Ridge. Andizan seismic station was the most distant observation point. And was within the Fergana valley.

Five from the nine observation points were located inside the depression. Three facial structures of the Tan-Shan conjugate within the Ketmen-Tube depression. They are the Nothern, Chatkal-Naryn and Southern zones. The facial structures are characterized by different tectonic history during Paleozoic when geosyncline stage has been completed. A number of deep faults had been formed to that time. The main of the faults is the Fergana-Talass fault. Alpine tectonics has formed modern

pattern of the Tan-Shan mountains with the ancient faults beeing renewed during the process. The Ketmen-Tube depression has been completed in early Quarternary period. The depression is separated from the Naryn plateau by Talass-Fergana fault at the south-west, and by the Takhtalyk deep fault zone at the south. The Ketmen-Tube depression creation began in upper chalk period. Down-going motion from that time with the highest intensity in the lower Oligocene prevailed and red sandstones, gravelstone and conglomerates of 150 m thickness have been formed at the continent. During Neogene, along with clay and sand, well spreaded thin galogenic sediments (salt and gypsum) were formed.

Bending rate varied inside the Ketmen-Tube depression with the highest intensivity to the north-east from the Talass-Fergana fault of the Toktogul valley. Neogene sediments here as thick as 1300 m.

The Ketmen-Tube depression was separated from the Talass and Susamyr Ridges by a system of sublattitude faults during the lower Quartinary period. Differential vertical motions are characteristic for that time within the Ketmen-Tube depression. This motion has created a set of uplifts and hollows boundaried by faults. The Torkent and Saragata valleys are the examples. Proluvium sediments represented by breccias prevail.

The Ketmen-Tube depression is characterized by low crossed relief. Eight river traces are distinguished which correspond to three complexes by age. The upper (V-VIII) terraces are represented

by the middle Quarternary sediments and are formen by gravel with sand and gravelly layers. The thickness of these middle Quarternary alluvial sediments is Of 40 to 150 m. Glacial sediments with big stones and gravel are also widely spreaded on the sides of ridges.

The upper Quarternary (Q_3) stage is presented by moraine sediments of the second ice period which are not well spreaded and filling narrow canyons along ridges slopes: proluvium sediments of cone shape downgoing into the Ketmen-Tube depression (gravel, crashed rocks, sandy loam) and mainly by river sediments forming the upper river terraces III and IV.

Modern stage Q_4 is presented by river sediments of the bottom and two upper terraces (gravel and sand) widely spreaded in all the canyons; proluvium sediments folding the upper stage (unsorted fragments and sand loam); slides and delluvium-gravitational complexes created near the sharp slopes.

It is common considering seismic effect as dependent on local geological condition beneath receiver. Following specific features beneath the seismic stations can be derived from geological conditions.

As was mentionad above, observational points seismic station Torkent, Torkent town, Kyzyl-Uran, Ozgorush, and Toktogul town were within the Ketmen-Tube depression. Its own pecularities, however, relate to each station. Seismic station Torkent is situated at outcrop of the upper Caledonian granitic intrusion without any sediments above. Torkent town (5 km down

the river Torkent) is situated in the center of the local Torkent depression formed by Neogene and Quarternary sediments. Kyzyl-Uran is within the Saragata depression filled by Neogene sediments. Ozgorush has to have thinner sedimentary layer beneath the station in comparision to Torkent and Kyzyl-Uran since it is near the Takhtalyk Ridge. Toktogyl town at river Chichkan is several kilometers from Naryn river and stays on thick sedimentery layer (N+Q) folding the Toktogul depression with the highest thickness of 1.5 km in the center.

Seismic oscillations' intensivity can be dependent on these pecularities. The observation sites in Kara-Kul, on the side of Toktogul dam and Tashkumyr town are in similar seismic geological condition but different from closer stations. They are situated within the Naryn massif formed by metamorphic rocks with little sediments above. The Talass-Fergana fault could effect on seismic records obtained at these stations. Seismic studies has shown that seismic waves amplitudes decreases in two times then crossing the fault. Finally, seismic station Andizan inside the Fergana valley stays on thick sedimentary layers with the sand upper layer.

According to the project of the explosion, the charges have been placed in galleries of the right bank (2.3 and 88 tons) and left bank (125, 18 and 470 tons) at Burlykyay river.

As measurements in nearby zone showed, all the charges detonated on each bank were fired simultaneously with time delay as short as 20-30 msec. Considering the highest seismic records

resolution of 20 msec, it is possible to assume that seismic signals have been generated by two charges of left (613 tons) and right (90 tons) banks. Time delay between the two charges is of 160 msec.

The left bank and right bank charges are far from each other. So they did not effect each other. Thus, resulting seismic wavefield is a linear superposition of the oscillation generated by each of the explosions. Time delay between two signals arrivals as well as predominant periods of oscillations will determine the possiblity to separate the two signals.

The record obtained at the Torkent seismic station (the closest site), is shown in Figure III.33. Two distinct arravals P_1 and P_2 following in 150 msec are clear. The signals have equal periods of 0.15 sec. Thus, synphase interference can be expected in the following parts of the record due to mentioned arrival time difference of 0.15 sec. It is worth noting that the first arrival corresponds to 88 tons explosion since 2.3 tons expllosion generates signals undetectable by the equipment.

Synphase superposition of P_1 and P_2 signals at the Torkent seismic station can be proved by relative theoretical and experimental amplitudes comparison. Theoretical amplitude ratio calculated by relationship

$$\frac{U_2^z}{U_1^z} = \left(\frac{q_2}{q_1}\right)^{0.8}$$

for the charges q_1 = 90 tons and q_2 = 703 tons for the waves P_1 and P_2 respectively is of 5.13 in good agreement with observed

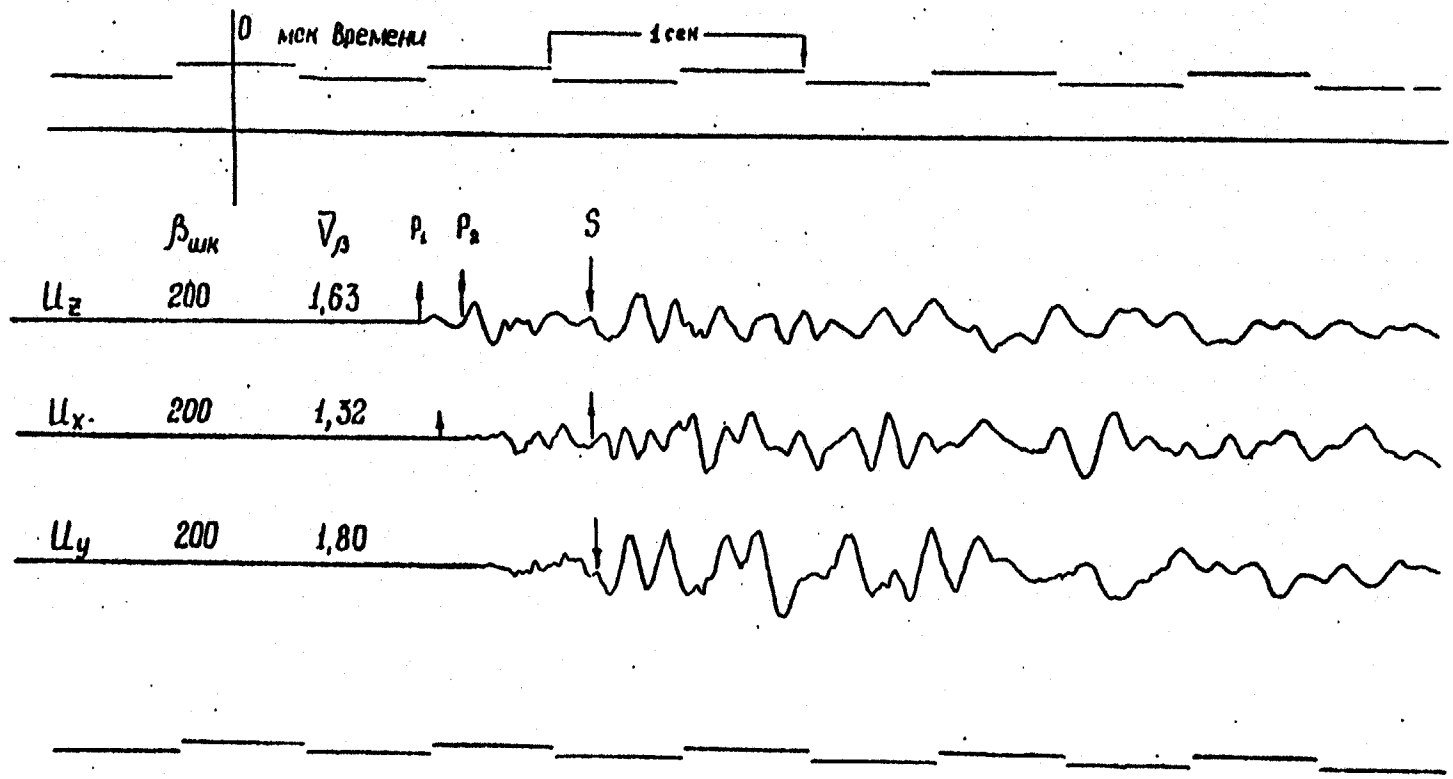

Figure III.33 Torkent seismic station records.

value U_2^z/U_1^z = 5.17 (Table III.26). In broader n range from 0.7 to 0.9 the amplitude ratio varies from 4.2 to 6.3.

"Pure" linear superposition of signals from the two explosions can be complicated by interference of different reflected and refracted inside the earth crust seismic phases. The more inhomogeneous is the crust the higher the complexity of record.

Records from almost all the stations showed distinct P_1 and P_2 phases corresponding to the left bank and right bank explosions respectively. Only the Andijan station with low recording rate (Table III.26) did not show the two phases. Averaged time delay between P_1 and P_2 from remote stations (Table III.26) is of 160 msec. Mean amplitudes ratio is of 5.1 to 5.2 with high data sccitering.

It is important noting that superposition of the oscillations with periods of 0.1 (Ozgorosh, Table III.26) and 0.3 sec (prevailing periods at some stations) corresponds to destructive interference decreasing total seismic effect. Maximum decreasing relative to synphase superposition, estimated from relationship (1) is of 30 to 40 percents for the given charges.

High-frequency and low amplitude phase disturbing the principal signals is clear at the Torkent seismic station records. This phase is traced to a large distance. Features of the phase make it possible to relate it to stone avalanches during the slopes collapse.

Table III.26 Time delay and relative amplitudes of two signals related to the main charges of the left and right banks

Point	Distance, km	Azimuth to epicenter (real)	Time delay, sec	Visible periods		Relative amplitude, vertical component	
				T_{P_1}, sec	T_{P_2}, sec	W_{P_2}/W_{P_1}	U_{P_2}/U_{P_1}
Seismic station "Torkent"	5.00	43°20′	0.15	0.15	0.15		5.17
v.Torkent	9.32	53°20′	0.17	0.14	0.15	3.5	5.0
v.Kyzyl-Uran	19.0	0°	0.16	0.07	0.07	8.3	2.9
v.Ozgorush	28.0	327°20′	0.15	0.10	0.10	4.50	5.75
t.Toktogul	27.8	88°40′	0.16	0.16	0.20	7.6-3.3	7.2-2.8
t.Kara-Kul	55.5	59°30′	0.26				
t.Tash-Kumyr	102.6	55°40′	0.16				

Two arrivals in 14.28 and 14.60 sec after the first P_1 arrival were recorded which correspond to air-shock wave. These signals have a period of 0.025 sec (40 Hz) and amplitudes ratio of 5, i.e. the same as measured from seismic waves. Arrival times difference is of 320 msec, however, in comparison with 150 msec measured from seismic records. This discrepancy can be explained by differences of seismic and acoustic waves generation or by different distances from the charges to the observation sites which is most imporvant for acoustic wave with low velocity of propagation.

The Earth's crust of the Eastern Uzbekistan and North-Western Kirgizia is characterized by complex blocky structure. The structure is studied by seismic observations of earthguakes and explosions. Large faults usually separate different blocks separating zones with different seismological features.

The Eastern Uzbekistan is studied thoroughly as well as the territory of Kirhgizia to the south from the Talass-Fergana fault. Kirhgizia in whole is studied in less detailes, however, and velocity models are limited by simple homogeneous layered medium for various regions.

Specific crust massif - the Fergana-Chatkal block is separated by different geological and geophysical tectures to the south from the Fergana-Talass fault where the stations in the range from 50 to 145 km have been established.

No detailed geophysical model of velocity distribution is

available now for the nothern region of the experiment (stations from 5 to 50 km) with the closest region - the Chui depression situated to the north of the Ketmen-Tube depression beeing studied in detail. Fergana-Chatkal's block and Chui's depression principal characteristics are presented in Table III.27. The former region is discribed by layered medium with gradients and the letter by simple homogeneous layered medium.

Geophysical interpretation allows to relate the layers with averaged velocities, V_p, from 4.5 to 5.0 km/sec as beeing Mezozoic complex of 4 km thickness, and the layers with $\overline{V}_p$ from 5.5 to 5.9 km/sec to high velocity Paleozoic complex of 20 km thickness. And, finaly, the layers with averaged V_p velocity from 6.1 to 6.8 km/sec relate to crustal granite-basaltic complex of the crust. Total crust thickness varies from 48 to 52 km over the territory of the Eastern Uzbekistan and Kirgizia.

Table III.27 Fergana-Chatkal block and Chui depression velocity models

Chui depression					Fergana-Chatkal block	
Depth range, km	First arrival range, km	$\bar{V}_p$, km/sec	$\bar{V}_s$, km/sec	$\bar{V}_{s-p}$, km/sec	Depth range	Velocity range, km/sec
0,2,3	0-17	5.0	2.9	7.0	0.7	5.0-5.7
2.3-6-15	17.5-75	5.9	3.45	8.3	7-22	5.7-6.3
6-15	75	6.2	3.6	8.8	22-28	6.0-6.1
					28-37	6.3-6.8
					37-46	6.1
					46-57	6.9-7.2
					58	7.8

A large number of different interfering seismic phases should be expexted due to a large number of different layers with velocity gradients and even low velocity layers. These phases should substitute each other in the first arrivals over the range of observations. Seismic stations placed at low velocity sedimentary layers showed much more complicated wave-field pattern due to reverberations in the upper low velocity layers.

Figures III.33 and III.34 present the records obtained at the observation sites put at hard rocks outcrops. The records are characterized by a simple shape of the waveforms with a few distinct arrivals in later parts (shear waves). Intensive and

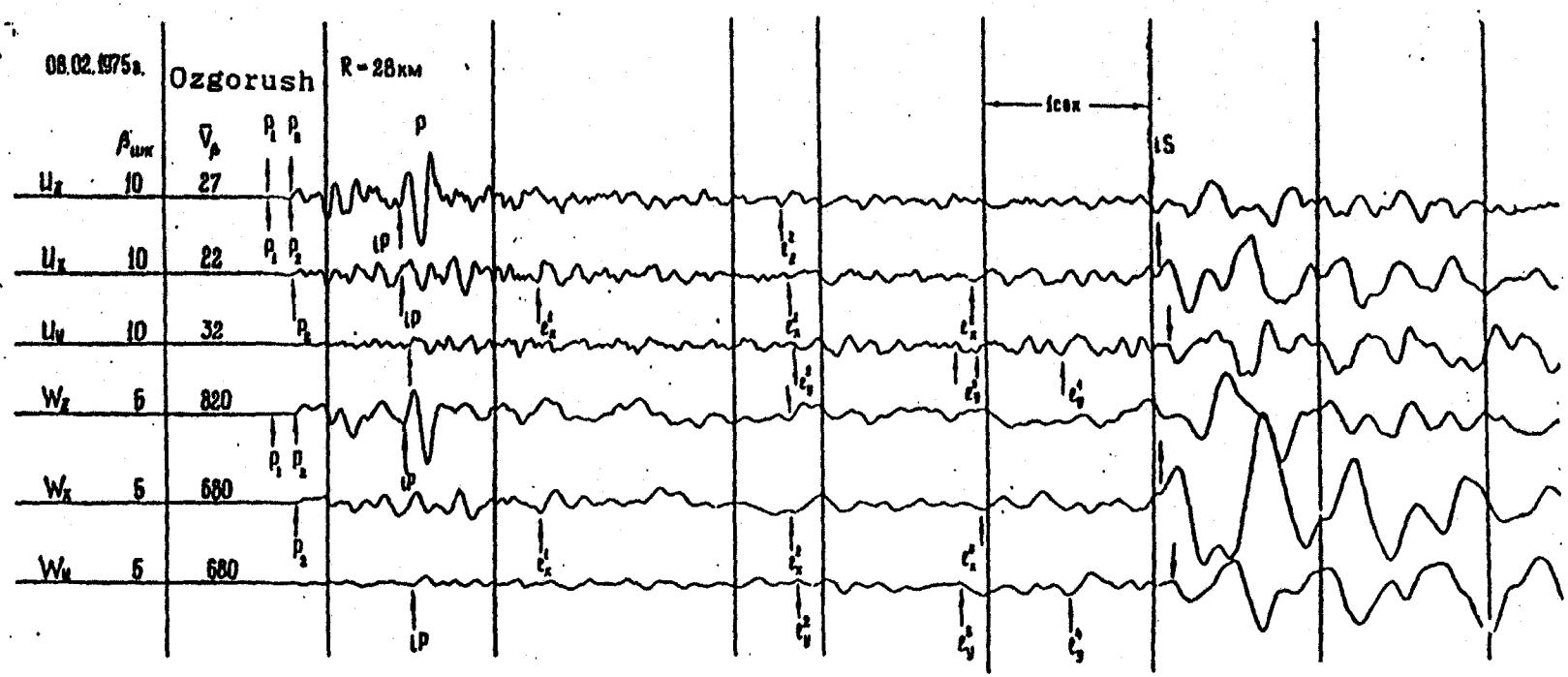

Figure III.34 V. Ozgorush records.

long oscillations are observed at the observation sites above thick sedimentary layers (Figure III.35). Shear wave arrival is practically unobservable and surface waves have larger amplitudes and duration.

It is hard to identify and trace seismic phases over the range of the observations due to different tectonic conditions and geological structures beneath the stations. These reasons as well as large spacing between the stations lead to high data scattering and low accuracy of time/distance curves.

Figure III.36 displays time/distance curves measured from seismic phases arrivals relative to Moscow time 10:00:00. All the first arrivals at the seismic stations were generated by the principal charge of 88 tons at the right bank, and the following arrivals were presumably generated by larger explosions of 595 or 613 tons yield detonated at the left bank of Byrlykyay river.

All the arrival times placed in Table III.28 can be recalculated into travel times of respective seismic phases considering absolute shot times of the first explosion to be 09:59:59.310±0.020 sec and that of the second one to be 09:59:59.4460±0.020 sec. These absolute times were estimated from averaged data on detonating signals, filming analysis, and seismic measurements in nearby zone (less than 1 km).

Dynamic characteristics: amplitude, period, wave shape were used in identifying of the seismic phases. Homogeneous layered model of the crust has been choosed with no refracted waves available. Refracted in the upper crust longitudinal waves, P_g

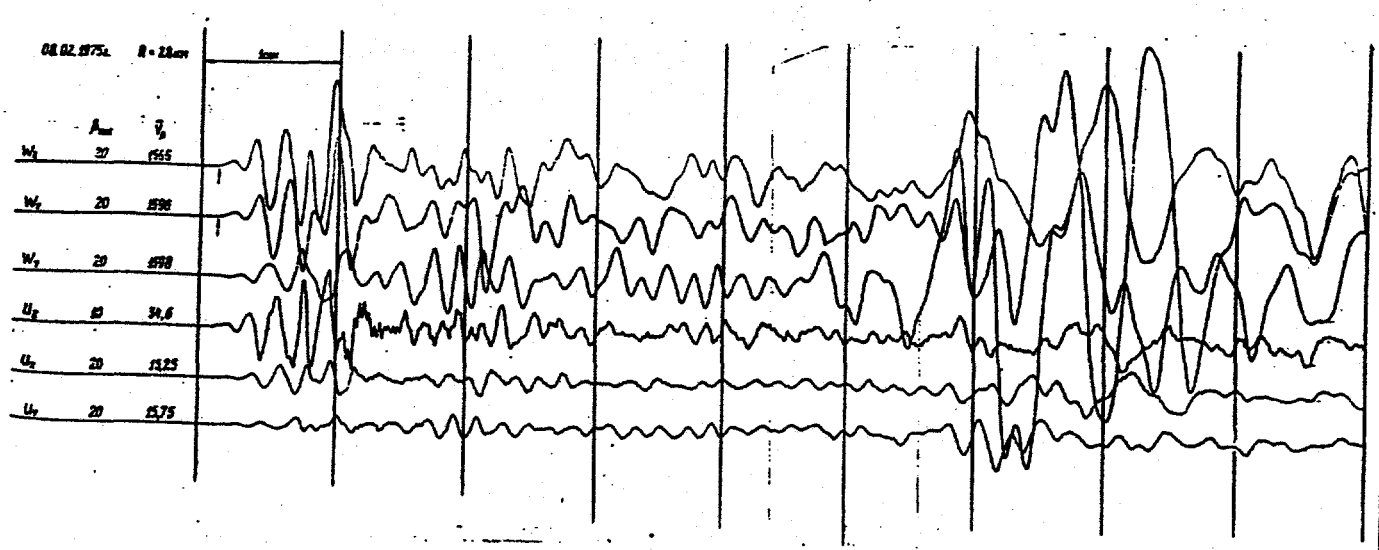

Figure III.35 Town Taktogul records.

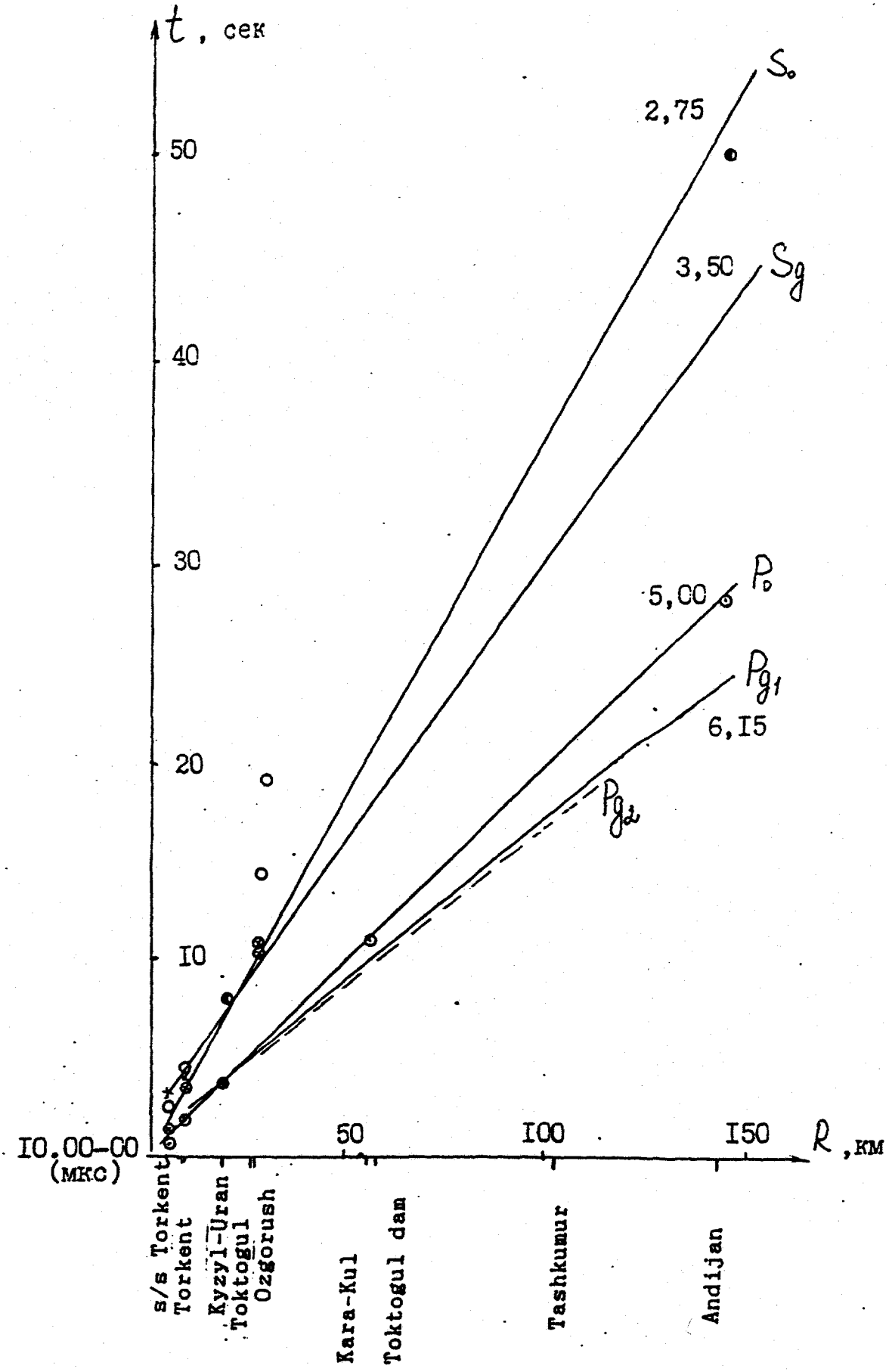

Figure III.36 Time/distance curves.

and P_o, in the first arrivals were, however, identified. Similar shear waves S_g and S_o observed in the following arrivals were also detected.

P_o- and S_o-waves with apparent velocities of 5.0 and 2.75 km/sec respectively can be interpreted as a wave refracted at the lower boundary of sedimentary complex (guide wave) (Table III.27). P_o-wave is in the first arrival from 5 to 25 km coming into followimg arrivals beyond 25 km with a few stations detected this phase. Modern and Neogene sediments induce some arrival time delay. Seismic stations Torkent and Ozgorush at hard rock outcrops measured arrival time 0.25 sec ahead of averaged time-distance curve. S_o-wave is distanct at these sites but hard to be distinguished from other oscillations at Torkent observation site staying on thick sediments. P_g- and S_g-waves are also refracted (or guide) and propagate presumably along the roof of crustal fundament (granite and basalt layers) complex. Measured apparent velocities of 6.15 and 3.50 km/sec are consisten with existing Fergana-Chathal block velocity models. P_g-wave is coming into the first arrival from 25-30 km. Seismic stations can be separated into two groups by the arrival times. The first group (Taktogul, Kara-Kul, Andijan) is characterized by larger travel times comparing to the second group (Ozdorush, Tashkumyr, Toktogul power station) staying at hard rock outcrops or shallow crustal fundament. Time differing is of 0.2 to 0.4 sec between these two groups. At Andijan station, arrival time is 1 sec late. This may be caused by thick sand sedimentary

Table III.28 Arrival times of selected seismic phases relative to absolute time 10ʰ00'00"

Point	km	Azimuth to epicenter, real	Azimuth magnetic	Longitudinal waves	Not identified phases of longitudinal wave	Shear waves	Not identified phases of shear and suface waves
1	2	3	4	5	6	7	8
s/s Torkent	5.0	43°20'	38°02'	iP^1_o 0.75 iP^2_o 0.90		iS_o 1.41 $i(S_e)$ 3.19	e 1.80 el 2.52
v.Torkent	9.32	53°20'	48°00'	iP^1_o 2.00 iP^2_o 2.17	e 2.65 e 2.80	iS_o 3.50 $e(S_e)$ 4.00	el 4.50
v.Kyzyl-Uran	19.0	0°	355°	iP^1_o 3.71 iP^2_o 3.87 $i(P_e)$ 4.00	e 5.14 e 5.54 i 6.14	iS_o 7.50	i 8.75 i 9.03 i 9.90
v.Ozgorush	28	327°20'	322°	eP^1_e 5.16 iP^2_e 5.31 $e(P_o)$ 5.50	iz 5.97 e 6.80 e 8.28 e 9.37 e 9.97	iS_o 10.54	el 14.27 el_2 19.01
t.Toktogul	27.8	88°40'	83°22'	iP^1_e 5.29 iP^2_e 5.47	iz 6.03 i 6.66 i 6.83 e 7.20 i 8.24 i 8.31	$e(S_e)$ 9.86 $i(S_e)$ 10.83	el_1 10.67
t.Kara-Kul	55.5	59°31'	54°45'	iP^1_e 9.94 iP^2_e 10.20 iP_o 11.03	e 11.94 i 13.40 e 14.40 i 15.24 e 17.01 i 17.31 e 17.64	$e(S_e)$ 18.28 eS_o 20.70	e 22.55 e 23.11
Toktogul dam	(56.5)	61°30'	56°45'	$eeP^1_{e_2}$ 9.78 $iP^2_{e_2}$ 9.90	$e(S_e)$ 15.98 eS_e 17.91		

1	2	3	4	5	6	7	8
t.Tashkumyr	102.6	55°40′	50°22′	$eP^1_{e_2}$ 17.16 $eP^2_{e_2}$ 17.32	e 5.14 e 5.54	iS 7.50	i 8.75 i 9.03
						iS_e 30.9	i 32.04 e 35.10
				iP_e 17.68	e 19.14 e 21.53		e 36.42 e 41.10
					e 24.16 e 25.05		e 43.10 e 44.70
					e 26.32 e 27.12		ee 45.97
					e 29.30		
t.Andijan	143	31°	26°	iP_{e_1} 25.25 iP_o 28.3	i 30.5 i 33.0	eS_e 42.5	i 46.0
					e 36.0	eS'_o 50.5	e 55.4
							el 39.0

layers know from geological survey. Two time-distance curves have been constructed for the two groups of stations marked by P_{g1} and P_{g2}. The stations at hard rocks outcrops show more distinct S_g and S_o arrivals.

Other arrivals can not be identified due to absence of stable dynamic characteristics and large spacing. Surface waves do not usually show distinct arrivals and can be traced only at some stations, with those beeing impossible to detect at some stations due to intensive previous oscillations. Thus, no time/distance curves have been constructed for surface waves.

Seismic waves' dynamic parameters were analysed only for the whole group of body waves because of large spacing and uncorrelated principal waves over the range of observations. In the body waves group before surface wave arrival peak displacement amplitude is W_{max}, with related period T_{Wmax}, and peak particle velocity amplitude is V_{max}, with related period T_{Vmax}. Also, dynamic parameters of only longitudinal waves W_p, V_p, T_{Wp}, and T_{Vp} were measured. All the there components: vertical Z, radial X, and tranversal Y were measured.

P-wave group: Peak displacement and velocity in P-waves against distance are presented in Figure III.37. Only vertical and radial components are shown as in other amplitude curves. Transversal component is always lower than radial and is not shown.

It is clear from Figure III.38 that vertical and radial components are commensurable but their ratio varies depending on

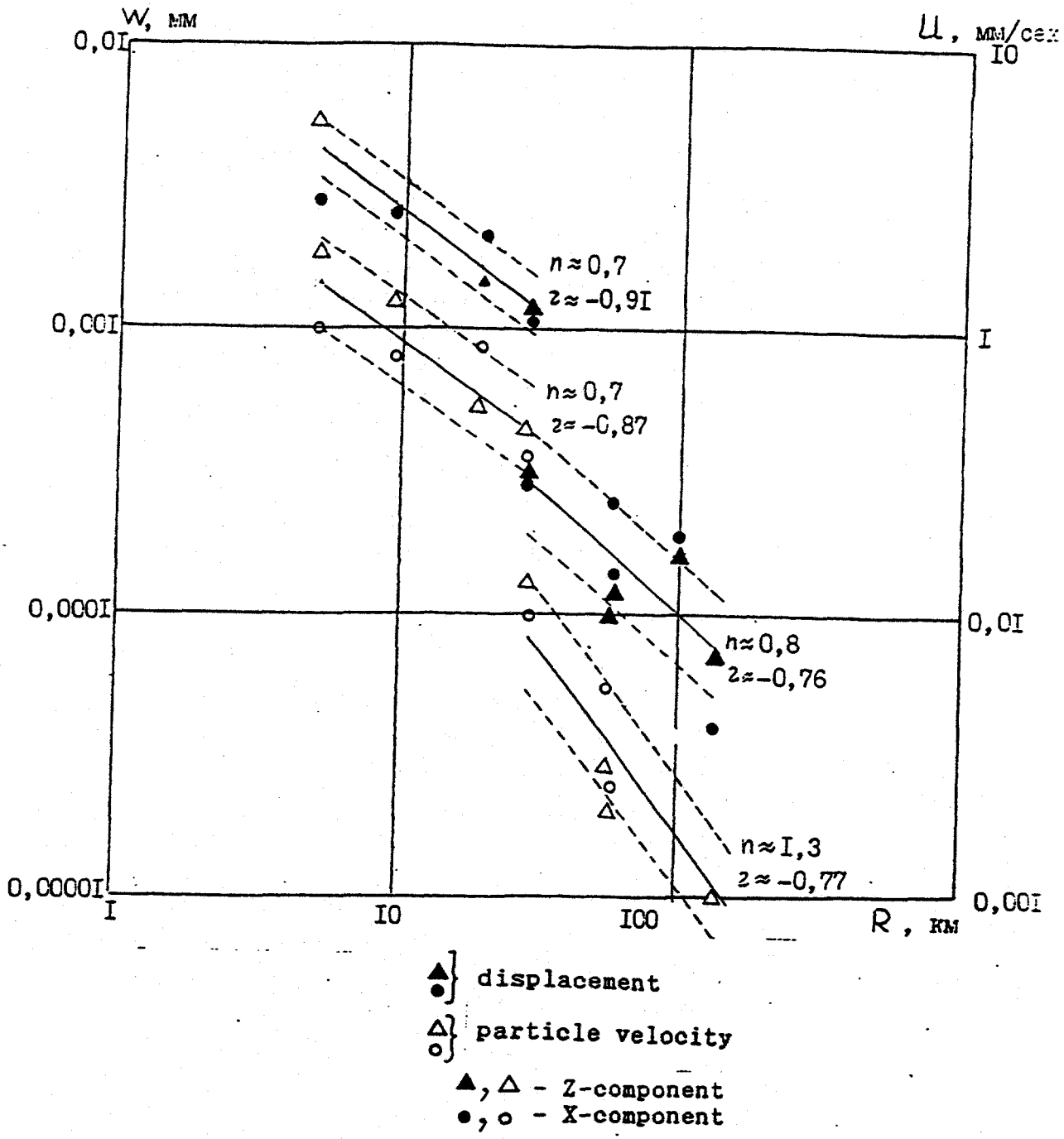

Figure III.37 Peak particle velocity and displacement in P-waves.

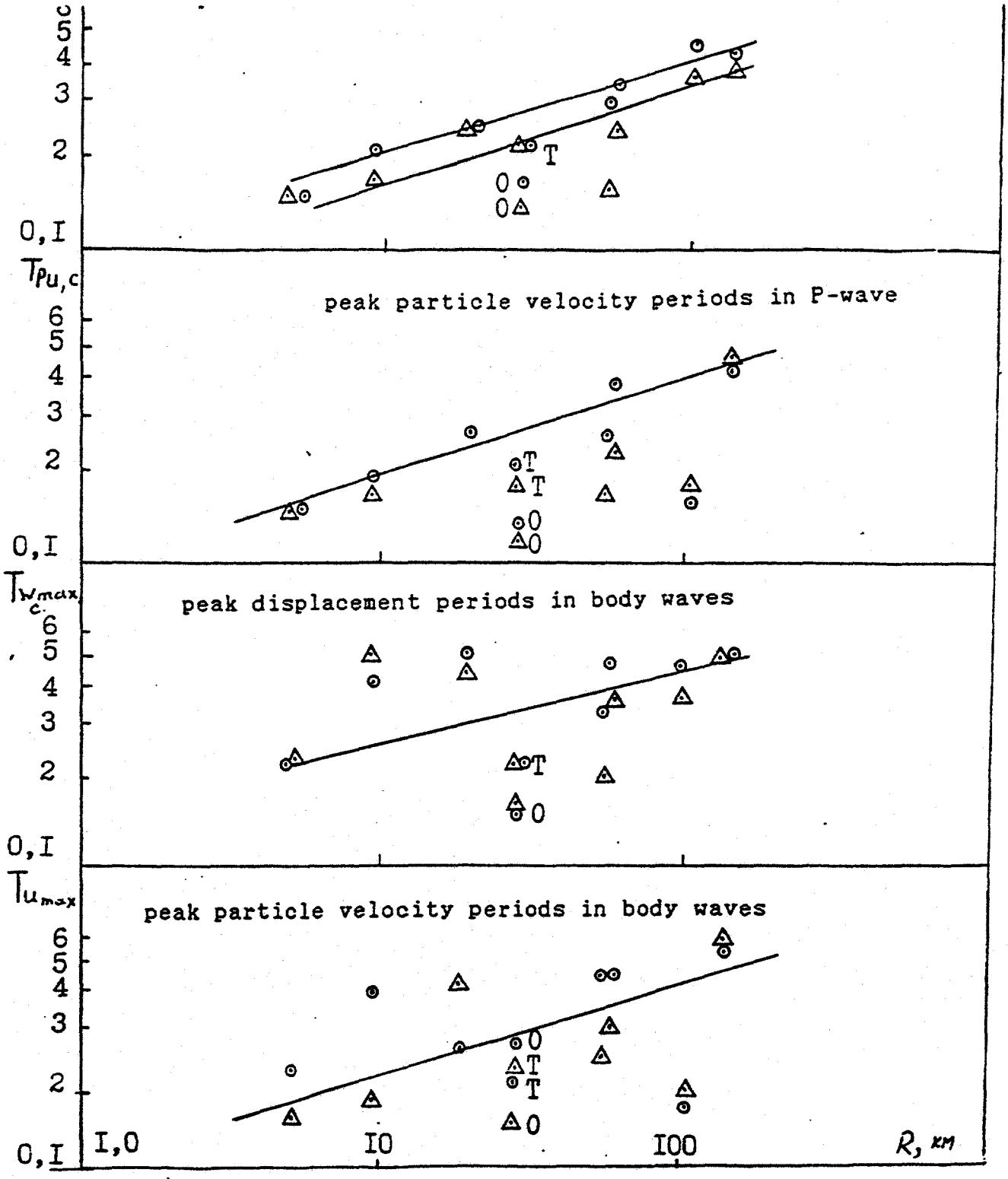

Figure III.38 Visible periods of peak phases in body waves.

station. Radial component is usually equal or smaller than vertical. Only Kyzyl-Uran (1.5 times) and Kara-Kul (2.5 times) stations showed larger radial component. Therefore, all the measured values were used to calculate linear regression by the least squares.

Two parts of amplitude curve can be separated. the first part of linear dependence is from 5 to 28 km and second one is from 28 to 140 km. The second part lays well below the first one. Peak displacement amplitudes measured at Ozgorush and Toktogul at the same distance of 28 km from the epicenter differ in four times for vertical as well as radial components. The larger the distance the higher data scattering. It is interesing to mentio that Tashkumur data (Z as well as X components) lay two times higher than averging line. Horizontal component of displacement at the side of Toktogul hydro-electric power station only half as large as that measured by Kara-Kul station at the same distance of 56 km while vertical components are almost the same.

Figure III.38 also shows P-wave periods related to peak displacement amplitudes. The periods are in the range from 0.5 to 1 sec. Exponential period increase with increasing distance with an exponent $m \simeq 0.3$ is characteristic. Both radial and vertical components obey this relationship, horizontal component period beeing usually larger than that of vertical component in P-wave group. The periods measured at Ozgorush observation site are half as large as those of Toktogul seismic station beeing at

the same distance.

Peak particle velocity vs. distance curves are also characterized by two ranges of linarity (Figure III.37), second part laying much lower. Similar displacement's curves features can be derived. Peak velocity amplitude measured at Ozgorush a quater as large as at Toktogul seismic station. Tashkumyr's peak amplitudes three times larger than the approximating line. Kara-Kul's horizontal velocity component is two times larger that of dam side.

The periods related to peak velocity values lay in the range from 0.5 to 1 sec, increasing as $R^{0.3}$. Ozgorush and Tashkumur stations have recorded anomalously low periods.

Body waves group (joint analysis). Figure III.39 displays peak displacement amplitude against distance in the whole body waves group. P, S and F characters near the points indicate that peak amplitude has been measured in P-wave, S-wave or following coda respectively. As clear from the Figure, peak amplitudes in all the cases except Tashkumur relate to unidentified oscillations group or coda wave. Vertical component is usually lower or close to horizontal one. The amplitude curve can be separated into two parts, as for P-wave curves, distance ranges beeing the same. The lines slopes in the ranges are the same and are of 0.9 to 1.0. Ozgorush and Toktogul horizontal component ratio of 3.5 holds, but vertical components ratio is of 2. Kara-Kul's and power station's horizontal components ratio also holds. Peak vertical displacement at Tashkumur was measured of

P-wave and radial one of S-wave. Figure III.38 also shows the periods.

Periods range from 0.15 to 0.5 sec with high data scattering. Thus regression is complicated, but one can note period increase with increasing distance. Both vertical and horizontal components' periods measured at Ozgorush as well as vertical component's period at Kara-Kul are anamalously low.

Table III.29 Regression coefficients obtained by the least squares

Component	first part			second part			all measurements		
	n	ρ	$\pm\sigma_{\lg A}$	n	ρ	$\pm\sigma_{\lg A}$	n	ρ	$\pm\sigma_{\lg A}$
	0.72	0.91	0.125	0.84	0.76	0.150	-	-	-
	0.99	0.91	0.140	0.88	0.76	0.155	-	-	-
	0.68	0.86	0.145	1.3	0.77	0.155			
	only radial component						1.66	0.97	0.155
	1.15	0.93	0.135	0.84	0.65	0.155	-	-	-

Peak velocity amplitudes in body waves for both vertical and horizontal components are presented in Figure III.39.

In most cases, peak displacement and velocity values relate to coda wave (F). Both vertical and radial components peak amplitudes at Tashkumyr were measured in P-wave as well as vertical peak amplitude at Torkent village. Vertical component is 1.2 times lower than radial one, as a rule. Both components were used in regression analysis. Two ranges (5 to 28 km and 28 to 145) are also separated for peak velocity measured in the

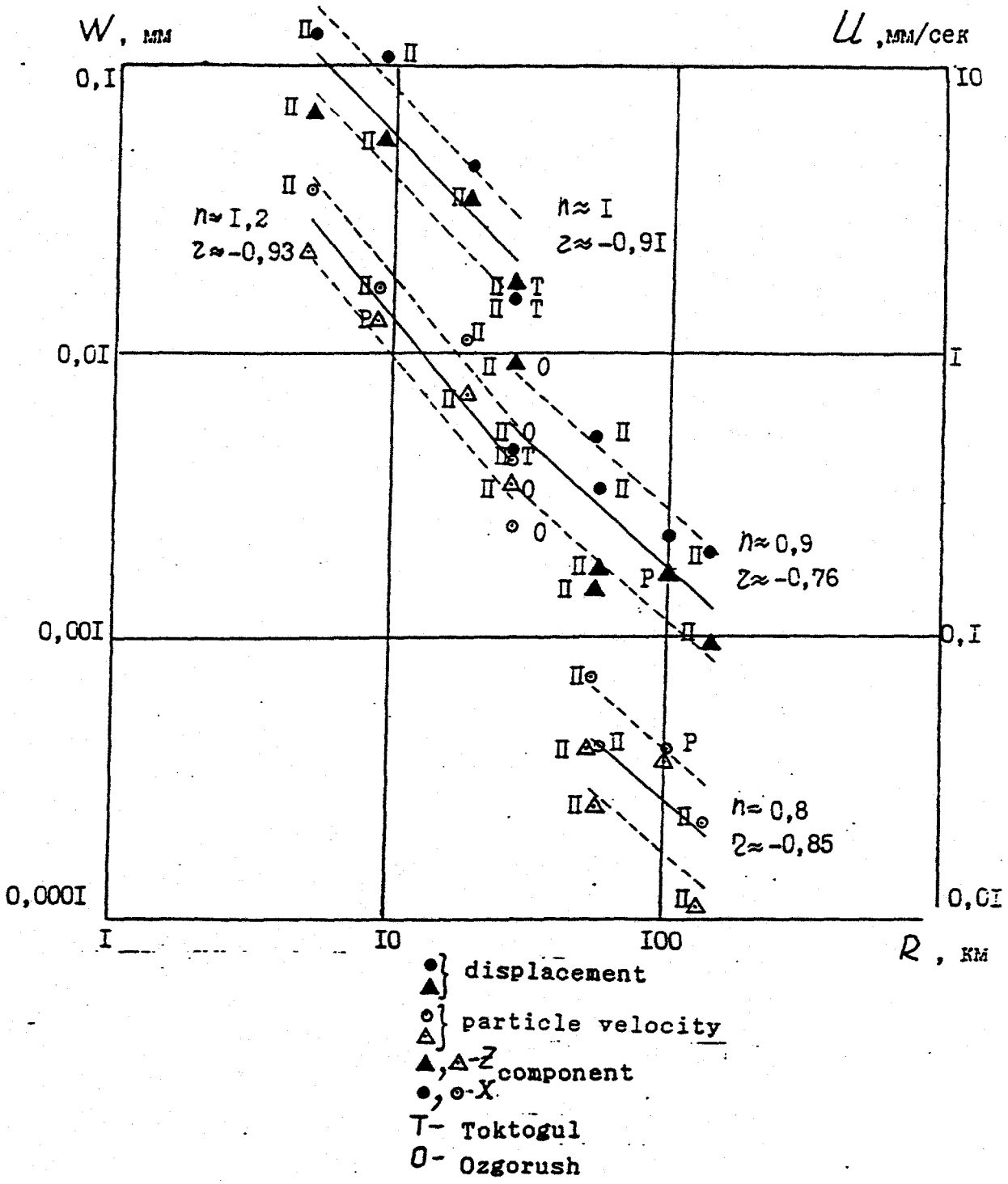

Figure III.39 Peak displacement and particle velocity in body waves group.

whole body waves group as previously for amplitude curves shown in Figures III.38 and III.39. These two parts of the amplitude/distance curve also differ in amplitude and are characterized by the same attenuation (Table III.29). Ozgorush measured amplitudes are also lower than those of Toktogul, but the ratio is smaller (only 1.5 instead of 3.5-4). Therefore , these two points are included in the first part of the amplitude curve, increasing the first regression line slope and decreasing the second one slope. Kara-Kul/Toktogul power station amplitude ratio holds for peak particle velocities in body waves group. Tashkumyr data are above the regression line.

The periods related to peak velocity grow with distance as $R^{0.3}$. Anomalously low periods were measured from both vertical and radial components at Tashkumyr and from vertical component at Ozgorush. Following conclusions can be derived from the amplitude/distance curves and periods analyzed above. All the amplitude curves can be separated into two parts with different linear regressions. These parts relate to the ranges below and beyong 28 km. The second regression line's level is lower than the first one, with the ratio at 28 km being of 4 to 5. This amplitude difference can be explained by local geological conditions. All the stations below 28 km are situated within the Ketmen-Tube depression. Other stations placed within the Naryn massif and Fergana valley are isolated from the explosion by the deep and wide Talass-Fergana fault. Station Ozgorush is the only exclusion. At all the amplitude curves except estimated from

peak velocities in the whole body waves group, Ozgorush data belongs to the second part. This phenomenon can be explained by following consideration. Station Ozgorush was near the Takhtalyk Ridge and installed at hard rock outcrop, while other stations were placed within the Ketmen-Tube depression at soft sediments of Neogene and Quarternary age. Geological conditions' effect is possible to illustrate by a comparizon of Ozgorush and Toktogul records. Station Toktogul stays at a sedimentary layer of about 1.5 km thickness and is characterized by considerally larger amplitudes and longer periods of oscillations than Ozgorush.

Other pecularities of the amplitude/distance curves can be also explained by effects of geological structure beneath the stations. For example, radial component measured at Kara-Kul is always higher than at Toktogul dam side because of the letter station is inside a tunnel, and the former one is inside Karasu river valley.

Besides regression analysis in the two ranges, whole range regression line was calculated. Only peak radial values were involved unlike other amplitude curves where both radial and vertical component of ground motion is of principal imporatnce for seismic hazard studies, seismic wave amplitudes are predicted by this curve. So, the regression line in the whole range was calculated to compare obtained and existed curves. Figure III.40 displays obtained curve as well as the curves for 1 kt explosion in granite, tuff, salt, and alluvium. Burlykyay's curve lays below that of granite, but total weight of the

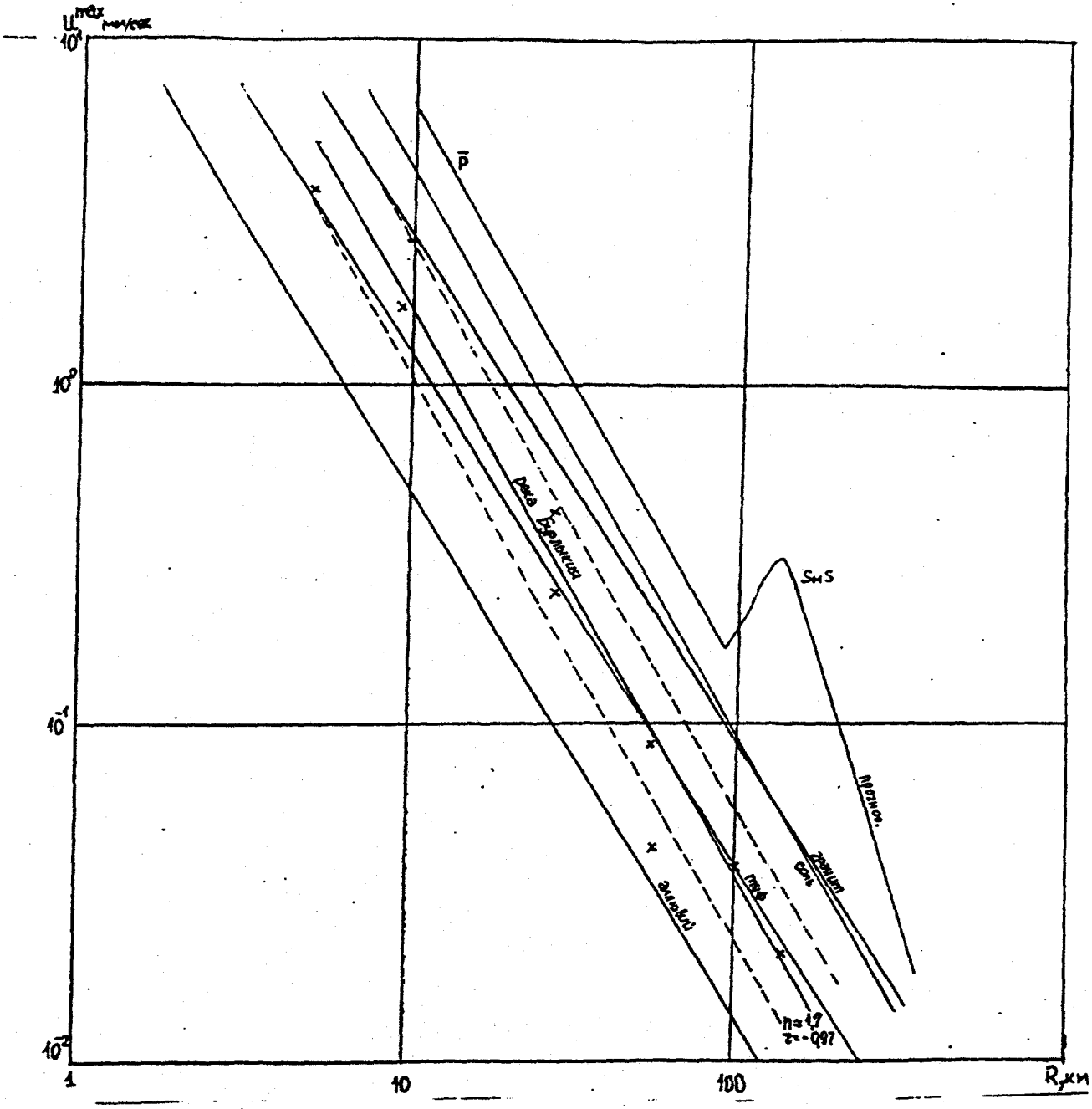

x- measured amplitude

r.Burlykyay - least squares regression line

- - - confidence level (standard deviation)

Figure III.40 Peak particle velocity from the Burlykya explosic and 1 kt explosion in various media.

explosion was only 0.7 kt with extra attenuation due to negative interference of the right and left bank charges. If comparing with 1 kt concentrated explosion Byrlykyay's signal amplitude could be from 1.4 to 1.7 times lower, the estimation including lower total weight and negative interference.

The whole range amplitude/distance curve is characterized by larger attenuation (proportional to $R^{1.7}$) comparing with the others curves. This is caused by large amplitude drop when seismic waves cross the Talass-Fergana fault (stations from 55 to 140 km). Measured amplitudes values are well approximated by regression line (correlation R=0.97). Only two points are beyond standard error ($\pm\sigma$). Geological conditions beneath these two stations can explain this deviation, as discussed above.

Investigations of Toktogul dam vibrations.

Before constructing Toktogul reinforced concrete dam, special investigations of the Naryn river canyon sides vibrations depending on height were conducted. It was shown that vibration amplitude increases with increasing height above the bottom, with horizontal component at the canyon side being several times larger than at the bottom. Dependence of vertical component is considerably weaker. Similar case has been investigated on an example of soil dam inside a canyon. The dam effect on the canyon side has been studied. It has been shown that the dam ridge (52 m high) and the adjacent canyon side has oscillated in similar way, but horizontal component along the canyon is four times larger than along the dam ridge. At the

natural period of the dam oscillations and far enouth from the dam, oscillations amplitude was 6 times lower than at the dam ridge. Construction of Toktogul dam had not been finished before the experiment. The dam body could be represented by reinforced concrete wedge 145 m high. The dam ridge was 210 m long and 75 m wide. The dam base was 15 m long and 250 m wide along the river.

To study the dam vibrations induced by the explosion at Byrlykyay river 56 km for from the dam the measurements of dispalcement and particle velocity were conducted in three points. Two observation points were inside the dam body: near the basement (absolute elevation 725 m) and near the ridge (absolute elevation 825 m). Both points were at one vertical axis centring the dam (respectively to the canyon axis). The third observation point had absolute elevation of 875 m and was placed inside test gallery of the left side of the canyon. The point was placed 20 m down river from the dam ridge axis and 25 m above the ridge. The distance from the point to the free surface in vertical direction was of 70 m.

Figure III.41 presents cross sections of the dam with observation point marked. Three components of motion displacement and velocity were measured at each point. Common seismometer was used for each component. Horizontal seismometers were oriented along (Y) and perpendicular (X) to the ridge (approximately along the canyon axis) then installed inside the dam body. When installed inside the canyon body, seismometers were oriented relative to the explosion epicenter, X-axis being

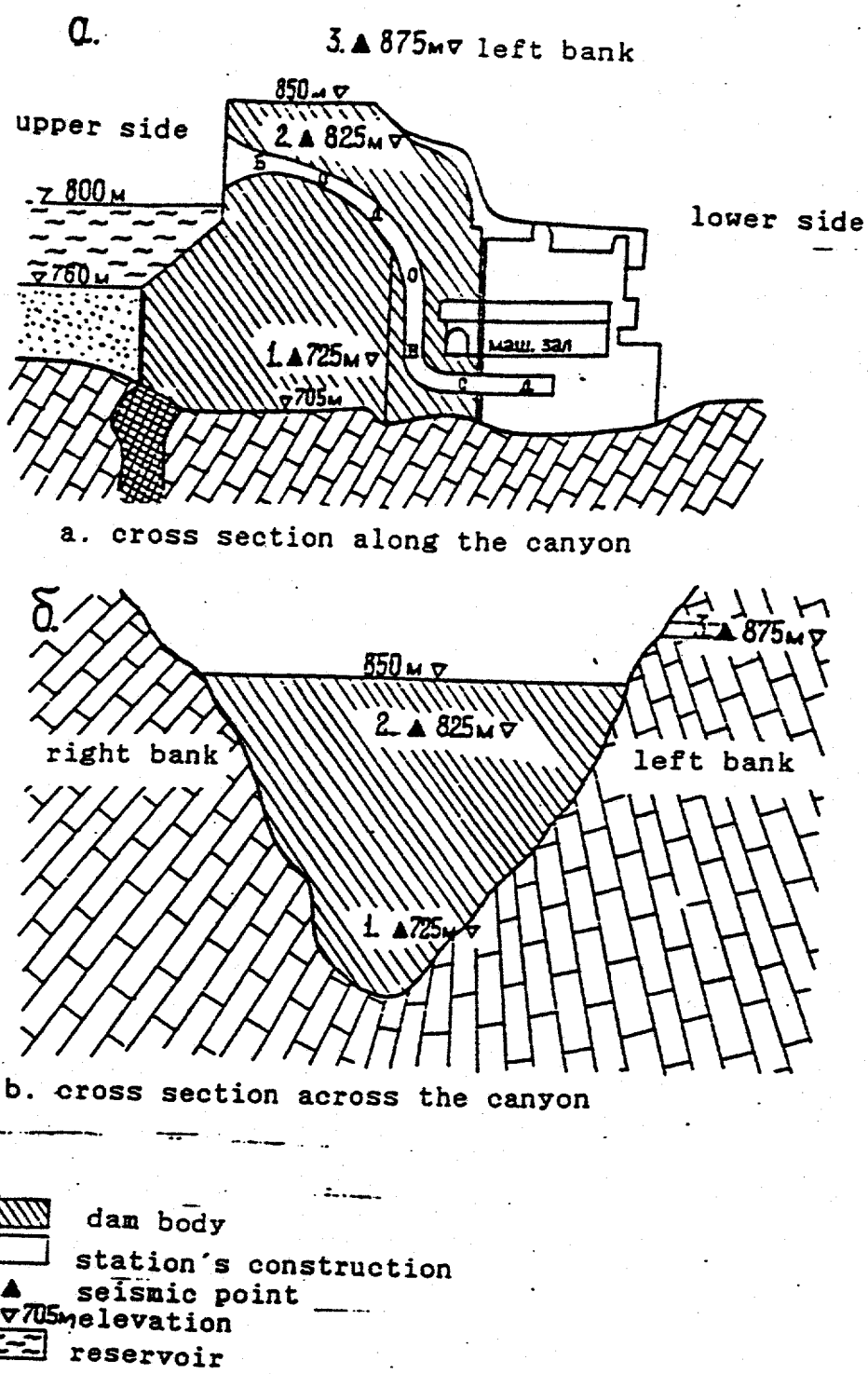

Figure III.41 Toktogul hydropower station dam.

practically parallel to the canyon axis.

Table III.30 presents peak values measured at each point. When analysing the data it should be taken into account that the measurements were conducted in different wave types which could be at one component and absent at another. Also, measured periods were estimated from complicated interferencing waveforms and could be inaccurate. The data show that maximum oscillations were observed at the canyon wall, and the lowerest amplitude relates to the dam basement, as was noted from previous studies. Displacement velocities at the dam ridge are 1.7 to 1.8 times large than those of the basement, but visible periods of oscillations of peak motion decreases at the ridge. Vertical component of displacement varies only little with height.

Relative amplitude variation with the dam height and inside the canyon body is better to trace by identical phases' amplitude comparison measured at all the points. This comparison is the most reliable and gives accurate quantitative estimates suitable for the study of the dam deformation.

Analyzing the data from Table III.31 it is possible to conclude that vertical oscillations in the canyon were 1.7 times larger than at the basement and horizontal oscillations were 2.5 to 3.1 times larger. In turn, amplitudes of horizontal oscillations at the ridge were 1.8 to 2.0 times larger than at the basement, with vertical component being the same or a little bit larger (10 to 20 percents). Amplitude increase in the canyon walls with heigh could be due to crashed rocks forming the upper

Table III.30 Peak parameters in body waves as measured at the Toktogul dam (R≅56 km)

NN	Location	Z			X			Y		
		W, mm	U, mm/s	T, s	W, mm	U, mm/s	T, s	W, mm	U, mm/s	T, s
1	Dam fundament	0.0014	0.018	0.22	0.0014	0.018	0.45	0.0013	0.019	0.48
2	Dam crest	0.0015	0.032	0.18	0.0014	0.033	0.2	0.0017	0.032	0.30
3	Dam side	0.0017	0.031	0.34	0.0033	0.040	0.50	0.0024	0.043	0.35

parts of the canyon. Increased ridge oscillations might be due to resonance.

Low amplitude oscillations with a period of 0.18 to 0.22 sec are visible in the following part of the records in the group of body waves. The oscillations are merged with principal signal and are distinct at X-component at the ridge. Fourier's amplitude spectra of X-component in the interval from 0 to 16 sec calculated for all the three points show extra maximum in the frequency range from 4 to 5.5 Hz (T = 0.25-0.18 sec). This maximum is 2.5 times larger at the ridge than at the basement. Thus, if considering this maximum as induced by resonance, natural dam period is from 0.18 to 0.25 sec.

Table III.31 Peak displacement and velocity ratio as measured at the basemant (b), ridge (r) and canyon wall (c)

Ratio	Z	X	Y
W_r/W_b	1.11±0.14 /15/	1.60±0.25 /14/	1.71±0.36 /13/
W_c/W_b	1.61±0.19 /15/	2.94±0.49 /13/	2.59±0.58 /12/
W_c/W_r	1.47±0.18 /15/	1.89±0.34 /13/	1.65±0.32 /12/
U_r/U_b	1.22±0.21 /15/	2.09±0.43 /14/	2.24±0.42 /14/
U_c/U_b	1.75±0.29 /20/	3.22±0.42 /21/	2.41±0.35 /22/
U_c/U_r	1.51±0.28 /20/	1.77±0.33 /23/	1.41±0.30 /24/

1. Number of measurements is in brackets.
2. Confidence interval at 0.9 probability level.

This natural period is smaller than principal natural

period T = 0.38 sec reported for a dam of 150 m height, but equal to second overtone. The dam oscillations should effect the canyon wall since the spectrum calculated from the records inside the wall shows the same maxima in the range from 4.5 to 6.5 Hz.

Oscillations along the canyon axis are larger than in perpendicular direction as clear from Table III.32. The ratio W_x/W_y had been of 0.71 before the dam construction and 1.38 after. This values characterise the dam effect.

Table III.32

Observation point	Basement	Ridge	Canyon wall
W_x/W_y	0.97±0.12 /10/	0.99±0.04 /10/	1.38±0.27 /17/
U_x/U_y	1.25±0.29 /13/	1.34±0.34 /14/	1.6 ±0.26 /24/

III.6 Tyrnyause explosion.

A large scale explosion of chemical explosive was conducted December 31, 1977 near Tyrnyause at the elevation of 3,000 m. The purpose of the explosion was to open a deposite. Total explosive weight was of 800 ton. The upper part of the ridge Karashiili has been thrown down. The ridge is situated within the "Mulukansky" quarry of the Tyrnyause nonferrous metallurgy plant (TNMP). The upper contour of a new quarry creation, opening the access for elimination of moving massive have been achived as a result of the explosion.

The large-scale explosion was conducted by a method of chamber charges of two-sided throwing down at elevation of 3,100 m. The charges positions are shown on Figure III.42. Total explosive weight was of 833 ton. There were six charging chambers.

Table III.33

Charge number	1	2	3	4	5	6	Total
m, t	388	88	132	132	44.6	48.5	823
q, t	433	98	146.7	146.7	49.5	54	928
W, m	36	22	20	20	17.5	18	
$W/q^{1/3}$, $m/kt^{1/3}$	4.75	4.77	3.78	3.78	4.77	4.76	

The explosives were following: 106 ton of ammonit 6GV (mixture of ammonium nitrate and trotyl), 394 ton grammonit 79/21, and 330 ton granulit AS-8. Specific explosive energy of the first two explosives was 1030 kcal/kg, and that of the

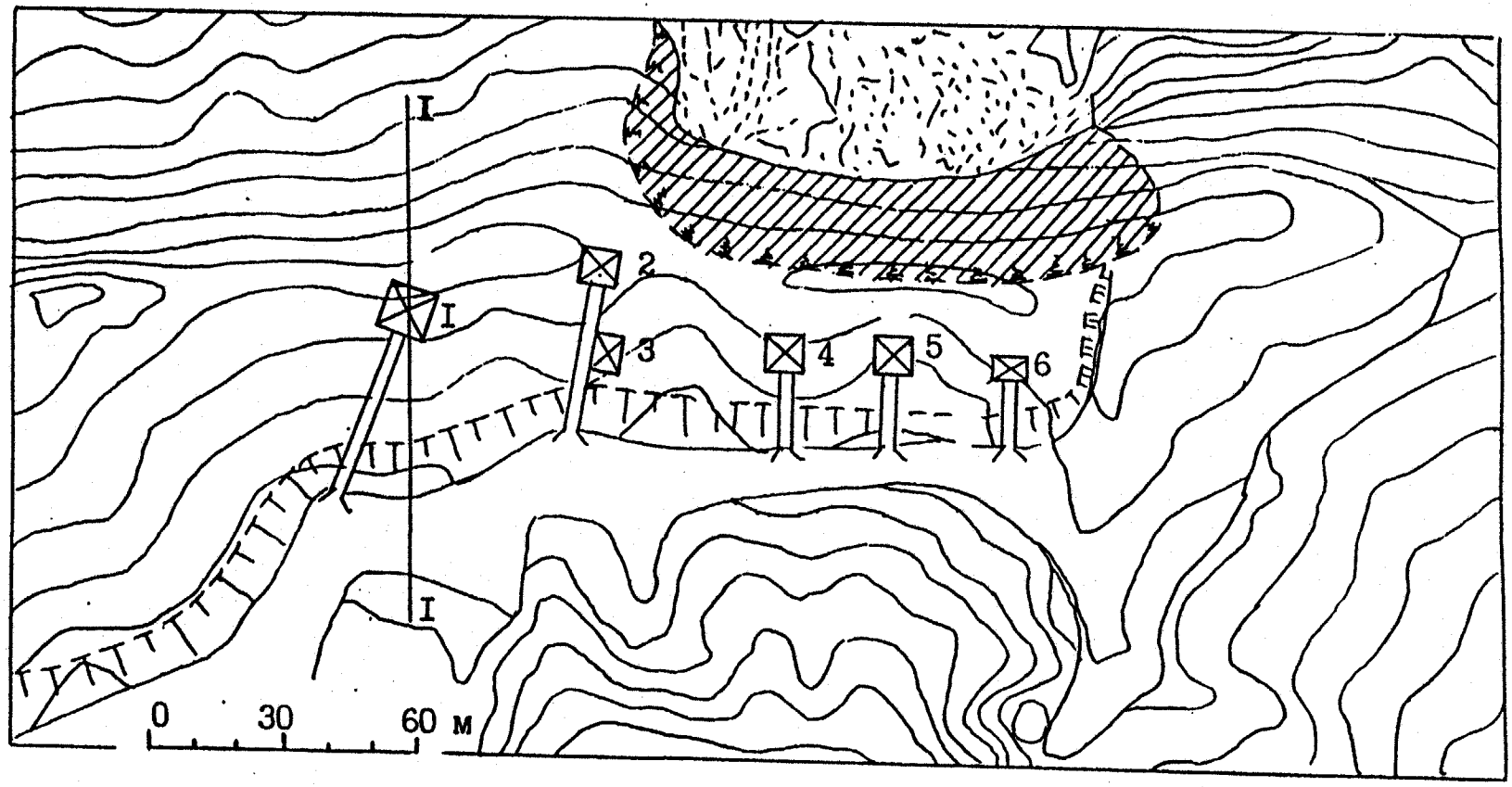

Figure III.42 Charges' locations.

latter was of 1242 kcal/kg. Equivalent charge's energy of trotyl explosion, q, is convenient to use in comparison of different explosives. Trotyl's specific energy is of 1000 kcal/kg. Equivalent trotyl yield of the Tyrnyause explosion is estimated as 928 ton. Table III.33 contains the information about the charges masses, m, explosion energy q, and the shortest distances to the surface, W.

The charges were detonated in two stages in order to reduce seismic effect. The charges 2 through 6 have been fired in the beginning with total weight of 445 ton (495 ton of trotyl), and then the first charge of 388 ton has been fired in 220 msec (trotyl equivalent weight of 433 t).

The ridge blown up has been formed by laminated recrystallized limestone (marble). Volumetric weight of the marble was of 2.73 to 2.8 g/cm^3, compressional strength 800 to 1000 kg/cm^2, extensional strength 50 to 70 kg/cm^2, the Poisson's ratio 0.3; longitudinal wave velocity 5.0 to 5.5 km/sec. The massif's rocks were crossed by deep cracks, which separated the massif into large blocks of a meter size.

Five observation points were arranged to measure the explosion generated signals. ~~Figure~~ Table III.34 presents the epicentral distances, R_{ep}, hypocentral distances from the center of the charge 4, R_h, azimuths, and absolute elevations.

Seismic and acoustic waves were measured at the observation points. The equipment at the points 1 through 3 was switched on by control automatics. The control point has been arranged at the point 3.

Table III.34

Point	R_{ep}, km	R_n, km	Azimuth, ^{o}	Elevation, m
1	0.6	0.602	76	3150
2	1.2	1.204	67	3200
3	2.3	2.3	145	3200
4	5.8	6.06	254	1350
5	5.8	6.07	283	1300

Special timing equipment was established at each observation point. The equipment complex consisted from calibrated time marker, marine chronometer, MX-6, which gave second time marks, and a radio channel of correct time which allowed recording of six time bips of Moscow time radiosignals. The system of automatic control has recorded absolute time of the first explosion $14^h59'59.59''$. Time delay between the first and the second explosions was of 0.22 sec. The shot absolute time was used to estimate seismic waves propagation velocities at large distances.

Mountanions relief and various geological conditions are characteristic of the region where the experiment and measurements were conducted. Three large tectonic faults cross the region separating massifs with different geological formation. The space between the faults is presented by granitic intrusion covered by skarns and recrystallized limestone. The intrusion is traced over the both sides of the canyon and has some outcrops. The explosion was fired at the top of this

granitic block. Schist massifs are at the both sides from the faults. The canyon bottom is covered by young river sediments of gravel and sand several meters thick.

The points 4 and 5 were at equal distances from the explosion and at opposite sides of the town separated by a fault. The point 4 was placed at river sediments of the left bank of the r.Baksan 20 to 50 m thick. The point 5 has been established in a mine excavated in the granitic massif to a length of 40 m at opposite side of the canyon. The explosion and point 5 were in the same granitic massif. Such observations were supposed to reveal possible fault as well as local geological conditions influence on seismic waves' parameters.

Total volume of rocks thrown down was estimated as 6.5 10^5 m^3 which is 2.2 times more than predicted for an explosion of such an yield. The volume increase can be explained by extra rocks collapse due to gravitational force. The nothern slope collapsed more intensively (lower right part of photos). The explosion specific energy outlay of 1.4 kg/m^3 was decreased by rocks collapsing. About 75% of the rocks have been thrown down to the nothern slope and other to the Mukulan canyon.

Recorders SD-725 were used to measure shock wave in the air. Figure III.43 presents peak overpressure in shock wave as a function of distance (curve 1). The highest overpressure (about 0.05 kg/cm^2) has been measured at the observation point 3 (R_{ep}= 2.2 km). It was even higher than at the point 2 (R_{ep}=1.2 km; ΔP_m=0.038 kg/cm^2) which has been shielded by back part of the ridge. Shock waves generated by different charges are clear on

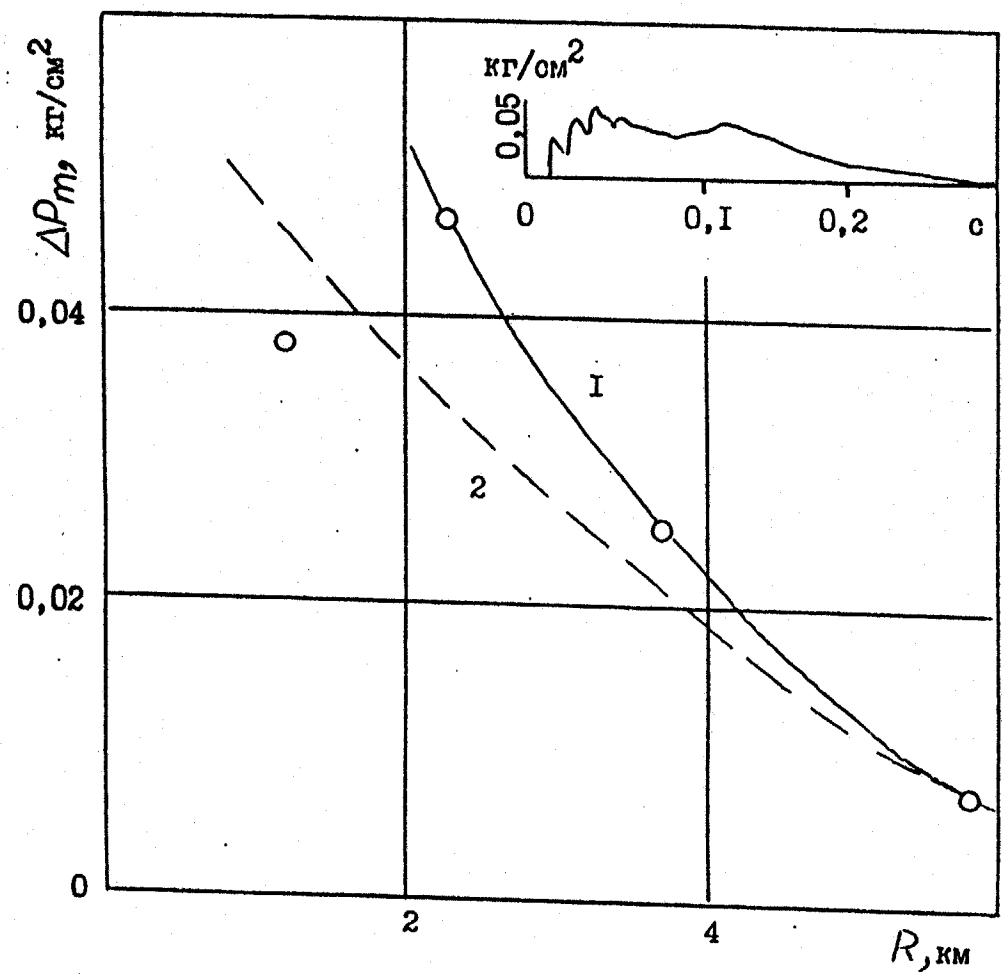

Figure III.43 Peak overpressure in acoustic wave.

the records. An example of record at the point 3 is shown in Figure III.43. The record is common for excavation explosions with shallow depth of burial: shock wave generated by upgoing wave is followed by gradual pressure growth induced by gaseous products of detonation ejection. Compression phase in the acoustic wave in the range of measurements was of 0.3 to 0.5 sec. Glasses in windows have been broken to a distance of 3 to 4 km where $\Delta P_m \geq 0.02$ to 0.03 kg/cm^2. The overpressure was less than 0.01 kg/cm^2 within the town.

Curve 2 in Figure III.43 presents prediction of Sadovsky's relationship for surface trotyl explosion which has to produce the measured overpressure at 6 km. Such an explosion yield is 230 ton from averaged overpressure and impulse measurements , i.e. 25% of actual total yield. High acoustic energy output shows that the charges were underburied. More intensive attenuation of peak pressure with distance in comparison to curve 2 corresponds to air pressure and density increase along the path of acoustic wave propagation. The air pressure variation was of 0.2 kg/cm^2 in the range of the measurements.

Seismic waves measurements were conducted at four points. Vertical, U_z, and radial, U_x, particle velocities were measured at the points 1 and 2. Seismometers S5S were used as sensors. The sensors were cemented to hard rock outcrops.

The points 4 and 5 were equiped by three-component seismometers to measure vertical (Z), radial (X) and transversal (Y) components of displacement (S) and particle velocity (U) in seismic wave. S5S seismometers were used at the point 4. The

point 5 was equiped by seismometers USF-3M, with natural period of To=1.5 sec and damping of 0.5 to 0.6. In order to measure displacement, low-frequency galvanometers with natural frequency of 5 Hz integrating a signal were included in recording channel. Particle velocity measurements were made by using high-frequency galvanometers with natural frequency of 120 Hz. The galavanometers were installed in oscilloscopes OMS-2M.

Seismic wavefield characteristics were effected by time delay between the two explosions almost equal in yield. Figure III.44 presents records of particle velocity U_x and U_z at each observation point.

Two arrivals are clear in longitudinal wave group, P_1 and P_2. Compressional wave velocity of 4.8 km/sec was estimated from the distance between the points 1 and 2 (0.6 km) and the measured arrival time difference. Shear and surface waves are also clear at the records from the points 4 and 5 by longer periods and amplitude growth.

The most complicated seismograms are characteristic for the point 4 as a comparision shows. Tectonic faults are responsible for this phenomenon. Reflected waves and refracted waves produced at the faults complicate the signals.

Inspite some shielding effect which is possible from faults, displacement at the point 4 is 3 to 5 times larger than at the point 5. Thick sediments is a possible reason of the local amplitude increase.

Table III.35 presents measured first motion amplitudes of displacement and particle velocity in P_1 and P_2 and those of

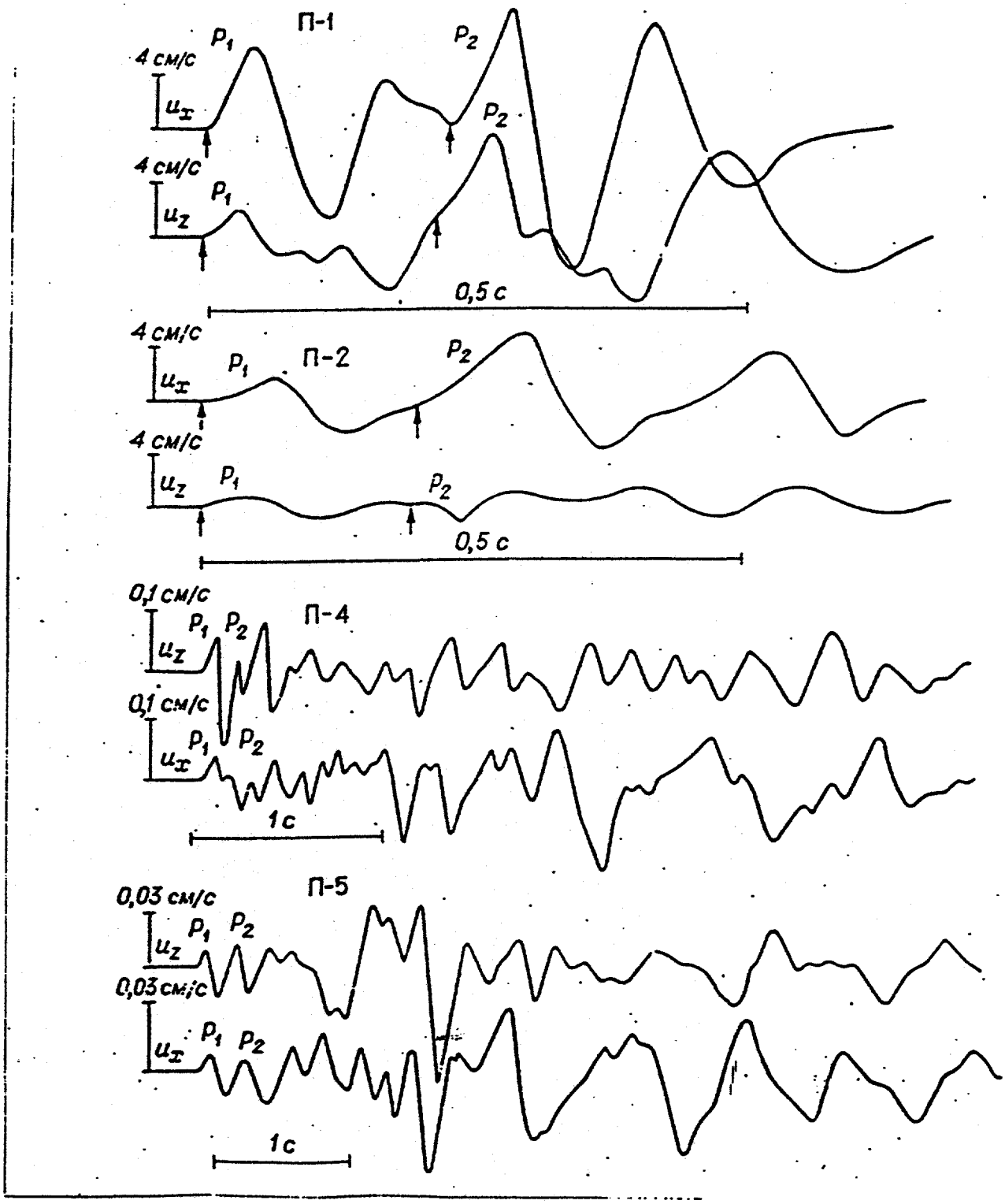

Figure III.44 Seismic records.

Table III.35

Point	Distance, km	Compo-nent	Longitudinal wave			Share wave			Body waves group			Surface waves		
			u,sm/s	t_-,s	s,mm	u,sm/s	t_-,s	s,mm	u,cm/s	T,s	s,mm	u,sm/s	T,s	s.mm
1	0.6	x	6.0	0.07	2.2	8.5	0.07	3.0	9.5	0.14	2.1			
		z	1.9	0.05	0.5	7.5	0.07	2.7	5.5	0.16	1.4			
2	1.2	x	1.6	0.09	0.74	2.0	0.08	0.8	4.2	0.16	0.1			
		z	0.54	0.7	0.2	1.3	0.05	0.35	1.2	0.14	0.3			
4	6.06	x	0.030	0.09	0.19	0.04	0.08	0.016	0.11	0.22	0.06	0.14	0.44	0.11
		z	0.055	0.066	0.027	0.084	0.12	0.025	0.08	0.11	0.07	0.027	1.0	0.044
		y							0.11	0.24	0.08	0.077	0.44	0.12
5	6.07	x	0.008	0.13	0.0054	0.007	0.20	0.0045	0.027	0.29	0.016	0.030	0.39	0.035
		z	0.009	0.1	0.0054	0.015	0.18	0.0057	0.015	0.19	0.007	0.048	0.31	0.044
		y							0.03	0.29	0.016	0.026	0.90	0.040

peak amplitudes of all the principal seismic phases observed.

In the closest zone (1-3 km) peak parameters are related to the first arrivals of compressional wave. Vertical component is 1.5 to 3 times lower than horizontal.

Horizontal peak particle velocite as a function of scaled distance $\bar{R}=R/q^{1/3}$ (km/kt$^{1/3}$) is a principal characteristic of seismic waves and is presented in Figure III.45 (curve 1)

$$U_x=4.3\ (\bar{R})^{-1.6}\ \text{(cm/sec)}$$

The measured particle velocity from this explosion is two times lower than that of standard relationship for horizontal velocity from a contained explosion of chemical explosive in granite (see curve 2 at Figure III.45) which is described by relationship

$$U_x=8.5(\bar{R})^{-1.6}\ \text{cm/sec.}$$

Such an amplitude decrease is not only due energy lost into the atmosphere, but also due measuring along the ridge.

Peak parameters in far-field (3 to 6 km) were observed from surface waves. The only except is vertical component at the seismic point 4 which had peak value in body waves.

Surface wave amplitude was 4 to 5 times larger than that of the first arrival. Peak horizontal particle velocity at the points 4 and 5 is shown in Figure III.45 with $\bar{R}=8$ km/kt$^{1/3}$. Horizontal component at the point 4 also larger than vertical. The ratio is of 1.8 at the point 5, horizontal component of particle velocity is 4.5 lower than predicted by relationship (1). It can be explained by shielding effect of the r.Baksan canyon which separates the explosion and the observation point 5. Vertical to horizontal amplitude ratio here is of 1.6.

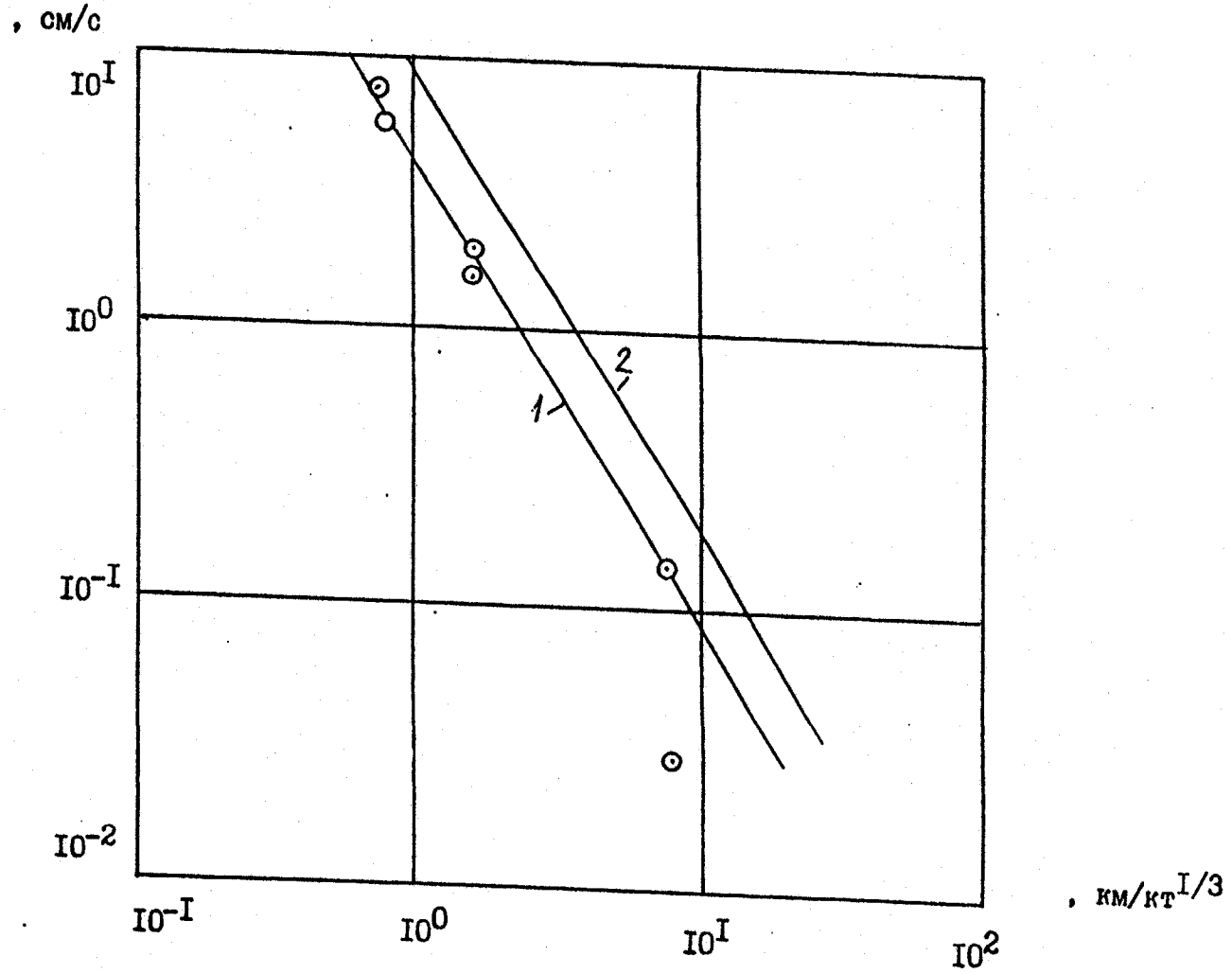

Figure III.45 Peak particle velocity VS. scaled distance.

. There were some underground tunnels beneath the explosion site in skarn massif (ρ=2.9 g/cm^3, f=17 to 19) and marble (ρ=2.7÷2.8 kg/cm^3, f=15÷17). The tunnels had a cross section of 6 to 7 m^2. Detailed survey after the explosion has shown that:

a) the tunnel at hor. 2690, R=400 to 450 m, $\bar{R}$=50 to 55 m/t$^{1/3}$ has not been damaged;

b) the tunnel at hor. 2827, R=250 to 300 m, $\bar{R}$=32 to 38 m/t$^{1/3}$ has not been damaged;

c) in the drift at hor. 2887, R=200 to 220 m, $\bar{R}$=25 to 28 m/t$^{1/3}$ local damages and falls out were observed;

d) in the tunnel at hor. 2945, R=200 m, $\bar{R}$=25 m/t$^{1/3}$ some cracks and faults opening of 2 to 5 cm wide were observed.

Some stones falled down. In this tunnel the roof has colapsed at R=170 m ($\bar{R}$=21 m/t$^{1/3}$) near the joint to another tunnel where the cross section area was of 10 to 12 m^2. Closer to the explosion at R=150 m ($\bar{R}$=19 m/t$^{1/3}$) some parts of the tunnel have also been collapsed. Enforced parts of the tunnel have not been damaged.

These observations as well as measurements of compressional wave in nearby zone described by standard relationship

$$U_m=200\ (R/q^{1/3})^{-1.75},\ \text{m/sec} \qquad (5)$$

where R is the distance in meters, q is the weight in tons, allowed to conclude that

1. weak damages (cracks, small collapses) occured in the range from $\bar{R}$=20 m/t$^{1/3}$ to $\bar{R}$=30 m/t$^{1/3}$ and 0.5 m/sec$\leq U_m \leq$1 m/sec;

2. in the range from $\bar{R}$=20 m/t$^{1/3}$ to 25 m/t$^{1/3}$ some collapses near joints are possible;

3. tunnel collapse was observed where $\bar{R}\leq$20 m/t$^{1/3}$ and $U_m\geq$1 m/sec.

III.7. R. Alinjachai explosion

An explosion contructed a dam in the canyon of the r. Alinjachai (Nakhichevan ASSR) was designed to meliorate dry soil. The explosion was conducted on September 4, 1984 in 13h (Moscow time). Total explosive weight was of 689 ton.

Mechanical and seismic effects of the explosion were measured. The dam size was also determined. This dam has been constructed by newly developed method. The explosion only damaged and loosened a massif with gravity doing all the job on rock movement. So, very low specific energy has been reached for dam construction. Some experience on long storage of explosive in a mine has been also obtained.

The explosion site was inside mountaneous region with absolute elevation of 1300m. The site is formed by pliocene extrusive rocks. Modern alluvium sediments 5 to 6 m thick cover the rocks near the river channel. The exploded massif is formed by diorite porfirite with volume weight 2.4 g/cm^3, compressional strenght of 1370 kg/cm^2, longitudinal velocity of 4300 m/sec, and shear velocity of 2300 m/sec. The rocks were dry. A charge has been positioned only at the right bank of the canyon. The canyon wall slope near the dam was of 70^o to 80^o. The right wall was 130 m high above the river bed, and the left was only 100 m high. Water outlay of the r.Alinjachai was of 0.35 m^3/sec at the moment of the explosion.

Charge and access tunnels scheme is shown in Figure III.46. Line charges' parameters are presented in Table III.36. The charge 1 has been fired in 0.70 sec after the second and third

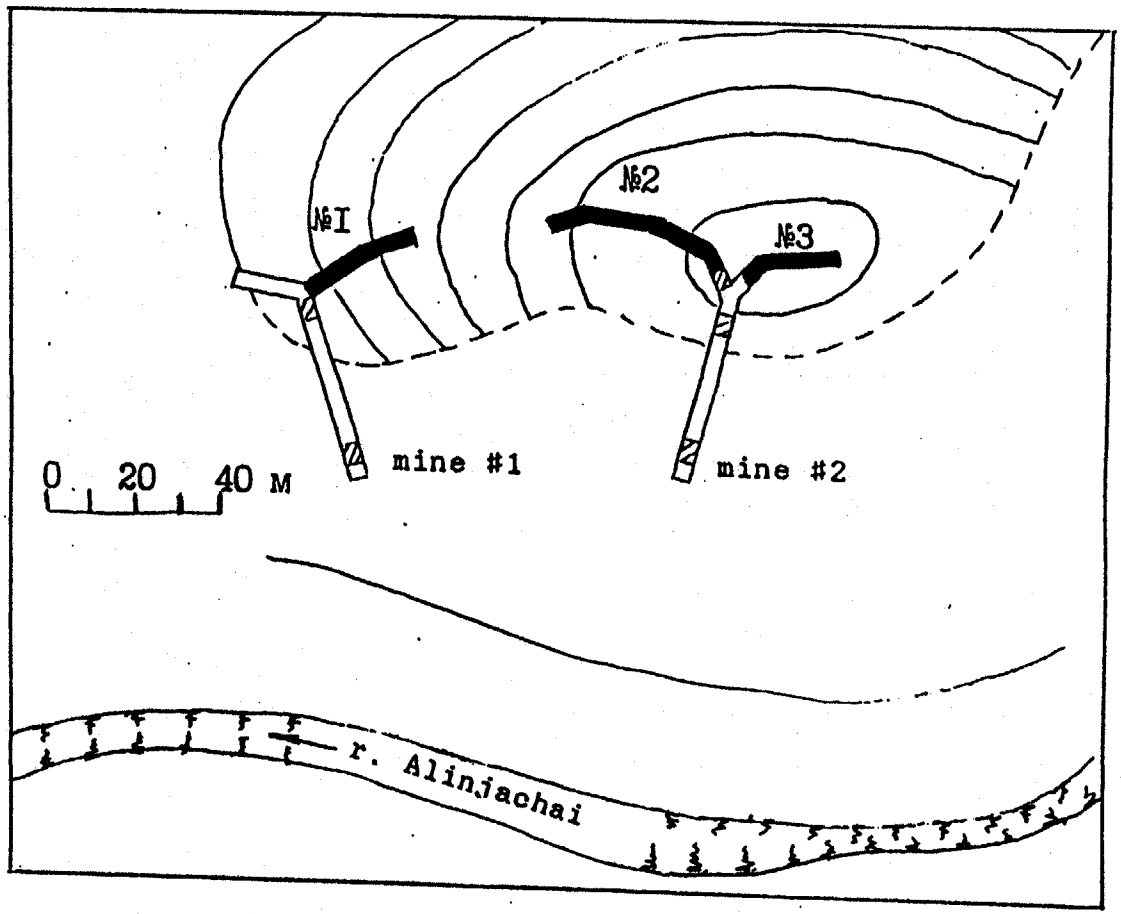

Figure III.46 Charges positions.

charges.

Table III.36

NN charge	SDS, m	Linear density q_1, t/m	Charge lenght l, m	Charge total mass Q, t
1	55	6.5	30	195
2	60	7.4	50	371
3	58	5.4	23	123

The access tunnels were closed by 5 concrete lockages. These lockages are shown by dashed areas in Figure III.46. Two parts 7 and 5 m long are filled by concrete in the tunnel 1, there parts 6,7, and 3 m long are cemented in the tunnel 2 (reference from the mouth). Thus, total concrete lockage lenght was of 28 m. The chambers containment had a special importance to provide proper massif damage to induce rock slide. Gas leakage in such a case could reduce mechanical effect.

The explosion development history was filmed from the upper point by two cameras (350 and 1800 m far from the mouth of the tunnel 2). Seismic and acoustic waves were also measured. The initial surface motion has been filmed from the closest point and overall explosion pattern from the distance point.

Seismic waves' parameters were measured at the free surface by SM-3 sensors established at distances 548 and 945 m from the center of the second charge. The sensors have been cemented to concrete fundaments at hard rocks. Three component motion was measured: radial (X), vertical (Z), and transversal (Y).

Recorders SD-725 were used to measure acoustic wave parameters. The sensors measured overpressure as a function of time. SD-725 have been established at the seismic points as well as at the more distant filming point.

The explosion process has been recorded by the closest camera in detail. Gas ejection from the tunnels has started 0.06 sec after the explosion with velocity of 75 m/sec. In 0.2 sec gas velocity increased to 300 m/sec. Locks damage is a reason of such an ejection history.

Vertical cracks at the front surface of the massif began to appear in 0.21 sec after the explosion. The largest crack went from the mouth of the second tunnel to the upper part of the massif. Gas ejection from the crack occured in 0.28 sec after the explosion.

All the equipment has been swithced on 3 sec before the explosion.

The initial surface velocity above the second charge was of 20 to 25 m/sec and at the upper part of 15 to 16 m/sec as measured from filming.

The upper part of the canyon slope has begun to collapse in 1.5 s after detonation above the second tunnel. Collapse of side part of the massif going to upper part started at the same time. Collapse has been finished in 20 to 25 sec.

A dam of total volume of 6.1 10^5 m^3 has been created as a result of the explosion. The maximum height was of 32 m and length of 195 m in basement. The crest length was of 165 m.

Figure III.47 presents the dam cross sections along (2) and

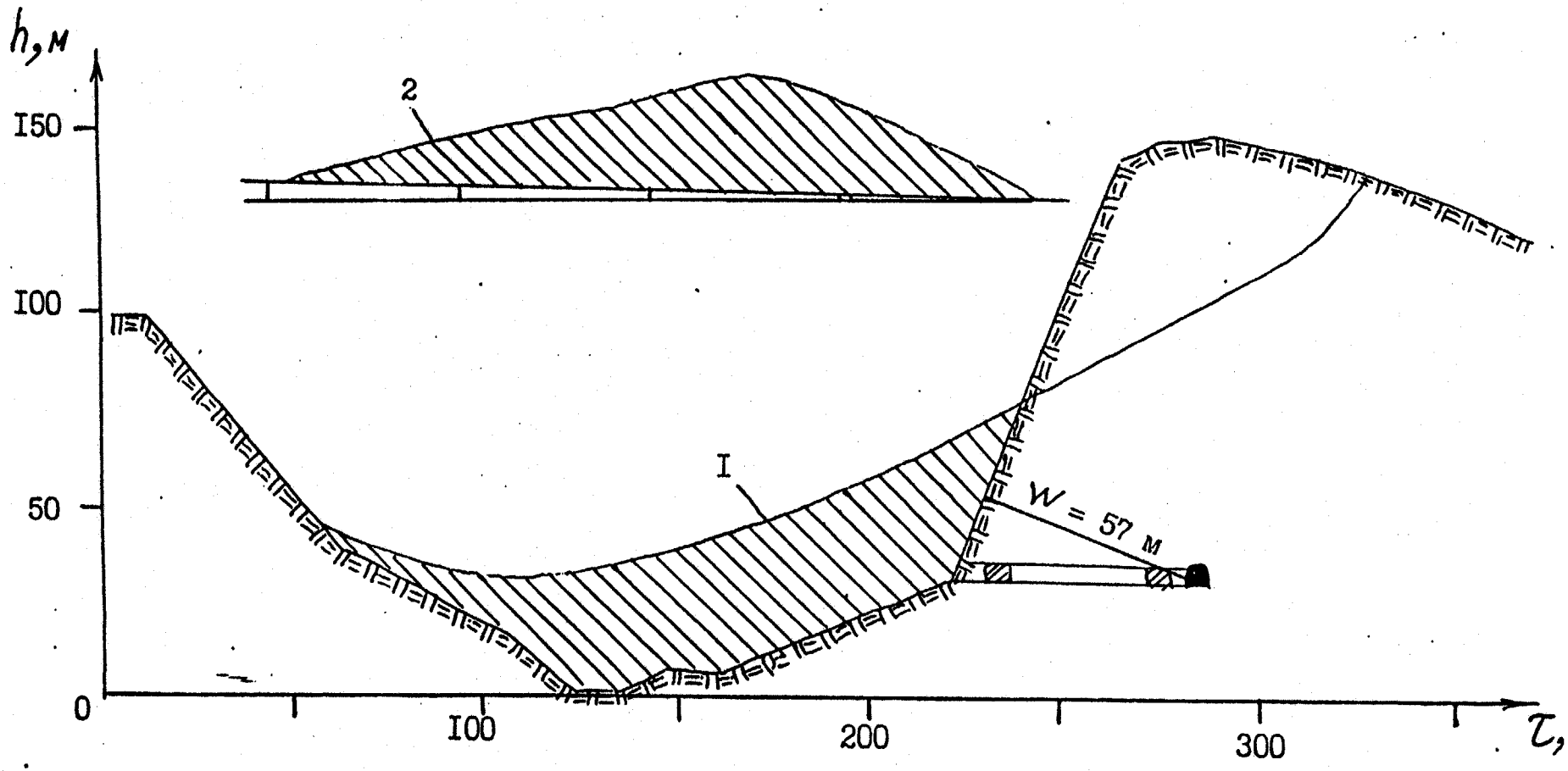

Figure III.47 Dam cross sections along (1) and across (2) the canyon.

acsross (1) the crest, where the dam is the highest.

Three-component records at 945 m are shown in Figure III.48a. Straight longitudinal wave, P_1, from the first by time of detonation charges 2 and 3 is distinct. This wave velocity as determined from time/distance relation is of C_p=3250 m/sec. Long period waves are observed after straight wave and have the highest amplitude. Straight wave from the second explosion, P_2, can be seen in 0.5 sec on the background of the long period wave. Time delay between P_1 and P_2 corresponds to designed one.

Table III.37 summarizes the results of measurements of particle velocity in the first arrival, U_p, peak particle velocity, U_m, and corresponding periods.

Table III.37

R, m	Component	U_p, cm/sec	U_m, cm/sec	T,sec
	x	9.1	-	-
548	y	0.7	-	-
	z	10.4	-	-
	x	1.1	5.9	0.37
945	y	0.9	1.9	0.22
	z	2.5	3.4	0.2

The measured values are well described by relationship

$$U=315\ (R/q^{1/3})^{-1.8}$$

which is obtained from the Medeo explosion data.

The record of acoustic wave measured at 945 m is shown in Figure III.48b. Two peaks of pressure are due to gas ejection

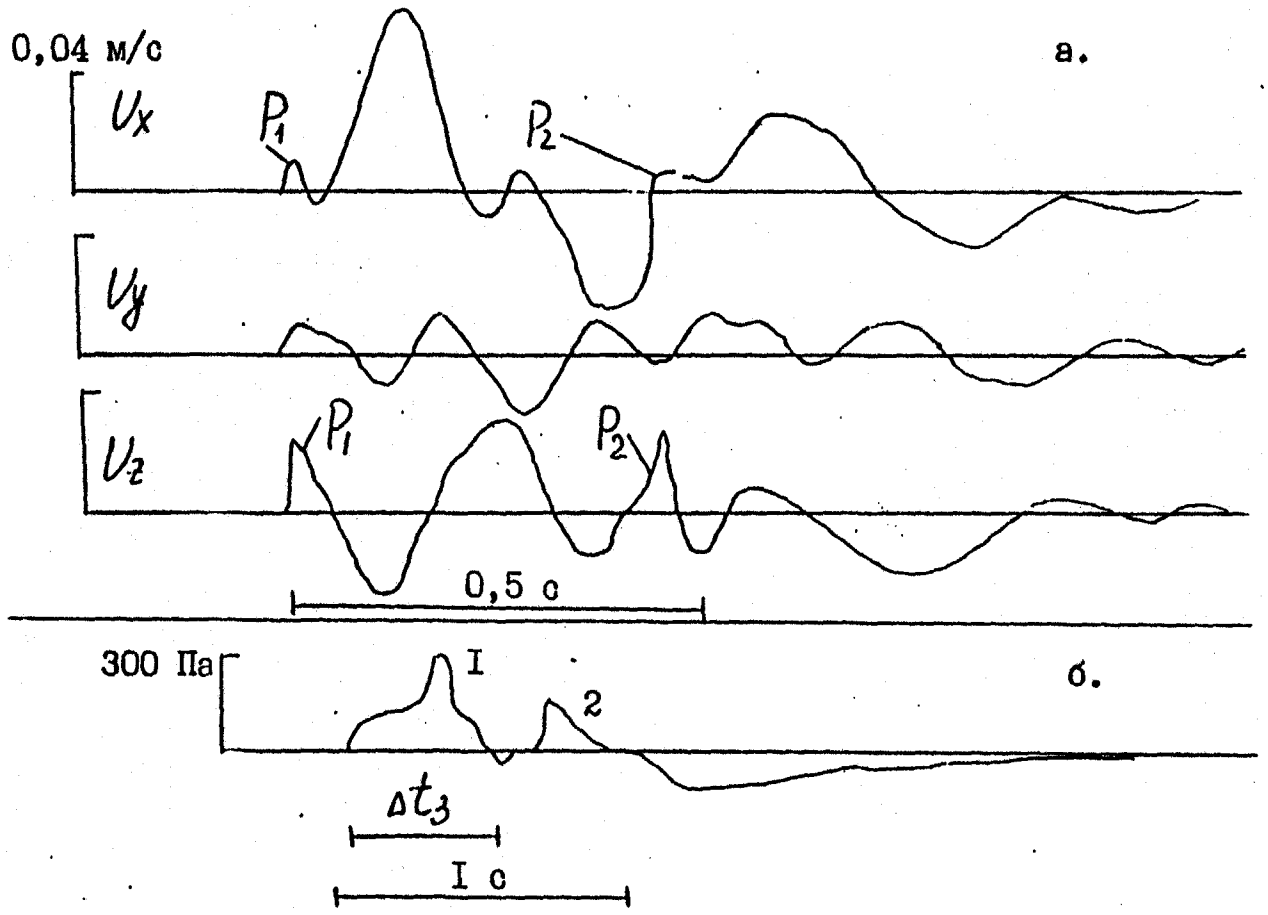

Figure III.48 Three-component seismic records at a distance of 945 m (a) and air shock wave (b).

from the tunnels 1 and 2. The first peak is of 280 Pa, and the second is of 140 Pa. These peaks follow by small overpressure steps induced by the free surface uplifts from the first and the second explosions. Time delay between the first and second peaks corresponds to time delay between the explosions of 0.5 sec, i.e. 0.2 sec shorter than real one. It is explained by 70 m shorter distance from the charge 1 to the point.

Energy share of acoustic wave can be estimated from the data. By using standard relationship for acoustic wave impulse of surface explosion,

$$J_+ = 350\ (q_e^{2/3}/R)\ [\text{Pa sec/m}^2]$$

one can estimate effective trotyl yield, q_e, as 0.5% of the total energy. Note, that for the Baipaza explosion this value was of 2%, and at the Burlykya was of 30%. Thus the explosion under consideration has been well contained

All the charges have been fired in proper manner as follows from the seismic and acoustic data which show good ratio of amplitudes related to the real explosions' yields.

The town of Kazanchi has been surveyed after the explosion. Building in the Kazanchi were constructed from stones cemented by clay. Only some buildings have been constructed from cemented bricks. Almost all the buildings have been damaged to some extent by seismic waves. Walls were cracked and roof was cracked also in some places. Three building had wall joints separation and opened cracks of 2 cm wide. Thus, such damages are related to 6-ball earthquake.

III.8 Explosion on r. Uch-Terek.

The Cambarata hydropower station N1 and N2 have been constucting during several years in Kirgizia on the Naryn River. Dam creation for the station was designed by large scale directed explosions. The dam formation of the Cambarata N1 station has been designed by landslide like collapse of a mountain slope induced by an explosion of 270,000 ton.

To support the part of the technical project of the Cambarata power station N1 dealing with dam construction a test explosion was conducted in the canyon of the Uch-Terek river on June 11, 1989 at 10h59'46" MSK. The epicenter of the explosion was located in 17 km to the south of the epicenter of the Burlykya explosion conducted on February 8, 1975. The Uch-Terek explosion was conducted in the river canyon. The canyon had slopes of 50^{o} and depth of 200 m. Rocks were presented by laminated sandstone (30-60 %) and aleurilite of middle, fine and large lamination. Layers' thickness was from 0.1-0.3 m to 2-3 m. The layers were close to vertical. Interfaces between lithological complexes are sharp and even along layering. Sandstone is grey, green-grey, brown, fine and middle grained, and sometime large granited up to gravelic. Maximum compression strenght is of 67-82 MPa. Aleurolite is grey, green down to black, middle and fine laminated. The rock is intensively cracked but hard in samples. Compressional strenght is of 47 to 55 MPa. Aleurolite and sandstone density is of 2.65 to 2.7 g/cm^{3}. The rocky massif is crossed by several tectonic discontinuities of different scale (from III to V). The upper

part of the massif is covered by alluvium sediments 6 to 7 m thick. Compressional wave velocity varies from 1.5 km/sec near the surface to 4.0 to 4.5 km/sec at a depth of 40 m.

Two linear charges were placed at two stages with absolute elevations of 1173 and 1208 m. The lower charge had a length of 145 m and the shortest distance to the surface of 50 to 57 m. Linear charge density was of 5.3 to 6.8 ton/m. Total explosive weight was 992 ton. The upper charge was 92 m long, had the shortest distance to the surface of 88 m, linear charge density of 7.5 to 8 ton/m and total weight of 701 ton. Linear density and total charges' weights were calculated for the explosive ammonit 6 GV (ammonium nitrate + trotyl). Actually, a mixture of ammonium nitrate (94.5%) and Diesel fuel (5.5%) was used. The mixture is called igdamite. The explosive effectiveness is of 85% from the ammonit 6 GV as lagre scale experiments had shown. Due to this fact, the charge total mass was estimated as of 1906 ton (1083+823 ton).

The lower charge was designed in a way to provide intensive rock landslide to the bottom of the canyon and to create a convenient path for accelation of collapsing of the upper stage. The upper stage rocks crashing was conducted by the upper charge with that of scaled depth of burial being similar to the scaled depth of burial designed for the Cambarata N1 dam construction.

Figure III.49 shows principal scheme of mine and access tunnels. The tunnels were of cross-section area of 14 to 15 m^2. All the mining tunnels were evenly filled by explosive to a height of 2 m (the lower charge) and 2.2 to 2.5 m (the upper

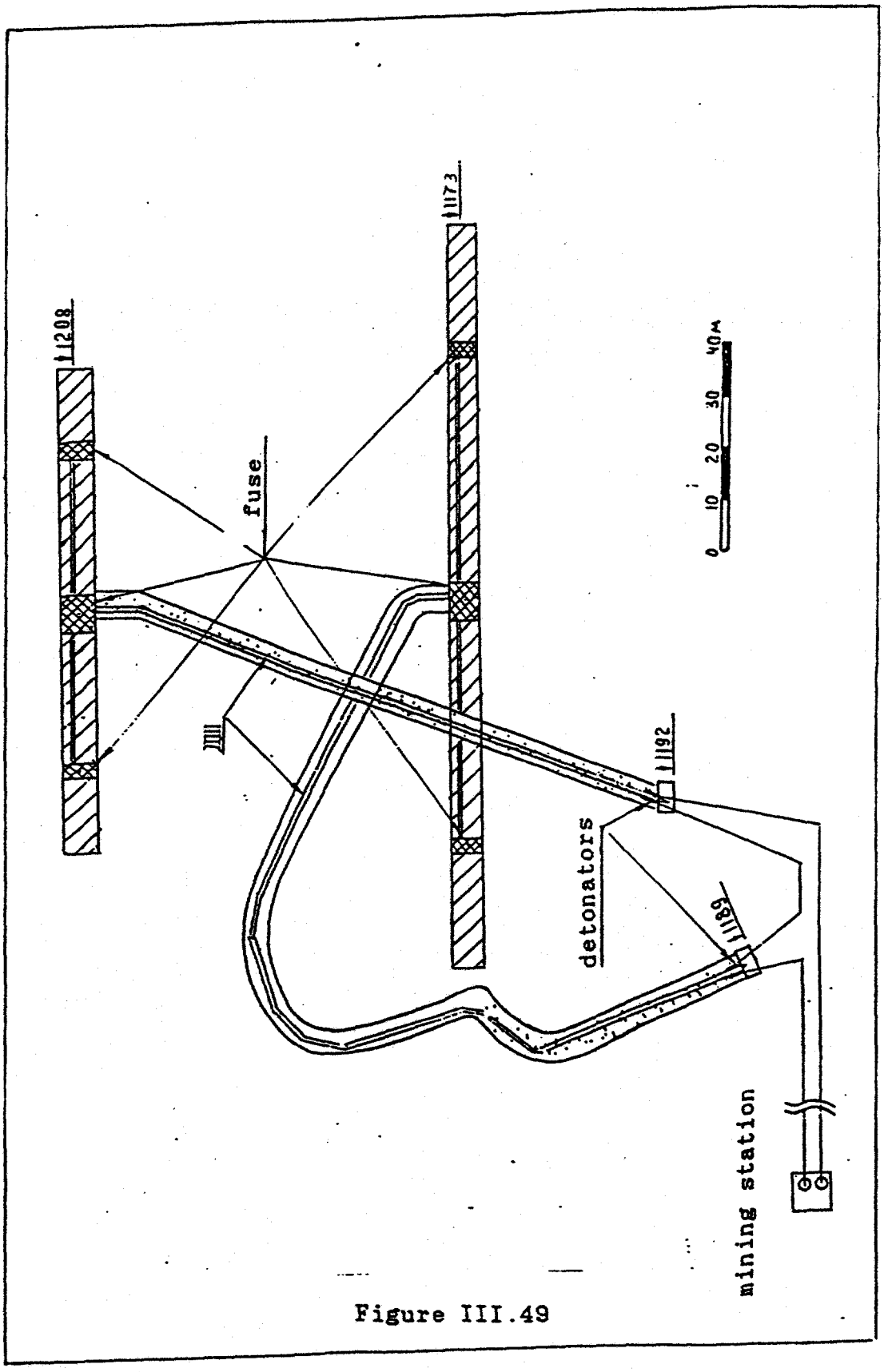

Figure III.49

charge). The ammonium nitrate was in three-layered paper sacks. Each five sacks were placed at each other and the sixth was cut and the explosive filled empty room between the sacks. This procedure increased explosive density.

Diesel fuel was supplied by special pipes mounted in the tunnels. Steel tubes were used to made the pipes. The tubes were 108 mm in diameter and had one hole of 5 mm in diameter per meter. The holes were made in the upper part of the tubes to spread Diesel fuel evenly along the charges. In order to avoid fuel throwing to the tunnels roof the tubes were covered by thin plastic band. There were formed special cavities of sacks with bottom covered by plastic band to gather Diesel fuel. The cavities have gathered about 25% of fuel. Other fuel moistened explosive between the sacks. In order to prevent fuel leakage in surrounding rocks the tunnels were cemented and covered by plastic band to a height of 2 m.

Diesel fuel was supplied to the charges during 1.5 days and was finished only one day before the explosion. To monitor fuel level special holes 1 m deep were made in several places of the charges. Preliminary calculations had shown that fuel level would be of 1.5 to 1.7 m, i.e. could be seen in monitoring boreholes. Then the wells were digged deeper almost to the tunnels bottom. But no free fuel have not been noted. Ammonium nitrate and the paper sacks were wet. These observations allowed to conclude that some fuel leaked from the tunnels. In general, it has to be concluded that the procedure of large indignit charge formation was wrong. The tunnels floor and walls had to

be isolated be compacted with higher density, and fuel should be spreaded over all free surface of the charges.

Ammonit 6 GV detonating fuses have initiated the charges. There were detonating fuse of 6 ton weight in the center of the charge, and two auxilary 2 ton detonating fuses situated at 1/6 of the charge length from the edges (see Figure III.49). The detonating fuses were connected by several detonating wires. Detonating wires from the main detonating fuse went to the tunnels' mouths. Here the wires were connected to detonators: 4 detonators for each charge. Two detonators were connected to the main detonaiting chain and two to the doubling one. The detonators were connected in sequence. Mining station was 2.7 km far from the shot point. Control automatics also have been installed there. All the measuring equipment situated closer than 2 km had to be run 1 second before the explosion from that control point. Seismic equipment at far points have been switched on manually from correct time marks of precise clocks.

It was presumed by the project to fire the charges at 11h00'00" sharp (MSK). Actually, the explosion had been detonated 12 seconds before that time. The cause of the early detonation was a damage in the detonating machine. The machine electric circuit had been broken and detonating circuit has been shorten when a handle has been rotating relatively slow. Preliminary machine testing had not revealed any damage inside.

Since the explosion had been detonated before planned time all the measuring equipment in closein zone have not been switched on. So, the information about the explosion development

is limited. Only photos of the explosion development, peak amplitudes of shock waves, and seismic data from remote stations are available.

Figure III.50 shows the photos of the explosion development which were made from 4 km. The film have been forwarded manually and no time marks are available. Some estimations show that the second photo have been made 2 to 3 sec after the explosion initiation. Time interval between the photos N2, N3, and N4 is estimated as 1 sec, i.e. time necessary to forward film in a camera. The first photo shows the canyon general view before the explosion: a portion of road going to the tunnels is visible. The photo 2 shows process of avalanche-like collapse of rocky massif induced by the upper charge. The lower edge of the collapsing mass is at a level of the road, i.e. about the point of the shortest distance to the surface from the lower charge. At that moment no signs of the lower charge detonation are visible. This means that the charges have been fired not simultaneously.

The third photo shows the beginning of ejection of gasous products of detonation through cracks created above the upper charge due to rocks collapsing. (It is worth noting that such a pattern is common for explosions at slopes). This photo also shows effects of the lower charge: collapsing rock are lifted in a dome-like shape that can be due to developing of the dome generated by the lower explosion.

The photo 4 presents gas ejection from the second explosion. Extra collapsing of the upper part of the slope is

Figure III.50

also seen.

Thus, from the photos it is possible to conclude that the second explosion was 4 to 5 sec later that the first one (the lower change). The fact that only one charge has been detonated instead of the two at the same time can be explained by improper voltage or duration of the initiating electric impulse which has been generated by occasion. The impulse was not enouth to detonators and only "the weakest" has been initiated. This detonator was connected by detonating wire to the upper charge. The problem of the second charge detonation in several seconds after the first one is complicated. There are some reasons for that:

a) Nichrom bridge heating in the detonators has not initiated detonation of tenerese but has caused decomposition followed by and detonation;

b) Collapsing of the tinnel roof under effect of the upper explosion caused multiplyed impacts of rocks and detonating wires which has initiated detonation;

c) The tunnel collapsing of the lower charge has compressed and heated amonium nitrate and fuel with following combustion.

Combustion in constrained conditions might cause detonation. In this case total energy output is lower as well as mechanical effect. In principle, there are some other causes of the lower charge detonation, but it is obvious that the lower charge has been detonated. A dam with following characteristics has been constructed as a result of the explosion:

- dam height was of 45 m (absolute elevation 1180 m);

- dam width across the river was 295 m;
- total loosen rock mass in the dense dam body was of 2.22 10^6 m^3, in loosen - 3.02 10^6 m^3;
- disconcentrating coefficient was of k=1.36.

The dam cross sections along and across the river and rock distribution in plane are shown on Figures III.51 and III.52 by line 1. Figures III.53 present photos of the r. Uch-Terek canyon before and after the explosion. The photos have been made from the points lower of the dam.

The explosion crater is horseshoe shaped and wider in the lower part. There are some vertical and subvertical scarps about 10 m high at the upper part of the crater. The crater width at a level of the SDS of the upper charge (elevation 1270 m) is of 220 m, i.e. the explosion effect coefficient is n=0.76 which is close to that of the charge center. The crater edges at a level of the SDS from the lower charge are covered by destroyed rocks 260 m wide. It is worth noting that such a width is traced from 1260 to 1180 m. It confirms absence of intensive throwing by the lower explosion.

The dam created by the explosion is relatively symmetric. The dam's slopes down and up the river are 1:3.4 and 1:3.1 respectively. Rocks crashed by the explosion lay in the upper part (1250 to 1320 m) of the crater with slope of 30^0 and in the lower part with slope of 20^0. At the opposite side of the canyon rocks lay about horizontally (see Figure III.52), i.e. no rocks have been thrown to the opposite side. No rocks have been also thrown far from the main heap and above the opposite slope.

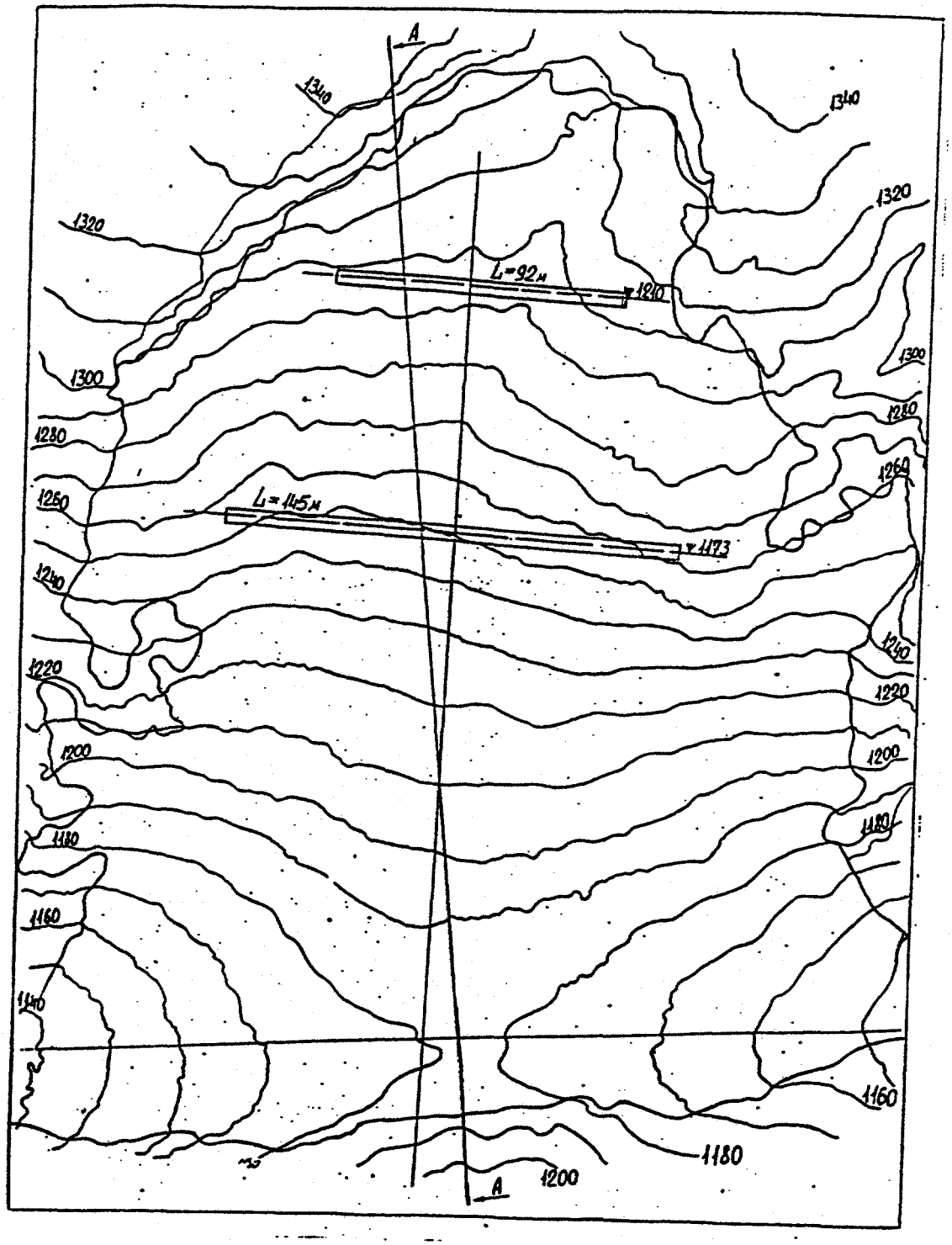

Figure.III.51

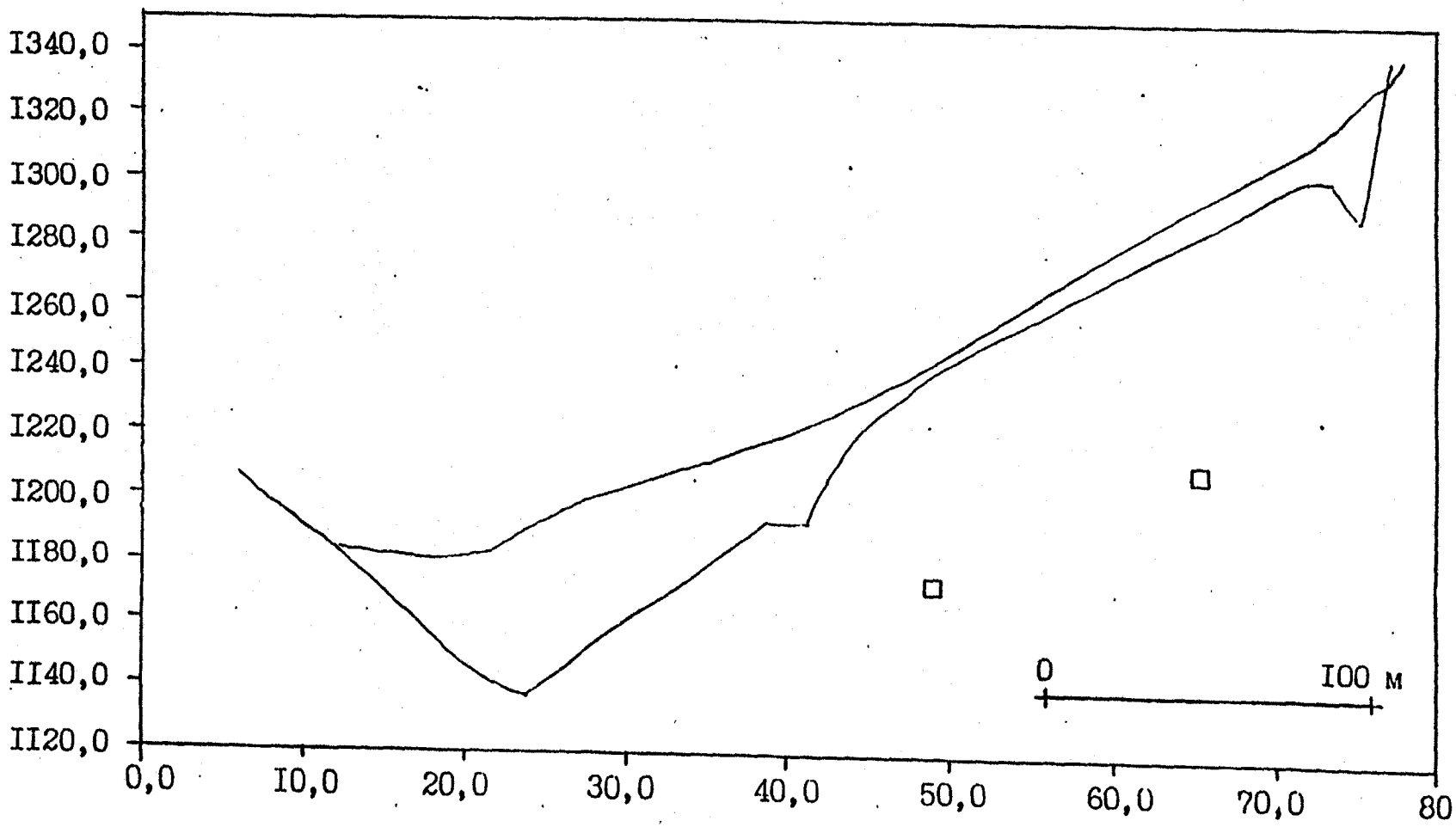

Figure III.52-a

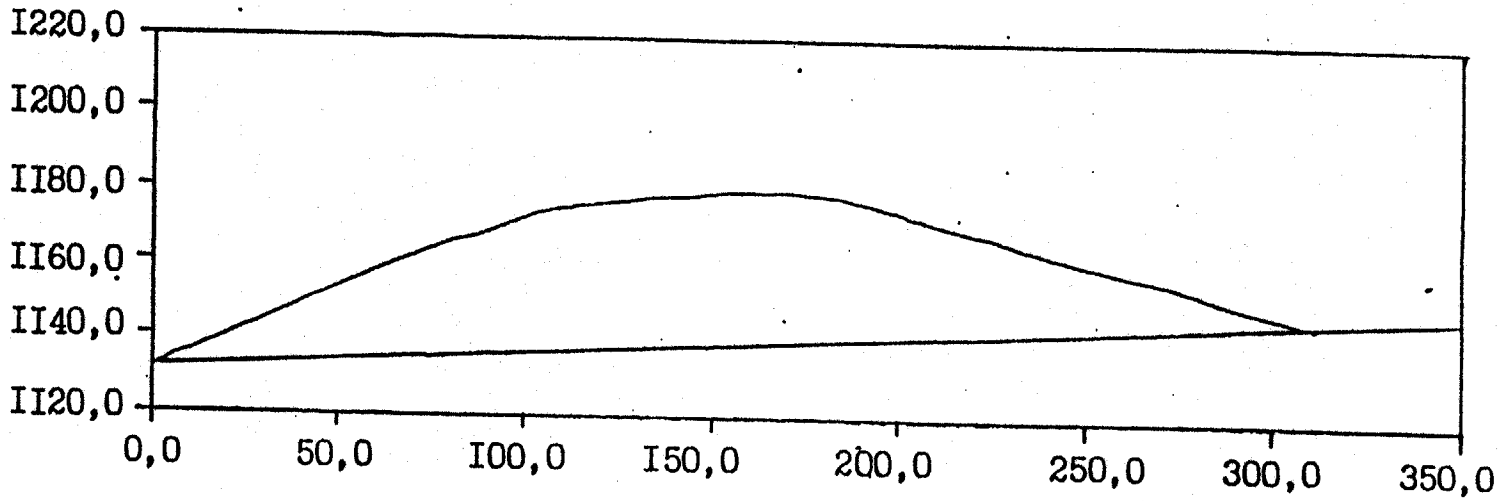

Figure III.52-b

Figure III.53

These observations also confirms the underdetonation of the second charge relative to designed value. Besides it, the second explosion effect have been influenced by the rocks collapse generated by the first explosion which covered the point of the SDS when the second charge has been detonated.

Acoustic wave. Air-shock wave from the explosion was measured by recorders SD-725. The sensors have been established at distances 570m, 800m, and 1800 m from the explosion epicenter. The sensors have measured only overpressure amplitude since the recorders have been switched on later then the explosion. Thus, air-shock wave shape was not measured. Figure III.55 presents peak overpressure amplitudes, ΔP, as a function of distance from the epicenter. Solid line on the Figure corresponds to overpressure in shock wave generated by trotyl air explosion of 32 ton. Thus, more than 1.7% of the explosion energy has been converted into acoustic wave.

A. Seismic effect of the explosion

The main goal of seismic observations during the explosion on the r.Uch-Terek was to obtain experimental data on generation and propagation of seismic waves in complex geological structures such as a region around the epicenter surrounded by ridges and valleys of the Tyan-Shan system. The data obtained were assumed to use in prediction of seismic effect in populated areas and on technological consructions from large scale explosions in the same area.

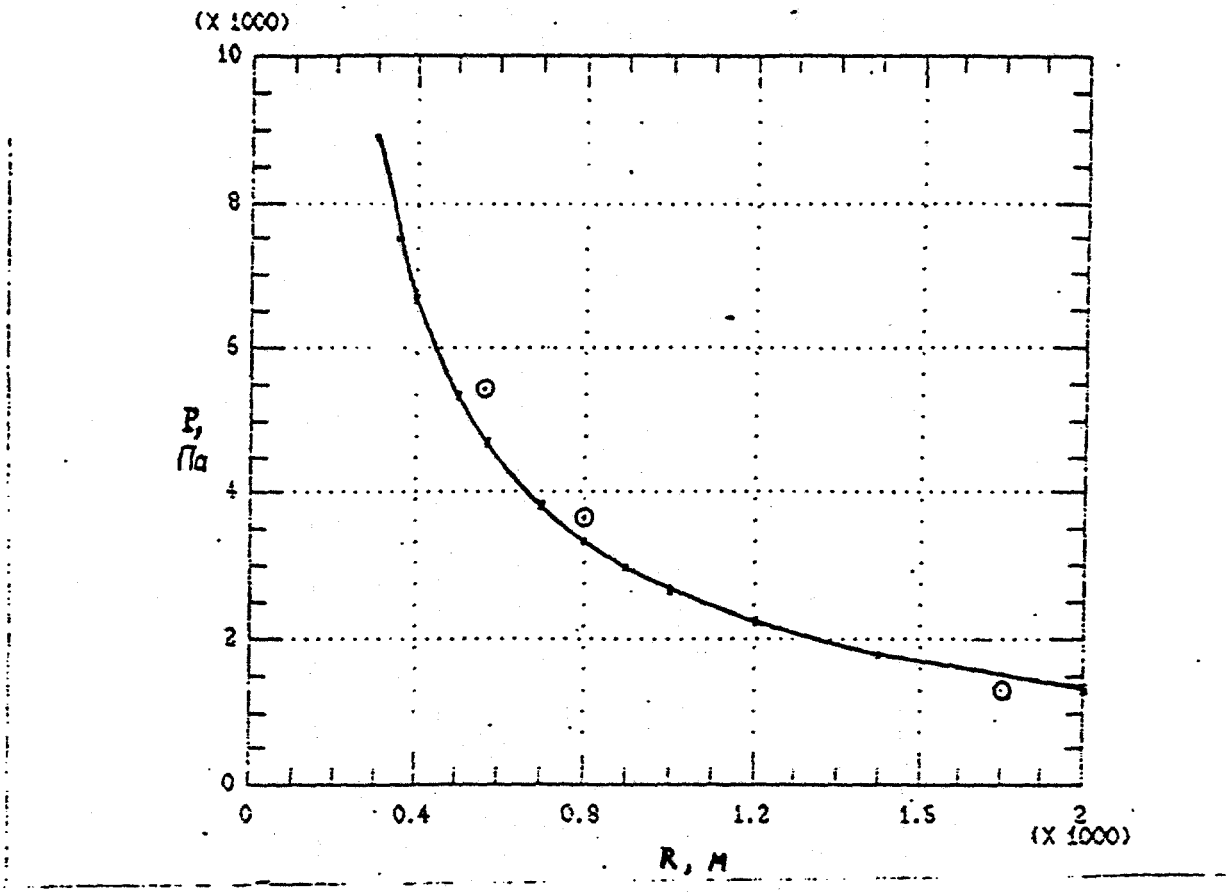

Figure III.55 Overpressure in air shock wave vs. distance
⊙ - experimental data

1. Observation system and measuring procedures.

Seismic observations have been designed in a way to solve the principal task - to reveal the populated areas with the highest seismic hazard. Thus, the system of obseravtions differed from usual profile observations which are the most informative for geophysics. Moreover, not only displacement but particle velocity was measured. Vertical (Z) and two horizontal (X) and (Y) components were measured to detect different seismic phases arrivals. X-component corresponded to radial motion with Y-component being perpendicular to X (transversal). At some points, however, X and Y were oriented NS and EW.

Nineteen points of observation have been established to measure seismic waves. The seismic points differed by equipment. Figure III.56 presents the observation points and there locations relative to the epicenter. Besides, Table III.38 contains list of the observation points including distances from the epicenter as well as azimuths and titles. The distances and azimuths have been determined from a 1:100,000 scale map. Due to low accuracy of the map, distances and azimuths errors were as high as several km and degrees.

Four pricipal groups can be distinguished from the nineteen stations. The first group numbered as 01 through 04 relates to the permanent seismic stations of the Complex Seismological Expedition of the Institute for physics of the Earth, Academy of Sciences of the USSR. The stations are equiped by "Turtle" type seismometers recording displacement in vertical (Z), north-south

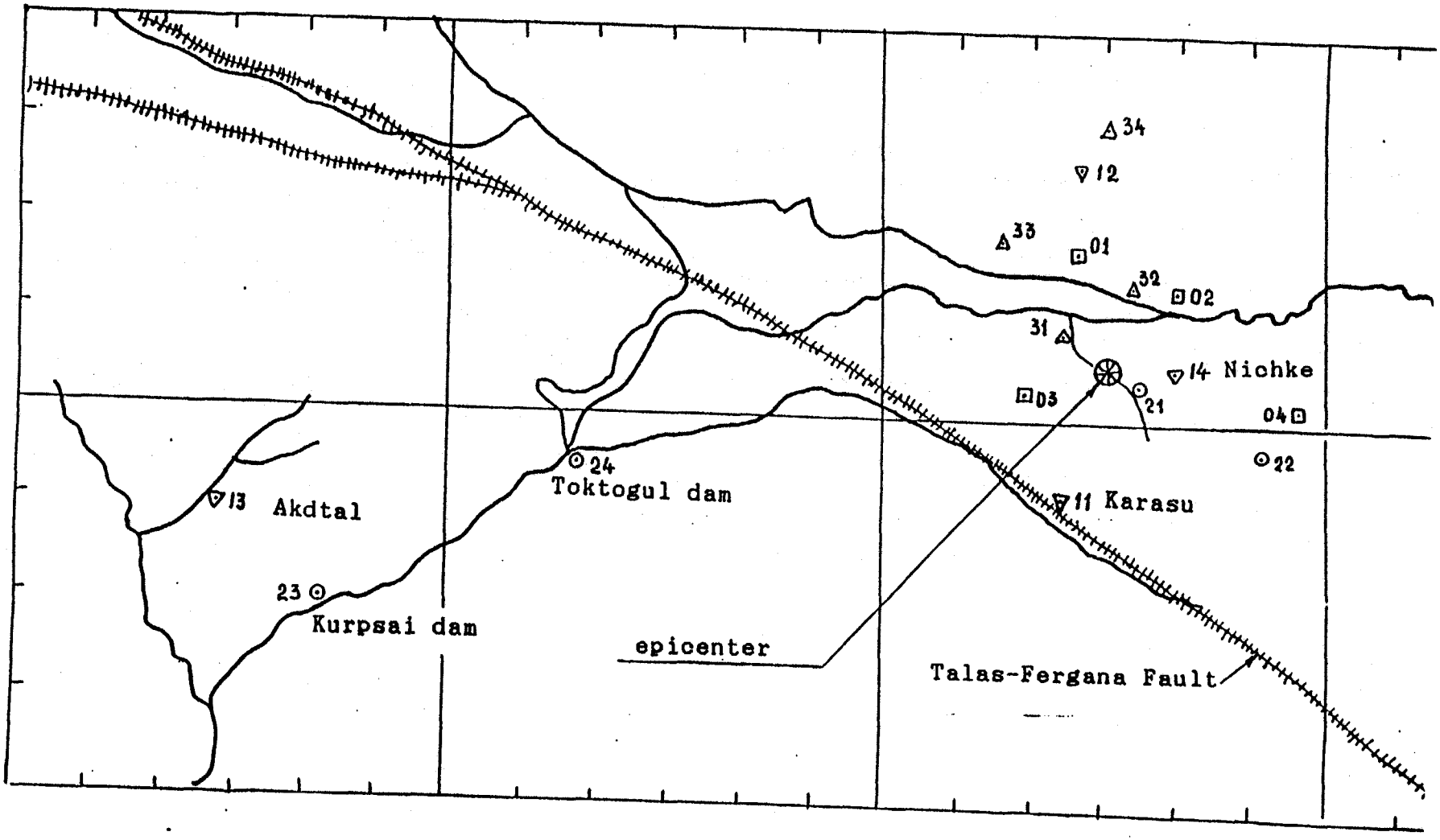

Figure III.56 Map of seismic points locations scale 1:500,000.

Table III.38

Seismic point #	r, km	Azimuth, φ°
01	11	346
02	10	41
03	8	252
04	19	103
11 (Carasu)	14	213
12 (Torkent)	19.6	353
13 (Akjal)	92.3	260
14 (Nichke)	6.4	95
15	41.7	269
16	53.4	274
17	58.9	263
21 (Kyzyl-Uran)	4.5	117
22 (Ozgorush)	18	117
23 (Kurpsai GES)	84.6	253
24 (Toktogul GES)	66.7	260
31 (Uch-Terek)	5	310
32 (Kyzyldjazy)	8.5	18
33 (Torkent)	16	322
34 (Sarsagul)	23	0

and east-west directions. The seismometers gain was of 50 in the frequency range from 1 to 10 Hz. The records obtained allowed to measure peak displacements and periods of longitudinal (P), shear (S) waves and their arrival times. The amplitudes and periods made it possible to estimate peak velocities in P and S waves. Surface waves' parameters, however, are disturbed and have not been measured and analyzed.

The second group of stations consists from seven permanent stations 11 through 17 equiped by displacement recording systems. The data from these stations were used to calculate time/distance curve for P, S, and R waves. The data from four stations have been analysed, however, and only Z-component. The sensors gain was of 100 in the range from 1 to 10 Hz. The data allowed to measure peak displacements in P and S-waves, as well as in surface waves. Wave periods and particle velocities have been measured only for surface waves since recording rates were of 2 mm/sec (i.e. very low).

The third group unites four temporary seismic stations 21 though 24 where collegues of D.D Sultanov worked. Each of the sites has been equiped by three USF-3M seismometers with natural period of 1.5 sec and damping of 0.5 to 0.7. Photographic paper was used for recordings by mirrow galvanometers GB-III and GB-IV on electromechanical oscilloscopes OMS-2M.

Three components of displacement Z, X, and Y were measured at these points as well as three components of particle velocity. To measure displacement, USF-3M was connected to overdumped GB-III-3 or GB-IV-S5 galvanometer with natural period

of 5 Hz. This connection gave flat responce (frequency independent) in the range from 0.05 to 1 sec with peak amplification ranging from 3000 to 5000 or from 25,000 to 35,000 respectively. Particle velocity was measured by using not damped galvanometers GB-IV-V3 with natural period of 120 Hz and damping in the range from 0.6 to 0.8. Responce of such a channel has the same shape as for displacement with peak amplification of 250 to 400. Seismic channels' gain was adjusted by using resistor set Shk-2, which allowed to change gain without responce shape disturbance by including in the seismometer/galvanometer circuit of r-shaped active resistor R_{1-r}.

Displacement and particle velocity were measured from the same seismometer. To avoid interaction between parallel galvanometers connected to a common seismometer, special large decoupling resistors, R_1, were included in the circuits. Some calculations show, that when R_1=500 Ohm ($\beta \geq 5$) interaction between two channels (electric current) with common sensor is less than 10% accurate if other channel influence is not considered.

Figure III.57 presents some typical responces of displacement (V_w) and particle velocity (V_n) channels, the scheme of parallel connection of two galvanometers to common sensor and a table of principal constants of seismic stations 21 through 24.

Second time marks are supplied to each seismogram in addition to records. The time marks are taken from chronometer MX-6 and accurate time from radio signals of a common

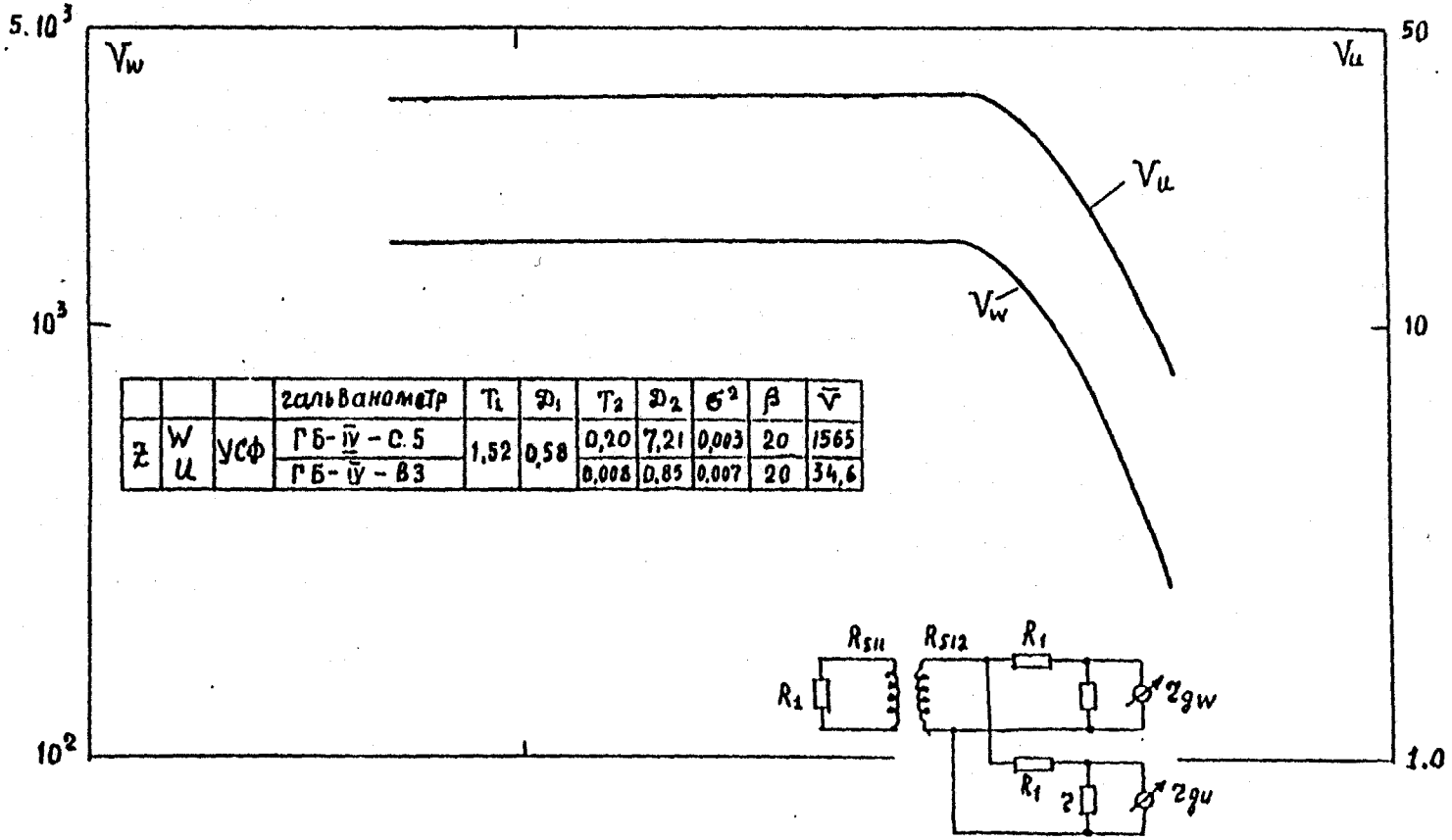

			гальванометр	T_1	$\mathcal{D}_1$	T_2	$\mathcal{D}_2$	σ^2	β	$\bar{V}$
Z	W	УСФ	ГБ-IV – С.5	1,52	0,58	0,20	7,21	0,003	20	1565
	U		ГБ-IV – В3			0,008	0,85	0,007	20	34,6

Figure III.57 Seismic channel responce.

3965

broadcasting system. The time marks allow to calculate seismic waves propagation velocities.

Recording rates at all the seismic stations were of 30 to 50 mm/sec which give time arrival accuracy of ±20 msec.

At the closest points 21 and 22, sensors were established in special vaults digged in soft soil. The vaults depth was of 0.5 m. Remote points 23 and 24 have been chosen at the sites with hard rock outcrops. Sensors have been established in tunnels. The distance from the tunnels mouth to the sensors was of 50 to 100 m.

The group four consisted from four postable seismic stations 31 through 34 where Dr. Kulikov V.I. worked with his collegues. Three seismometers SM-3KV have been established at the each point. The seismometers have natural period of 2 sec and damping of 0.5 to 0.7. Three-component particle velocity has been measured (X,Y,Z). GB-IV-B3 not damped galvanometers were used to record velocity. The galvanometers have natural period of 120 Hz and damping randing from 0.6 to 0.8. Electromechanical oscilloscopes OMS-2M were used for recording. The seismic channel responce was similar to flat responce shown on Figure III.57. The channels gain was of 3 to 20.

Chronometer MX-6 was used to make 1 second time marks. Recording rate was of 30 to 50 mm/sec.

One of the seismograms recorded at the point 04 (19 km from the epicenter) is shown in Figure III.58. The seismogram has a mark of component (WE,Z,NS). Different seismic phases' arrivals longitudinal (P), shear (S) and surface (R) are indicated by

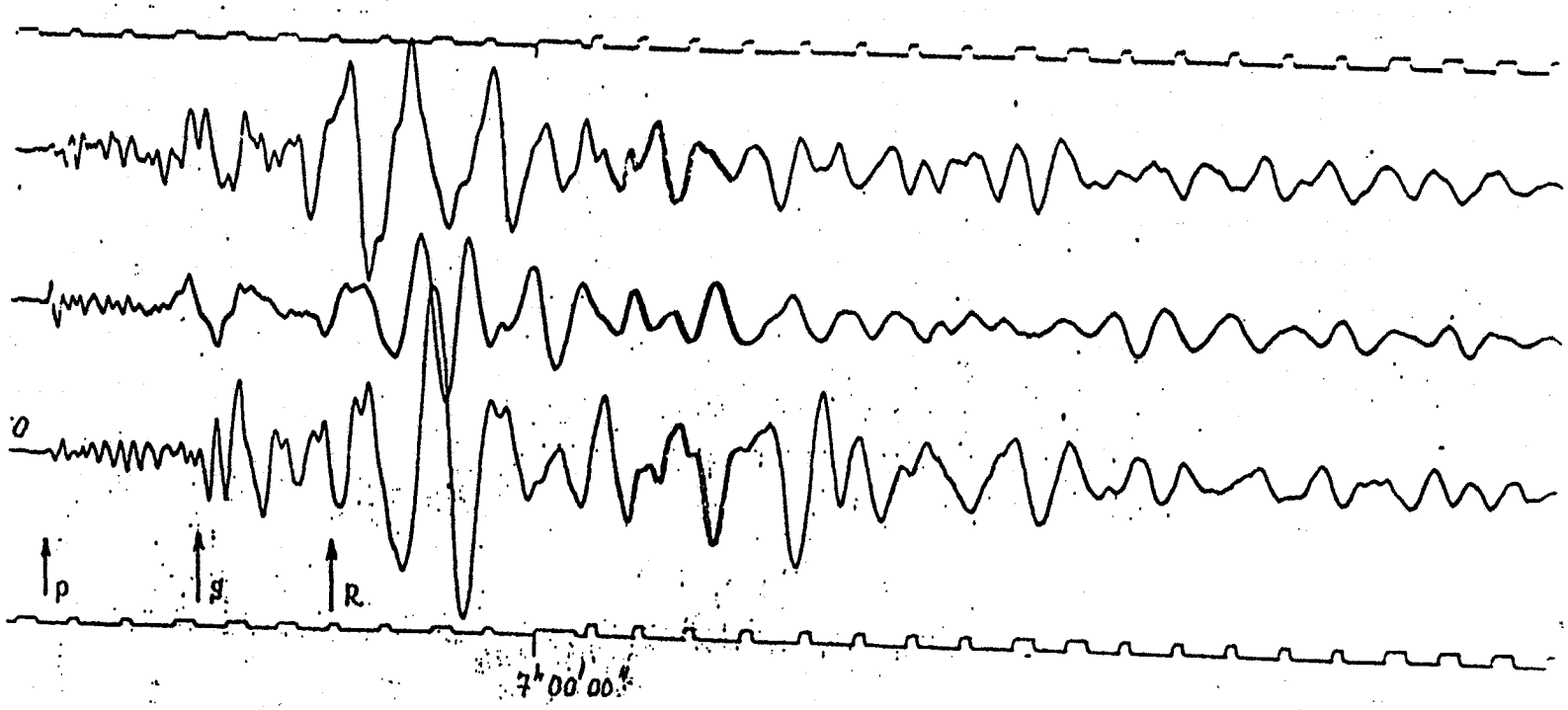

Figure III.58 Records from #04. Displacement, gain - 50.

Epicentral distance 19 km.

arrows. Second time marks as well as correct time 7 00′00″ (GMT) are also shown.

2.Wave pattern and time/distance curves.

Section III.5 discribes geological and tectonic structure of the region where the explosion at the r.Burlykya has been fired.

The data on absolute arrival times of longitudinal, t_p, shear, t_s, and surface, t_R, waves measured from the seismograms relative to Moscow time 10 59′00″ are presented in Tables III.39 and III.40. The time/distance curve for longitudinal wave shown in Figure III.59 was obtained from arrival times t_p. The experimental data put on that and other Figures are shown by signes corresponding to those on the map of the region (see Figure III.56). A straight line corresponding to apparent seismic wave velocity of 6.76 km/sec is drawn through the experimental points. The line extrapolation to R=0 makes it possible to estimate the shot time $t_{expe}=10^h59'48.18''$ (Moscow time). Figure III.60 presents all the arrival times of distinguished seismic phases from Tables III.39 and III.40. The seismic phases identification was carried out considering dynamic characteristics: amplitudes, periods, wave shapes. Apparent propagation velocities of P and S waves from the time/distance curves are 6.76 and 3.7 km/sec respectively. These velocities are high and indicate the waves are refracted propagating along the roof of crustal fundament - granitic/basalt complex.

Table III.39 Arrival times of selected seismic phases (stations 01-04; 21-24)

Point	r,km	Azimuth φ°	t_P	t_{S-P}	t_{R-P}	t_S	t_R
01	11	346	49.8	1.55	4.0	51.35	53.8
02	10	41	49.62	1.66	3.57	51.28	53.19
03	8	252	49.8	0.8	2.4	50.6	52.2
04	19	103	50.5	2.9	5.3	53.4	55.8
11	14	213	50.2	2.2	5.5	52.4	55.7
12	19.6	353	52.3	2.8	10	55.1	62.3
13	92.3	260	61.9	11.5	31	73.4	92.9
14	6.42	94.7	50.1	1.6	7.5	51.7	57.6
15	41.7	269	54.7	5.5	-	60.2	-
16	53.4	274	56.2	6.6	-	62.8	-
17	58.9	263	57.0	7.2	-	64.2	-

Note: Absolute arrival times are sums of t_P, t_S, t_R and $10^h59'$.

Table III.40 Arrival times of selected phases of sesimic waves (Seismic stations # 21-24 и 31-34)

Seismic station	r,km	Az. φ°	t_{P}	t_{S-P}	t_{R-P}	t_{S}	t_{R}
21	4.5	117	-	-	-	-	-
22	18	117	51.14	1.73	4.0	52.87	55.14
23	84.6	253	60.76	10.17	17.4	70.93	78.16
24	66.7	260	56.2	6.9	13.5	63.1	69.7
31	5	310	-	1.05	1.57	-	-
32	8.5	18	-	1.83	3.77	-	-
33	16	322	-	2.63	7.0	-	-
34	23	0	-	4.72	9.43	-	-

Note: Absolute arrival times of phases t_{P}, t_{S} and t_{R} are the sum of 10h59' and seconds presented in Table.

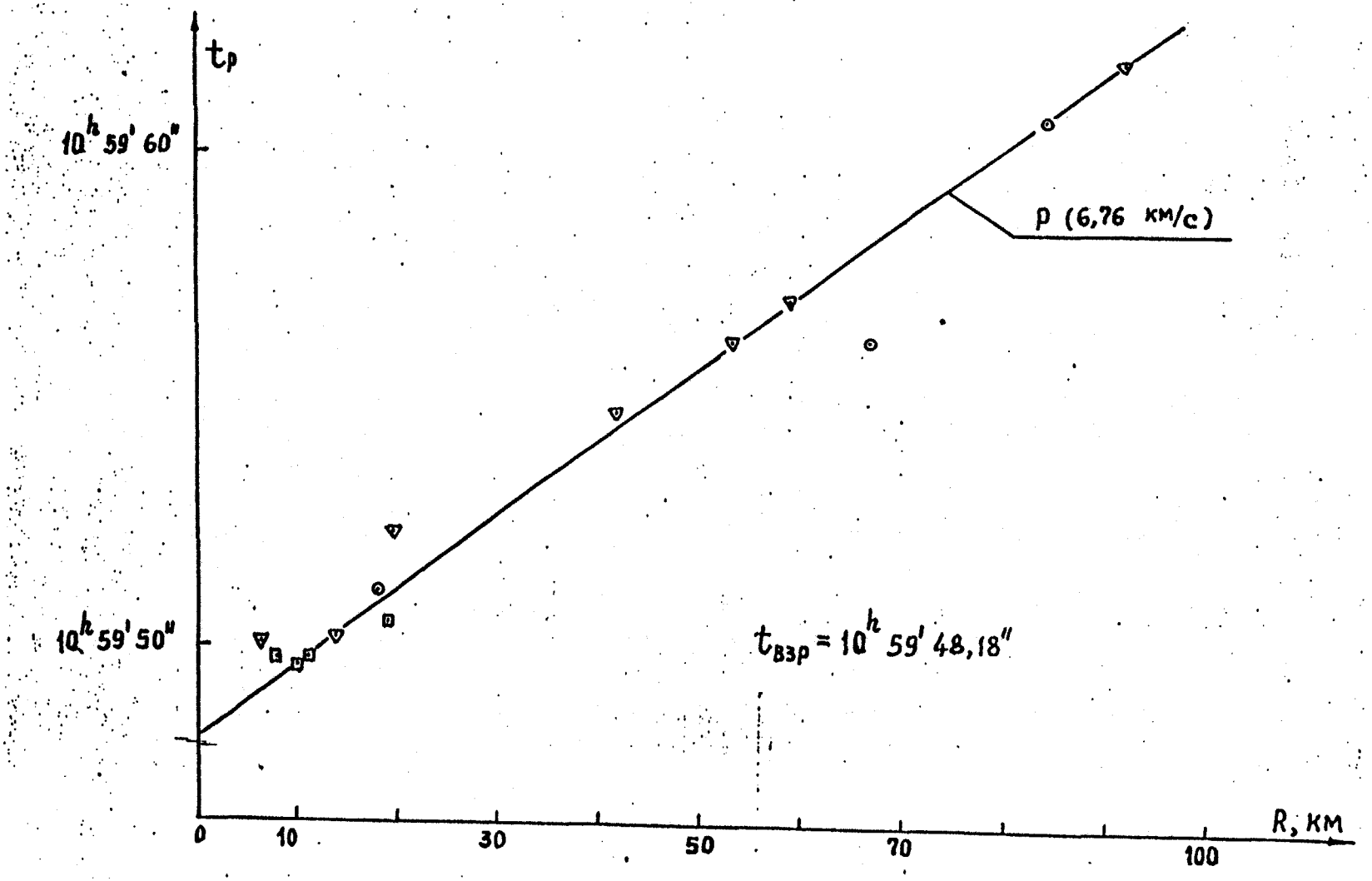

Figure III.59 Arrival time of P-wave.

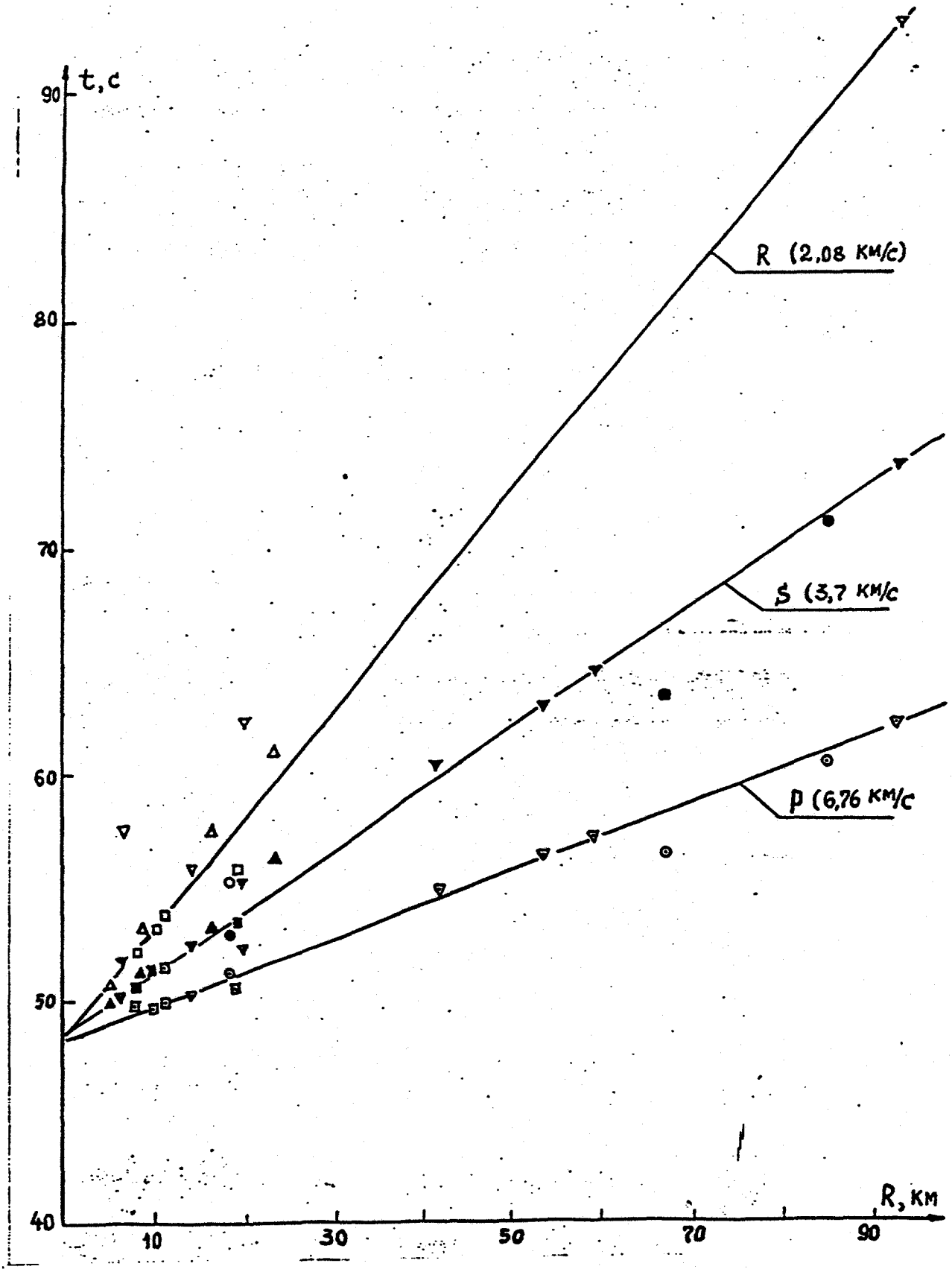

Figure III.60 Time/distance curves of P, S, and R-wave.

The apparent velocities obtained are consistent with the present understanding of the crust structure of the Fergana-Chatkal block (see Table III.38).

Surface waves are usually emergent and arrival times scattering is higher than for P and S waves as clear from Figure III.60. Surface wave apparent velocity from Figure III.60 is of 2.08 km/sec.

Although several seismic arrivals are seen on the seismograms, it is hard to identify them due to sparse observations (no profile).

3. Seismic waves' dynamic parameters.

It was hard to correlate different phases on the seismograms. Thus, dynamic parameters have been considered in different groups of longitudinal (P), shear (S), and surface (R) waves. Tables III.41 through III.44 present peak displacements, W, peak particle velocities, U, and periods in the groups. Particle velocities in the Tables from the seismic stations 01 to 04 and 11 to 14 have been estimated from relationship $U=\frac{2\Pi}{T}W$. Table III.43 contains the measured peak displacements W, and peak velocities V from the seismic stations 21 through 24. Table III.44 presents peak displacements calculated by relationship $W=\frac{T}{2\Pi}V$ from peak velocities obtained at the seismic stations 31 through 34.

Longitudinal waves. Amplitude/distance curve for longitudinal wave has been obtained from the data presented in Tables III.41

Table III.41 Seismic waves parameters (Raileigh wave parameters are not analyzed below)

NN	R, km	Azimuth φ°	Compo-nent	W_P, mm	U_P, mm/s	T_P, s	W_S, mm	U_S, mm/s	T_S, s	W_R, mm	U_R, mm/s	T_R, s
01	11	346	Z	0.09	2.17	0.26	not	visible		0.52	3.2	1.0
			E-W	0.02	0.50	0.25	on	record		0.3	1.7	1.1
			N-S	0.035	0.92	0.24				0.4	2.5	1.0
02	10	41	Z	0.048	1.21	0.25	0.066	1.04	0.40	0.24	1.88	0.8
			E-W	0.020	0.74	0.17	0.070	0.98	0.45	0.15	1.18	0.8
			N-S	0.02	0.63	0.2	0.15	1.71	0.55	0.21	1.39	0.95
03	8	, 252	Z	0.21	–	–	–	–	–	–	–	–
			E-W	0.20	5.7	0.22	0.28	5.02	0.35	1.24	9.73	0.9
			N-S	0	–	–	0.24	6.55	0.23	1.68	16.2	0.65
04	19	103	Z	0.08	2.18	0.23	0.126	0.66	1.2	0.31	2.16	0.9
			E-W	0.056	1.67	0.21	0.1	1.26	0.5	0.45	2.46	1.15
			N-S	0.040	1.0	0.25	0.22	3.45	0.4			

Table III.42 Data of the measurements of seismic waves (Periods ofP , S waves and particle velocity in P and S wave are not analyzed)

NN seismic station	R, km	Az., φ^{o}	Compo-nent	W_P, mm	U_P, mm/s	T_P, s	W_S, mm	U_S, mm/s	T_S, s	W_R, mm	U_R, mm/s	T_R, s
11	14	213	Z	0.04	1.26	0.2	0.025	-	-	0.06	0.47	0.8
12	19.6	354	Z	0.12	2.5	0.3	0.085	1.78	0.3	0.04	0.31	0.8
13	92.3	260	Z	0.02	0.18	0.7	0.05	0.39	0.8	0.025	0.13	1.2
14	6.4	94.7	Z	0.60	16.8	0.22	0.48	4.31	0.7	1.1	6.9	1.0

Table III.43 Data of the measurements of seismic waves

NN seis. sta.	R, km	Az. φ°	Com-po-nent	W_P, mm	U_P, mm/s	T_P, s	W_S, mm	U_S, mm/s	T_S, s	W_R, mm	U_R, mm/s	T_R, s
21	4,5	297	Z							0.65	7.55	0.65
(Kyzyl			X							1.3	11.5	0.7
Uran)			Y							1.4	13.0	0.7
22	18	297	Z				0.012	0.41	0.20	0.12	0.7	1.1
(Ozgo-			X				0.035	1.0	0.20	0.08	0.6	1.2
rush)			Y				0.02	0.60	0.20	0.11	0.6	1.2
23	84.6		Z	0.0025	0.080	0.20	0.004	0.035	0.8	0.0024	0.025	0.80
(Kurp-			X	0.0013	0.043	0.20	0.002	0.038	0.3	0.0016	0.023	0.90
sai Dam)			Y	0.0023	0.069	0.23	0.002	0.05	0.3	0.0016	0.023	0.70
24	66.7	80	Z	0.0036	0.115	0.20	0.0046	0.060	0.4	0.0042	0.044	0.70
(Tokto-			X	0.0033	0.115	0.20	0.010	0.12	0.55	0.0063	0.083	0.8
gul Dam)			Y	0.0030	0.070	0.20	0.014	0.15	0.6	0.0055	0.06	0.85

Table III.44 Data of measuring of seimic waves

NN seis. sta.	R, km	Az. φ°	Com-po-nent	W'_p, mm	U'_p, mm/s	T'_p, s	W^2_p, mm	U^2_p, mm/s	T^2_p, s	W'_-, mm	U'_-, mm/s	T'_-, s	W^2_-, mm	U^2_-, mm/s	T^2_-, s	W_R, mm	U_R, mm/s	T_R, s
31	5	310	Z	0.31	11.3	0.11					≈0					0.75	8.14	
			X								4.54					1.1	10	
			Y													0.59	6.03	
32	8.5	18	Z	0.09	4.4	0.13	0.12	5.45	0.23		≈0					0.34	2.95	
			X	0.035	1.44	0.15	0.13	3.18	0.26	0.05	1.73	0.18				0.30	3.32	
			Y	0			0			0.05	1.48	0.23				0.59	5.03	
33	16	322	Z	0.02	0.60	0.2	0.009	0.39	0.15	0.06	0.71	0.5	0.036	0.53	0.43	0.20	1.45	
			X	0.014	0.41	0.22	0.026	0.82	0.2	0.043	1.36	0.2	0.038	0.95	0.25	0.19	1.42	
			Y	0						0.043	1.0	0.27	0.064	1.74	0.23	0.15	1.36	
34	23	0	Z	0.085	5.36	0.10	0.032	1.26	0.16	0.047	0.89	0.33	0.10	2.9	0.22	0.043	0.44	
			X	0.049	2.58	0.12	0.10	3.58	0.18	0.029	5.53	0.33	0.19	4.2	0.28	0.11	1.74	
			Y	0.039	2.04	0.12	0.054	1.89	0.18	0.19	3.79	0.31	0.29	7.95	0.25	0.16	2.42	

through III.44. Figure III.61 shows in log-log scale peak vertical velocity in longitudinal waves, V_p^z, as well as radial, U_p^x. Figure III.62 presents peak vertical displacement, W_p^z, and peak radial displacement, W_p^x. Vertical measurements are shown by signes with a dot inside (U_p^z and W_p^z), and radial by opened signes (U_p^x and W_p^x). The parameters shown on the Figures are underlined in Tables III.41 through III.44.

Tangential component of motion (Y) is usually much lower than radial and vertical as the experience of seismic waves measurements from large explosions shows. Such a rule is confirmed by the data obtained from the r.Uch-Terek explosion as Tables III.41 through III.44 show. Thus, Y-component is not shown on Figures III.61 and III.62 and is not analysed.

Vertical and radial components are usually same from the same experience. Thus, it is natural considering all the parameters together. It can be seen from the data obtained during the explosion on the r.Uch-Terek, that for all the seismic stations except two vertical components, U_p^z and W_p^z, are large than radial, V_p^x and W_p^x. Vertical to radial amplitude ratio varies with station but is lower than two. Thus, averaging relations on Figures III.61 and III.62 have been calculated from all the data set. The experimantal data have been approximated by the least squares procedure. Following relations have been obtained:

$$U_p^{z,x} = 107\ r^{-1.58}\ [mm/sec]$$

$$W_p^{z,x} = 3.58\ r^{-1.53}\ [mm]$$

which are presented by solid lines on Figures III. 61 and

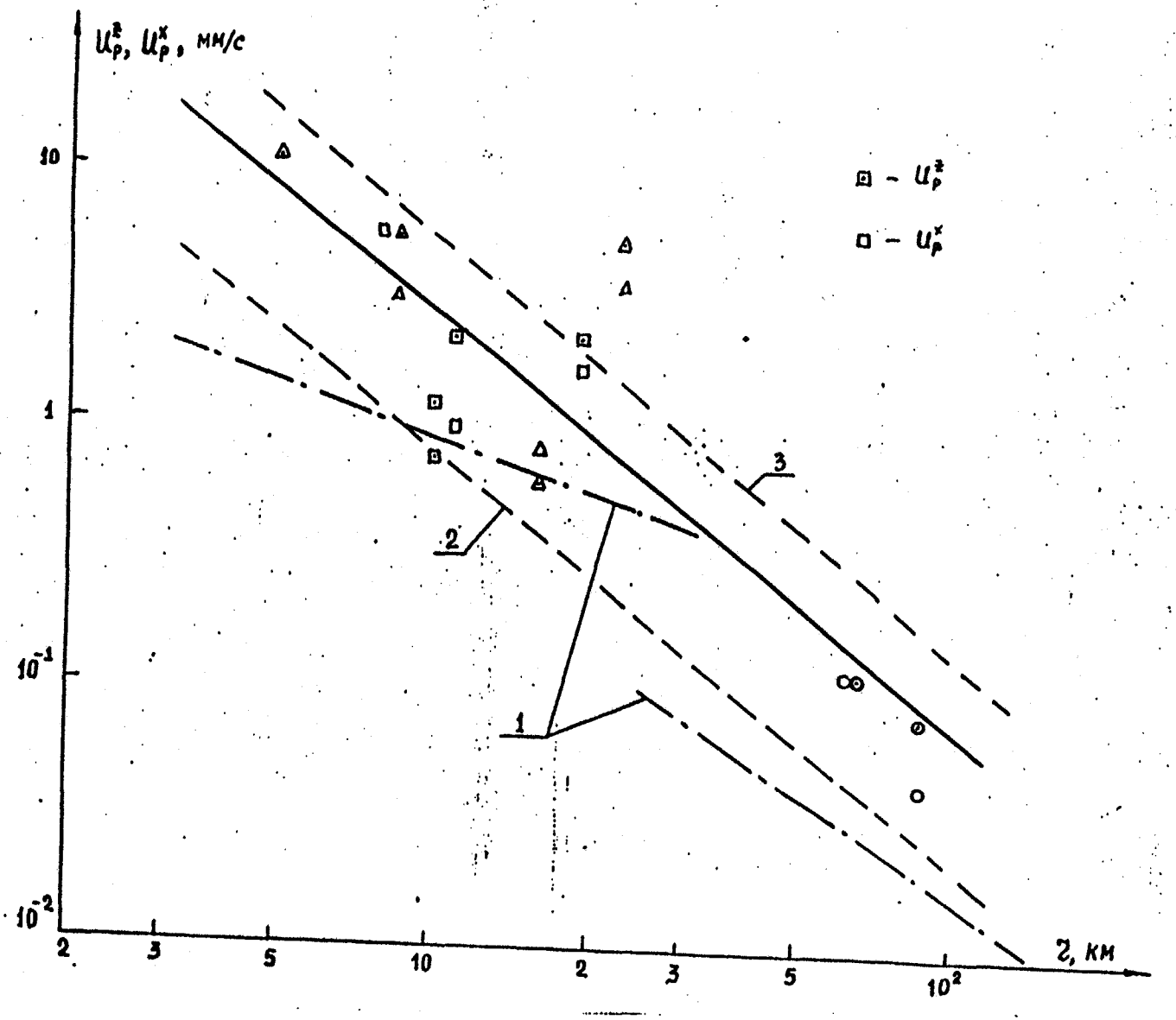

Figure III.61 Peak particle velocity in longitudinal wave.

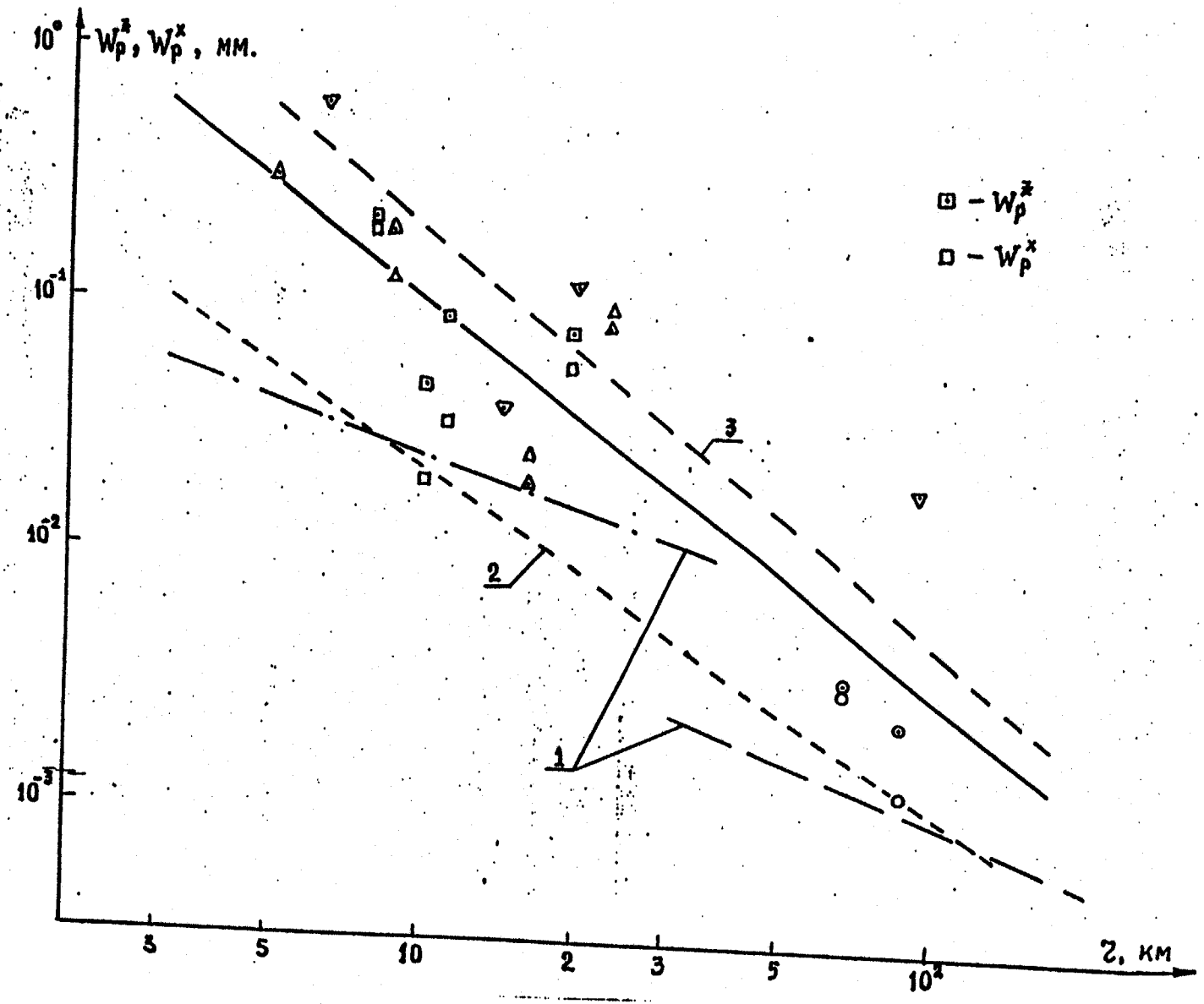

Figure III.62 Peak displacement attenuation in longitudinal wave.

The experemental data scattering is high, as clear from the Figures. Particle velocities, U_p^z and U_p^x, measured at the Sarsagul (point 34) are five times higher than approximated values. Local geological conditions are of principal importance for the scattering. For example, particle velocity amplitude at the point N03 is 1.4 times higher than approximated, and at the point 02 is 2.8 times lower, although the two points are at the same distance. But the point 03 was situated on thick sediments, and the point 02 was on hard rocks. So the difference is natural.

Vertical displacement, W_p^z, at the Carasu station (point N11) is 1.6 times lower than predicted by the approximated line. The Talas-Fergana fault near the town may be a reason for that.

The same scattering is observed at the remote (60 to 100 km) stations. Displacement at the Akdjal (point N13) is 5 times larger than approximated. From the other side, displacements, $W_p^{x,z}$, measured at the Kurpsai hydropower station (point N23) and the Toktogul dam (point 24) are lower than approximated.

The latter amplitudes can be lower due to the points location. The two points have been established in tunnels at distances of 100 m from mouths. Previous investigation of the explosion on the r.Byrlykya has shown that displacement amplitude, W_p^z, measured in the living zone of the town Karakul (56 km) is 2 times larger than in a tunnel which is close to Karakul. Hence, geological conditions are of high importance for amplitude as well as distance.

Amplitude/distance curves obtained from the r.Burlykya explosion, $U_p(R)$ and $W_p(R)$, are also shown by dashed lines on Figures III.61 and III.62 for a comparison. All the experimental data are averaged here together to obtain these relations which is different from section III.5. According to this consideration, the amplitude/distance curves are approximated by relationships $U_p^{z,x} \sim r^{-1.56}$, and $W_p^{x,z} \sim r^{-1.31}$. These relationships are close to those obtained from the explosion on the r. Uch-Terek. Dashed lines (2) are lower than solid lines averaging the Uch-Terek data. It is consistent with larger yield of the r. Uch-Terek explosion.

Empirical relationships for P-waves from tamped nuclear explosions in granite (scaled to 1 kt) are also shown on Figures III.61 and III.62 by dashed lines (3). Exponents in these relations are the same for displacement and particle velocity and are equal, n=1.6. Comparing all these relationships, it is possible to conclude that seismic waves attenuation with distance is almost the same for tamped nuclear explosions and the explosion under consideration, but absolute amplitudes of the latter are lower than for 1 kt tamped explosion.

This differenc can be explaned by lower seismic efficiency of excavating explosions as well as different physical parameters of explacement medium.

Figure III.63 presents periods of longitudinal waves related to peak displacement or particle velocity. Such a relation, $T_p(r)$, obtained from the explosion on the r.Burlykya is shown by solid line. Despite high scattering of the

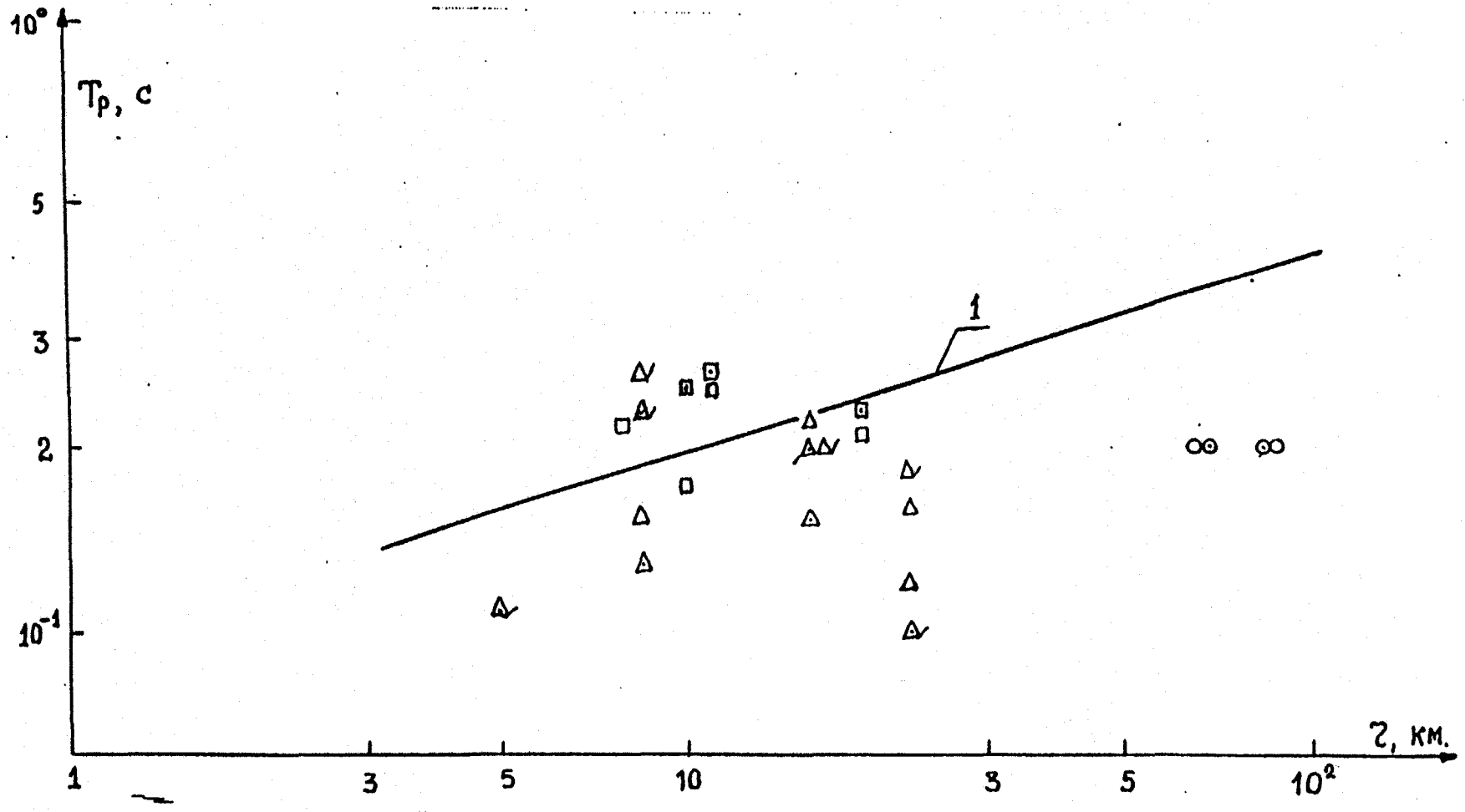

Figure III.63 Periods of surface waves.

experimental data, periods from the r.Uch-Terek and r.Burlykya explosions are consistent. The periods should be consistent since T_p almost not depend on yield.

Body waves. Buildings and constructions interact with seismic waves as oscillators with a given natural periods. Five-stage buldings and lower are usually characterized by natural period of 0.1 to 0.5 sec. Thus, construction responce to seismic motion is dependent on spectral characteristic of a signal as well as its duration.

In the very beginning of the explosions hystory, when only shallow explosions of several tons were conducted, seismic waves were not of long duration and contained only several periods in body and surface waves. Surface waves were of the highest danger for buildings (by periods and propagation distance) in such a situation. Geological structures did not influence this interaction much. Seismic hazard was relatively simple to estimate and empirical criterion of critical velocity of 10 cm/sec has been established.

As a scale of explosions increased, seismic waves duration and periods also increased. Buildings and constructions damaged when seismic waves parameters were lower than considered as safety in seismic enjeeniring. This phenomenon was the most distinct of underground nuclear explosions. It occured necessary to reduce critical particle velocity causing damages or destruction of buildings and constructions due to periodical process of induced oscillations similar to earthquakes.

Destructivity of explosions was estimated by intensity balls in this situation. MSK-64 scale was used which has been eleborated from earthquakes. Each ball of the scale has its own characteristic damages and ground motion velocity.

The experience has shown that horizontal components of ground motion velocity is of the highest importance for constructions. It is also obvious that short period waves with periods close to those of natural of constructions have the highest damaging effect. Surface waves oscillations can be excluded from consideration, since those periods are of much longer periods and particle velocities are lower than in body waves.

From the previous discussion, it is natural that peak radial velocity in longitudinal wave, U_p^x, and peak radial and transversal velocity, $U_s^{x,y}$, in shear waves have been analyzed in order to estimate seismic hazard of the explosion on the r. Uch-Terek. Figure III.64 presents the experimental data on U_p^x and U_s (points) averaged by the least squares method (solid line).

It is clear from Figure III.64, that amplitudes of P and S-waves are similar, with number of seismic stations where $U_p > U_s$ being the same as where $U_s > U_p$. Amplitude/distance curve from the data can be approximated by relationship

$$U=98.4\ r^{-1.54}\ [mm/sec]$$

Similar relationship obtained from the explosion on the r. Burlykya is shown by dashed line (1) on Figure III.64. This relationship lays lower and is characterized by higher

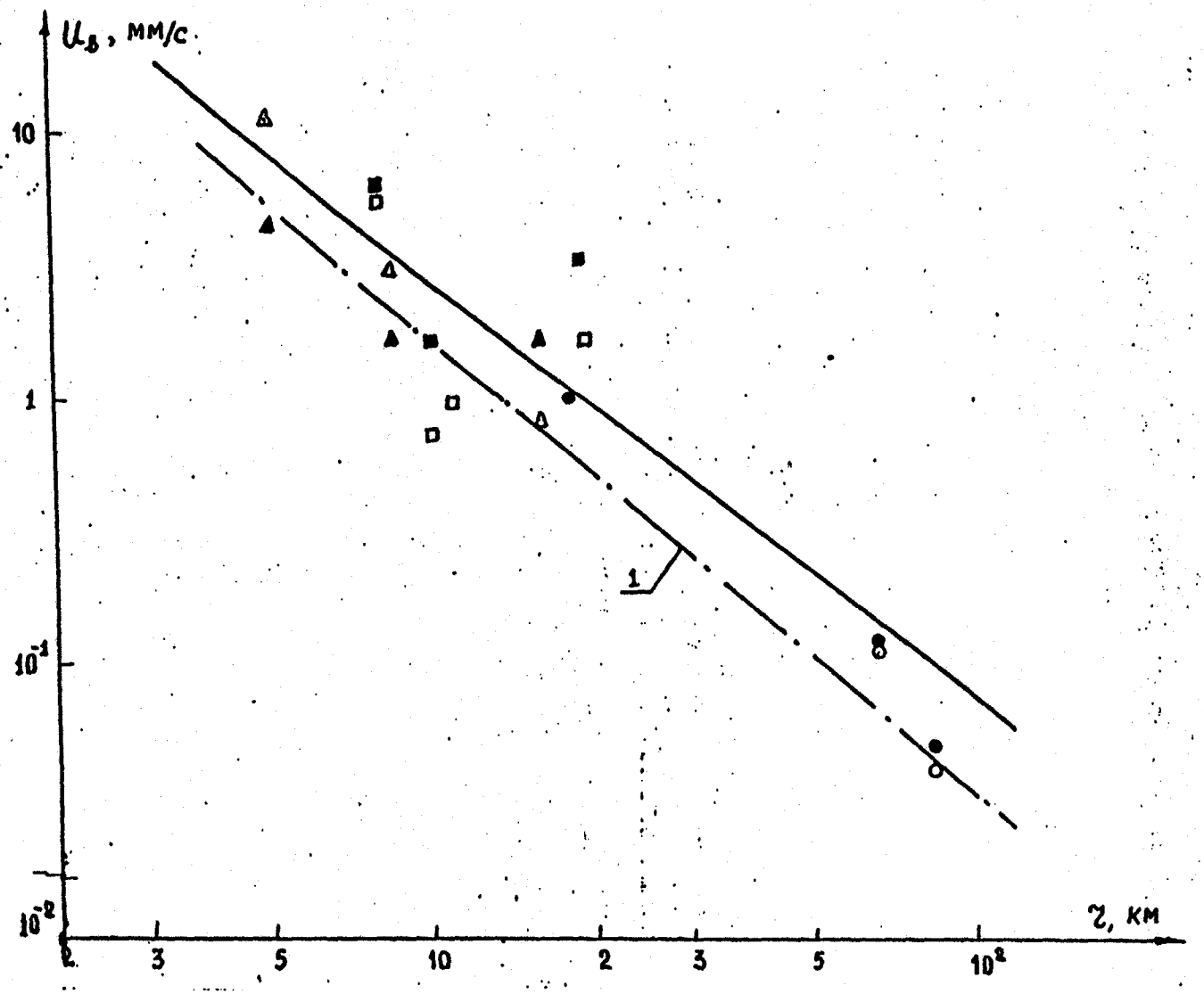

Figure III.64 Peak particle velocity attenuation in body waves.

attenuation ($r^{-1.7}$) than that of the Uch-Terek explosion. So those of comparison is complicated. If to compare amplitudes at a distance 20 km from the two explosions, the difference is of 1.86 times.

Assuming amplitude/yield relation $A \sim q^{0.65}$, which is usual for underground nuclear explosions, it is possible to estimate the Uch-Terek/Burlykya yields ratio. It is of 2.6.

Surface waves. Surface waves' parameters are presented in Tables III.41 through III.44. Large displacements and low ground velocities are characteristic of these waves. Surface waves periods are 2 to 6 times longer than those of body waves.

Points in Figure III.65 present vertical and radial displacements in surface waves. Regression line obtained by the least squares method is presented by solid line:

$$W_R^{z,x}=19.95\ r^{-1.88}\ [mm].$$

The data scattering is lower. This lower scattering can be explained by lower influence of the crust inhomogeniety due to larger wavelength.

The Burlykya data are shown by dashed line ($W_R^{z,x}(r)$). This line slope is less than from the Uch-Terek data.

Similar relationship for 1 kt tamped explosion in granite is shown by dashed line (3).

Particle velocities, U_R^z and U_R^x, as well as regression lines are shown on Figure III.66 by solid lines. Similar data from the Burlykya explosion are shown by dashed line (1) in Figure III.66. The data scattering is also lower due to the reasons

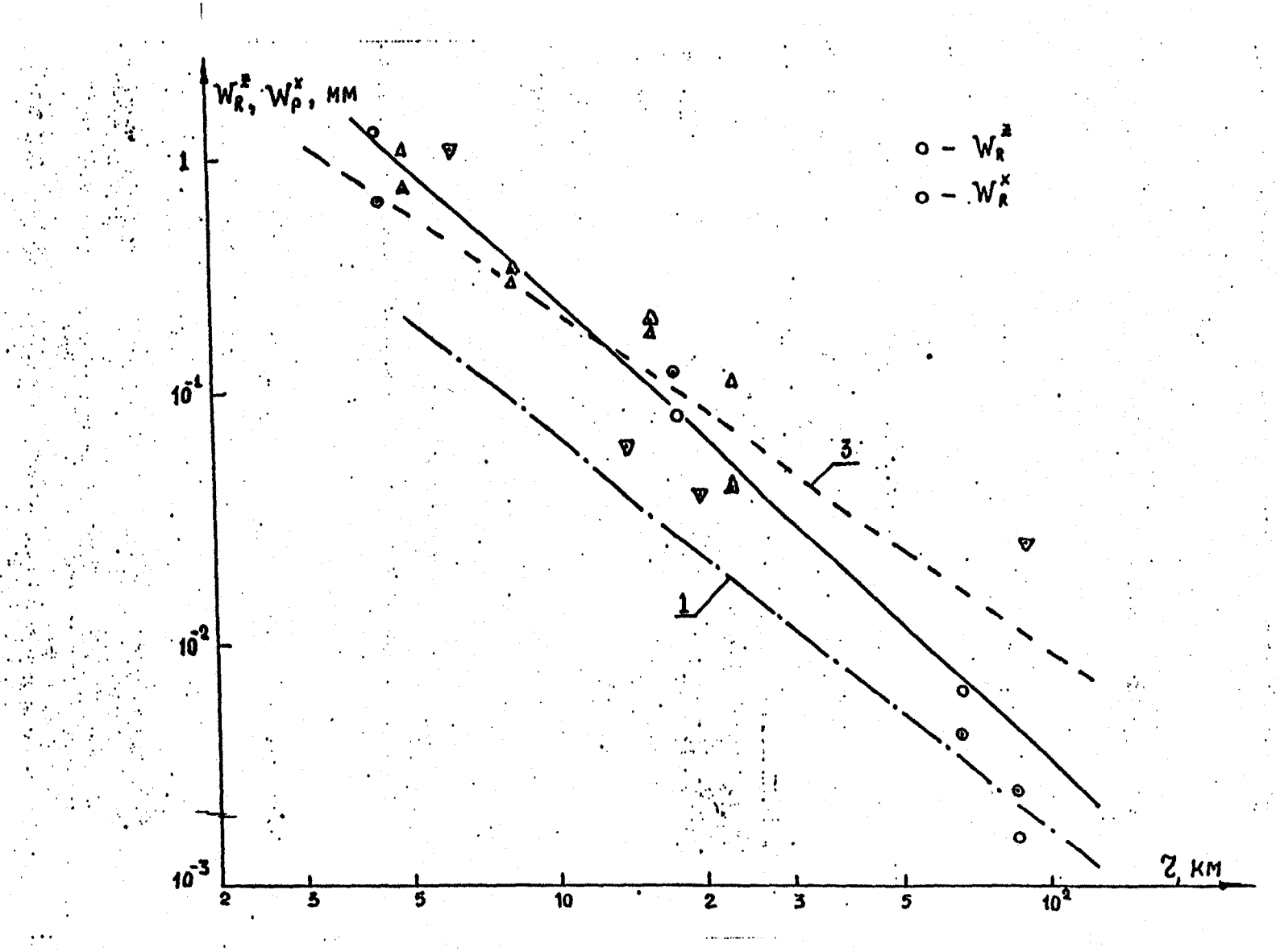

Figure III.65 Displacement in surface wave.

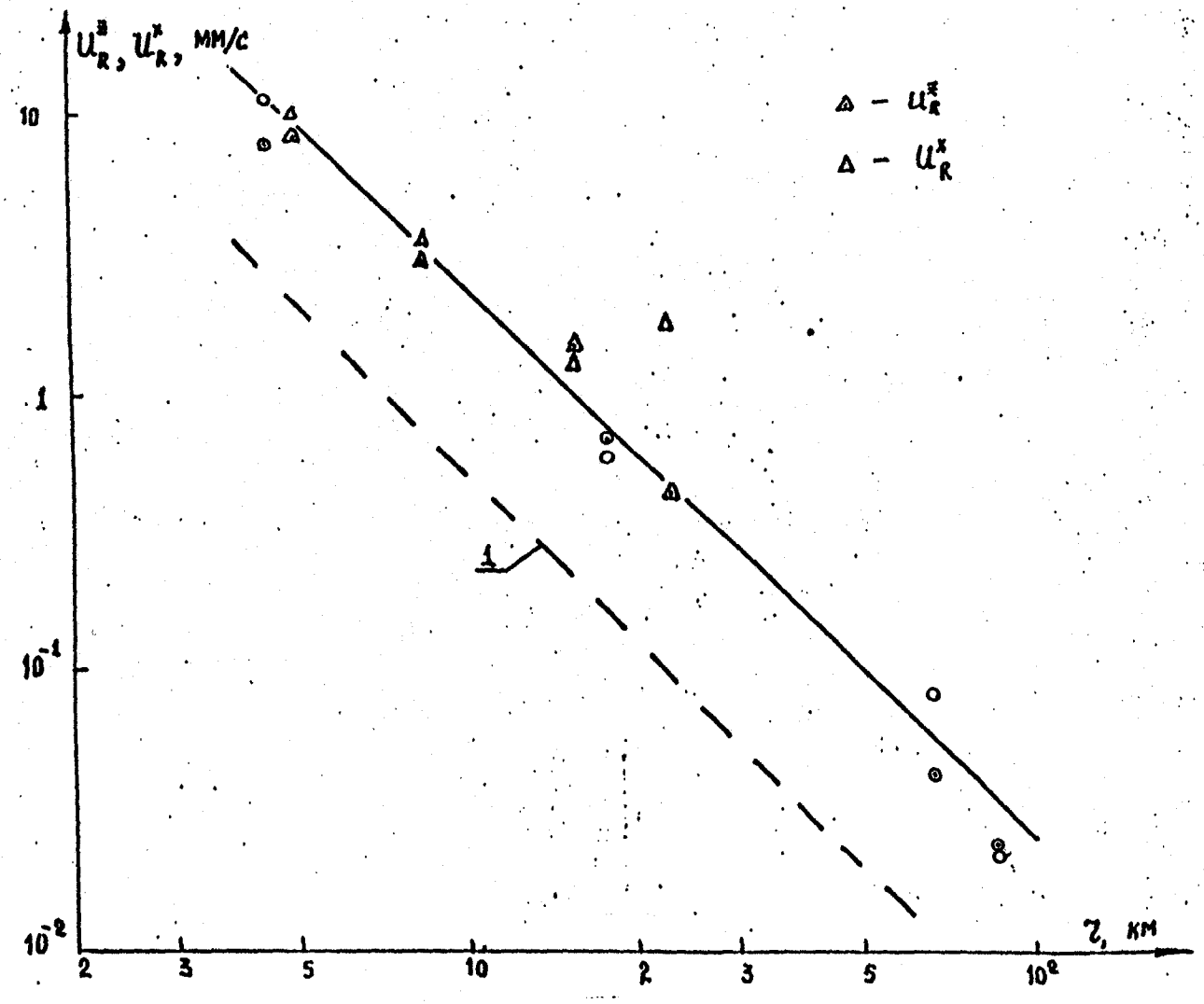

Figure III.66 Particle velocity in surface wave.

discussed above. Attenuation is almost the same for the two explosions.

Periods of surface waves are presented in Figure III.67. The periods are much longer than those of body waves, as clear from the data. The Burlykya relationship is shown by dashed line (3), as well as $T_R(r)$ for 1 kt underground nuclear explosion in granite. The experimental data are consistent with relationships (1) and (3).

B. Investigation of induced seismicity by the explosion on the r. Uch-Terek.

Number of large explosions conducted for peaceful purposes, including dam construction, have been increasing in recent years. Due to this fact, importance of possible toctonic earthquake triggering by seismic waves generated by large scale explosion is very high, especially in active regions. Explosion influence on seismic activity in regions surrounding it as well as remote regions have been studing from the very beginning of underground testing (60-ties).

Test explosion of June 11, 1989 on the river Uch-Terek, Kirghizia was used to conduct such an investigation through seismic monitoring of epicentral and adjacent regions diring long time before and after the explosion. Relatively low yield of the explosion has, of cource, limited a scale of its effects on environment. But high natural seismic activity of the region (8 balls) and many active faults around allowed to suppose measuring possible induced seismicity. Moreover, since the

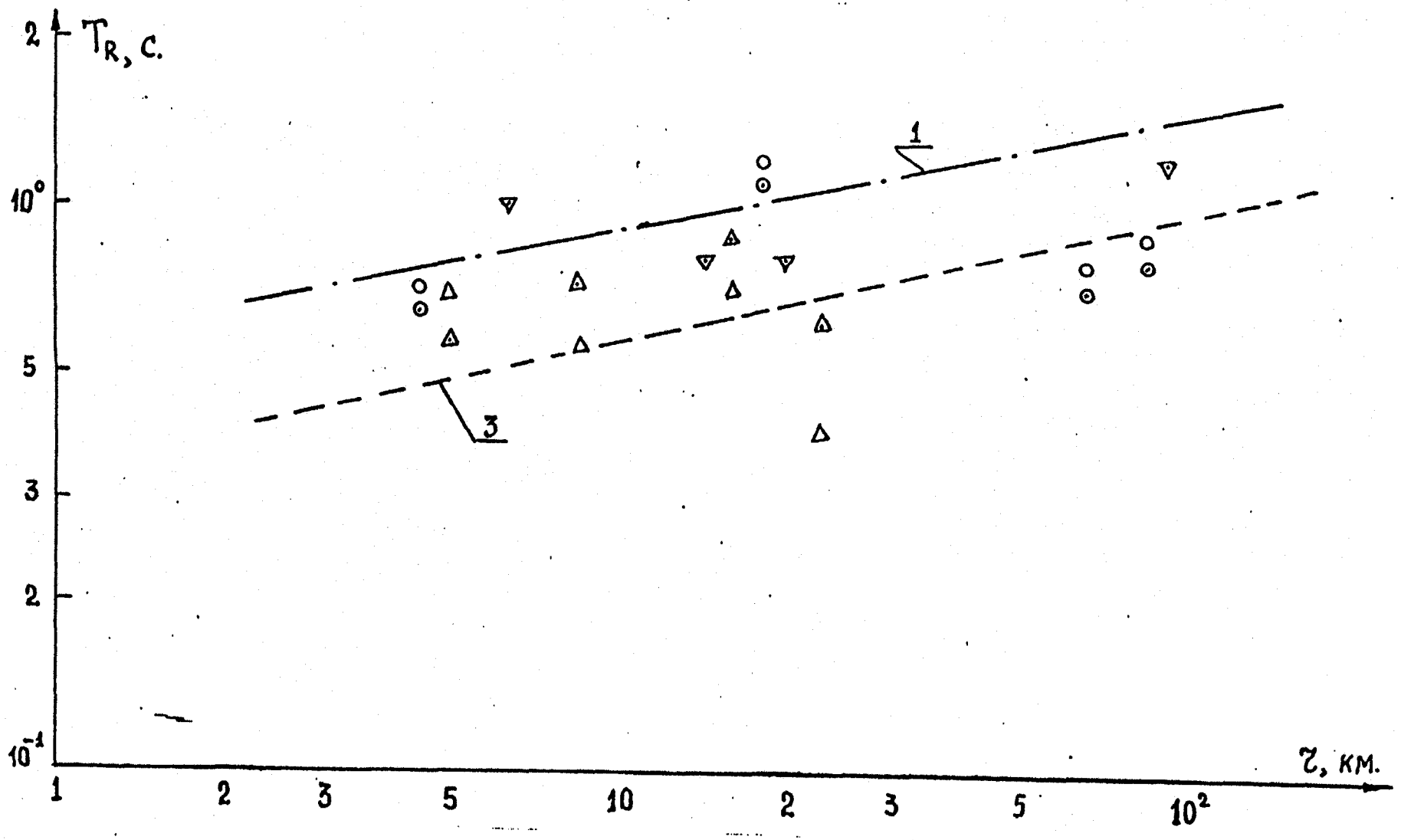

Figure III.67 Periods of surface waves.

explosion has not been tamped (contained) no seismic events related to the explosion cavity collapse, following subsidence and residual strain around the explosion could take place. In this case, only natural tectonic strain field "disturbed" by transient explosion wave is related to possible seismicity changes after the explosion.

No induced earthquakes with energy higher than explosion energy have been still mentioned after explosions. The highest energy induced earthquakes have been measured in several seconds after explosions when strong explosion generated wave passes through the source region of prepared earthquake. The zone of possible influence of an explosion in tectonic regions is smaller than 20 to 40 km for the explosion of Mt class.

It is possible to imagine that a triggered earthquake can be larger than regional seismic intensity (in balls). For example, there were rockbursts after mining explosions, seismic effect increase from shallow earthquakes, relief and soil conditions effect.

1. Tectonic conditions and natural siesmicity around the Cambarata dams.

The site of the Cambarata dams construction is within large tectonic structure - the Naryn graben. The graben is complex and actively developing structure. It is the eastern part of the Ketmen-Tube block of the Earth crust which is characterized by high density of discontinuities and active tectonic movements along deep buried zone. In modern time, the lower part of the

graben is lifted, but adjacent mountains are uplifted with higher rate. Such a differential uplift strain field. The graben structure as well as that of the Ketmen-Tube block is highly inhomogenions and is separated by many tectonic discontinuities.

A sheme of tectonic faults of different sizes around the Cambarata dams and adjacent regions is shown in Figure III.69. There are some large and deep faults at the territory of the region and around it. They are the Talas-Fergana fault, the Nikolaev line and others. These faults are active and seismic. The faults are characterized by geological data as a zone of seismic events with magnitudes of 7.5 (Talas-Fergana fault) and of 6.5 (Nikolaev line). The set of the deep faults is extended by regional and local faults. The latter faults are shallower and smaller. At the territory of the Naryn graben the maximum possible magnitude is predicted to be of 5.0 near the dams.

Tectonic activity of the region is governed by the Indostan/Euroasia lithospheric plates collision. Compressional stresses in meridional direction and thrusts are prevailed. Seismic activity of the region is constrained by tectonic motion and geological structure.

Earlier investigations (1965-1977) has established that the Cambarata region's seismic activity is lower in comparison to southern regions. There were only several earthquakes with magnitudes from 2.8 to 3.5 between the Talas-Fergana fault and r. Naryn in that period of time. There were also observed more earthquakes with lower magnitudes. During 1985 through 1987 seismic measurements were conducted by high sensitive equipment.

There were of 72 earthquakes in 1985, 110 in 1986, and 54 in the first six months of 1987. The earthquakes magnitudes were from 0.5 to 4 with 2/3 of the total amount being of magnitude from 1.5 to 2.0. The majority of the earthquakes and the highest from them were near the Talas-Fergana fault. There were observed only several earthquakes beneath the constructed dams with magnitudes of M=2.0. Considering seismic equipment sensitivity change, it is possible to conclude that seismic activity near the Cambarata dams has not changed during 12 year period from 1975 to 1987 and was low.

Despite relatively low seismic activity near the Cambarata dams, seismic hazard is constrained by strong earthquakes at the Talas-Fergana fault (M=7.5), Nikolaev and Naryn (M=7.0-6.5) seismic zones situated at distances from 20 to 50 km. Thus, the region is characterized by seismic intensity of 8 balls.

The obtained level of seismic activity of 7 to 10 earthquakes per month allowed to designe 20 days long seismic monitoring after the explosion June 11, 1989 at the r. Uch-Terek. If the explosion has really changed local seismic activity, several tens of earthquakes could be detected similar to previons experience.

2. Results of observations of seismicity in the period of the r. Uch-Terek explosion.

To reveal possible induced seismicity from the explosion at the r. Uch-Terek data from a telemetric set of seismic stations as well as temporary seismic stations of the Institute for

physics of the Earth of the Academy of Sciences of the USSR have been used.

The data were obtained in the period of time from May 1 to June 30, 1989. Figure III.68 presents a scheme of the seismic stations' locations. Table III.45 summarizes the stations locations and elevations.

Table III.45 Locations and elevations of seismic stations

NN	Tag	Stations name	Coordinates latitude N	Coordinates longitude E	Elevation, m
Telemetric set					
1	TG01		41°39.0′	72°35.2′	2000
2	TG02		41°41.9′	72°46.6′	2200
3	TG13		41°49.8′	72°39.0′	2500
4	TG15		41°48.2′	73°22.0′	2100
5	TG16		41°52.3′	72°29.8′	2000
6	TG17		41°46.5′	73°32.7′	2100
7	TG10	Toktogul	41°51.5′	72°56.5′	980
Temporary stations					
1	TK01	Karasu	41°35.9′	73°10.2′	2050
2	TK02	Torkent	41°53.5′	73°13.8′	1400
3	TK03	Akjol	41°34.3′	71°12.5′	920
4	TK25	Nichke	41°42.4′	73°20.6′	1700

Catalog of earthquakes and explosions for that period of time is in Table III.46. The region is limited by coordinates 41°10′ - 42°30′ N and 71°50′ - 74°00′E. The catalog contains origin times (GMT), hypocenters (coordinates and depths), energy (energy class and local magnitude), and number of stations used to determin the hypocenters.

Energy class, K, characterizes seismic energy, E_s, of earthquake in Joles by relationship $K=\log E_s$. Earthquake magnitude, M, can be determined from empirical formula:

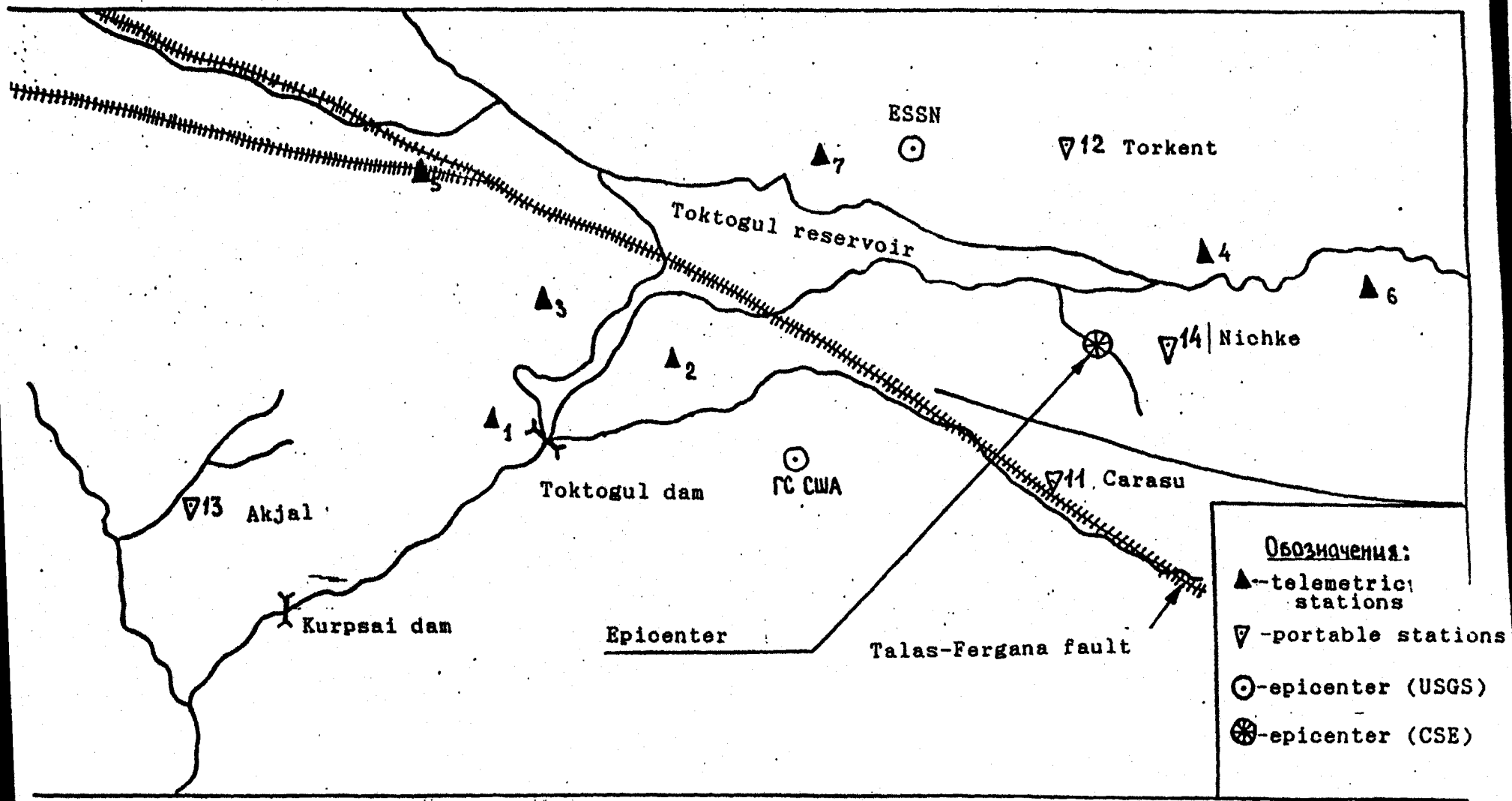

Figure III.68 Scheme of seismic observations.

M I:500 000

$M=2/3\ (K-5),\ M \leq 2.0$

$M=0.6K - 2.8,\ M>2.0$

extra to standard definition. Magnitude can be also determined from seismic wave duration, by relationship $M=2\log\tau-1.27$.

The data on the explosion June 11, 1989 in the catalog are given in three versions. The most reliable is the first version (first line). The determined epicenter is close to the real one, and is shown in Figures III.68 and III.69. Origin time was determined by a procedure independent on hypocenter depth and corresponds to detonation 11.8 sec before planned time. The explosions energy class is K=10.4 and magnitude M=3.5. The latter is lower that teleseismic value of 3.75.

The catalog for the region under investigation contains data on 57 crustal earthquakes with magnitudes from 1.1 to 3.1. One earthquake with magnitude M=3.7 should be considered more carefully due to several reasons. A half of the earthquakes (27) had magnitudes ranging from 2.0 to 2.4. In the range from 1.1 to 1.9 there were 17 earthquakes and in the range from 2.5 to 3.1 - 12 earthquakes. There were of about 1 earthquake per day in average.

The catalog has been separated in to three parts 20 days long each:

- May 1 through 21 (40 to 20 days before the explosions) - 14 earthquakes;
- May 22 through June 10 (20 to 1 day before the explosion) - 19 earthquakes;- June 11 through 30 (20 days after the explosion) - 24 earthquakes.

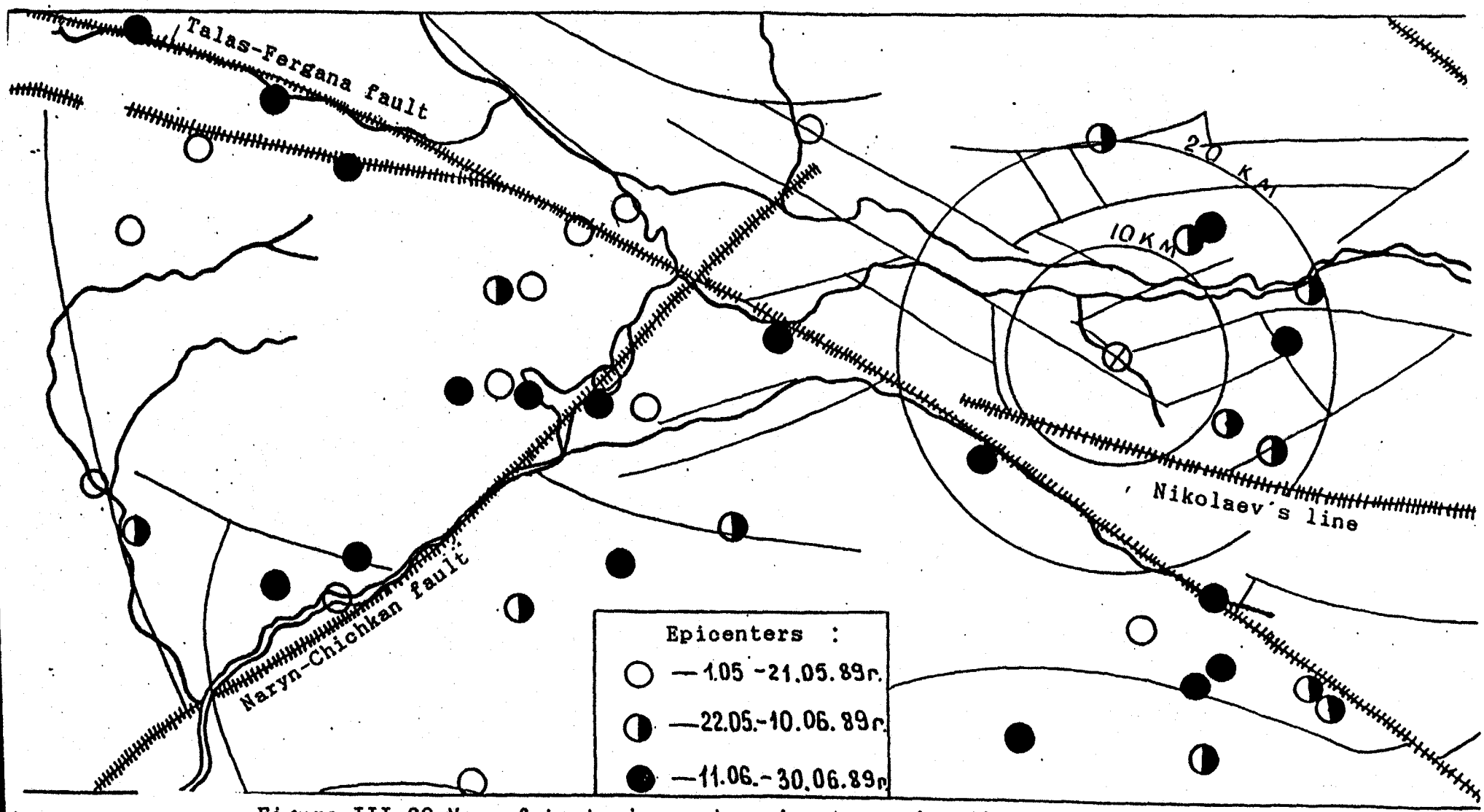

Figure III.69 Map of tectonics and epicenters in the working region.

M. I:500 000.

Statistic estimate can not be of high reliability, of course, due to short time of observations and relatively low seismic activity change. Thus, apparent small (20 to 30%) increase of earthquakes number per 20 days can not be considered as a statistically representative.

Figure III.69 shows the map of the epicenters of the recorded earthquakes in the three time intervals as well as principal tectonic structures of the region. The zones of 10 and 20 km radius around the epicenters are related to the deep Talas-Fergana, Naryn-Chatkal faults and Nikolaev line. Some of the epicenters are related to regional faults shown on the map.

There were no earthquakes inside 10 km zone during all the period of observations. There were 8 earthquakes between 10 and 20 km from the epicenter. Most of the earthquakes were to the east and north-east from the epicenter. During 20 days before the explosion there were 5 earthquakes with magnitude of 2.0 to 2.4 in the nothern and eastern parts of the zone. There were only 3 earthquakes during 20 days after the explosions with magnitude from 1.6 to 2.2. Two of tham were in the same zone, and one to the south-west from the epicenter near the Talas-Fergana fault.

Thus, inside 20-km zone around the Uch-Terek explosion there was no seismicity increase during 20 days long period of observations.

It is worth noting that in the adjasent region of the Toktogul hydropower station situated 50 km west from the explosion epicenter there was observed seismicity increase of

earthquakes with similar magnitudes ML 2.5 during the reservoir filling (when water level reached 100 m and during high rate of filling), i.e. during another type of industrial activity. This fact, by our opinion, is an evidence of possible influence on natural seismic regime of different types of artificial activity which is dependent on physical michanism and scale of an impact.

There were four earthquakes with M=2.0 to 2.5 near the Talas-Fergana fault during 20 days after the explosion at distances less than 30 km from the epicenter. At the same time, there were only one earthquake during 40 days before the explosion in this region. The apparent activity increase hardly to be related to the explosion influence, since explosion generated wave at such a distance should be of low amplitude due to attenuation during propagation. Moreover, no post explosion seismic activity has been mentioned previously from explosions of kiloton class at distances larger than 10 km. Stochastic variations of seismic activity may be a possible reason of such an activity change. Following explosions near the Cambarata dams should by monitored during 8 to 12 months period to understand possible activization of deep and large faults at large distances.

Catalog of earthquakes compiled by the Institute for seismology of the Academy of Sciences of the Kirghizia SSR for the period from April 1 to Augest 1, 1989 was also available. The catalog has been compiled from the data of 31 regional seismic stations established at the territory of Kirghizia.

There were only four earthquakes observed 1.5 mouths before

the explosion and four 1.5 mouths after included in the catalog within the area under investigation. Energy class of the earthquakes was from 7 to 8 (M=1.1-2). Thus, the catalog also has not shown seismic activity increase.

C. Teleseismic observations from the explosion at the r. Uch-Terek.

Teleseismic measurements up to 84^{o} (9300 km) were conducted to estimate some parameters of the Uch-Terek explosion, which have not been determined from local measurements. Absolute origin time and total yield are two of them. The teleseismic data will be used to estimate maximum distance and detection threshold of seismic methods in future. These estimates are of principal importance for verification of methods of monitoring of underground nuclear testing under test ban treaties.

Seismic bulletines of the OME IPE AN USSR include data from 29 seismic stations ranging from 135 to 2500 km from the epicenter. These stations are located in the Sovies Middle Asia, Ural, Cancasus, and Baikal region. The explosion origin time from the data is 06h 59m 48.4 sec. This time is close to meassured from local data 06.59.48.23 (see appendix 1). The explosion location from the data is 25 to north-west from the real epicenter (Figure III.68).

Averaged magnitude from the data of the Kirovabad, Bakuriani, and Zakamensk stations is 4.63. Only peak vertical displacement in longitudinal waves was used to estimate this magnitude, M_{pv}. Surface waves magnitude obtained from vertical

component measured at four stations is of M=3.75, which is higher than from local observations, M=3.5.

The USGS bulletin data are limited. The bulletin contains the data only from 8 stations in Iran, Pakistan, Norway, Africa and Canada (4 stations) ranging from 1300 to 9300 km. Absolute origin time has been determined with low accuracy due to larger distances from the epicenter and only few stations involved. Hypocenter depth has not been determined and substituted by H=33 km. The USGS determined epicenter is 30 km south-west from the real epicenter. Magnitude, M_{pv}, determined by 4 station data is of 4.65.

Teleseismic magnitude is a characteristic of seismic wave amplitude. It is usually used to determine explosion yield. Teleseismic yield determination, by our opinion, is better than that of obtained from similar regional data. It is due lower frequency used in teleseismic determination. Low frequency signal is more stable relative to disturbance by real inhomogenieties . Teleseismic waves propagate mainly through the upper mantle which is more homogenious than the crust. Thus, teleseismic estimates of yield are more accurate and stable.

The total explosive mass (yield) of the Uch-Terek explosion was determined from relationship

$$m_p=0.82 \log W_{kt}+4.43$$

which was usually used in the FSU for contained explosions in hard rocks (granite, sandstone, etc.). The explosion yield from magnitudes 4.63 (FSU) and 4.65 (US) is of 1.75 to 1.35 kt (trotyl). The estimates accuracy is relatively low due to only a

few stations were used.

Table III.46 Seismological bulletin from the data obtained at local distances for the period from May 1 to June 30, 1989.

NN пп	Date	Arrival time hh mm ss	Coordinates		h, km	Class K	Magnitude m	Number of stations	Notes
			φ°N	λ°E					
1	2	3	4	5	6	7	8	9	10
1.	01.05.89	09-09-45.22	40 56.03'	73 09.54'	0.0	9.7	2.6	5	n/r
2.	04.05	07-50-04.09	41 40.88'	72 33.96'	7.8	7.0	1.2	3	
3.	05.05	09-30-39.74	41 25.81'	72 13.26'	5.0	8.2	2.0	7	b
4.	05.05	11-18-30.04	41 34.73'	73 46.94'	12.4	8.8	2.3	6	
5.	06.05	06-15-32.42	41 25.40'	72 16.43'	5.7	8.5	2.2	7	b
6.	06.05	20-00-52.63	42 53.86'	72 54.61'	4.3	7.8	1.1	3	
7.	07.05	17-43-19.67	41 52.68'	72 13.59'	8.0	8.5	1.5	3	
8.	07.05	20-11-00.52	41 30.28'	72 21.76'	35.2	8.7	2.2	7	
9.	09.05	17-48-48.37	41 28.89'	73 16.11'	12.2	8.5	2.3	8	
10.	10.05	23-34-35.68	41 40.00'	72 43.82'	19.7	8.2	3.1	5	
11.	12.05	07-57-00.31	41 21.83'	72 22.55'	1.4	8.5	2.5	5	b
12.	12.05	08-43-05.66	41 37.24'	72 06.86'	5.5	8.3	1.6	3	
13.	12.05	15-54-07.14	41 45.71'	72 36.08'	10.0	7.2	1.6	3	
14.	13.05	02-03-49.74	40 50.65'	72 01.05'	5.2	7.5	2.5	3	n/r
15.	16.05	22-06-29.43	42 43.22'	73 08.15'	0.0	9.0	2.6	8	n/r
16.	17.05	00-40-39.73	41 11.00'	73 24.29'	44.0	9.3	2.3	7	
17.	18.05	01-17-52.38	41 40.99'	72 41.08'	10.4	7.4	1.8	3	
18.	18.05	06-12-24.57	41 26.11'	72 19.09'	18.2	8.6	2.3	7	b
19.	18.05	08-06-26.74	41 22.43'	72 14.57'	7.4	7.7	2.3	3	b
20.	18.05	08-36-27.89	41 30.40'	72 23.64'	18.2	8.8	2.1	4	b
21.	19.05	06-34-21.90	41 47.85'	72 39.24'	12.4	7.2	1.3	3	
22.	19.05	09-15-54.98	41 28.73'	72 14.51'	18.3	8.4	2.1	6	b
23.	21.05	00-24-06.00	41 48.61'	72 08.35'	36.8	9.2	2.7	5	
24.	21.05	13-05-24.69	41 50.12'	72 42.38'	17.7	6.7	1.5	5	
25.	22.05	21-33-32.26	41 08.00'	72 38.10'	2.1	8.2	2.2	5	n/r
26.	24.05	15-21-38.84	41 51.54'	72 24.40'	13.6	7.0	1.7	4	
27.	25.05	04-35-47.91	42 10.66'	73 00.14'	0.8	7.7	1.9	3	

1	2	3	4	5	6	7	8	9	10
28.	25.05.89	11-21-54.43	41 45.18'	73 27.19'	10.8	7.2	2.2	4	
29.	25.05	19-38-48.45	41 25.03'	73 27.85'	2.5	8.4	2.6	7	
30.	25.05	23-10-37.92	41 26.87'	73 28.63'	4.4	8.2	2.2	6	
31.	26.05	06-39-52.23	41 19.68'	72 17.13'	1.4	8.7	2.4	8	b
32.	26.05	13-21-24.30	41 22.57'	73 20.49'		9.8	2.4	4	
33.	26.05	22-57-24.67	41 45.95'	72 34.17'	22.2	7.7	1.7	7	
34.	28.05	03-09-11.58	42 14.56'	71 44.38'	4.4	10.3	2.4	3	n/r
35.	30.05	04-13-37.37	40 53.67'	72 57.18'	4.6	10.3	2.6	3	n/r
36.	30.05	09-30-31.10	41 20.34'	72 23.06'	1.4	8.8	2.7	7	b
37.	31.05	08-08-31.36	41 54.40'	73 14.75'	28.9	8.4	2.4	8	
38.	01.06.89	06-56-07.97	41 00.52'	73 01.58'	1.8	7.8	2.5	5	n/r
39.	01.06	10-07-44.31	41 16.69'	72 10.35'	30.5	10.0	3.0	7	
40.	02.06	08-08-24.22	41 51.51'	71 52.76'	6.1	8.4	2.2	4	
41.	02.06	11-11-19.94	41 39.77'	73 21.58'	14.9	7.3	2.0	5	
42.	02.06	13-33-00.18	41 38.61'	73 25.23'	2.1	7.7	2.0	6	
43.	03.06	13-27-07.66	41 01.57'	73 23.85'	4.1	8.2	2.3	3	n/r
44.	03.06	19-23-55.80	41 34.12'	72 50.13'	1.0	7.2	1.4	3	
45.	06.06	05-46-13.25	41 20.98'	72 31.34'	5.0	9.1	2.1	3	
46.	06.06	07-46-05.65	41 20.46'	72 21.11'	16.9	8.9	2.4	3	b
47.	08.06	07-34-02.19	41 20.42'	72 21.29'	5.6	8.0	1.9	3	b
48.	08.06	12-12-09.68	41 48.83'	73 20.06'	16.3	7.8	2.0	5	
49.	09.06	04-26-12.42	41 02.86'	72 28.46'	1.0	9.6	2.8	8	n/r
50.	09.06	17-40-25.63	41 14.69'	72 54.52'	1.4	8.8	3.0	4	
51.	10.06	00-49-03.24	41 30.07'	72 35.71'	1.4	8.4	2.8	3	
52.	10.06	07-30-11.88	41 21.78'	72 16.79'	1.3	7.8	2.1	8	b
53.	10.06	13-31-00.43	41 33.60'	72 08.89'	32.8	9.1	3.1	7	
54.	10.06	19-26-29.62	41 17.53'	72 39.51'	0.8	8.6	2.5	9	
55.	11.06.89	06-59-48.23	41 42.89'	73 15.04'	10.2	10.4	3.5	7	b
		48.12	43.01'	15.70'	11.3	10.4	3.5	7	Uch-Terek
		47.42	38.40'	17.21'	15.2	10.6	3.5	7	explosion
56.	11.06	13-08-03.26	41 09.22'	73 01.95'	10.3	9.5	2.6	3	n/r
57.	13.06	18-33-26.21	42 37.20'	72 58.00'	0.0	9.5	2.8	7	n/r

1	2	3	4	5	6	7	8	9	10
58.	14.06.89	08-33-03.12	41 24.88'	72 15.64'	0.0	9.1	2.7	8	b
59.	14.06	09-15-47.67	41 17.11'	72 43.97'	0.1	8.9	2.4	7	
60.	15.06	02-11-32.91	41 11.51'	73 50.40'	5.7	8.1	2.4	3	
61.	15.06	15-54-24.43	41 23.15'	73 07.51'	0.7	8.7	2.7	6	
62.	16.06	02-36-37.22	41 59.61'	72 08.97'	17.4	8.7	2.3	10	
63.	16.06	06-00-31.03	41 31.07'	72 18.65'	22.1	7.4	2.0	6	
64.	17.06	19-11-50.55	41 27.42'	73 22.03'	13.9	7.9	2.3	4	
65.	19.06	06-00-04.89	41 05.66'	73 23.43'	4.3	7.3	2.1	5	n/r
66.	19.06	09-00-38.25	41 22.11'	72 11.73'	22.8	8.7	2.4	5	b
67.	19.06	15-10-24.04	41 40.30'	72 40.91'	9.6	7.0	1.4	3	
68.	20.06	01-31-15.53	41 17.46'	72 56.67'	0.6	7.9	2.0	7	
69.	20.06	05-00-46.49	41 25.46'	72 16.47'	28.5	8.8	2.2	6	b
70.	20.06	07-10-02.85	41 21.62'	72 20.35'	32.5	9.4	2.8	9	b
71.	21.06	08-57-30.21	41 29.30'	72 18.91'	15.3	8.0	2.2	8	b
72.	22.06	06-29-04.74	41 42.53'	72 52.25'	16.9	8.0	2.2	9	
73.	22.06	09-51-51.54	41 00.59'	72 50.36'	2.5	9.2	2.5	5	n/r
74.	22.06	18-20-36.48	41 37.26'	73 06.81'	17.7	7.4	1.6	4	
75.	23.06	07-13-35.24	41 48.95'	73 20.30'	10.0	6.8	2.2	6	b
76.	23.06	07-51-11.55	41 32.22'	72 23.96'	22.7	8.8	2.2	5	
77.	24.06	09-05-53.35	41 28.48'	72 19.27'	6.1	8.6	2.4	10	
78.	24.06	11-28-16.65	41 40.46'	72 31.64'	15.3	7.0	1.3	4	
79.	25.06	21-39-44.36	41 55.50'	72 19.35'	1.7	7.8	2.4	6	
80.	26.06	00-52-07.18	41 43.49'	73 26 21'	20.3	7.7	1.7	5	
81.	26.06	01-16-14.46	41 10.72'	72 39.11'	1.4	9.2	2.6	9	
82.	26.06	05-15-17.91	41 40.61'	72 35.54'	3.8	5.6	1.4	3	
83.	26.06	15-17-23.05	42 09.56'	72 41.70'	15.8	9.3	2.6	7	
84.	27.06	08-02-22.12	41 26.21'	72 19.56'	16.0	8.2	2.4	9	b
85.	27.06	16-46-36.07	41 18.90'	72 46.04'	1.0	10.0	3.7	4	
86.	27.06	20-19-16.94	41 32.06'	72 41.19'	8.6	7.1	2.1	8	
87.	28.06	06-47-42.12	41 30.54'	72 19.26'	27.5	7.6	2.1	5	b
88.	28.06	09-31-44.88	41 25.76'	72 25.95'	1.4	6.8	2.2	3	b
89.	29.06	06-09-26.35	41 21.19'	72 21.00'	1.4	7.2	2.0	4	b
90.	29.06	09-39-50.55	41 29.30'	72 24.61'	26.4	7.7	2.0	4	b
91.	29.06	13-18-09.22	41 18.20'	73 25.80'	1.7	8.2	2.2	3	

1	2	3	4	5	6	7	8	9	10
92.	29.06.89	20-14-01.78	41 26.17'	73 20.14'	7.4	8.0	2.0	6	
93.	29.06	20-37-10.06	41 30.59'	73 20.74'	7.5	8.5	2.6	7	
94.	30.06	07-37-26.7	41 22.46'	72 12.74'	1.4	8.2	2.5	8	b
95.	30.06	19-59-34.33	41 13.77'	73 53.42'	5.7	9.3	2.2	3	

Note: "b" - explosions in coal mines and at industrial sites

n/r - epicenter out of the region of investigations

Table III.47 Seismological bulletin of OME of the IPE of Soviet Academy of Sciences for the Uch-Terek explosion

General data : 11 June 1989 T_o=06h 59m 48,4s (GMT)

Region:48716 Kirghiz φ=41,86°N

λ=73,06°E H=3,0km

Error ellipce parameters :A =5,2km

B=12,8km

L=-35,6°

S=212,5km²

RMS time residual T_o:

0,66s from 28 (of 29) stations (S_σ)

Station	St-on code	Dist. Δ°	Az. to stat. °	Phase	Arrival time hh mm ss	S_σ, s	Sensor type	Amplitude (microns)			Period, s	Magnitude			
												m_{PV}	m_{PH}	m_{LV}	m_{LH}
1	2	3	4	5	6	7	8	9			10	11	12	13	14
ndijan	ANR	1.22	205	iPg	07-00-10.6	-2.6	SPZ								
				Pm	11.2		SKM			0.3	0.6				
				eSq	34.4	4.6									
				Smax	48.0		SM3		3.5		1.4				
amangan	NAM	1.36	230	iPg	07-00-14.4	-1.8	SPZ			7.8	1.2				
				Pmax	18.0		SKM								
				eSg	38.9	2.0									
				Smax	39.3		SM3	8.2			0.4				
runze	FRU	1.51	49	iPg	17.0	-2.0	SPZ								
				Pmax	19.8		SPZ			0.66	0.6				
				iSg	41.0	1.2	SPE								
				Smax	51.2		SPE		1.8		1.4				
				Lmax	01-(0)		MP	4.2	6.0	4.0	6.0				

1	2	3	4	5	6	7	8	9			10	11	12	13	14
Fergana	FRG	1.76	213	iPn	07-00-20.6	-1.1	P								
				Pmax	21.5		SKM			1.15	0.6				
				iSmax	45.3	0.7									
					47.8		SKM	1.05			1.3				
Tashkent	TAS	2.87	261	iPn	07-00-38.0	0.8	SPZ								
				Pmax	39.2		SKM			0.100	1.2				
				eP*	43.0	0.6									
				Pmax	46.0		SKM			0.58	1.2				
				ePg	47.0	0.6									
				Pmax	48.0		SKM			0.60	1.4				
				eS*	01-21.0	5.2									
				eSg	23.5	-3.2									
				Smax	27.0		SKM	2.5			1.0				
Alma-Ata	AAA	3.20	63	ePn	07-00-41.4	-0.4	SPZ								
				eP*	45.3	-3.1	SPZ								
				eS*	01-28.9	3.1	SPN								
				Smax	32.0		SP	1.6	2.5	0.7	3.0				
Talgar	AAB	3.37	65	iPn	07-00-4(8).5	0.2	SPZ								
				iP*	49.0	-2.0	SPZ								
				Pmax	49.5		SPZ			0.500	0.5				
				eS*	01-33.5	2.6	SPN								
				Smax	35.5		SP	0.67	1.03		1.0				
				Lmax	02-01.0		MPZ			1.5	8.0		3.4		
				Lmax	01.0		MP	1.0	1.8		10.0				3.5
Murgab	MUP	3.51	168	iPn	07-00-45.8	-0.4	SPZ								
				eS*	01-32.8	-2.2									
Garm	GAP	3.54	217	iPn	07-00-47.5	0.9	P								
				eSn	01-30.2	0.8	P								
Przevalsk	PRZ	4.03	79	ePn	07-00-52.0	-0.6	SPZ								
				Pmax	56.0		SPZ			0.03	0.5				
				eS*	01-50.0	-0.4	SPE								
				Smax	55.0		SP	0.310	0.42		0.8				
				Lmax	02-40.0		MP	2.0	2.3	2.5	8.0		3.9	3.8	

1	2	3	4	5	6	7	8	9	10	11	12	13	14
Obigarm	OBG	4.04	220	ePn	07-00-53.0	0.4	SPZ						
				eSn	01-44.0	1.9	SPN						
Bogi-Zagon	BGG	4.18	217	-iPn	07-00-55.1	-0.4	SPZ						
Tadjik				eSn	01-40.7	-6.0	SPN						
SSR													
Kalaidasht	KLT	4.22	221	ePn	07-00-55.4	-0.6	SPZ						
Tadjik				eSn	01-40.7	-6.0	SPN						
SSR													
	CGT	4.37	224	ePn	07-00-57.6	-0.6	SPZ						
				iSn	01-54.5	4.0	SPN						
Djirgital	DZE	4.44	228	iPn	07-00-59.0	-0.2	SPZ						
Langar	LNA	4.47	221	ePn	07-00-58.5	-1.1	SPZ						
				eS*	01-59.9	-3.5	SPN						
Horog	KHO	4.53	196	iPn	07-00-59.9	-0.5	SPZ						
				Pmax			CKM		0.500	0.8			
				eSn	01-48.9	-5.5							
				Smax			SKD	0.500		0.8			
Carasu	KRU	4.60	224	ePn	07-01-00.8	-0.6	SPZ						
Tadjik				eSg	02-22.3	-2.6	SPN						
SSR													
Dushanbe	DSH	4.63	226	iPn	07-01-01.5	-0.3	SPZ						
				Pmax			SKM	0.420		1.0			
				eS*		1.9							
Kulyab	KUL	4.86	214	ePn	07-01-01.6	-0.9	MPZ						
				eP*	14.9	0.5	MPZ						
				e	35.8		MPE						
				Sn	02-00.4	2.2	MPN						
				Smax			MPE	0.800		1.0			
				iSg	22.7	-5.0	MPE						
				Pmax			MPE	1.1		1.2			

1	2	3	4	5	6	7	8	9			10	11	12	13	14
Samarkand	SAM	5.11	247	-ePn	07-01-08.5	0.0	SPZ								
				iPg	28.0	-3.8	MPZ								
				Pmax	36.0		MPZ			0.400	1.0				
				e	02-05.6		MPE								
				Sn	12.0	3.2	MPE								
				iSg	38.9	-3.0	MPN								
				Smax	55.0		MPN	1.2			2.0				
Agalyk	AGL	5.26	246	iPn	07-01-08.8	-1.8	SPZ								
Uzbek				Pmax	10.8		SPZ			0.046	0.3				
SSR				iS*	02-32.0	-3.6	SPE								
				iSg	41.9	-5.8	SPE								
				Pmax	58.2		SP		0.246		0.1				
Nurata	NUT	5.79	260	iPn	07-01-15.3	-2.8	SPZ								
Uzbek				Pmax	19.2		SPE			0.08	0.2				
SSR				eSn	02-21.9	-4.1	SPE								
				Smax	31.4		SPN	0.280			1.0				
Semipala-tinsk	SEM	9.89	28	eP	07-02-13.6	-1.0	SPZ								
Vannovskaya	VAN	12.13	256	-iP	07-02-41.4	-3.7*	SPZ								
				i	04-43.6		SPN								
				Smax			SPN	0.03			1.0				
Sverdlovsk	SVE	16.98	336	eP	07-03-48.8	0.4	SPZ								
				Lmax	10-10.0		MP	0.200	0.200	0.200	7.0			3.9	3.8
Kirovobad	KRV	20.06	276	iP	07-04-24.0	-1.6	SPZ								
				Pmax	28.0		SPZ			0.02	1.0	4.6			
Bakuriani	BKR	21.98	280	-iP	07-04-47.0	1.8	SPZ								
				Pmax	48.5		SPZ			0.085	1.4	5.2			
Zakamensk	ZAK	22.49	57	eP	07-04-50.5	0.2	SPZ								
				Pmax	52.0		SP		0.006	0.006	1.0	4.1	4.2		
				e	13-10.0		MPZ								
				Lmax	27-32.0		MPZ			0.290	16.0			3.8	

Table III.48 Seimological bulletin of the USGS for the explosion at the r.Uch-Terek, Kirghizia.

11 June 1989. T_o=06hh59mm50,58s$\pm$0,97c (GMT)

φ=41,622°$\pm$13,9km

λ=72,902E$\pm$20,6km H=33km

RMS arrival time error:

0,9s (8st.)

Stan. code	State	Dust. Δ°	Az. to stan. °	Phase	Arrival time hh mm ss	S_σ, s	Longitudinal wave		
							Amplitude, nm	Period, sec	Magnitude, mb
MAID	Iran	11.71	247	eP	07-02-38.0	-0.4			
				e	04-46.0				
QUE	Pakistan	12.38	205	eP	07-02-47.2	-0.4			
				e	57.0				
NAO	Norway	41.50	319	P	07-07-35.6	-0.2	1.8	0.7	3.9
BNG	CAR	60.89	248	P	07-10-03.6	+1.1	5.0	0.4	5.0
MBC	Canada	62.15	3	eP	07-10-09.5	-0.7	5.0	0.7	4.8
INK	Canada	68.61	10	eP	07-10-51.0	-0.8			
YKA	Canada	76.06	4	eP	07-11-36.5	+0.6			
FFC	Canada	83.93	357	eP	07-12-19.0	+0.9	9.0	0.8	5.0

IV. Seismic wave source of large-scale underground explosions.

1. Principal characteristics of seismic wave source

Concentrated underground explosion is usually considered as a source of expanding spherical elastic wave. Such a representation allows relatively simple determination of principal parameters of generated longitudinal wave from, so called, reduced displacement potential, Φ, and it's derivatives.

Following relationships can be derived for displacement U(R, t), particle velocity V(R, t), and stresses σ_R (radial) and σ_φ (tangential)

$(\tau = t - R/c \geq 0)$

$$U(R,t) = -\frac{\partial}{\partial R}\left[\frac{\Phi(\tau)}{R}\right] = \left[\frac{\Phi'(\tau)}{Rc}\right] + \frac{\Phi(\tau)}{R^2}$$

$$(1)\quad V(R,t) = \frac{\Phi''(\tau)}{Rc} + \frac{\Phi'(\tau)}{R^2}$$

$$\sigma_R(R,t) = -\rho c^2\left[\frac{\Phi''(\tau)}{Rc^2} + \frac{2(1-2\nu)}{(1-\nu)}\left[\frac{\Phi'(\tau)}{R^2c} + \frac{\Phi(\tau)}{R^3}\right]\right]$$

$$\sigma_\varphi(R,t) = -\rho c^2\left[\frac{\nu}{1-\nu}\frac{\Phi''(\tau)}{Rc^2} - \frac{1-2\nu}{1-\nu}\frac{\Phi'(\tau)}{R^2c} - \frac{1-2\nu}{1-\nu}\frac{\Phi(\tau)}{R^3}\right],$$

where R is the distance from the source, c is the longitudinal wave velocity, ρ is the density, and ν is the Poisson ratio. Derivatives by τ are indicated by marks '.

Initial values of $\Phi(0)$ and $\Phi'(0)$ are equal to zero: $\Phi(0)$ =

$\phi'(0) = 0$ because of zero initial displacement at the moment $\tau = 0$. Similar conditions are usually used for the second derivative of the reduced displacement potential, i.e. $\phi''(0)=0$. Such a condition implies that particle velocity grows gradually after wave arrival. In principle, step velocity or stress propagation is possible on the wave front.

The Fourier transform is used to characterize the spectra of the generated wave. Common representation for broad classes of functions f(t) and f(ω), where ω is the angular frequency, are as follows

$$(2)\quad f(\omega) = \int_{-\infty}^{\infty} f(t)e^{-i\omega t}dt;\quad f(t) = \frac{1}{2\Pi}\int_{-\infty}^{\infty} f(\omega)e^{i\omega t}d\omega$$

By using (1) and (2) one can obtain following useful relationships:

$$U(R,\omega) = \frac{1}{R^2}\left[1+\frac{i\omega R}{c}\right]\Phi(\omega)$$

$$(3)\quad V(R,\omega) = \frac{1}{R^2}\left[1+\frac{i\omega R}{c}\right]\Phi'(\omega),\ \Phi'(\omega) = i\omega\Phi(\omega)$$

$$\sigma_R(R,\omega) = -\frac{\rho c^2}{R^3}\left[\frac{2(1-2\nu)}{1-\nu} + \frac{2(1-2\nu)}{1-\nu}i\omega\frac{R}{c} - \left[\frac{\omega R}{c}\right]^2\right]\Phi(\omega)$$

Relationships (3) can be used to estimate spectral

characteristics of the reduced displacement potential, if the functions $U(\omega)$, $V(\omega)$ or $\sigma_R(\omega)$ are known at a given distance R. For example, having the function $\sigma_R(\omega)$ one can obtain from (3) following expression:

$$(4)\quad \Phi(\omega) = -\frac{\sigma_R(\omega)R^3}{\rho c^2}\ \frac{i\omega}{\left[\frac{2(1-2\nu)}{1-\nu} + \frac{2(1-2\nu)}{1-\nu}\ \frac{i\omega R}{c} - \left[\frac{\omega R}{c}\right]^2\right]}$$

Some special features of the reduced displacement potential Φ can be derived from relationship (4). Thus, if the radius of unelastic source zone is Ro and the pressure at this radius is a step fuction with a constant amplitude Po, which can be treated as a function $P(\tau)=Poe^{-\alpha\tau}$, where α 0 and $P(\tau)=0$, $\tau<0$, then from (4) it follows

$$(5)\quad \Phi(\omega) = \frac{PoRo^3}{\rho c^2}\ \frac{1}{\left[d+d(i\omega Ro/c) - (\omega Ro/c)^2\right]}$$

where $d=2(1-2\nu)/(1-\nu)$. The Poisson ratio for common rocks is of $\nu=1/3$, and d=1. One can derive low- and high--frequency limits of $\Phi(\omega)$ from (5). When $\omega \rightarrow 0$, and assuming from (1) that for t ∞ $\frac{PoRo^3}{\rho c^2 d} = \Phi o$, where Φo is the asymptotic value, we obtain

$$(6)\qquad \Phi'(\omega) = \Phi o.$$

High-frequency limit of (5) gives

$$(7) \qquad \phi'(\omega) = \frac{\phi_{od}}{(\omega R_o/c)^2} \sim \frac{1}{\omega^2}$$

So called corner frequency determines the frequency where relations (6) and (7) are separated. The corner frequency is estimated from relationship

$$(8) \qquad \omega_c = c/R_o.$$

Thus, the values ϕ_o and ω_c can be treated as the principal parameters of generated seismic signal or seismic wave source. Relationship (5) can be generalized easily by using different pressure functions at the elastic source radius, R_o. This problem is well known as Sharp's problem and is often discussed in the different works devoted to explosion source. It should be noted, however, that the pressure function $P(\tau)$ has to be determined together with the elastic radius R_o, where it acts. It means that when analizing experimental data one should evaluate in which zone the data were measured and to which extent nonlinear and effect can influence the reduced displacement potential estimates. Theoretical calculations play a principal role in solving these complicated problems and our understanding of processes occuring during actual explosions in real rocks. Monographie [1,2] should be mentioned, which

summarize theoretical results obtained before 1970-1971. It has been shown by comparing of natural observation results with theoretical calculations by different schems [1], that some complicated processes of rock behaviour under high loading should be included. In particular, delatancy effects, i.e. rock density changes under pure shear stress, were obtained.

Following investigations [3,4] have shown that sophisticated medium models including different factors have to be elaborated for the theoretical calculations, as a result, these models include a lot of parameters which are not well determined for real rocks behaviour in nonlinear zone of explosions. So, the models are misleading sometimes. In this work, we will use more simple but more clear approaches to the problem of seismic wave generation by the explosion in hard rocks [5,6,7].

The authors of [5,6] numerically study the spherically symmetric case of an explosion. Their approach is very close to elastic case but includes plastic yielding which is one of the principal processes during an explosion. It is assumed, that yielding is govered by von-Mizes criterion

$$(\sigma_R - \sigma_\varphi)^2 = 3Y^2 \qquad (9)$$

where Y is the elastic limit under shear stress.

It was found that two plastic zones are created by the

where $\phi_o = 0.9\ (Y/\rho c^2)b^3$, $\theta_o = \tau_{1/2} = 0.28 b_m/c$

Reduced displacement potential will be as following

$$(12) \qquad \phi(\tau) = \phi_o/\theta \int_0^{\tau} \left[\frac{1}{2} x^2 e^{-x}\right] d\tau = \phi_o \int_0^{x} \left[\frac{1}{2} x^2 e^{-x}\right] dx$$

It follows from (12) that when $\tau \to \infty$, $\phi(\tau) \to \phi_o$, i.e. ϕ_o is asymptotic value of reduced displacement potential.

The spectrum of $\phi'(\omega)$ can be obtained from (11)

$$(13) \qquad \phi'(\omega) = \phi_o/(1+i\omega\theta_o)^3.$$

The spectrum (13) falls beyond the corner frequency faster that the spectrum (5). The corner frequency of (13) is $1/\theta_o$. These differences arise due to gradual pressure or velocity increase in the wave front which is opposite to step function used in (5).

Relatively simple approximation for low-frequency part of seismic wave, generated by an explosion was eleborated in [7] by analysing of the principal processes occuring during explosion cavity expansion in hard rocks.

According to this approach, the final stage of the cavity expansion is characterized by the existance of two regions: plastic zone around the cavity ($r \le R \le b$) and elastic zone ($R > b$). In the first zone the relation between principal stresses σ_R and

σ_φ is well known in rock mechanics as law

(14) $$\sigma_R - \sigma_\varphi = K/2\ \sigma_R - \sigma_s$$

In particular, when K=0 (14) coinsides with (9), and $\sigma_s=(3)^{1/2} Y$. In elastic zone it is assumed that stresses distribution at a given time is close to static one, i.e.

(15) $$-\sigma_R(t) = \sigma_*(b(t)/R)^3$$

at the interface between the plastic and elastic zones R=b the relationship of displacement and stress is as follows (ν = 1/3):

(16) $$U(t) = (\sigma_*/\rho c^2)\ b(t)$$

In equations (15) and (16) the value σ_* is used as a strenght, when k=0, $\sigma_* = 2/3\sigma_s = (2/3)Y$.

Following expression for maximum cavity radius can be obtained from the equations of motion and boundary condition (16):

(17) $$r_m = \frac{0.45}{A^{1/3}}\left[E/\sigma_*\right]^{1/3},\quad A = 5\,\frac{\sigma_*}{\rho c^2}.$$

It is possible to assume from the estimates that the pressure in the cavity is equal to zero and whole the explosion

energy E is transfered into the medium on the previous stage. This stage is not considered here since its parameters variation do not influence the final, quazistatic stage of the cavity growth with characteristic time t_m (time when the maximum radius is reached) given by:

$$(18) \qquad A^{1/2} t_m c/r_m = \int_x^1 \frac{dx}{x\left(\frac{1}{x^3} - 1\right)^{1/2}}, \quad x = r/r_m$$

The expressions for the maximum values of the unelastic zone b_m, displacement u_m when $R = b_m$ and t_m are as follows ($k=0$, $\nu=1/3$)

$$(19) \qquad \begin{aligned} b_m &= 0.2(E/\sigma^*)^{1/3} (\rho c^2/\sigma^*)^{1/3}; \quad \phi_0 = b_m^3(\sigma^*/\rho c^2) \\ U_m &= (\sigma^*/\rho c^2) b_m; \quad t_m c/b_m \cong 2. \end{aligned}$$

To determine the reduced displacement potential, $\Phi(\tau)$, it is enouth to known a source radius, which is b_m, and a function $\sigma_R(b_m,\tau)$ at this radius. It follows from (15) that

$$-\sigma_R(b_m,\tau) = \sigma^*(b(t)/b_m)^3$$

Calculations show that $\sigma_R(b_m,\tau)$ can be approximated by

$$(20) \qquad -\sigma_R(b_m,\tau) = \sigma_*(1-e^{-\alpha\tau}),\ \alpha = \frac{2}{t_m},\ \tau \geq 0$$

When substifuted in (4), it gives

$$(21) \qquad \phi'(\omega) = \frac{\phi_0}{\left(1+i\omega\frac{b_m}{c}\right)\left[1+i\omega\frac{b_m}{c} - \left(\frac{\omega b_m}{c}\right)^2\right]}$$

where $\phi_0 = (\sigma_*/\rho c^2)b_m^3$, i.e. the value of $\phi(\tau)$, when $t \longrightarrow \infty$, and $\phi'(\omega)$, when $\omega \longrightarrow 0$.

Expession (21) has the same spectrum roll-off beyond corner frequency as (13). The corner frequency is $\omega_c = \frac{c}{b_m}$. To obtain $\phi(\tau)$ one can use the inverse Fourier transform of (21).

The data measured from the explosion Salmon in salt are used to compare the results of calculations by the two discribed schems. The data from the explosion Salmon were thoroughly analized by many researchers. It is worth noting two recent papers [8,9] where all the principal previons investigations are mentioned. The total energy release of the Salmon was E = 2.2 10^{13}J as follows from the yield of 5.3 kt. It was adapted in the calculations from [8] and other sources that ρ = 2.2 g/cm^3, c = 4.55 km/sec. The main problem is how to estimate σ_* or Y which are very similar, as was mentioned above, for the both approaches. We adopted conventional relation $\sigma_*/\rho c^2 \simeq 10^{-3}$ for rocky massifs [1]. When $\sigma_*/\rho c^2 \simeq Y/\rho c^2 \simeq 10^{-3}$, one can obtain for rocky salt σ_* = 460 bar. For this Y value from the first approach iy follows

b_m = 150m, $\phi_o = 3\ 10^3 m^3$, θ_o = 9.4 ms,

$\omega_c = 1/\theta_o = 100\ 1/s$

It was assumed that for the explosion with high initial energy density in the cavity $P_1 \cong \rho c^2$.

The calculations from the second approach give:

b_m = 155m, $\phi_\infty = 3.7\ 10^3 m^3$, $\omega_c = c/b_m = 30\ 1/s$.

As clear from the values, b_m and ϕ_o are very close, but ω_c are quite different.

Figure IV.1 displays the result of the calculations of the potential (upper frame) and spectrum $/\phi'(\omega)/$ (lower frame) by the two methods. Solid line represents the methods and dashed line is for quazistatic approach. The results of the actual measurements are also shown by different marks. The data on the potential [10] at different ranges are shown in the upper frame of Figure IV.1. The potential rize time grows with distance and the final value, ϕ_o, decreases. Small rise at closer ranges can be explained by high-frequency component of the signal and are better simulated by the first method. When range increases the high-frequency component effectively attenuates and the signal is better described by the second method which does not include the initial part of the wave. These differences are confirmed by the spectra of seismic waves measured at large distances. The data from [11] are shown on the lower frame as well as the

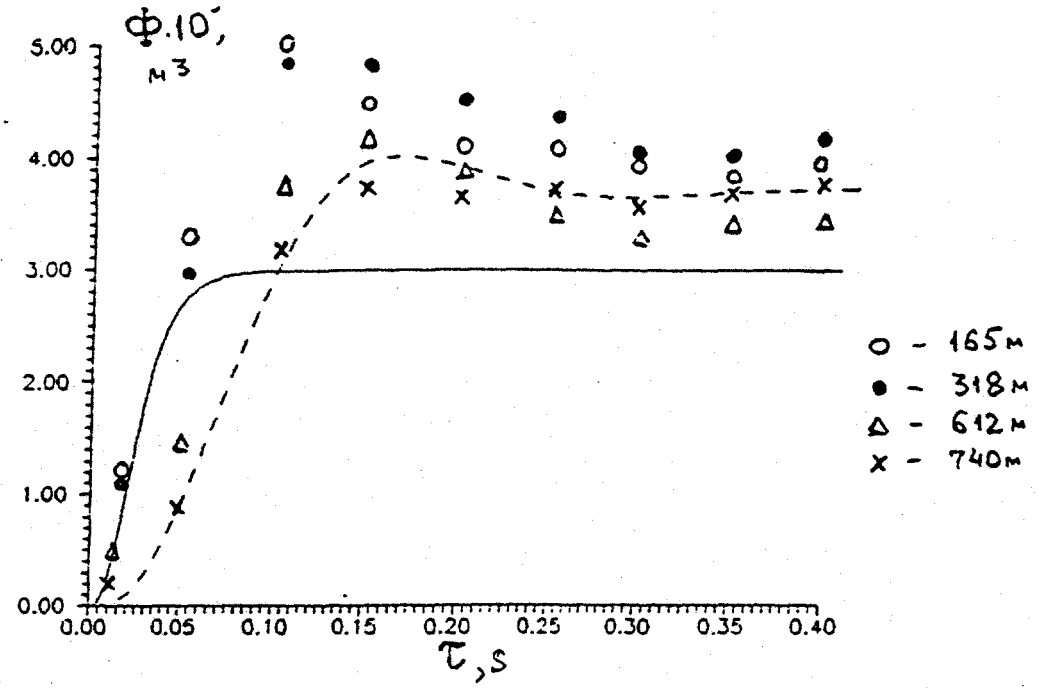
Φ.10⁻, м³
5.00
4.00
3.00
2.00
1.00
0.00
0.00
0.05
0.10
0.15
0.20
0.25
0.30
0.35
0.40
τ, s
○ - 165м
● - 318м
△ - 612м
× - 740м

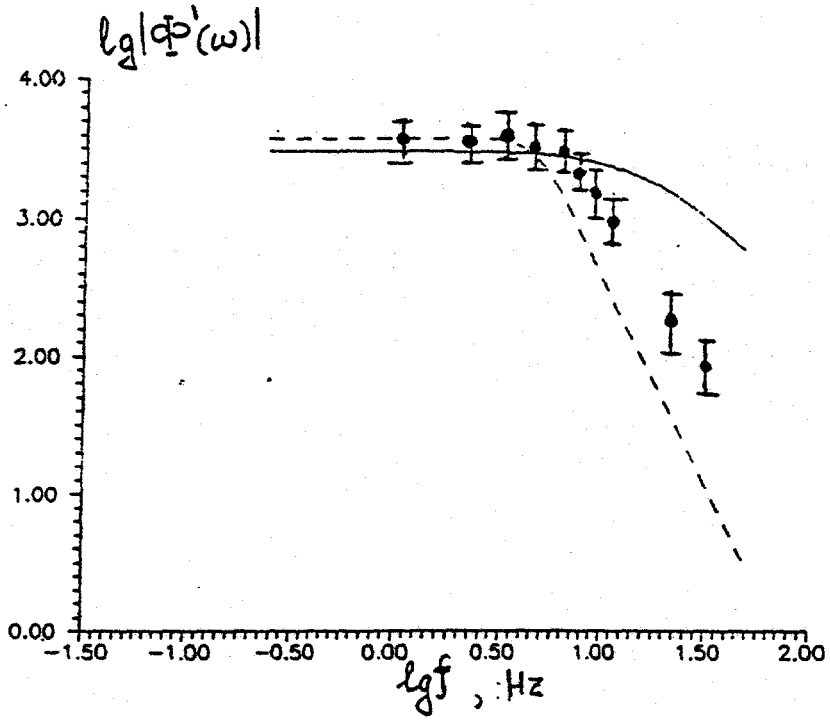
lg|Φ'(ω)|
4.00
3.00
2.00
1.00
0.00
−1.50
−1.00
−0.50
0.00
0.50
1.00
1.50
2.00
lgf , Hz

Fig. IV.1

calculated spectra. The data dispersion is shown by bars.

2. Some special characteristics of explosion generated seismic waves attenuation in rocky massif

Seismic wave amplitude attenuation with distance (R) is usually described by power law

$$A = B/R^n. \tag{22}$$

Such a relationship is also often used in processing of experimental data from underground explosions, with maximum particle velocity (V_m) used to evaluate seismic hazard. The exponent, n, and coefficient B depend on the type of explosion and properties of rocks. Naturally in this case, the effects of individual cracks and faults are averaged over different scales characteristic for actual rocky massif.

More detailed investigation of experimental data, however, allows to retrieve the influence of individual discontinuities [12]. As an example, we will describe the results of measuring of horizontal particle velocity from an explosion in granite. Figure 2 displays the recordings of sensors placed in the horizontal mine at different distances from the explosion. The same time scale for all the records is used for the sake of convenience (timing from the compressional wave arrival). The amplitudes are also scaled (multiplied) by corresponding

distances what allows to account for spherical spreading in the first approximation. It is worth noting, that second term is negligable in the known relation for spherical wave.

As can be seen from Figure IV.2, the shapes of the wave at the distances 350m, 400m, and 460m are similar. At the distances 700m, and 800m. however, the amplitudes change, and the rize time to the peak value (t_r) and positive phase duration increase. Fugure IV.3 shows these effects more carefully, where points shows V_m and crosses are for t_n.

Note, that in the range from 600 to 700m there is deep fault crossing the massifrevealed by geological survey. Following simple appoach will be used to describe the influence of the fault on the compressional wave generated by the explosion. Let us assume that a crack can be represented by a flat and plane layer of a thickness l_T which is much shorter that wavelength. The layer is filled by the material with strenght lower than that of surrounding rocks. Assuming that the wave is normal to the crack we use quazistatic approximation to describe deformation of the material inside the crack [13]. In such a case, normal stresses on the both sides of the crack are the same and equal to the relative thickness change multiplied by the strenght of the material, i.e. $\rho_T c_T^2$ (ρ_T is the dencity, c_T is the wave velocity; compressional stress is positive).

The sum of the stresses in the incident and reflected waves is equal to the stress in the refracted wave ($\sigma_0=\rho c V_0$, $\sigma_2=-\rho c V_2$,

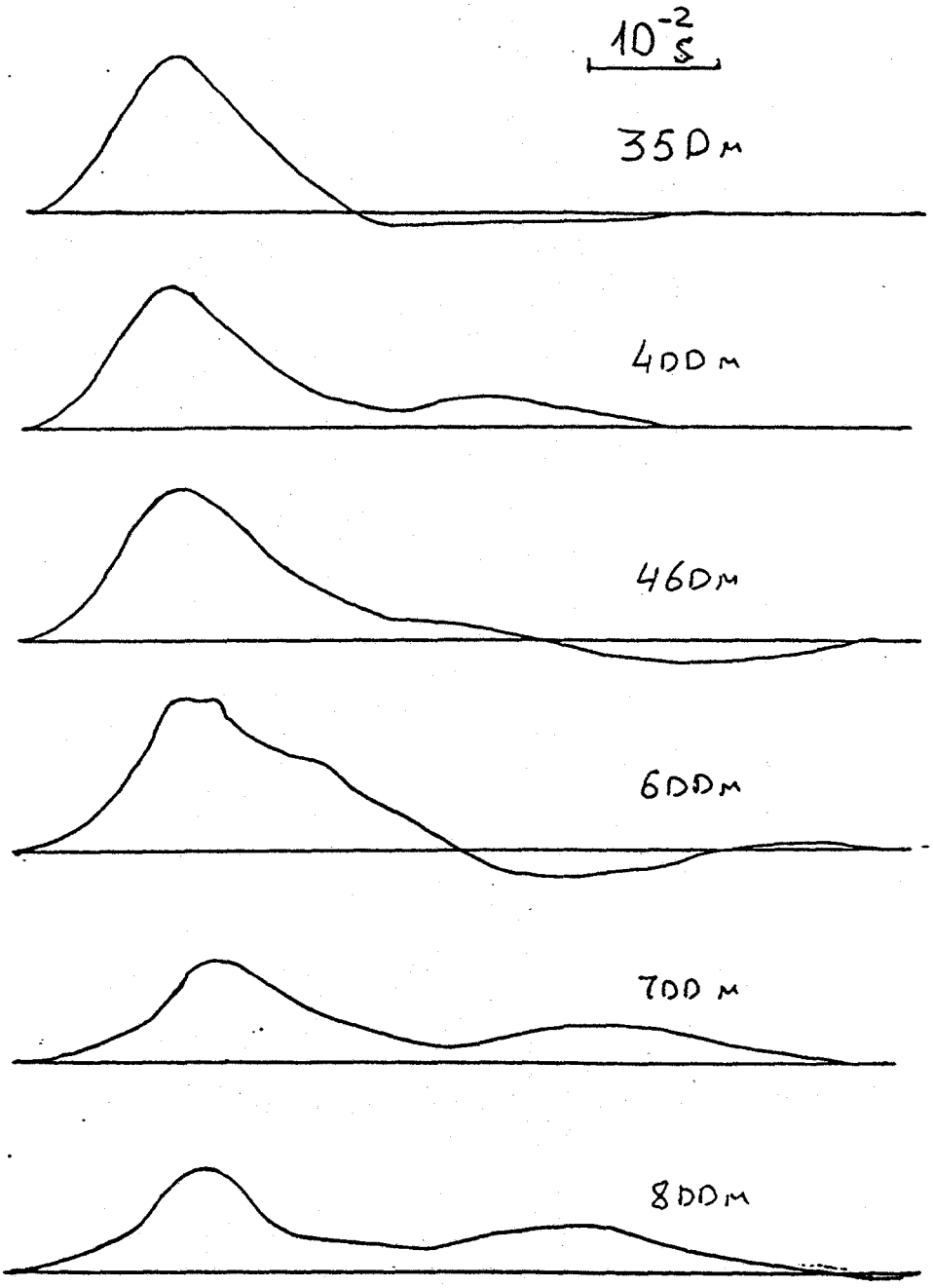

Fig. IV.2

$\sigma_1=\rho c V_1$; $\sigma_0 + \sigma_2 = \sigma_1$). The crack thickness change is equal to the difference of the relative positions of the crack boundaries. Following equation for the velocity in the transient wave, V_1, can be obtained from the above assumptions:

$$\theta \frac{\partial V_1}{\partial t} + V_1 = V_0 \tag{23}$$

where V_0 is the particle velocity in the incident wave, $\theta = \frac{l_T \gamma}{2c}$, $\gamma = \rho c^2/\rho_T c_T^2$, c is the compressional velocity, ρ is thedensity. Reflected wave (V_2) amplitude is determined by relationship

$$V_2 = V_0 - V_1 \tag{24}$$

The solution of (23) can be represented in the form

$$V_1 = e^{-x} \int_0^x V_0(x) e^x dx, \quad x = t/\theta. \tag{25}$$

The results of the calculations are presented in Figure IV.3 where V_1 and V_2 are shown for a given function V_0 which is close to the measured function from Figure IV.2. The same scale is used for convenience. Characteristic time, θ, is of 10^{-2} sec. The amplitude of the refracted wave is 1.5 times lower than of the incident one and rise time t_r increased to 1.5 10^{-2} sec. Note, that the reflected wave (V_2) has a sharper and shorter

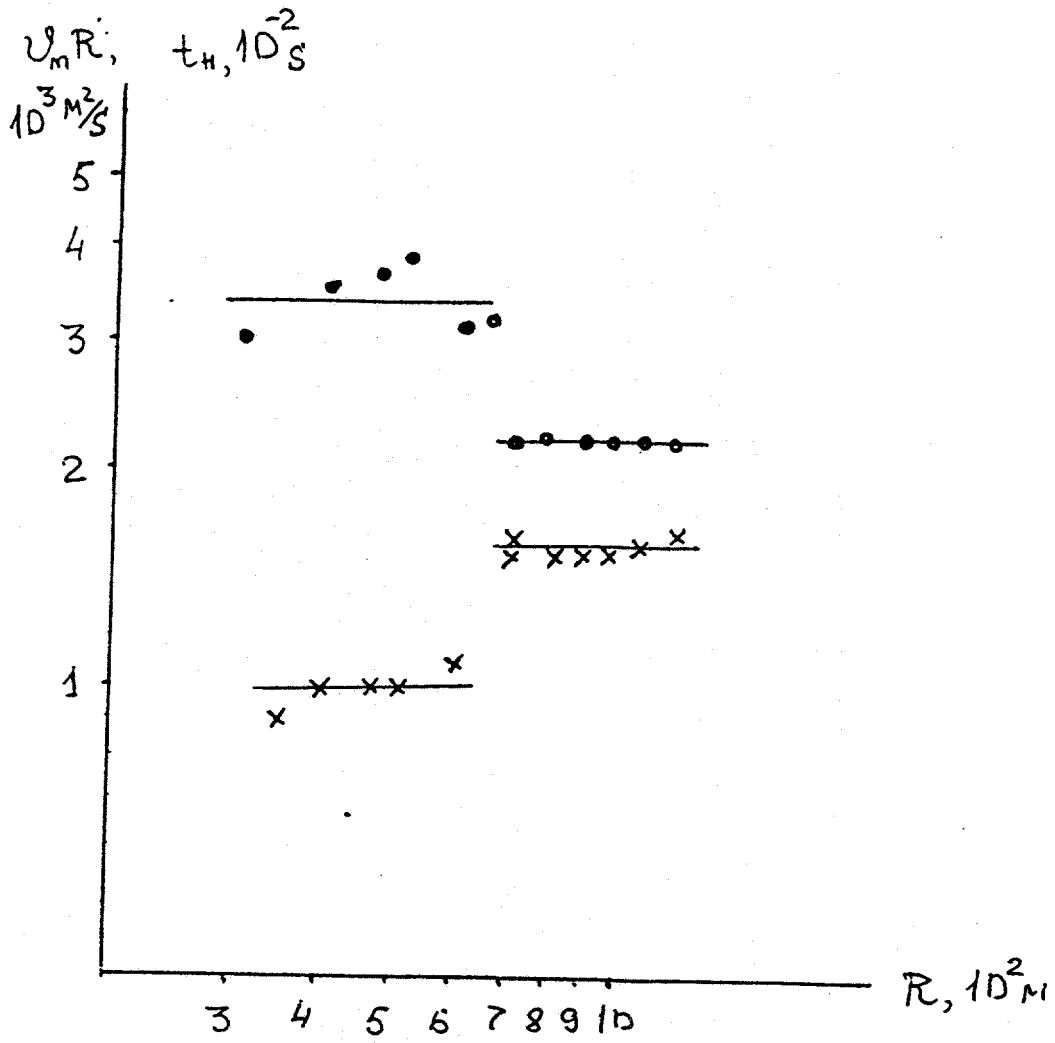

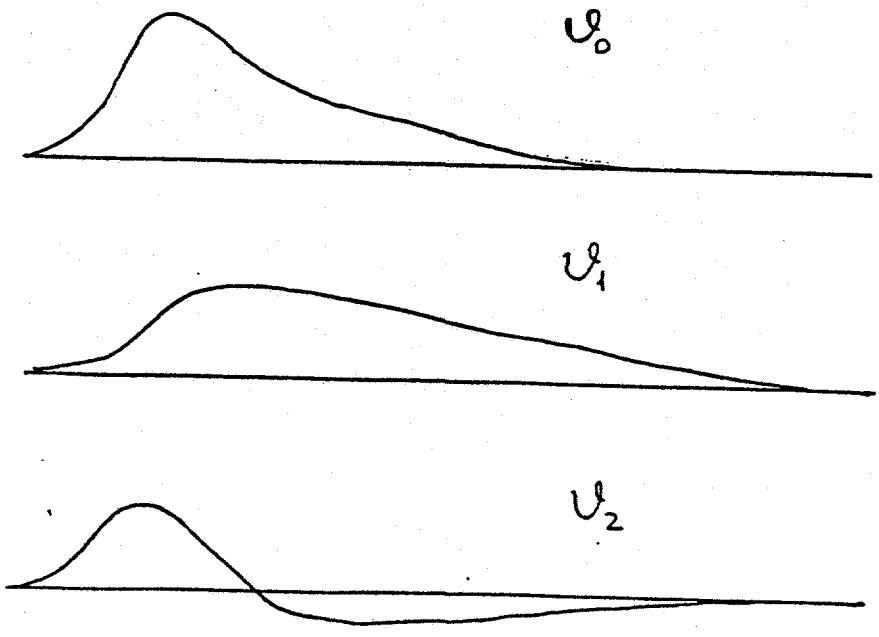

Fig. IV.3

compression phase and relatively long negative phase. Particle velocity can be larger when the reflected and incident waves merge, but stress and deformation are lower.

The results of peak velocity measurements from another explosion in granite are shown on Figure IV.4. As clear from the Figure, three separated horizontal parts can be distinguished where V_mR is pratically the same (i.e. $V_m \sim 1/R$). Characteristic times of two faults can be estimated from the offsets. The estimated values are close to that mentioned above ($\theta \cong 10^{-2}$ sec).

By using known values of θ and l_T (approximately 1 m) one can estimate γ, i.e. relative strength of the crack and massif materials:

$\gamma = 2c\theta/l_T = 10^2$ (c = 5km/sec). Since $\rho c^2 = 10^5$ MPa,

and $\rho_T c_T^2 = 10^3$ MPa, c_T = 700 m/sec, if $\rho_T = 2\ 10^3$ kg/m^3.

Thus, the material filling the cracks is close to sand or gravel by its mechanical properties. It is obvions, that such a material is common for cracks and small faults to depths of tens or hundreds of meters. For larger faults one can expect more hard material.

To estimate larger fault strenght we use the data obtained from the explosion conducted at the river Burlykya [14]. It was

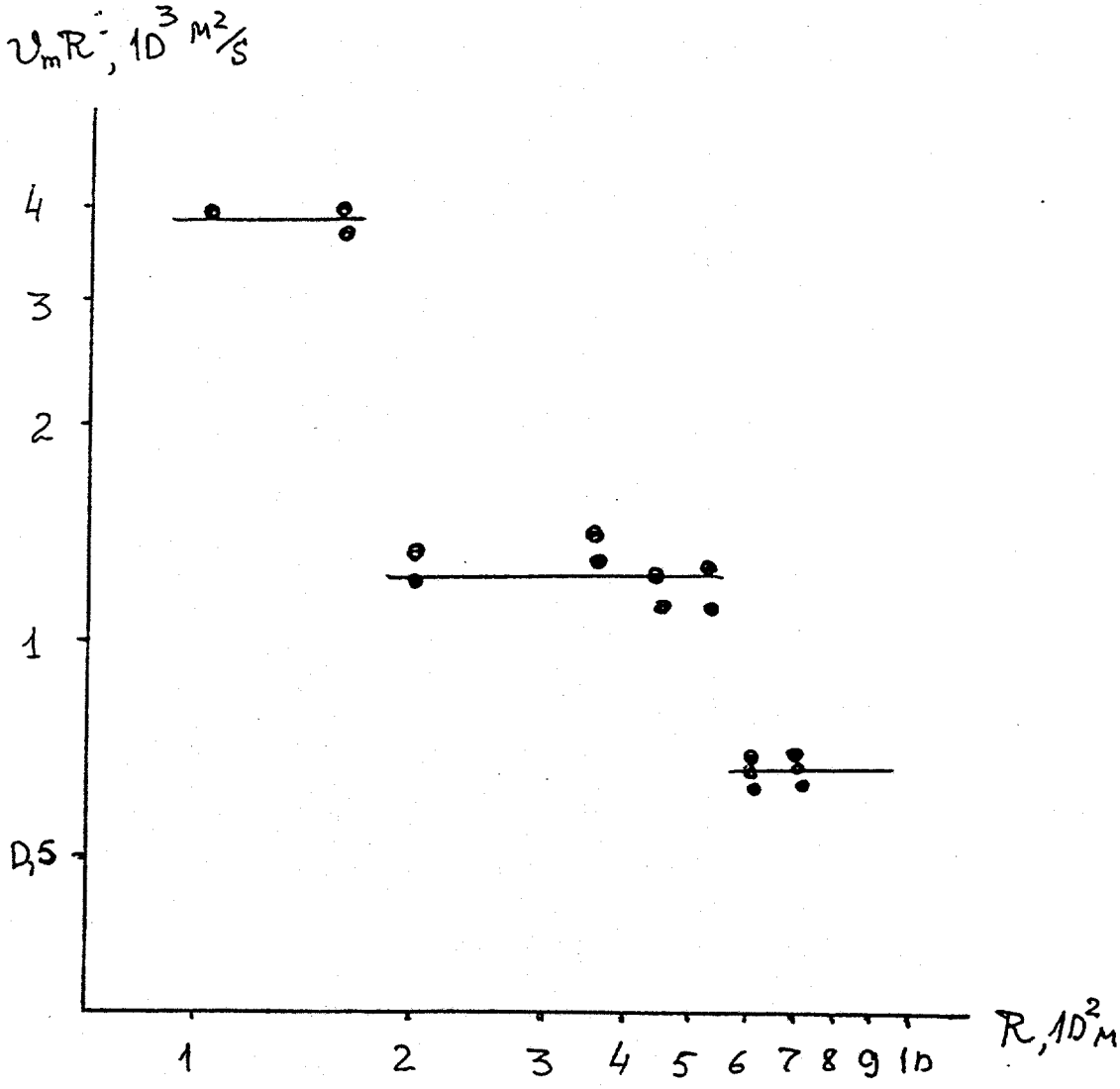

Fig. IV.4

established that seismic waves amplitudes drop from 3 to 4 times then crossing the Talass-Fergana fault. The period of oscillations in longitudinal wave was of 0.2 to 0.3 sec. Compressional wave velocity was of 5.5 km/sec. Let us use equations from [13] in estimating the parameters of the fault. According to the equations, amplitude change of a wave with a period T when it crosses a fault is equal to $(1+q^2)^{1/2}$, where $q = \pi l_T \gamma/cT = 2\pi\theta/T$. Assuming the thickness of the fault $l_T = 10^2$m, $q = 3$, and $c_T = 2\ 10^3$m/sec characteristic time is estimated as $\theta = 0.1$ sec.

The range of γ values ($10 \le \gamma \le 10^2$) can be treated as typical for natural rock massifs. For lower γ, a fault is not contrasting to surrounding massif. Higher γ's relate to unusually soft materials. Note, that we are not considering opened cracks here, as well as annealed.

Compressional wave meets cracks and faults of different scale when spreads from the center. Naturally, there are some regions with high crack density. In such a case, attenuation is high, i.e. amplitude drops fast, rize time and positive phase duration increase with distance. Exponent n in (22) may be larger than 1. At the same time, there are some regions (see Fig. IV.4) where only spherical spreading effects amplitude (n=1).

It is worth noting one important fact which should be considered when comparing explosions of different scale. In

practice, the range where relations of (22) type is determined depends on the explosion scale (cube root scaling of yield). Low yield explosions generate short period waves and smaller cracks with lower θ ($q \sim \theta/T$) are important. Larger cracks and faults are usually avoided in such a case. Seismic waves generated by large-scale explosions are not effected by small cracks, but larger faults should be considered.

Thus, by changing of scale of explosion one change the characteristic size of the cracks which determine attenuation. As a result, in the near-field zone of an explosion (particle velocity $V_m > 10 \frac{cm}{sec}$) the exponent n in (22) varies in the narrow range from 1.5 to 2, but change of yield in broad range does not influence the similary of principal wave parameters [1]. The similarity (scaling law) does not hold at larger distances. For example, wave periods depend on yield very weak. At these distances attenuation will be effected by the characteristic set of cracks and faults in a massif. Very important in this case is hierarchy in the blocks sizes and related discoutinuities [15]. The hierarchy is characterized by particular set of characteristic times θ.

The spectra $V_1(\omega)$ and $V_2(\omega)$ can be obtained from (23) and (24):

$$V_1(\omega)/V_0(\omega) = \frac{1}{1+i\omega\theta} = \frac{1}{q+1}; \quad q = i\omega\theta \tag{25}$$

$$V_2(\omega)/V_0(\omega) = \frac{i\omega\theta}{1+i\omega\theta} = \frac{q}{1+q}$$

The spectra allow to consider a fault or crack as a low-frequency filter for transient wave and high-frequency filter for reflected wave. Note, that when the wave passes through a crack its spectrum is multiplied by 1/1+q. As a result, the spectrum roll-off (asymptotic behaviour) changes. Passing several cracks (n) the wave spectrum is multiplied by $\left(\frac{1}{1+q}\right)^n$. This effect leads to strong attenuation at high frequencies. The reflected waves should be considered, however, in this case. The problem has to be treated separately, but the results of multiplied reflections consideration [13] show that follows from experimental seismograms.

Let us consider the results of plane harmonic longitudinal wave interaction with a set of parcallel cracks [13]. Incident P-wave is normal to a set of N blocks separated by the cracks of different scale, i.e. having different θ.

Potential for each block is written in the form

$$\varphi_n = A_n e^{i\omega(t-x/c)} + B_n e^{i\omega(t+x/c)} \tag{26}$$

where $1 \leq n \leq N$, x is the coordinate of a chosen point, A_n and B_n are the functions of frequency. In the quasistatic approximation, deformation of a crack between two adjacent blocks n and (n-1) is characterized by equal normal stresses, σ_x, at the boundaries, and relative deformation at any given time is equal to $\sigma_x/\rho_T c_T^2$. By using these boundary conditions one

can obtain the system for A_n and B_n:

$$A_n = (1-q_n)\,A_{n-1} - q_n\,B_{n-1}\,e^{i\omega 2x_n/c}$$

(27)

$$B_n = q_n\,A_{n-1}\,e^{i\omega 2x_n/c} + (1+q)\,B_{n-1}$$

where $q_n = i\omega\theta_n$, x_n is the coordinate of the crack boundary (the crack thickness is neglected). System (27) should include input signal $A_o(\omega)$, as well as boundary conditions at the last crack and beyond it. System (27) with $A_o(\omega) = 1$ have a fundamental solution for δ-function, $G(x,\omega)$ which can be used for different input signals. Note, that when $q_n \to 0$, i.e. $\theta_n \to 0$, or when $\omega \to 0$ it follows from (27) that $B_n = 0$, $A_n = A_o$, $n = 1,2,\ldots,N$.

It means that incident wave is not disturbed when $\theta_n = 0$. When $\omega \to 0$, the blocky system has the response coinciding with the low-frequency characteristic of initial (incident) signal, and, if $A_o=1$, $G(x,\omega) \to 1$.

The problem solution for particle velocity has the form

$$\tau = t - x/c$$

(28)

$$V(x,\tau) = \frac{1}{2\Pi}\int_{-\infty}^{\infty} G(x,\omega)\,V_o(\omega)\,e^{i\omega\tau}d\omega$$

where $G(x,\omega)$ is determined by the relation of particle velocity and potential φ_n:

$$V_n = \frac{\partial^2 \varphi_n}{\partial x \partial t} = -\omega^2/c \; (A_n - B_n \, e^{i\omega 2x/c}) \; e^{i\omega t},$$

from where

$$G(x,\omega) = (A_n - B_n \, e^{i\omega 2x/c}).$$

If $A_o(\omega)$ is the spectrum of potential of the input signal, $V_o(\omega) = -\omega^2/c \; A_o(\omega)$.

Note, that (28) determines the signal characteristics at the moment of time relative to the arrival at a given point, i.e. time is shifted by x/c.

The equation (28) can be used in calculating wavefields from a spherical source assuming that the wave propagates normal to a set of parallel cracks. Far enouth from the center, only the first term in (1) is important and ray approximation can be used which accounts for spherical spreading by multiplying of particle velocity by R.

Moreover, when the Poisson's ratio ν=1/3, normal stress ($\sigma=\sigma_R$) and particle velocity relationship are the same as for plane wave, i.e. $\sigma_R = -\rho c V$ is accurate to the third term in (1) for σ_R. Thus, the method of seismic wave propagation through a fault [12,13] can be also used for two-terms expression (1) for V(R,t) in the spherical wave. Scipping some problems of discussion dealing with seismic wave propagation through a system of cracks and faults, we now turn to the analysis of some experimental results from large-scale explosions in hard rocks.

3. Hard limestone explosions data analysis.

Two explosions were conducted in a massif formed by hard limestone. Concentrated charge of 190 tons of trotyl was fired in the experiment N1, and the second charge was of 660 tons [16]. Principal experimental data measured in the horizontal mine are presented in Tables 1 and 2.

Table IV.1. Experiment N1, Q = 190t.

Range, m	Sensor type	V_mR, m^2/s	τ_1, ms	U_mR, m^2
19.5	IMSG	520	-	-
29	-"-	250	~5	-
42.5	-"-	230	~6	-
43	-"-	210	~10	1.2
44	-"-	230	~10	1.2
44	VIB-A	260	17	1.3
100	VIB-A	210;280	18;18	2;2.1
100	IMSG	130	-	-
110, right	-"-	100	-	-
hole	VIB-A	100;120	27	1.3
100, -"-	VBP-3	150	23	1.7
100	VIB-A	85	26	1.2
240	VBP-3	70	23	0.8
240	VIB-A	55;60	29;31	1;0.9
460	VBP-3	46	23	0.5
460	VIB-A	37	34	0.64
800	-"-	15	29	0.25
1550				

Table IV.2. Experiment N2, Q = 660t.

Range, m	Sensor type	V_mR, m^2/s	τ_1, ms	U_mR, m^2
43	IMSG	468	-	-
92	VIB-A	290	-	-
145	-"-	210	29	3
160	VBP-3	150	~30	2
359	VIB-A	83;100	33;32	1.5;1.7
710	-"-	60	38	1.3
1460	-"-	33	42	0.9

Tables IV.1 and IV.2 summarize the measured values of peak velocity, V_m, peak displacement, U_m, and positive phase duration, τ_1, in longitudinal wave. For the sake of convenience of further analysis, the values of V_m and U_m are multiplied by R to exclude spherical spreading. Figure IV.5 presents V_mR and τ_1 as a function of the range (circles and crosses). The results of calculations by both methods for blocky structure considered in the previous sections are also shown by triangles. Filled tringles represent the results of calculations by the first method where initial elastic signal was estimated from (10)-(13). Following source parameters were obtained: b_m =42 m, θ_0=2ms, ϕ_0=64 m^3. Longitudinal wave velocity from the measurements was of c=6 km/s, and ρ=2.7 kg/m^3. Initial pressure in the cavity was adopted as $P_1=10^5$ kg/cm^2, and the ratio $Y/\rho c^2$

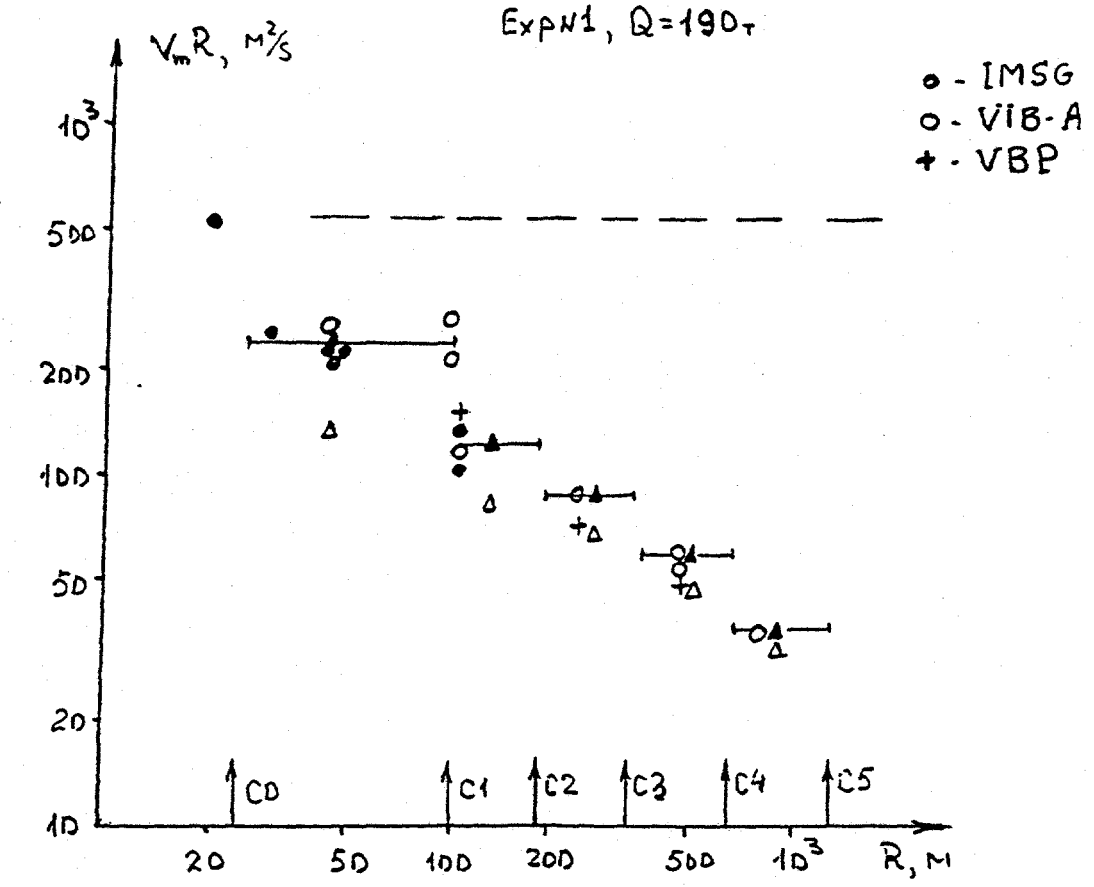
Exp N1, Q=190т
o - IMSG
o - VIB-A
+ - VBP
$V_m R$, м²/с
10^3
500
200
100
50
20
10
C0
C1
C2
C3
C4
C5
20
50
100
200
500
10^3
R, м

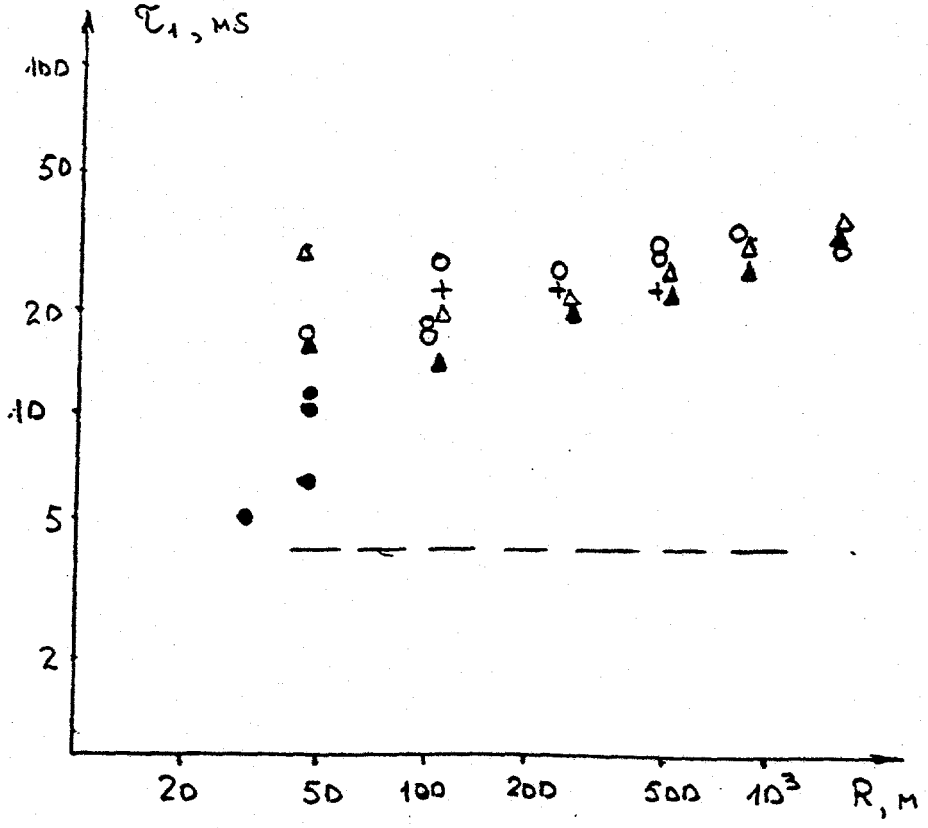
τ_1, мс
100
50
20
10
5
2
20
50
100
200
500
10^3
R, м

Fig. IV.5

$=10^{-3}$. The second explosion is characterized by b_m=64 m, θ_o=3 ms, ϕ_o=230 m^3.

A system of faults was adjusted to fit experimental theoretical relationships between VmR and R. The principal parameters of the system were the faults locations and their characteristic times θ. The faults C0, C1, C2, C3, C4, and C5 are indicated by arrows on the upper frame of Figure IV.5. The faults separate the principal blocks and determine the offsets of V_mR. Elastic solution for V_mR is shown by dashed line. Longitudinal wave source is chosen from the first method. The fault C0 is placed at the boundary of the principal zone of plastic destruction by the explosion generated wave. The radius of this zone is $R_o \geq b_m/2$=24m. This radius was chosen as an initial value in the further calculations of the wave propagation by the equations (26) and (27) for plane waves. The function $V(R,\tau)R$ was calculated from (28) and (3) by the equation ($x=R-R_o$)

$$V(R,\tau)\,R = \frac{1}{2\Pi}\int_{-\infty}^{\infty} G(x,\omega)\left[\frac{1}{R} + \frac{i\omega}{c}\right]\Phi'(\omega)e^{i\omega\tau}d\omega \qquad (29)$$

The parameters of $\Phi'(\omega)$ were chosen from (13) in the first method, and from (21) for the second method. The function $U(R,\tau)R$ was calculated by integrating of particle velocity records. Following parameters were derived from (19) and (21)

for the second method, when Q=190 tons: ($\sigma_*/\rho c^2=10^{-3}$)

$$b_m=40 \text{ m}, \quad \phi_0=(\sigma_*/\rho c^2)b_m^3=64 \text{ m}^3.$$

Note, that the parameters b_m and ϕ_0 are almost the same in the two methods.

The results obtained from the second mothod are presented in the Figures by opened triangles. The locations and characteristic times of the faults C1÷C5 were the same as in the first method, but the fault C0 was not included since it is situated in the nonlinear zone of the explosion.

The values of θ were equal for the faults C1, C2, and C3: θ=4 ms. Characteristic time, θ, for the fault C4 was 6 ms, and for C5 was of 14 ms. It should be noted, that geological survey has revealed two discontinuites near the fault C3 which were presented as a fault in the calculations. Intensively cracked zone was found at the fault C5 situated near the mine mouth. This phenomena can, obviously, explain the large observed offset of V_mR which leads to high θ value of the fault C5. Note, that the characteristic time values in the range from 4 to 14 ms are close to the values reported in Section 2.

Figure IV.6 shows predicted values of particle velocity as a function of distance (the first method). The records are shifted by R/c time corresponding to the longitudinal wave arrivals. Amplitude changes as a function of distance, rise time

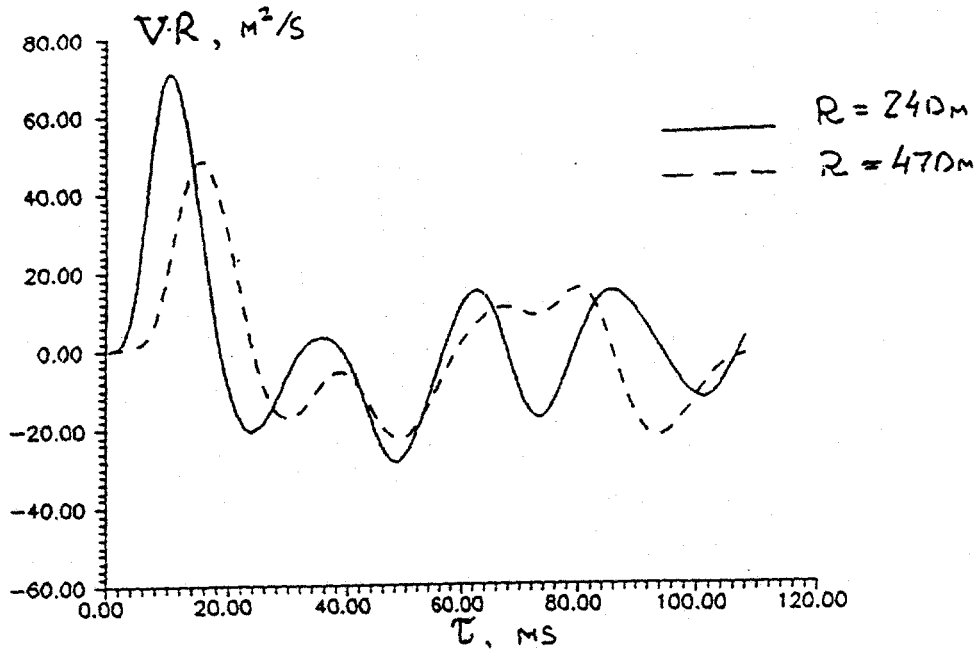
V·R, M²/S
80.00
60.00
40.00
20.00
0.00
-20.00
-40.00
-60.00
0.00
20.00
40.00
60.00
80.00
100.00
120.00
τ, MS
R = 240M
R = 470M

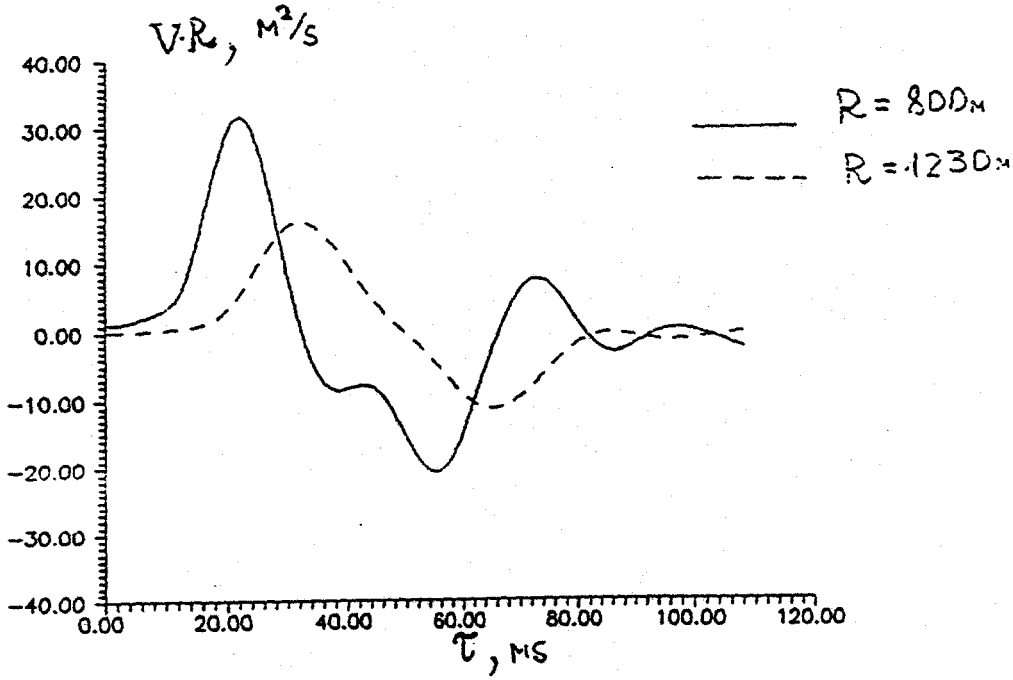
V·R, M²/S
40.00
30.00
20.00
10.00
0.00
-10.00
-20.00
-30.00
-40.00
0.00
20.00
40.00
60.00
80.00
100.00
120.00
τ, MS
R = 800M
R = 1230M

Fig. IV.6

and the first positive phase duration increase are clear from the Figure. The following oscillations are related to reflected by different faults waves. At larger distances, sinusoidal-shaped oscillations arise instead of sharp impulse. Figure IV.7 shows corresponding displacements at the same distances. The displacement rise time to peak value increases with distance in accordance to τ_1 increase. At larger times, the oscillations occure near the residual displacement discreasing with distance.

Reduced displacement potential, $\phi(R,t)$, can be obtained from (1) by using $U(R,t)R$ or $V(R,t)R$ at each given distance R.

Figure IV.8 shows reduced displacement potential calculated from $V(R,\tau)$ shown on Figure 6 by the relationship

$$\phi''(\tau)-\frac{c}{R}\phi'(\tau) = RcV(\tau).$$

The first derivative, $\phi'(\tau)$, was calculated by

$$\phi'(\tau) = e^{\tau c/R}\int_0^{\tau} RcV(t)e^{-tc/R}dt,$$

and integration of $\phi'(\tau)$ gave $\phi(\tau)$. As can be seen from Figure IV.8, the potential $\phi(\tau)$ reaches its final constant value with increasing time. This value is of $\phi_o=64\ m^3$. Increasing rize time of $\phi(\tau)$ with distance is clear. Some overshoot [9] of $\phi(\tau)$ is

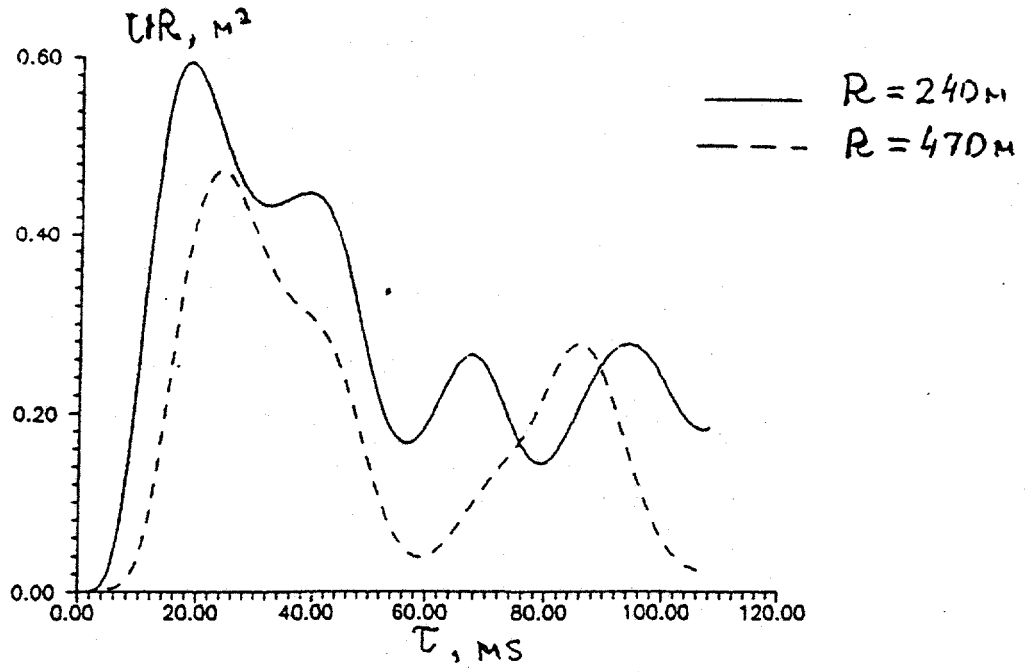
UR, M²
0.60
0.40
0.20
0.00
0.00
20.00
40.00
60.00
80.00
100.00
120.00
τ, MS
R = 240 M
R = 470 M

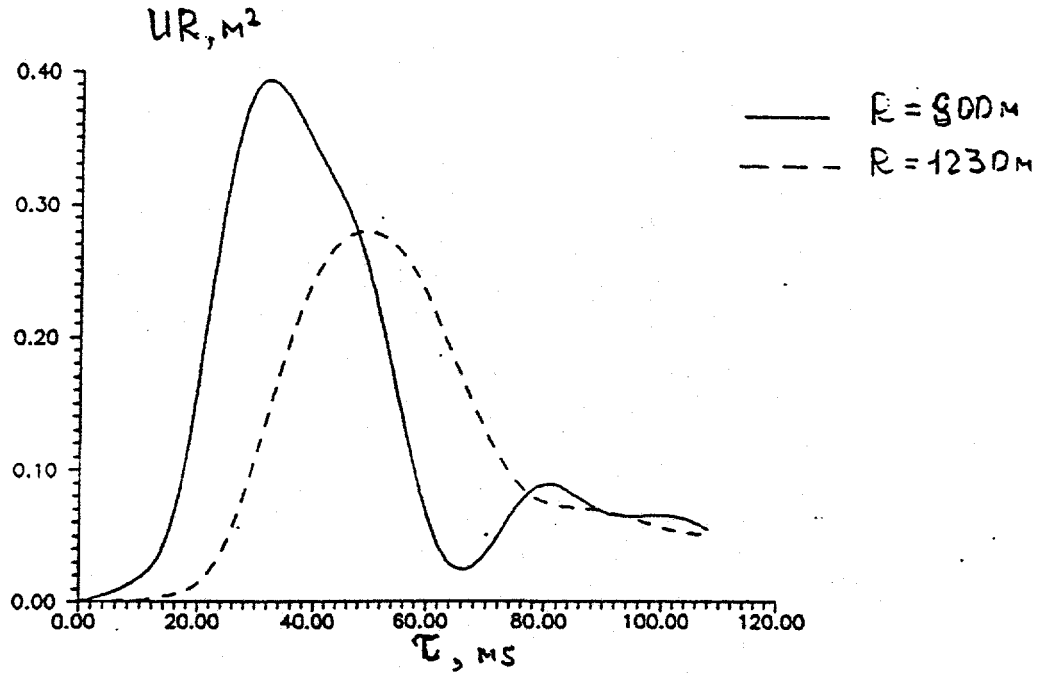
UR, M²
0.40
0.30
0.20
0.10
0.00
0.00
20.00
40.00
60.00
80.00
100.00
120.00
τ, MS
R = 800 M
R = 1230 M

Fig. IV.7

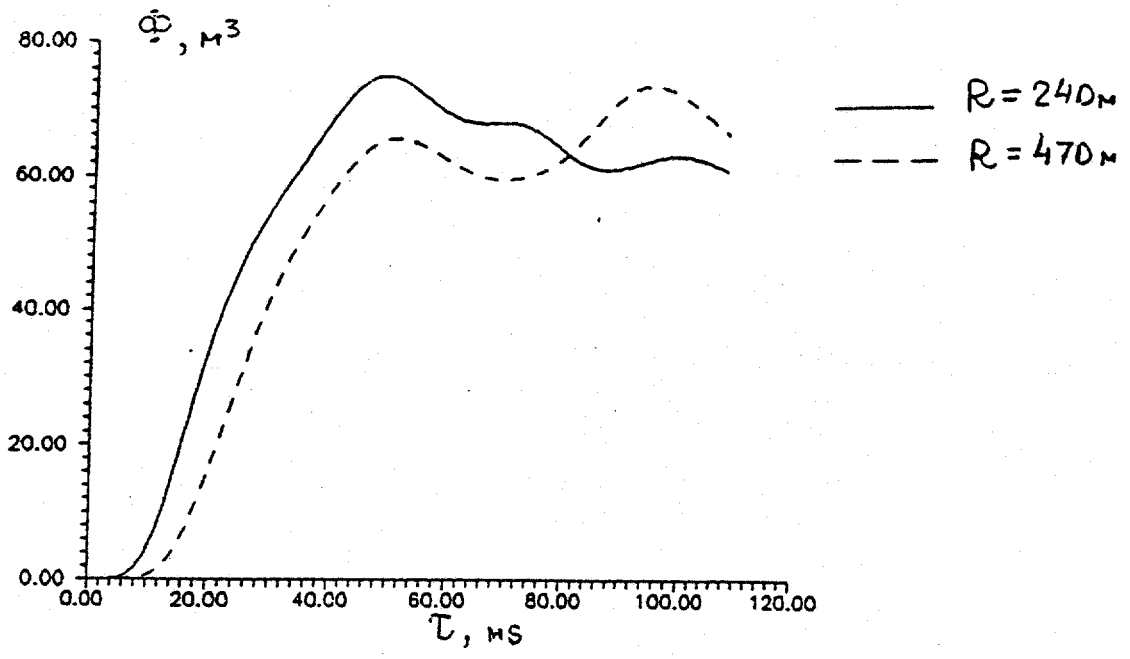
Φ, м³
80.00
60.00
40.00
20.00
0.00
0.00
20.00
40.00
60.00
80.00
100.00
120.00
τ, ms
R = 240 м
R = 470 м

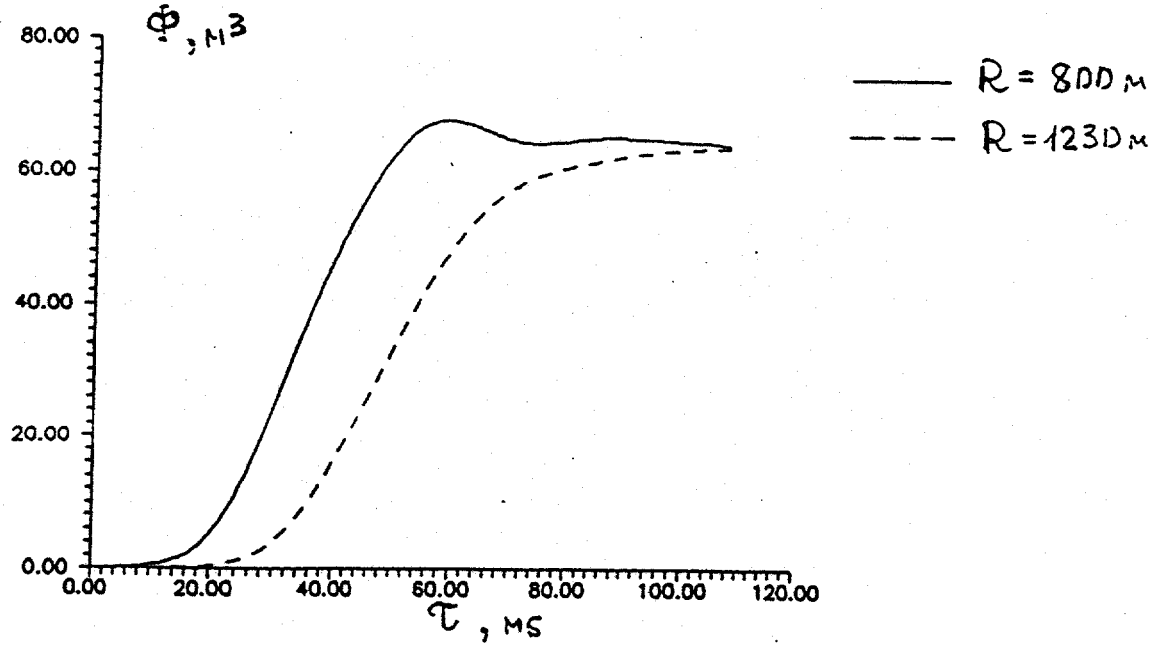
Φ, м³
80.00
60.00
40.00
20.00
0.00
0.00
20.00
40.00
60.00
80.00
100.00
120.00
τ, ms
R = 800 м
R = 1230 м

Fig. IV.8.

also may be seen at some curves.

Figures IV.9 through IV.11 show the results obtained by the second method. Dimensionless values of displacement, potential and spectra are given at three distances. Dimensionless values were obtained from relationships:

$$\bar{U} = UR/(\sigma*/\rho c\ b_m^2),\ \bar{\Phi} = \Phi/(\sigma*/\rho c^2 b_m^3) = \Phi/\Phi o;$$

$$S = \lg(|\dot{\phi}|/(\sigma*/\rho c^2 b_m^3)) = \lg(|\Phi'(\omega)|/\Phi o).$$

Corresponding elastic values of $\bar{U}$, $\bar{\Phi}$ and $\bar{S}$ are presented by dashed line. The comparison of the values indicates the effects of the faults increasing with distance: $\bar{U}$'s and $\bar{\Phi}$'s rise time increases and amplitude drops. The final value Φo, however, does not change, but some overshoot is clear. The change of the parameters discussed above is related to the spectral characteristics changes. The derivative of reduced displacement potential, i.e. $|\Phi'(\omega)|$, represent these changes very well. As clear from Figures IV.9 thru IV.11, $|\Phi'(\omega)|$, when $\omega \rightarrow 0$, does not change with distance and is equal to Φo. But at high frequencies, attenuation increases with distance. The latter phenomena can be formally described by the relationships (13) or (21) by including an effective corner frequency or bm. Quazistatic approximation for crashed zone expansion used at closer distances (Figure 9) describes relatively well averaged

R=42м

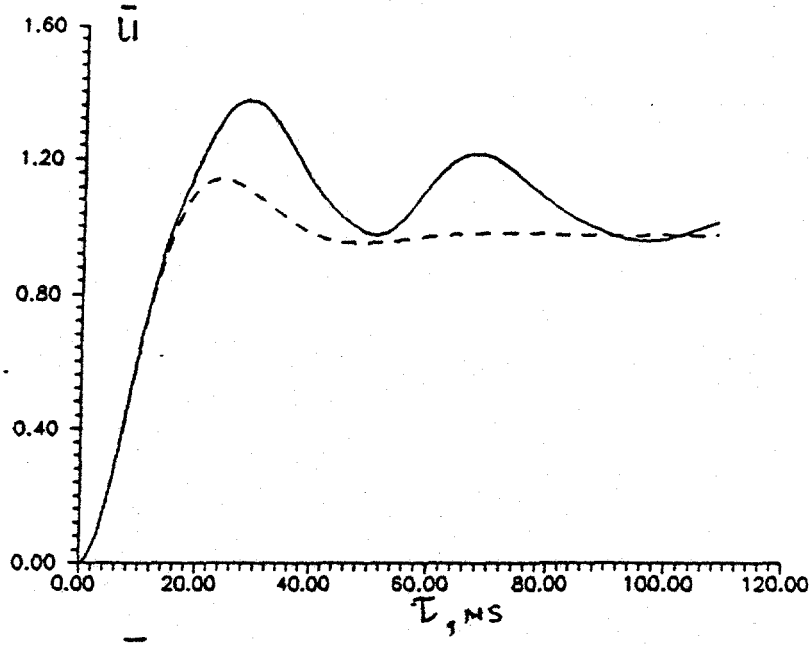
$\bar{U}$
1.60
1.20
0.80
0.40
0.00
0.00
20.00
40.00
60.00
80.00
100.00
120.00
τ, мс

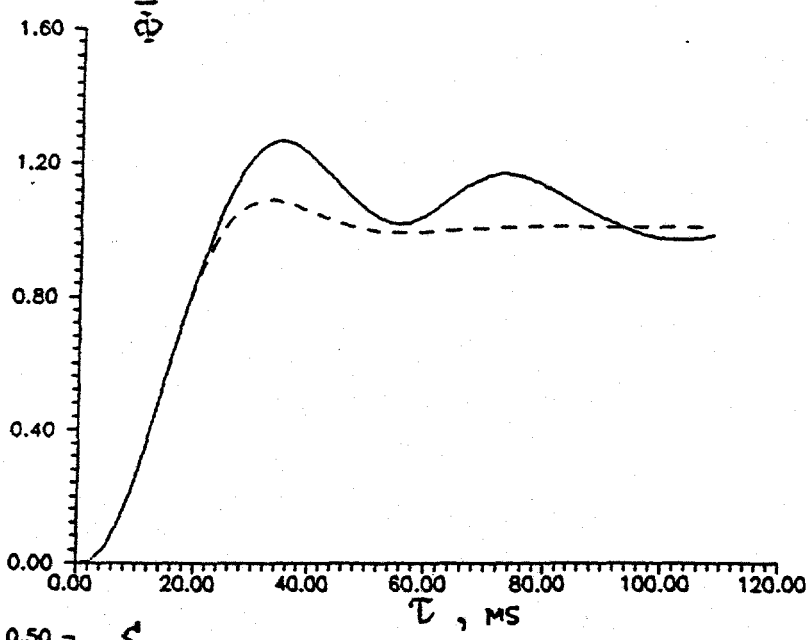
$\bar{\Phi}$
1.60
1.20
0.80
0.40
0.00
0.00
20.00
40.00
60.00
80.00
100.00
120.00
τ, мс

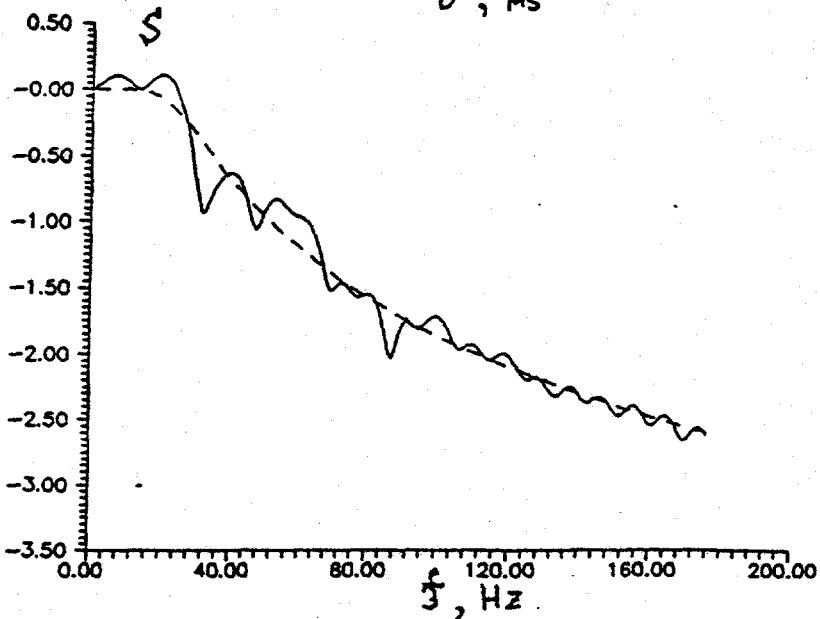
S
0.50
-0.00
-0.50
-1.00
-1.50
-2.00
-2.50
-3.00
-3.50
0.00
40.00
80.00
120.00
160.00
200.00
f, Hz

Fig. IV.9

R = 240 м

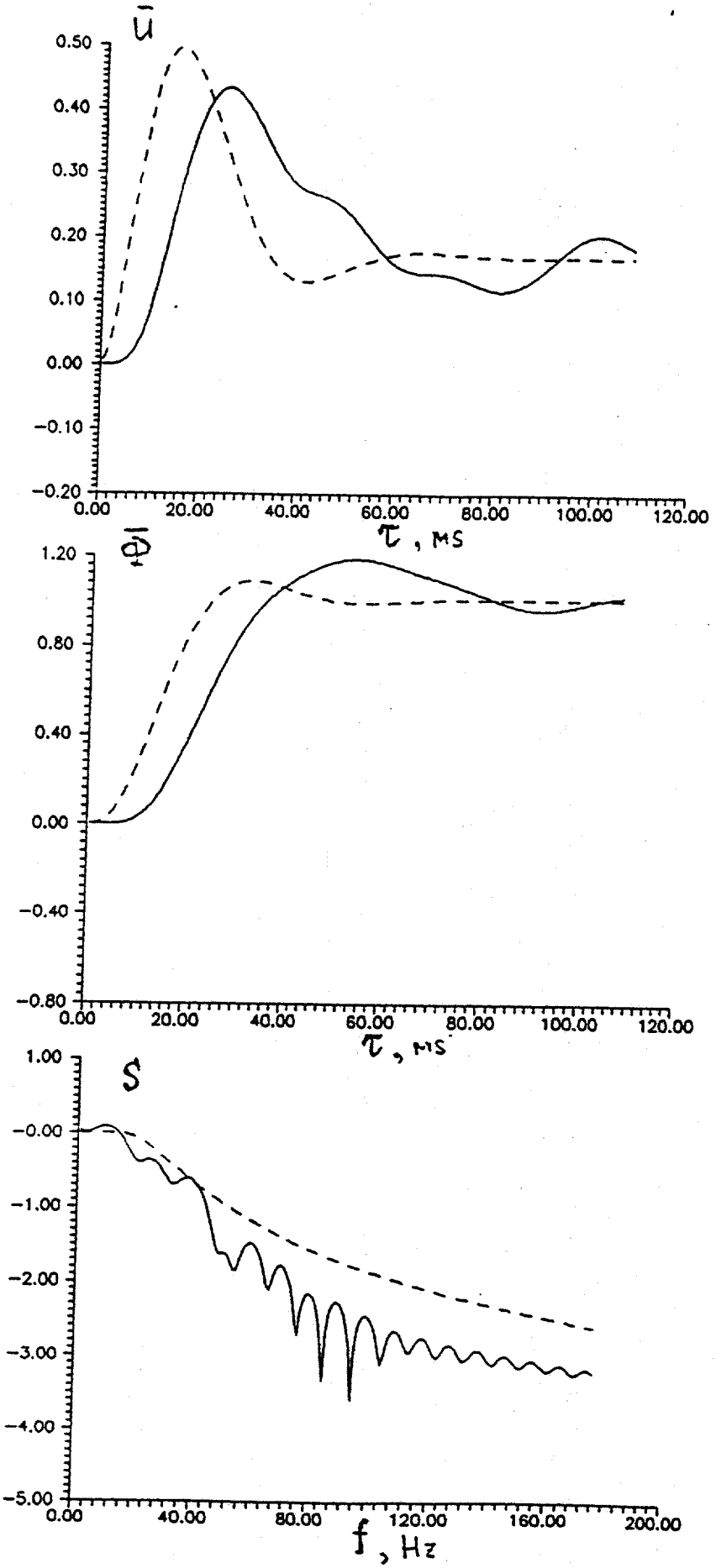

Fig. IV.10

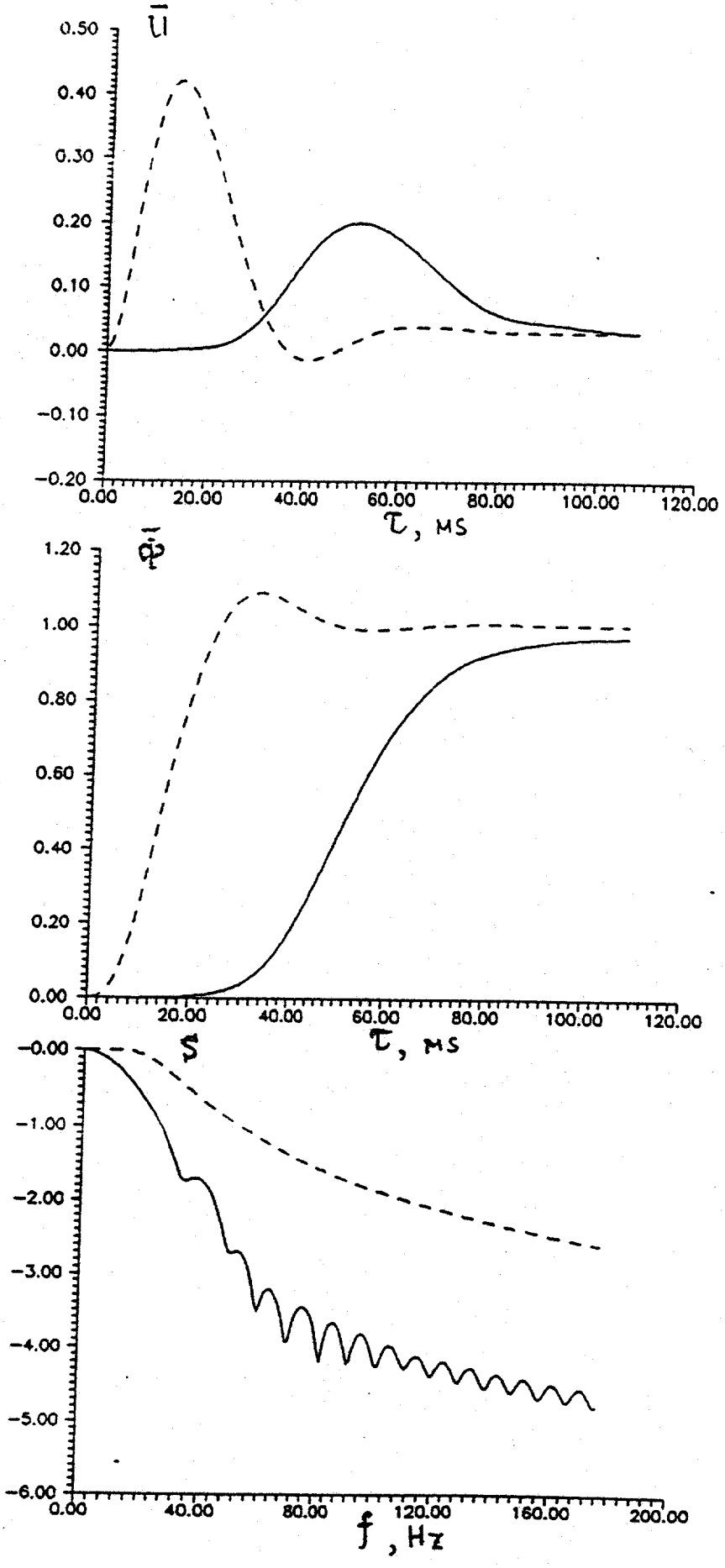

R = 1230 м

Fig. IV.11.

spectrum with the parameters b_m=40 m and $f_c = \frac{\omega_c}{2\pi} = \frac{c}{2\pi b_m}$ = 24 Hz. But if to include high-frequency asymptotic roll-off, i.e. $|\phi'(\omega)| \sim \left(\frac{b}{\omega}\right)^3$, the corner frequency and effective radius b_* are following: at R=240 m, f_c=12 Hz, b_*=80 m; and at R=1230 m, f_c=5 Hz and b_*=200 m. Thus, the effective source radius increases with distance in the medium containing cracks and faults. This effect is well known of the medium with attenuation, but no attenuation was included in the models, nethertheless, the result is similar. Quantitative comprison of the results demands a special consideration, but if to use standard attenuation relation $A \sim e^{-\delta R/\lambda}$, the decrement δ should be unreasonably large. The experimental and theoretical values of peak displacement are shown on Figure IV.12. As before, filled tringles shows the data from the first method, and opened - for the second. The two methods give close results, but peak particle velocity (see Fig. IV.5) at closer distances from the second method is much lower. Elastic solution for U_mR from the first method is shown by dashed line on the upper frame of Figure IV.12. The lower frame of Figure IV.12 shows the calculated values of $U_mR\tau_{1c}$. This value has a dimension m^3, i.e. the same as ϕ. The value ϕ_0 is shown by dased line in the Figure. As clear from the Figure, at large distances R the results from the two models are close to ϕ_0. This result follows from (1) for displacement. According to (1) at large enouth R only the first terme is important and

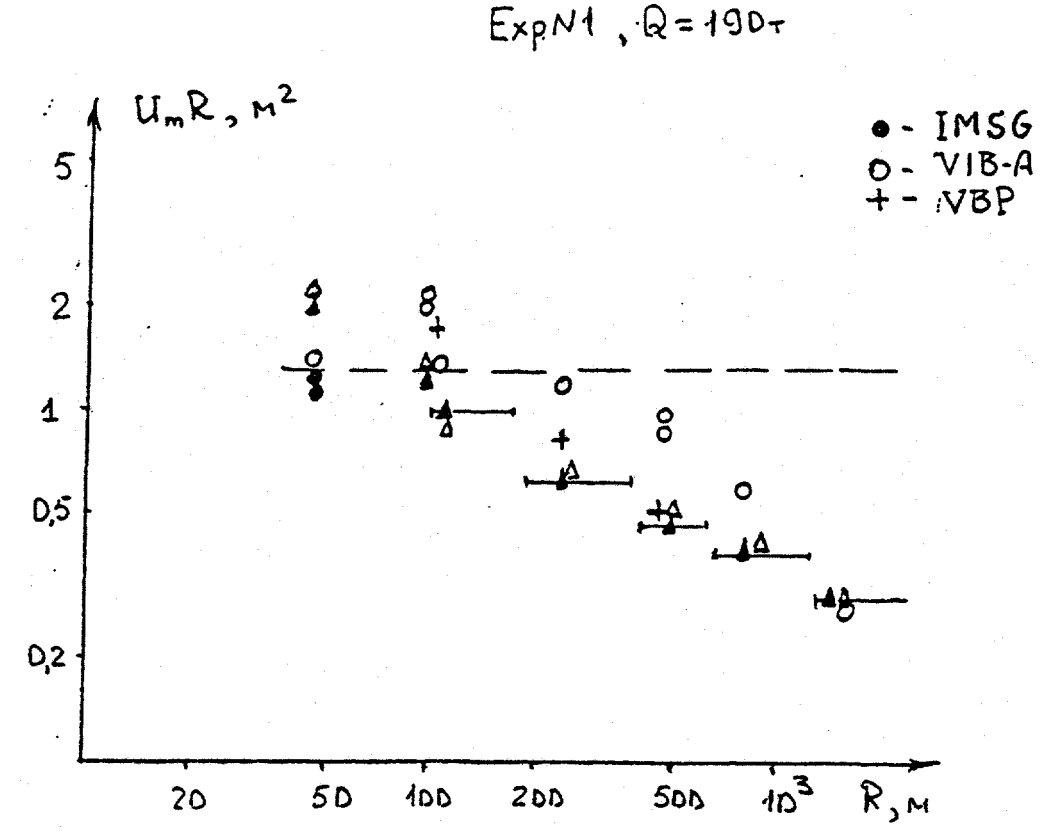
Exp N1 , Q = 190т
$U_m R$, м²
● - IMSG
○ - VIB-A
+ - VBP
5
2
1
0,5
0,2
20
50
100
200
500
10³
R, м

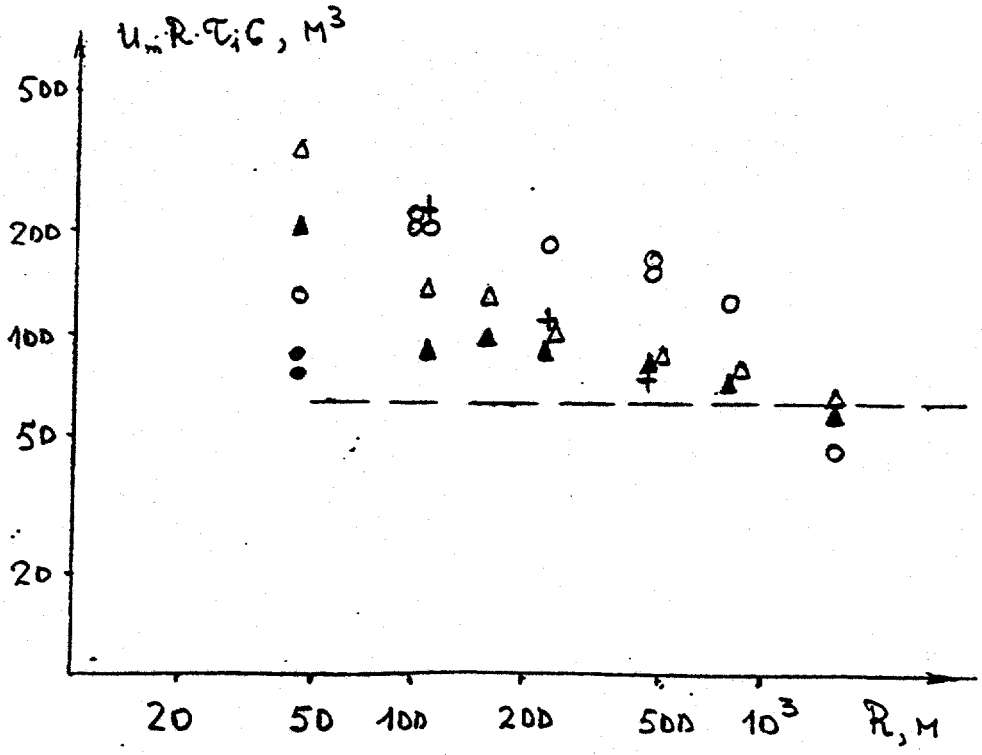
$U_m R \cdot \tau_i C$, м³
500
200
100
50
20
20
50
100
200
500
10³
R, м

Fig. IV.12

$$\phi(\tau) = Rc \int_0^{\tau} U(\tau)d\tau$$

Assuming that $U(\tau)$ is quazisinusoidal with a halfperiod of $\sim 2\tau_1$ we have $\phi(\tau) \cong RcU_m\tau_1 \cong \phi_o$ since at large distances ϕ_o final value is reached after the first phase passed. The same method used for closer distances gives overestimation of the potential. The experimental data under consideration are usually larger than theoretical calculations. But it concerns only the data obtained by integrating of VIB-A's particle velocity records. The data recorded by VBP sensors are in better consistence with the theoretical.

The results of the calculations by the first method for the second explosion are illustrated by VR, UR, and ϕ values at four distances (150m, 372m, 710m, and 1240 m), presented in Figures IV.13 thru IV.15. The same pattern as during the first explosion is obvious. The faults are shown by arrows on the upper frame of Figure IV.16, where the results of calculations are shown by triangles. Dashed line stands for the medium without the faults. The fault "c" is chosen at the boundary of the plastic zone as for the first explosion and has the same characteristic time θ=6 ms. The faults C2 thru C5 correspond to the same faults, but their relative positions are shifted according to the position of the second explosion. The characteristic times of the faults are the same except C3 which

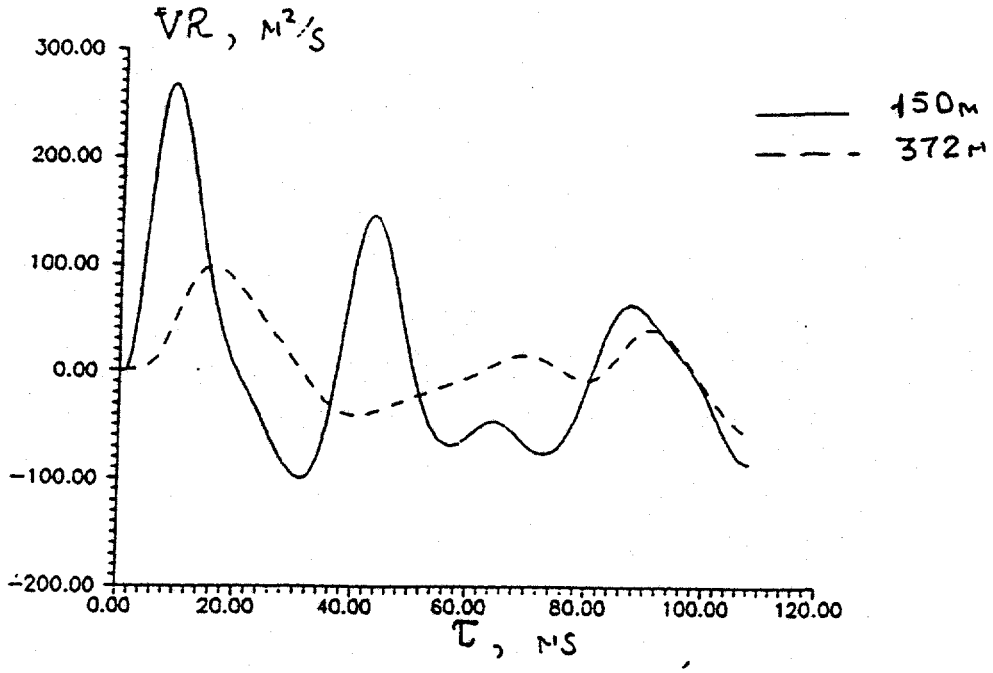
VR, M²/S
300.00
200.00
100.00
0.00
-100.00
-200.00
0.00
20.00
40.00
60.00
80.00
100.00
120.00
τ, MS
150M
372M

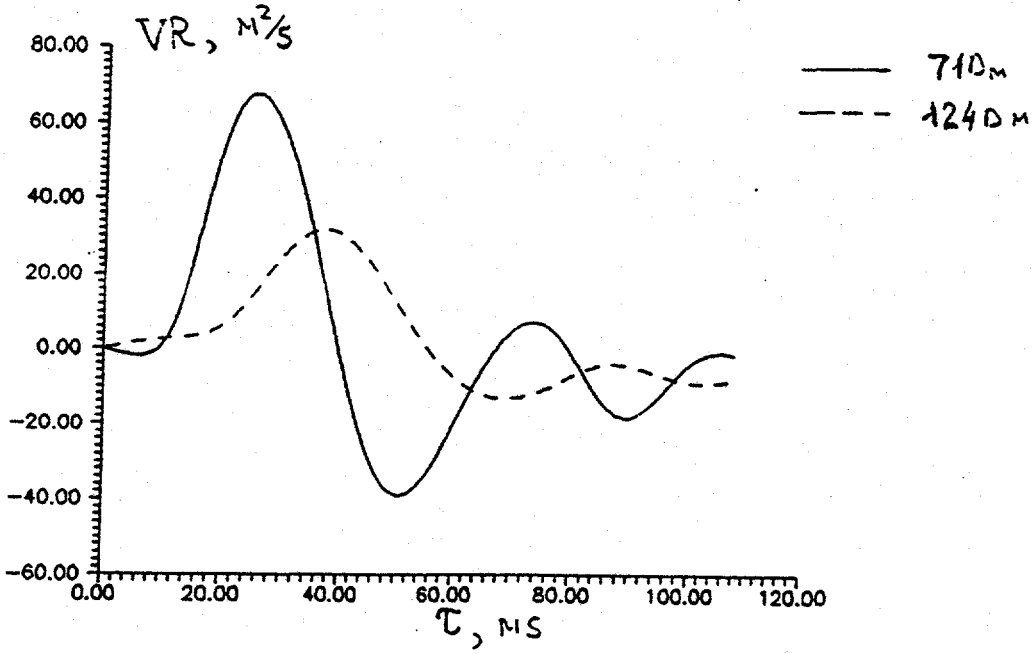
VR, M²/S
80.00
60.00
40.00
20.00
0.00
-20.00
-40.00
-60.00
0.00
20.00
40.00
60.00
80.00
100.00
120.00
τ, MS
710M
1240M

Frg. IV.13

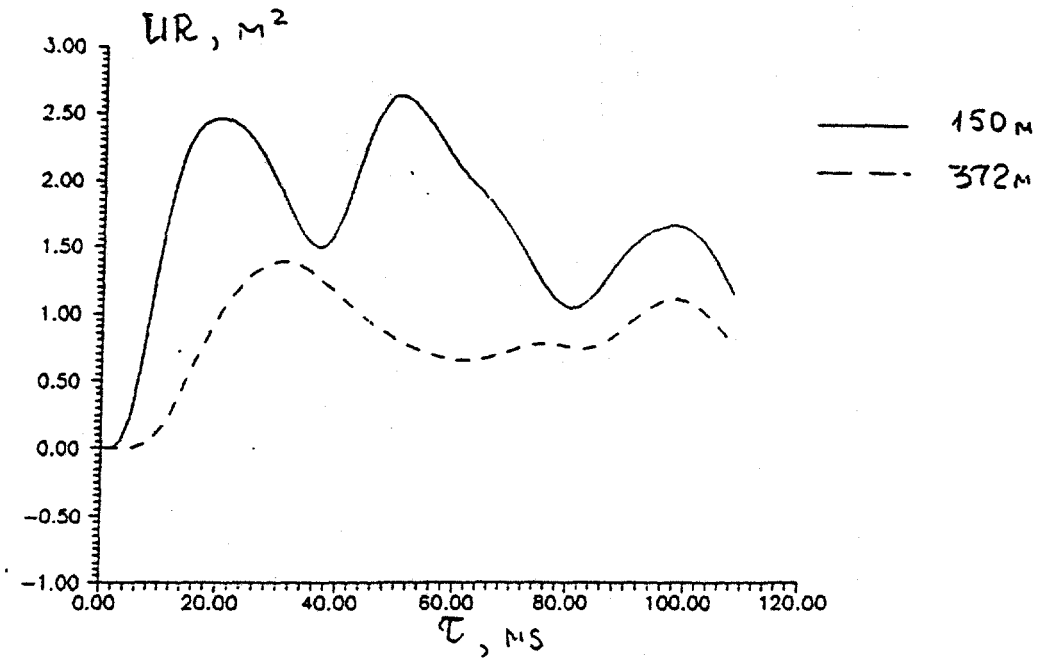
LIR, M²
3.00
2.50
2.00
1.50
1.00
0.50
0.00
−0.50
−1.00
0.00
20.00
40.00
60.00
80.00
100.00
120.00
τ, MS
150 M
372 M

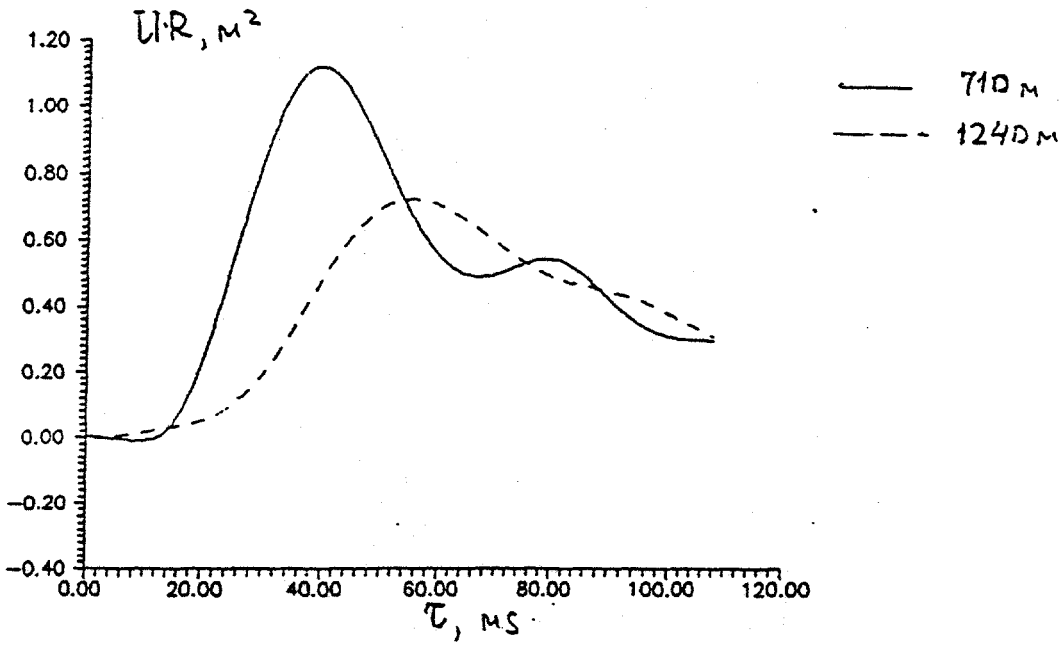
LIR, M²
1.20
1.00
0.80
0.60
0.40
0.20
0.00
−0.20
−0.40
0.00
20.00
40.00
60.00
80.00
100.00
120.00
τ, MS
710 M
1240 M

Fig. IV.14

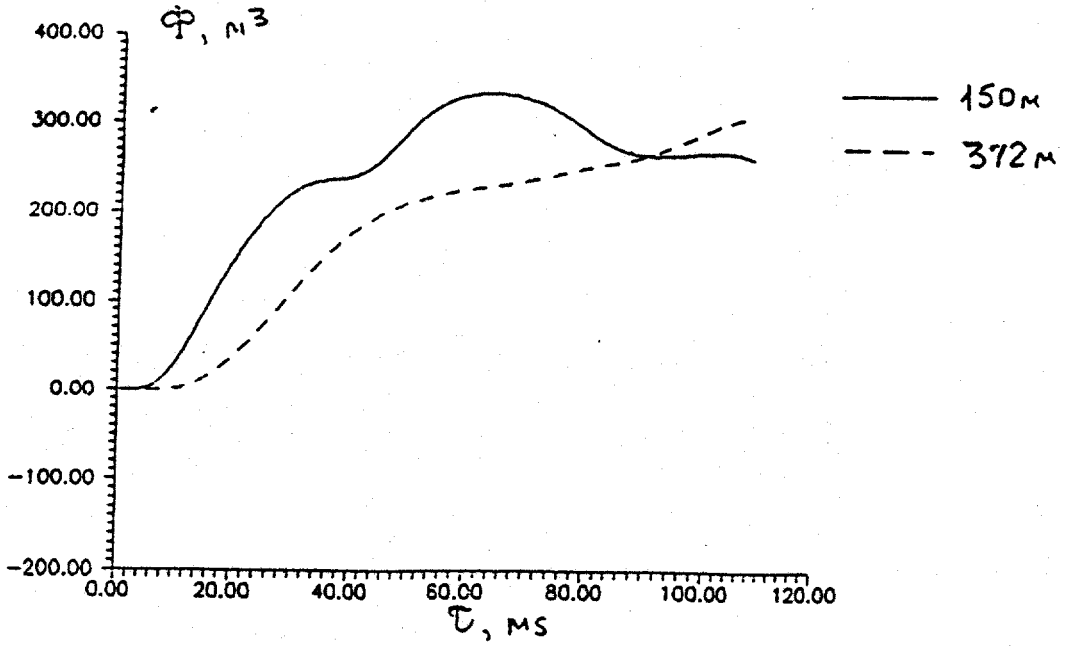
Φ, м3
400.00
300.00
200.00
100.00
0.00
-100.00
-200.00
0.00
20.00
40.00
60.00
80.00
100.00
120.00
τ, ms
150м
372м

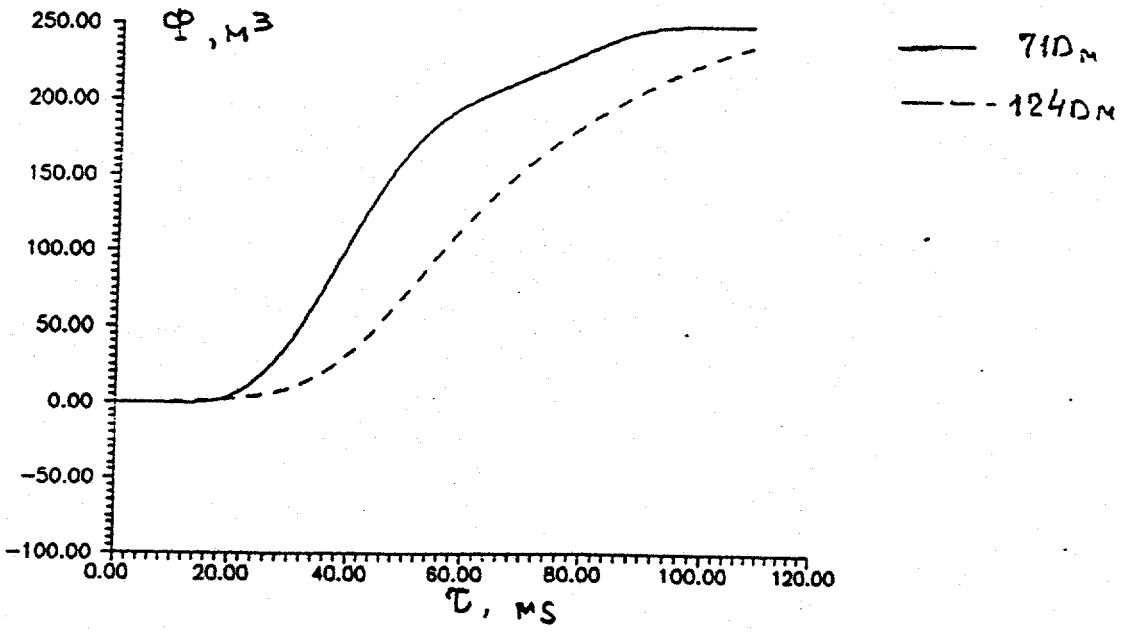
Φ, м3
250.00
200.00
150.00
100.00
50.00
0.00
-50.00
-100.00
0.00
20.00
40.00
60.00
80.00
100.00
120.00
τ, ms
710м
1240м

Fig. IV. 15

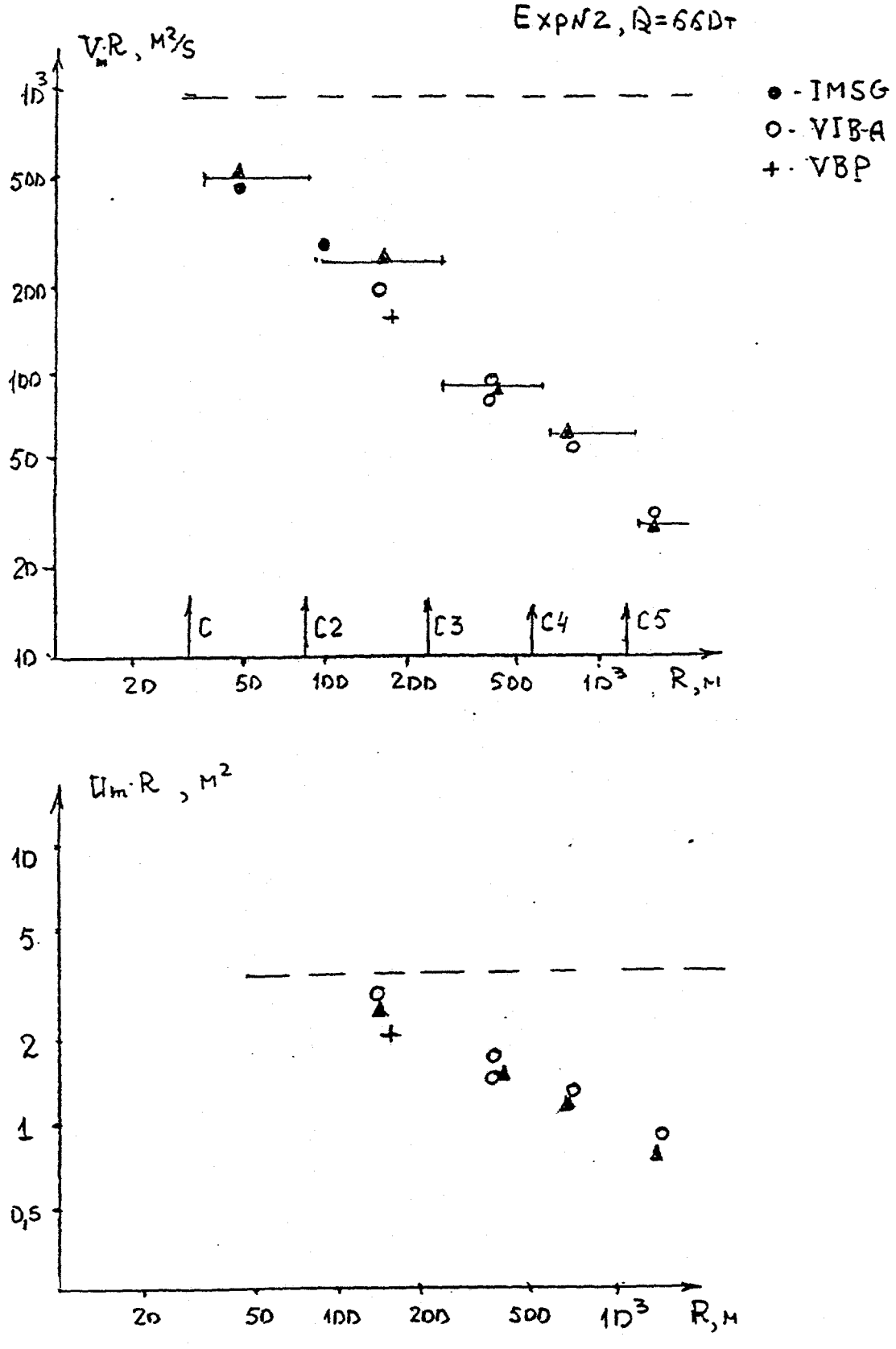
Exp N2, Q=66Dт
$V_m R$, $м^3/с$
10^3
500
200
100
50
20
10
● - IMSG
○ - VIB-A
+ - VBP
C
C2
C3
C4
C5
20
50
100
200
500
10^3
R, м
$U_m \cdot R$, $м^2$
10
5
2
1
0,5
20
50
100
200
500
10^3
R, м

Fig. IV.16.

characteristic time became 3 times larger. This variation can be explaines by the effect of the first explosion. Remember, that two large discontiniuties were revealed near the fault C3.

The lower frame of Figure 16 shows the comparison of the theoretical peak displacement in the first phase of compressional wave with the experimental data. Dashed line stands for U_mR for the medium without faults. The experimental and theoretical results coincide well. Note, that the value $V_mRc\gamma_1$ at large distances is close to ϕ_o for the second explosion (ϕ_o=230 m^3).

Thus, it is possible to conclude, that the method used in the work in estimating the effects of large structural discontinuities of fault type describes the principal characteristics of explosion generated compressional wave propagation well. The method allows to reveal the influence of a fault on the principal parameters of the seismic wave near a source which are usually used to estimate seismic source potential. The results of the calculations make it possible to analyze the experimental results and to estimate an accuracy of the measured parameters in estimating of potential. It is also worth noting that some methodical errors can disturbe the measurements. To illustrate this fact, the theoretical and experimental waveforms at close distance are compared in Figure IV.17. The VIB-A's record from the first explosion is shown by dashed line, and theoretical seismogram is shown by solid line.

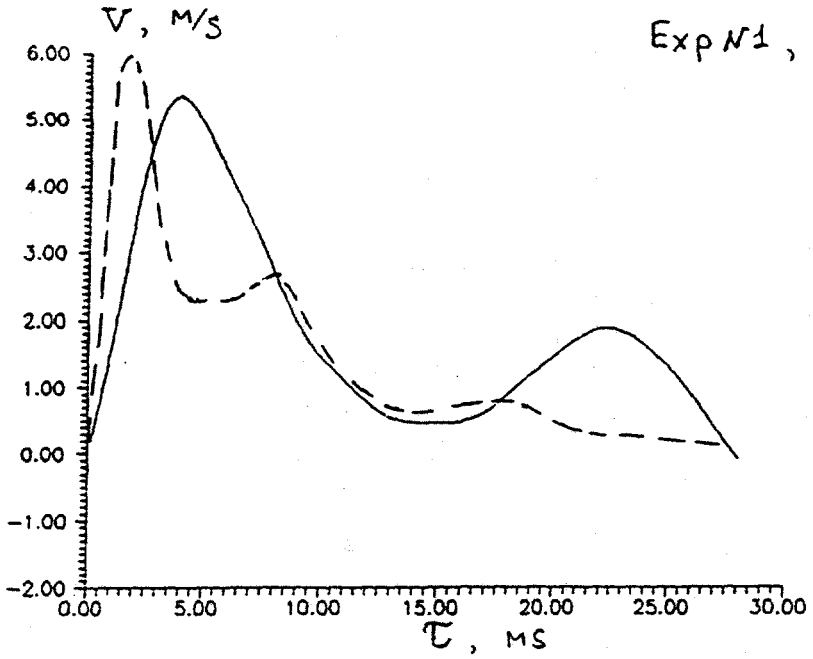
V, M/S
Exp N1, R=44M
6.00
5.00
4.00
3.00
2.00
1.00
0.00
-1.00
-2.00
0.00
5.00
10.00
15.00
20.00
25.00
30.00
τ, MS

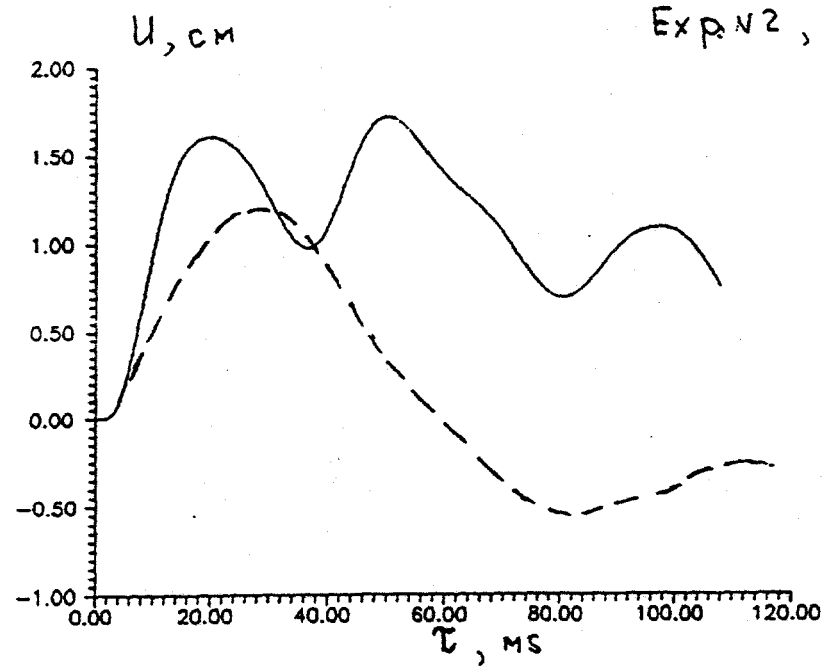
U, CM
Exp N2, R=160M
2.00
1.50
1.00
0.50
0.00
-0.50
-1.00
0.00
20.00
40.00
60.00
80.00
100.00
120.00
τ, MS

Fig. IV. 17

In the lower frame of Figure IV.17 displacement records from the second explosion are compared (dashed line-VBP's record, solid line - theoretical). As clear from the Figure the experimental and theoretical amplitudes are close. But at large times, the shapes of the records are different, especially for displacement, where the shorter first phase was meassured and, moreover, the negative phase at $\tau \geq 60$ ms. Here should be noted, that some effects were not included in the calculations . The most important is free surface effect. The effected waves can arrive in 50 to 100 ms after the first arrival.

Conclusions

The principal characteristic of longitudinal wave propagation near the explosions in hard limestone were revealed by joint analysis of the measured and theoretical data. The peak amplitude attenuates relatively fast with distance. The amplitude/distance relationship can be described by power law (22) with an exponent from 1.6 to 1.8. Such an attenuation in hard rocks can be explained by the effect of local discontinuities of fault type which are characteristic of rocky massifs. The periods increase and high-frequency component strong attenuation are also the result of the faults influence. As a result, such a parameters of source as corner frequency, ω_c, changes with distance. Thus, there is no reliable method to determine an actual source size, b_m, as an emmiter of elastic

wave, but some estimates of ω_c and b_m can be obtained from local data. The final potential value, Φ_o, is the most stable characteristic of the seismic source. The value Φ_o depends (according to (10)) on the total energy E, strength Y and ρc^2 by the following relationship

$$(30) \qquad \Phi_o \cong \frac{Y}{\rho c^2} b_m^3 \sim \left(\frac{E}{\rho c^2}\right)\left(\frac{\rho c^2}{Y}\right)^{0.78}\left(\frac{\rho c^2}{P_1}\right)^{0.12}$$

The ratio $\rho c^2/P_1$, where P_1 is the initial pressure in the explosion cavity, allows to estimate the effect of initial energy density. Chemical (trotyl) explosion is characterized by $P_1 \cong 10^5$ kg/cm^2, and nuclear explosion can be characterized by $P_1 \cong \rho c^2 \cong 10^8$ kg/cm^2. This estimate leads to the conclusion that trotyl explosions are 1.2 times more effective than nuclear. This difference is not too large. This conclusion is consistent with the results of [9], but the calculations in [4] shows, that trotyl explosions have seismic efficiency two times higher than nuclear.

Seismic moment, M, can be also estimated from (30) by using Φ_o value:

$$(31) \qquad M = 4\pi\rho c^2 \Phi_o \sim E(\rho c^2/Y)^{0.78}\,(\rho c^2/P_1)^{0.12}$$

Note, that relative seismic moment value, M/E, depends on $(\rho c^2/Y)$. If this value does not depend on rock type ($\rho c^2/Y = 10^{-3}$ in our calculations) the value M/E is constant. For example, calculations show that for nuclear explosions in salt $M/Q = 3\ 10^{13}$

kg m/kt, and for hard limestones $M/Q=3.31\ 10^{13}$ kg m/kt.

Thus, different by strenght rock types are characterized by similar M/Q values. The same conclusion was published in [9]. Thus, the simple methods of seismic source parameters calculation show that M/Q depends on relative strenght of rocks. It is clear, that the parameter $Y/\rho c^2$ influence is hard to understand without experimental data. From this point of view, the data obtained from the explosions of various yield in granite are very prospective.

REFERENCES

1. Rodionov, V.N., V.V. Adushkin, V.N. Kostuychenko et.al., Mechanic effect of underground explosion, Nedra, 1971. (in Russian).
2. Rodean G., Seismology of nuclear explosions, 1974
3. Zamyshlaev, B.V., Evterev, L.S., Models of dynamic deformation and destruction of rocks, Nauka, 1990. (in Russian).
4. Bychenkov, V.A., S.V. Dem'yanovsky, G.V. Kovalenko et.al., Seismic efficiency of tamped underground explosion, Problems of nuclear science and engineering, Ser. Theoretic and applied physics, N2, 1992. (in Russian).
5. Korotkov, P.F., B.M. Prosvirnina. Numerical simulation of explosion in elastic-plastic medium and some problems of

simulation. Doklady AN SSSR (Reports of Academy of Sciences), 1976, N.228, N1.(in Russian).

6. Korotkov, P.F., B.M. Prosvirnina. On the scaling law and energy distribution of explosion in elastic-plastic medium, PMTF, 1980, N2. (Applied Mathematics and Theoretical physics). (in Russian).
7. Kostuychenko, V.N., V.N. Rodionov. On the generation of seismic waves by large-scale underground explosions in hard rocks. Izv. AN.SSSR, Ser. Earth's physics, 1974, N10. (in Russian).
8. Denny M.D., Goodman D.M. A case Study of the Seismic Source Function: Salmon and Sterling Reevaluated. J.Geophys. Res, 1990, 95, N B12
9. Denny M.D., Johnson L.R. The explosion Seismic Source function: models and scaling laws revived. Explosion Source Phenomenology, Am. Geophys UN., 1991
10. Hensinkveld M.F. Calculation on seismic coupling of underground explosions in salt. Lawrence Livermore Nation. Labor., CA, UCRL-53103, 1981
11. Springer D., Denny M., Healy J., Mickey W. The Sterling experiment: Decoupling of seismic waves by a shot-generated cavity. J. Geophys. Res., 1968, 73, 5995-6011
12. Sadovskyi, M.A., V.N. Kostuychenko. On the explosion generated seismic wave attenuation in rocky massif. Doklady AN SSSR, 1988, v.301, N6. (in Russian).

13. Kostuychenko, V.N. On the propagation of seismic waves through cracked rocky massif. Doklady AN SSSR, 1985, v.285, N2. (in Russian).

14. Sultanov, D.D., E.I. Lyuke, O.P. Kuznetsov. The results of far field seismic observations during the explosion on river Burlykya. Vzryvnoe delo (Explosions) N82/39, Nedra, 1980. (in Russian).

15. Sadovsky, M.A., L.G. Bolkhovitiniv, U.F. Pisarenko. Deformation of geophysical medium and seismic process, Nauka, 1987. (in Russian).

16. Rulev, B.G. Dynamic characteristics of seismic waves from underground explosions. Vzryvnoe delo, N64/21, Nedra, 1968. (in Russian).

*This work was performed under the auspices of the U.S. Department of Energy by Lawrence Livermore National Laboratory under contract No. W-7405-Eng-48.